University of Southampton

Institute of Sound and Vibration Research

# THE SELECTION AND APPLICATION OF A VISCOELASTIC MATERIAL FOR USE IN AN ARTIFICIAL DAMPING TREATMENT ON INTEGRALLY STIFFENED PANELS.

by

C.T. Coote, B.Sc.

Submitted for the Degree of

Doctor of Philosophy

M. Phil. awarded (1974)

February 1974

ABSTRACT

FACULTY OF ENGINEERING AND APPLIED SCIENCE

INSTITUTE OF SOUND AND VIBRATION RESEARCH

Doctor of Philosophy

THE SELECTION AND APPLICATION OF A VISCOELASTIC MATERIAL FOR USE IN AN ARTIFICIAL DAMPING TREATMENT ON INTEGRALLY STIFFENED PANELS.

by Christopher T. Coote

The work described in this report can be conveniently divided into two sections, the first arising out of a need to obtain more detailed information on viscoelastic materials incorporated in artificial damping treatments due to the lack of detailed information available in the literature, and the second section of the work describing the application and performance of the selected material used in a specific damping configuration. The first section concerned the selection and testing of various silicone based elastomers for use in damping treatments. The development of a forced vibration method for testing damping materials in shear is described, with results of the dynamic shear properties detailed in the form of graphs. Of particular interest was the performance of these materials over wide temperature ranges for possible use in adverse environmental conditions. The testing apparatus was developed to enable measurements to be made over the temperature range -60°C to +150°C by the incorporation of environmental test chambers. Careful consideration was given to the separation of the various test parameters so that the effects of changing frequency and strain applied could be accurately determined. Testing was carried out over the ranges 200 - 1000 Hz and at shear strains of .0004 to .01. In addition changes in the basic material were investigated by varying the filler content and curing techniques. The methods of specimen moulding are described in detail to enable future investigators to avoid some of the difficulties encountered. The most successful material tested in terms of overall

performance was a filled fluorinated silicone rubber which was selected for further use in a particular type of artificial damping treatment utilising the material primarily in shear. The manufacture of shear damping beams is also described in detail.

The second section of the work concerned the effects of adding shear damping beams to the response of a resonating integrally stiffened flat panel. The reductions in the resonant multi-modal response, to both acoustic and single point excitation, obtained by the addition of such dampers, are described. Detailed mode shape investigations and energy dissipation measurements were made to determine the response reductions in a quantitive manner. In addition the effects of such dampers on the response of two full scale aircraft structures is described. As a parallel to the experimental investigations of panel response, theoretical investigations are described in which attempts have been made to incorporate significant amounts of artificial damping in the usual response estimations. The most successful theoretical model consists of a transfer matrix analysis of a beam on elastic supports in which the effects of shear damping are included. The trends indicated from this theory which incorporated mathematical models of the damping material behaviour as measured in the first section, agree well with the effects observed in the practical panel response investigations. It was shown that for a weight addition of only 2%, displacement and hence stress response can be reduced to 60% of the undamped response by the addition of a shear damping beam.

ACKNOWLEDGMENTS

The author would like to thank Professor B.L. Clarkson of the Institute of Sound and Vibration Research, University of Southampton, for his supervision of the work and his many helpful comments and advice. The writer would also like to express his gratitude to all his colleagues at the Institute, and in particular Mr. F. Cicci, for their valuable discussions and suggestions on the work. He also thanks the technical staff at the Institute for their valued advice and assistance in the design and construction of the test apparatus.

The author would like to express his gratitude to Dr. D.K. Thomas of the Materials Department, Royal Aircraft Establishment, Farnborough, and his staff in the Rubber Materials Laboratory, for their invaluable help in the selection and supply of the various silicone rubbers used and their assistance in moulding the test specimens and shear damping beams. Finally he would like to thank the British Aircraft Corporation, especially Mr. D.C.G. Eaton of the Acoustics Department, Filton, for their sponsorship of the author during the period of study.

CONTENTS

## LIST OF FIGURES AND PLATES

LIST OF TABLES

## NOMENCLATURE

| | | |
|---|---|---|
| A | - | area of a single rubber shear face for both shear test specimens and damping beams. |
| $BM_i$ | - | bending moment in beam at station i. |
| $C_1, C_2$ | - | constants in W.L.F. equation. |
| D | - | shear damping beam parameter for transfer matrix analysis. |
| E | - | complex Young's modulus of elasticity for the defined material. |
| E' | - | real part of E. |
| E'' | - | imaginary part of E. |
| F | - | excitation force. |
| G | - | complex shear modulus of damping material. |
| G' | - | real part of G. |
| G'' | - | imaginary part of G. |
| H | - | excitation moment for 3 beam theoretical model. |
| Hpq | - | frequency response function at q to excitation at p. |
| I | - | second moment of area of the defined bending section. |
| K | - | complex stiffness of rubber spring or equivalent bending stiffness of stringer. |
| K' | - | real part of K. |
| K'' | - | imaginary part of K. |
| M | - | moving mass (either of shear test specimen or stringer) |
| $M_j^r$ | - | bending moment to right of station j in beam element. |
| P | - | excitation force for energy measurements. |
| R | - | stringer equivalent rotational stiffness. |
| S | - | cross sectional area of rubber "spring". |
| SFi | - | shear force in beam at station i. |
| T | - | test temperature for shear damping specimens. |
| $T_o$ | - | reference temperature for method of reduced variables. |
| $T_{oo}$ | - | common temperature in W.L.F. equation. |
| $T_t$ | - | glass to rubber transition temperature for damping material. |
| $T_1$ | - | $T_t + (50 \pm 5)^oK$ - as in third version of W.L.F. equation. |

$^{l}_{k}(T)^{r}_{j}$ - transfer matrix from L to R of station i, k.

V - shear force in a beam element.

X - displacement response of base of single slug specimen.

$X^{r}_{k}$ - displacement to right of station k in beam element.

Y - displacement response of top of single slug specimen.

$Z^{r}_{k}$ - state vector to right of station k in transfer matrix theory.

a - frame pitch of test panels.

f - test frequency in Hz.

h - height of test panel stringers from skin line.

$h_{pq}$ - impulse response function at q to impulse at p.

$\ell$ - width of one skin bay or test panel or length of equivalent portion of shear damping beam.

t - thickness of rubber shear layer.

w - excitation frequency.

y - peak resulting displacement for energy measurements.

$\alpha$ - phase angle lag between excitation and response.

$\alpha_{ij}$ - receptance between stations i, j of structure.

$\Omega$ - ratio of test frequency to natural frequency $w/w_n$

$\delta$ - structural damping ratio of bare panel.

$\epsilon$ - horizontal displacement of stringer tip during stringer rotation.

$\eta$ - hysteretic damping ratio of "rubber" material.

$\theta$ - angle of rotation of stringer from vertical.

$\lambda_i$ - frequency parameter for beam i $= 4 \frac{w^2}{EI}$

$\mu$ - weight per unit length of beam.

w - excitation frequency.

$w_n$ - resonant frequency.

# I. INTRODUCTION

## I.1 Integral Structures

In recent years the trend in lightweight structures has been away from the conventional fabricated or built-up structure to one of the more modern developments. These include honeycomb sandwich, fibre reinforced plastics, bonded metal structures, and integrally machined structures. Of these the integrally machined structure comes closest to simulating the conventional built-up structure and is thus widely used. Hence this type of structure is to be investigated in this report.

The most common application of such structures is in the aerospace field where weight is of paramount importance. However the applications to other vehicles are increasing as designers realise the cost advantages of lightweight structure. The improvement in stress analysis techniques has also enabled designers to reduce safety factors, thus leading to cheaper and lighter structures. Since most of the problems associated with these structures originate in the aerospace field, reference will be made to this application in particular.

For aircraft use the main application of these types of structure is for the external skin and engine nacelle structure. Large portions of the skin will be in a very hostile acoustic environment for most if not all of the aircraft operating time. Even if the skin is not subjected to high stresses by normal flight loads, it may be within a severe acoustic pressure field. This is produced mainly by high speed jet noise and turbulent boundary layer, with possible contributions from ground reflections and larger scale air turbulence. Stresses induced by normal flight loads and air turbulence are of a low frequency nature and will usually only involve a few of the overall bending or torsion modes of the particular sub-structure such as the wing or fuselage. Stresses induced by the

acoustic pressure field are in general of a very localized high frequency type and can cause severe fatigue problems.

It is these stresses that it is sought to reduce (by artificial means). The stresses are usually bending stresses caused by transverse vibration of the skin excited by short wavelength fluctuating acoustic pressures. The response of a stiffened skin to these pressures is almost always multi-modal. Thus stresses will be induced over a range of frequencies. If the excitation were over a limited frequency range, it might be possible to eliminate the major resonances at the design stage. Lin et al (1) suggest designing structures so that the stringer torsion and stringer bending modes bracket the excitation frequency range to eliminate major resonant response. Mead (2) also explains the significance of these modes. This method cannot be applied to the integral panel because of its difference in behaviour compared to conventional structure, as described by Clarkson and Cicci (3). They show that due to the relative similarity in order of magnitude of the stringer bending and torsional stiffnesses, the modes of vibration are no longer grouped in bands as shown by Lin et al (1, 4, 5). Results obtained by Olsen and Lindberg (6) confirm this. Also with jet noise excitation which contains energy over a wide portion of the spectrum it is hardly ever possible to use this approach. The best that can be done is to estimate the bounds which the induced stresses will reach by methods such as those developed by Clarkson (7), and if these are too high to find some artificial means of reducing them to an acceptable level.

It is well established (8) that when dealing with vibrations in the high frequency range, it is not necessary to study the structure as a whole. Instead it is usually possible to identify the prominent modes of vibration as either resulting from displacements of the support structure, or displacements of the skin and its associated stiffeners.

As has been mentioned previously the main high frequency effect is due to displacements of the skin. Thus it is possible to study the vibration characteristics of one skin panel with its associated stiffeners and gain a knowledge of the vibration characteristics of the whole structure. This approach is adopted in this report, and an investigation into reducing the vibrations of a single integrally stiffened panel made.

The conventional built-up structure is defined as one made up of flat skins periodically reinforced in one direction with open or closed section stiffeners (stringers) which are usually bent up from flat sheet or extruded. The stiffeners are attached to the skins by rows of rivets. This system although requiring the minimum of capital equipment to manufacture is becoming an increasingly costly process as the cost of labour rises. The system does not lend itself to automatic production and is virtually "hand-made" from start to finish. The integrally machined structure as its name implies does not involve the same amount of joining as the conventional structure. The integral structure starts out as a solid billet of material which is then machined away leaving the stiffeners standing proud of the skin. The choice of stiffener cross-section is usually limited to simple rectangular or "T" shapes and up to 99% of the billet may be machined away. However since the system lends itself to high speed production on numerically controlled machines, the cost compares very favourably with that of the conventional structure.

One of the major problems with the conventional structure is its resistance to fatigue. The multiplicity of rivet holes create stress concentrations throughout the whole structure, and the many crevices created are ideal galvanic and stress corrosion centres. Rivet fit is also difficult to control and loose or missing rivets can cause fretting of the structure and further fatigue problems. Integrally stiffened structures overcome these problems and were first developed to increase

the "classical" fatigue resistance of stiffened structures by eliminating many of the joints and providing generous fillet radii at all changes of section. Thus it can be seen that the integral structure has several advantages over the conventional and this explains the increasing use of this type of construction. However because of the nature of the integral structure it has several disadvantages compared to the conventional. Since the integral structure eliminates a large proportion of the joints within the structure, the opportunity for movement and thus friction between structural members is reduced. In a resonant situation the one factor which limits the resonant vibration amplitude and hence stress, is the structural damping. Since the majority of structural damping comes about due to fretting and internal friction, it can be seen that the integral structure may experience resonant vibrations which can build up to a higher level than in the conventional structure. Nelson (9) has shown measurable differences in response of a resonant beam with small variations in structural damping and Mead has shown (10, 11) via tests on rivetted joints in beams, that the structural damping is at least an order of magnitude lower in the "integral" structure. Kennedy-Pancu (12) vector plots of resonant response on an integral plate have also shown this order of difference in structural damping compared to a conventional plate of similar size. Cicci (13) has shown that the vibration characteristics of an integral plate differ from those of a conventional plate in that the siffeners bend with the skin rather than acting as line stiffeners on the skin. This can induce very high bending stresses on the free edge of the stiffener and as there is no discontinuity in the material at the skin/stringer interface, cracks can propagate freely into the skin area with possibly disastrous results.

Thus it can be seen that although the integral structure offers superior characteristics in terms of static strength and cost of production,

it suffers from severe limitations caused by its lack of internal damping and the ease with which cracks can propagate through it. If a means could be found of increasing the structural damping and thus reducing the resonant vibrations of the integral structure, the system would be even more attractive and would create structures of greater efficiency.

I.2 Artificial Damping Treatments

Attempts to produce a metal with much higher internal or structural damping, out of which to manufacture integral panels, have been made. These are usually alloys containing boron and beryllium and thus do not compare favourably on cost with duraluminium. Most effort on increasing structural damping has been by the addition of some artificial damping treatment containing a high damping plastic. Lazan (14) describes a wide variety of such treatments and Jones and Trapp (15) show the effectiveness of various treatments on real structures with simple equations for stress estimates. First attempts were to apply what is known as an unconstrained damping layer. This merely consisted of a uniform layer of high damping material stuck to the vibrating surface. As the surface vibrated, the unconstrained layer spaced away from the neutral axis of vibration by some proportion of the skin thickness, was subject to plain extensional and compression strain. Warnaka et al (16) give design charts showing the optimum stiffness and thickness for the damping material to obtain a given response reduction. This method is not very efficient since the vibrating skins are usually thin and the strains applied to the damping layer are small. Jones (17) shows the effect when applied to a stiffened panel and suggests the advantage of spacing the material away from the vibrating skin to magnify the damping effect. Thus to obtain any worthwhile increase in damping, large (and therefore heavy) amounts of damping material have to be applied. This

system was applied to an integral panel by Lyons (18) using L.D. 400 synthetic material. For a weight addition of nearly 20% stress reductions of the order 65% were observed. Although the stress reductions were significant, the considerable additional weight was unacceptable.

A modification of this method is the constrained layer. This consists of a uniform layer of damping material attached to the vibrating surface with a stiffer constraining layer applied over the top of the damping material. As the panel vibrates, shear strains are induced in the damping material. Tests by the author using Viton damping material and aluminium constraining layers on an integral panel, showed no significant advantage over unconstrained Viton layers - however no optimisation was attempted. The ultimate developments of this method are damping tapes. These consist of a layer of adhesive damping material backed by metal foil. This can then be stuck on to the areas where vibration control is desired. Many authors have suggested that the use of damping materials in shear is the most efficient method, Ungar and Kerwin (19) describe beam designs incorporating damping material shear cells within the flanges, Lamarce and La Barge (20) describe increased resistance to sonic fatigue by using sandwich panels with a damped core; similar results using damping tape are described by Jones (21), and Potter (22) describes increased reliability of rotor systems by using elastomeric shear dampers. Kerwin (23) showed the effect of single layers of damping tape applied to simple beams with good correlation between wave propagation theory and experiment. Attempts by Ungar, Ross and Kerwin (24) to improve the performance of damping tapes by applying several layers showed that the addition of a third or fourth layer had very little additional effect since hardly any strain was being transmitted to these tapes by the relatively soft material below. In fact it was demonstrated that a three layer tape system was no more effective

than a single tape containing equivalent amounts of damping material and metal foil. Lazan et al (25) developed theory for several material bands of various types (elastic, rigid, uniform and non-uniform thicknesses), but the experimental results on beams are at too low a frequency to be comparable. Torvick and Lazan (28) suggested a corrugated spacer to be applied to the vibrating panel with the damping tape on top of this. Since this increased the distance of the tape from the neutral axis of vibration the damping effect was increased considerably. Simmons et al (27) developed a multiple tape system and overcame the problem of transmitting shear strain to the upper layers by anchoring alternate ends of the constraining foil of the tapes in solid blocks of epoxy resin. In this way the upper tape was just as effective as the tape adjacent to the skin. In experiments on typical skin / stringer panels the resonant amplification factor was reduced by a factor of 5 for a weight addition of only 1.5%.

The tuned vibration absorber is a familiar mechanism, and several workers have modified the simple mass/spring system by incorporating damping in the absorber itself. This has the effect of making the tuning less sharp and the method can be made effective over a frequency range. Henderson (28) develops the theory for this and shows the possibility of extending the effective frequency range. Jones et al (29) demonstrate the practical effect on a radar antennae connection, but the problem here was essentially to eliminate only one major resonance peak. Jones (30) also describes the application of small tuned beams to a stiffened panel with the middle of each skin bay connected to a tuned beam via a damped link. Theory and experiment showed that the natural frequency of the tuned beam was critical, in relation to the frequencies of the stringer bending and torsion modes, if the system was to have a broad-band effect. Thus with an integral panel where the stringer bending and torsion modes are closer as described previously (3, 31) the effective

band width of useful stress reduction would be reduced. Bruns (32) described a system using rings of damping material to support tuning masses, a ring and mass being placed in the centre of each skin bay of a stiffened panel. Results show a fairly broad band effect, but again the major reduction in amplification factor from 30 to 6 was measured at a single predominant resonance peak. From the results of this survey of literature on tuned dampers it was concluded that this type of treatment would not be suitable for broad band stress reduction on an integral panel.

Lyons (18) utilised the natural spacing effect of the rectangular section stiffeners of an integral panel by suspending a layer of stiff damping material across the stringer free edges, thus utilising the ideas of Torvik and Lazan (26). Lyons demonstrated significant stress reductions over a broad frequency range using what was effectively a spaced unconstrained damping layer. Further investigations by Cicci (31) confirmed the effectiveness of this method when the panel was excited by an acoustic pressure field. However, the material used possessed damping properties which were very sensitive to temperature changes. This was so marked that a change in room temperature had a considerable effect on the stress reductions obtainable in the integral panel. To overcome this a shear damping beam technique has been developed. This maintains the use of the spacing effect of the panel stiffeners, whilst using a material in shear to obtain a superior performance as suggested in (27, 33, 34, 35.)

I.3 Shear Damping Beams

The shear damping beam system is shown diagrammatically in Figure 1 and consists of a sandwich beam attached to the tips of the panel stiffeners. The beam consists of a continuous upper aluminium layer,

visco-elastic centre and discontinuous aluminium lower layer. Each of the lower layers is attached to a stiffener (stringer) tip. As the panel vibrates causing rotation of the stiffeners, the lower sandwich layers induce a shear strain in the visco-elastic centre layer. The sandwich beam is also excited in its own flexural modes, inducing further shear strain in the centre layer. Initial tests by Cicci (31) have shown that for a .025m. (1"") wide beam attached across the centre of a .530m. x .555m. (21" x 22") integrally stiffened panel, r.m.s. stress reductions of the order 70% can be obtained for a weight addition of only 2%. The system responds to all the natural modes of vibration of the plate and is effective in damping the response both to discrete tone acoustic excitation and random noise excitation. Theoretical studies of sandwich damping treatments (36) indicated that a material of low shear modulus (of the order $8 \times 10^4$ Kg/m$^2$ (600 lb/in$^2$) was desirable, in conjunction with a value of loss factor as high as possible.

1.4 Damping Material

The choice of damping material is important not only for its damping properties but also for its capability of withstanding the general aircraft environment. The environment is severe with a temperature range of -60°C to +150°C and exposure to all the usual aircraft fuels, lubricating and hydraulic oils. Thus the material must maintain its damping properties and be resistant to aircraft fluids over this wide temperature range. The use of various types of rubber and plastic as seals on electrical and other types of aircraft connectors and covers has shown that the silicone rubbers are the only generally satisfactory materials. Potter (22) describes the selection of silicone rubber shear dampers for stress reduction in rotor systems, Jones (37) Nashif (38) and Ruzika (39) have also demonstrated the suitability of silicone rubbers for use in structural damping treatments. Hence silicone based elastomers were selected for use in the shear damping beam.

Owens (40 has shown the temperature sensitivity of the damping properties of many commonly used materials, to be too high for use in applications involving large temperature changes. He suggested two techniques for improving the workable temperature range. The first was to modify the material chemically to increase cross-linking within the material, the second was to blend several different materials to broaden the effective range. Turner (41) also suggests blending for shear damping materials whilst Blenner (42) shows the results of blending on an unconstrained extensional damping treatment. Here the effective temperature range is nearly doubled by this technique. Because of lack of facilities no blending operations were carried out to improve the basic material, but an attempt was made to increase cross-linking within the material by chemical modification.

Since there exists virtually no literature on the shear damping properties of these materials it was necessary to develop a technique for testing the materials to obtain their basic dynamic shear properties before using the material in the shear damping beam system.

Three basic types of rubber supplied by the Materials Department at R.A.E., Farnborough were tested. These were:- methyl-vinyl silicone rubber, phenyl-methyl silicone rubber and flourinated silicone rubber. The most promising of these was flourinated silicone rubber, and repeat tests were made to investigate variations in the dynamic shear properties with varying filler content and applied strain plus tests at sub-ambient temperatures. The results for phenyl-methyl rubber were very poor and are thus not included since the performance of this compound was at least an order of magnitude less than that of the methyl-vinyl and flourinated rubbers.

## II. MEASUREMENT OF THE DYNAMIC PROPERTIES OF VISCOELASTIC MATERIALS

In order to be able to produce viable shear damping beams it was necessary as stated previously to develop a method for testing the basic damping material,to ensure that it was capable of performing well over the required environmental range. This chapter describes the basic mathematical models used to describe the behaviour of such materials and reviews the methods available to obtain the parameters defined by the mathematical models. The choice of a particular testing technique is described together with the basic theory underlying the method, including an error analysis.

### II.1 The Concept of Viscoelasticity

Most elastomers used in damping treatments have a response to dynamic strains which may be described as viscoelastic. Bishop (43) suggests the dynamic shear properties can be represented as a complex shear modulus, $G = G' (1 + i\eta)$ where G' is the real part of the complex shear modulus G,and $\eta$ is the loss factor. Ungar and Kerwin (44) define the hysteretic loss factor $\eta$ in terms of energy ratios for both single degree and multi-degree of freedom systems. This simple definition agrees with that of Bishop and is the most commonly used. Crandall (45) demonstrates the limitations of this simple hysteretic model, but states that the material properties based on this definition are useful for comparison. The author agrees with this view and thus all the measured material properties are based on a simple linear viscoelastic model.

The dynamic properties of most viscoelastic materials, including silicone rubber, are strongly dependent upon temperature, excitation frequency, and applied strain. Ungar (33) and Ruzika (39) show typical frequency dependencies of the dynamic properties of rubber type materials whilst Hatch et al (29) show frequency, temperature and strain dependencies for a wide range of materials including synthetic rubbers. If such

materials are to be of use in damping the typical multi-modal response of stiffened panels, the frequency and strain dependency of the dynamic shear properties should be small or ideally constant. In modern aircraft the temperature range experienced in flight can be of the order $-60^{o}C$ to $+150^{o}C$. Thus the variations in the dynamic shear properties should also be small within these limits.

The behaviour of viscoelastic materials through a wide temperature range may be described by three regions, see Figure 2. At the lower temperatures the material is "glassy" showing a high modulus, but little capacity for damping due to the material being brittle. At the higher temperatures the material is "rubbery" being very flexible and with little resistance to deformation. In between these two conditions is the "transition" region (40), (47), where the material has a reasonable stiffness and a good resistance to deformation. The damping capacity is at a maximum in this region (48), thus it was desired to find a viscoelastic material with a transition region wide enough to cover the temperature range $-60^{o}C$ to $+150^{o}C$.

## II.2 Measurement Techniques

There are four basic methods for measuring the dynamic properties of damping materials, these are:-

(a) Free vibration measurements of frequency and the logarithmic decay of amplitude, usually involving a coated cantilever beam (49), (50).

(b) Wave propagation measurements of frequency and decay rates (51), (52).

(c) Resonance tests with results obtained from measurements of the response curve (53), (54).

(d) Forced oscillations method with measurements of excitation force, displacement and phase angle between them (55), (46).

Method (a) is unsuitable owing to the very high rate of decay resulting from these high damping materials. The signals obtained would be of very short duration and difficult to analyse. The method using a coated beam as first suggested by Oberst (56),suffers from problems due to the multi-modal response of the beam. Even if excited at the fundamental frequency, the high system damping will cause considerable coupling of the higher modes. This will cause the decay curve to show a beating effect, amplitude being modulated at the beat frequency. Thus any measurements of logarithmic decrement would have to take this into account, which would further complicate the analysis of results. Adkins (57) describes some modifications to the coated beam technique which overcome these problems, but the system is limited to the testing of relatively stiff materials in extension and compression, not in shear. Abdulhadi (58) describes a three layer composite beam test using a soft viscoelastic material as the core. Knowledge of the natural frequencies and system loss factors of the composite beam enable calculations to be made to estimate the basic core material properties. This also suffers from neglect of the higher order mode coupling. Estimates of the first four mode factors of a cantilever are used, but as these are approximations the final calculated properties could be in considerable error.

Method (b) involves very small strains indeed, thus the results would not demonstrate any strain dependency of the dynamic properties. The signals obtained would be of very short duration as for method (a) and therefore difficult to record and analyse.

Method (c) is unsuitable for materials whose dynamic shear properties are dependent on strain, as the amplitude of vibration at resonance is not controlled by the experiment, but depends solely on the properties it is desired to measure, i.e. damping. Frequency

variation over the desired range involves large changes of vibrating mass, thus this method can be impractical. McConnell (59) suggested an electronic mass cancellation or addition device built with operational amplifiers. Use of this method by Cicci (31) has shown that at present the amplifiers available have too great a phase shift within them to enable the system to work. With a simple single degree of freedom system as described by Nashif (60), an upper frequency limit is reached with soft materials. Assuming an effective vibrating mass of 1/3 that of the viscoelastic spring, with no further mass addition, an upper frequency limit of the order 500Hz is not uncommon. Thus this method is unsuitable for testing soft materials over a wide frequency range.

Method (d) overcomes these problems since the experimenter can set the strain and excitation frequency accurately. Provided that instruments can be found to measure the excitation force, displacement of the moving mass, and phase angle between these two, to the required degree of accuracy, this method is suitable. Since such instruments are available, this method was chosen for the tests described in this report.

To determine the variation of the dynamic shear properties with temperature, it was necessary to keep the other variable i.e. strain, constant. This was achieved by testing at constant displacement amplitude, this being associated with a calculated acceleration level at each test frequency. Thus an acceleration signal could be conveniently used to control the response of the specimen. Any variations in the damping properties could then be attributed solely to variations in temperature and frequency. When testing for the strain dependency of the damping properties, values of acceleration for different displacement amplitudes were calculated and these used for controlling the response in constant temperature tests.

## II.3 Forced Oscillation Method

### II.3.1 Theory

The specimen is shown in Figure 3. If the centre block is subject to an excitation force, the system responds as a single degree of freedom system, with the spring stiffness provided by the rubber layers in shear.

Consider the vector diagram of forces for the steady state vibration of a single degree of freedom system (Figure 4).

$\alpha$ = phase angle between inertia and excitation forces

M = mass of moving block and link above force sensing element

F = magnitude of excitation force

X = displacement of moving block

$\ddot{X}$ = acceleration of moving block

K = complex spring stiffness

K' = real part of spring stiffness

K" = imaginary part of spring stiffness

$\eta$ = loss factor of rubber

G' = real part of shear modulus of rubber

G" = imaginary part of shear modulus of rubber.

Resolving in the direction of inertia force:

$$M|\ddot{X}| - K|X| + F\cos\alpha = 0. \qquad (3.1.1)$$

Resolving in the direction perpendicular to inertia force:

$$K\eta|X| - F\sin\alpha = 0. \qquad (3.1.2)$$

Thus $$K|X| = \frac{F\sin\alpha}{\eta}$$

Substituting in (3.1.1)

$$M|\ddot{X}| - \frac{F\sin\alpha}{\eta} + F\cos\alpha = 0$$

Thus

$$\eta = \frac{F\sin\alpha}{M|\ddot{X}| + F\cos\alpha} \qquad (3.13)$$

Note this is a general equation and if the system is driven at

frequencies greater than the natural frequency, i.e. $\alpha > \pi/2$, then

$$\eta = \frac{F \sin \alpha}{M |\ddot{X}| - F |\cos \alpha|}$$

By definition $\eta = {}^{K''}/_{K'} = {}^{G''}/_{G'}$ (34), (44)

Now $G' = \dfrac{\text{Shear stress in phase with shear strain}}{\text{Shear strain}}$

Thus $G' = \dfrac{\text{Force in phase with shear strain}}{\text{Shear area x Shear strain}}$

$$= \frac{M |\ddot{X}| + F \cos \alpha}{\text{Shear area x shear strain}} \qquad (3.1.4)$$

Thus by measuring the force required to maintain oscillations at a given frequency, the acceleration of the moving mass, and the phase angle between the force and acceleration, the properties G' and $\eta$ can be calculated from equations 3.1.3 and 3.1.4.

II.3.2 Error Analysis

Whenever results are calculated from measured quantities, there is always the danger that errors in the measured data may lead to magnified errors in the calculated quantities. Hence an error analysis was performed to determine whether any such error magnification would be present in these experiments.

It was thought that the only measured quantity subject to appreciable error would be the phase angle $\alpha$ between the excitation force and acceleration of the moving block.

The dynamic characteristics of the force transducer give rise to some phase change over the frequency range tested, also changes in temperature of the sensing element caused by conduction down the threaded linkages could cause phase variation. Although phase-matched amplifiers were used, the accuracy of matching is not guaranteed to greater than 2% by the manufacturers. Thus phase mis-match in the

amplifier chains could amount to 4%. Accurate measurement of phase by the phase meter is difficult to achieve, the accuracy required being of the order 1 to 2% ideally. The meter used was guaranteed accurate to 2.5% on the absolute scale, and 1.3% on the relative measurements, it also had a very sensitive scale ($12^{o}$ full scale deflection) which was useful in obtaining accurate readings at the lower test frequencies.

Hence an error analysis was carried out to investigate possible error magnifications in the calculated values of $\eta$ and G' due to errors in the measurement of the phase angle $\alpha$ .

Using the notation of 3.1 above, the equation of motion of the system in Fig. 2 is:-

$$M\ddot{X} + K(1 + i\eta)\, X = F \sin \omega t \qquad (3.2.1)$$

Thus it can be shown that:

$$\{-M\omega^2 + K(1 + i\eta)\}\ X = F \sin(\omega t - \alpha) \qquad (3.2.2)$$

Where $\alpha = \tan^{-1} \dfrac{K\eta}{(K - M\omega^2)}$

If the natural frequency of the system is $\omega_n = \sqrt{K/M}$,

Define $\Omega = \omega/\omega_n$ then $\tan\alpha = \eta / 1 - \Omega^2$ (3.2.3)

Differentiating w.r.t. $\eta$, $\sec^2\alpha\, d\alpha = \dfrac{d\eta}{1-\Omega^2}$

Thus $$\left\{1 - \frac{\eta^2}{(1-\Omega^2)^2}\right\} d\alpha = \frac{d\eta}{1-\Omega^2}$$

$$\frac{d\eta}{d\alpha} = \frac{(1 - \Omega^2)^2 - \eta^2}{(1 - \Omega^2)}$$

Thus it can be seen that for high values of $\Omega$, the error magnification is of the order $\Omega^2$, so this region is to be avoided. For low values of $\Omega$, assuming a typical value of $\eta$ (e.g. 0.5) the error magnification is less than unity, hence percentage error is reduced. At the point of resonance the error magnification is large but at frequencies just above

and below resonance e.g. $\Omega$ = 0.9 the error magnification drops to the order of unity.

Hence it was concluded that the error magnification in calculating the value $\eta$ would be negligible if the frequency range were restricted to $0 < \Omega < 1.5$ and the point of resonance avoided ($\Omega = 1.0$). Since the lowest resonant frequency found was 650 Hz. and testing was confined to the range 200 to 1000 Hz, these conditions were satisfied.

From equations (3.1.1) and (3.1.2) solving these simultaneously for K gives:

$$K = \frac{M|\ddot{X}| + F\cos\alpha}{|X|}$$

If the surface area of one face of the moving block (Fig. 1) is A, and the thickness of the rubber layer is t, from equation (3.1.4)

$$G = \frac{K\,t}{2\,A}$$

$$= \frac{(M|\ddot{X}| + F\cos\alpha)t}{2\,A\,|X|}$$

Differentiating w.r.t. $\alpha$ leads to:-

$$\frac{dG}{d\alpha} = -\frac{F\,t\sin\alpha}{2\,A\,|X|} \qquad (3.2.4)$$

From equations (3.1.1) and (3.1.2) it can be shown that:

$$|X| = \frac{F\sin\alpha - \eta F\cos\alpha}{-\eta M\omega^2}$$

Also remembering that $M = K/\omega_n^2$ and $K = \frac{2\,A\,G}{t}$

$$|X| = \frac{-(F\sin\alpha - \eta F\cos\alpha)}{\eta\Omega^2} \times \frac{t}{2AG}$$

Substituting in (3.2.4) and using equation (3.2.3) leads to:-

$$\frac{dG}{d\alpha} = G\eta \quad \text{or} \quad \frac{dG}{G} = \eta\, d\alpha$$

Thus the percentage error in G is $\eta$ times the error in $\alpha$ measured in radians. This is acceptable for the range of values of $\eta$ and $d\alpha$ encountered.

## III. APPARATUS FOR THE DETERMINATION OF DYNAMIC SHEAR PROPERTIES OF VISCOELASTIC MATERIALS

The apparatus necessary for performing the forced oscillation type tests had to be designed with some care to ensure that certain important parameters were well controlled. The first sections of this chapter describe the design philosophy behind the apparatus in addition to a description of the final configuration. The method of testing and calculation of results is also shown in some detail, to reveal the importance of closely controlling the various parameters involved.

The results from the forced oscillation tests showed some slightly unusual trends, and it was decided to check that these were a feature of the material rather than the testing technique, by repeating the tests on similar material using a different testing technique. This "single slug" technique is described and the results obtained compared with those for the forced oscillation method. The final sections of the chapter describe the moulding techniques used for producing all the specimens, including the shear damping beam, used in this study.

### III.1 Apparatus Design

The aluminium specimen is shown in Figure 3 and Plate 3, it consisted of a fixed "U" shaped block, with the moving mass in the centre. The moving block was bonded to the legs of the fixed block by two layers of rubber approximately $^{1}/_{16}$" thick. Aluminium was chosen in order to keep the moving mass and hence inertia forces low, enabling the desired strains to be achieved with the vibrator available. It was also thought that any damping treatment for aircraft use would involve bonding of the rubber to aluminium, thus an aluminium specimen would test the integrity of typical bonds.

Since the material being tested was only $^{1}/_{16}$" thick, the bonding between rubber and metal faces was a serious problem. Any deterioration

in the bond would lead to large errors in the measured quantities and any adhesive used to bond the rubber and aluminium would be of comparable thickness to that of the material under test. The properties of such a specimen would then be some combination of the properties of the rubber and adhesive. Hence it was decided to bond the rubber direct to the aluminium at the vulcanizing stage. A mould was therefore made to press cure the rubber direct in the specimen block. Full details of this procedure are given in Section III.6.

Since the rubber layers were so thin and the rubber to metal contact area large enough for good heat conduction, it was thought that the temperature of the rubber would be very close to the air temperature within the environmental chamber. Thus a mercury in glass thermometer, with its bulb arranged adjacent to the centre of the moving mass, was used to measure the air temperature. Jones et al (61) have demonstrated that the dynamic heating of a rubber shear layer is very small, thus it was thought that embedding thermocouples in the rubber would yield no advantage. Embedded thermocouples could also cause stress concentrations and subsequent errors in the measured properties.

A small fan was used to direct cooling air over the force transducer and some air flowed over the heating coil. However, it was found that temperature gradients within the coil were negligible, the temperature variations on each side of the specimen were undetectable with the thermometer used.

The main frame and base plate of the rig were made from 2" x 1" and 1" thick steel respectively. This relatively massive construction plus a mounting on a substantial concrete base, was used to avoid any significant spurious structural resonances. To test the effectiveness of these precautions, the specimen block was maintained at an acceleration of 1.0g for a range of frequencies, whilst another accelerometer was attached to various parts of the structure with wax. Only two small responses were measured on the support structure and specimen

"U" block. These were less than 2½% of the moving block acceleration and, therefore, thought to be negligible.

It was found during these tests that the measured acceleration of the moving mass was up to 20% less than that of the vibrator head at certain frequencies. It was thought that this was caused by losses in the threaded connectors used between the vibrator head and the moving block of the specimen. Thus it was necessary to mount an accelerometer direct to the moving mass within the heating chamber. An accelerometer was used in conjunction with a charge amplifier, as this had a negligible change in sensitivity for temperatures up to 150°C. It was found that this type of accelerometer was sensitive to side loads at low frequencies. Hence the accelerometer lead was taken out through a ½" diameter hole in the bottom plate to avoid any possibility of the lead touching the sides of the hole, and so putting a side load on the accelerometer and giving rise to spurious signals.

III.2 Apparatus

The apparatus is shown diagrammatically in Fig. 5. Photographs with and without the cooling drum in place are shown in Plates 6 and 7. The aluminium "U" block of the specimen was attached to the steel frame by two screws, clamping the top plate of the environmental chamber against the support frame. The heating chamber consisted of a steel drum wrapped with a 1 kilowatt heating tape, the cooling chamber was similar but wrapped with copper tube and glass-fibre insulation. The specimen was completely enclosed within the environmental chamber with an aluminium connector projecting through the bottom plate to thread onto the force transducer. The force transducer was attached to the vibrator head by an adjustable threaded steel link.

The force transducer used was a piezo-electric device which was cooled by a fan placed behind the main frame of the rig. The force and acceleration signals were fed to a phase matched charge amplifier,

this reduced any phase shift or change in sensitivity due to changes in capacity of the transducers caused by temperature variations. Further amplification of the signals was carried out in another phase matched amplifier to obtain the necessary 100 mV minimum signal levels for correct functioning of the phase meter. A block diagram of the instrumentation used is shown in Fig. 8.

III.3 Method of Testing

The temperature within the heating chamber was set to the desired value by passing a pre-determined current through the heating coil and allowing the temperature to stabilise. (See Fig. 9). The oscillator was then set to 200 Hz. and the output adjusted until the calculated acceleration level of the moving mass for that frequency was shown on the valve voltmeter. Readings of the force transducer output and the phase angle between force and acceleration signals were then noted. This procedure was then repeated for other frequencies up to 1000 Hz. Another test was then made at a different temperature until a range of tests over the temperature range 20°C to 150°C had been completed for each specimen.

Specimen 1 was then tested at sub-ambient temperatures by assembling the test apparatus with the cooling chamber in place. (Plate 7). The Thermos container was then filled with liquid nitrogen. The two tubes emerging from the Thermos lid were of different lengths, one extending to the bottom of the container and connected to a gaseous nitrogen supply, the other just penetrating the lid and connected to the copper tube coil surrounding the cooling chamber. A small over-pressure was applied from the regulator on the gaseous nitrogen supply, forcing cold nitrogen vapour around the copper coil. This was exhausted to atmosphere outside the building. When the temperature within the cooling chamber had stabilised at the desired value, testing was carried out as before.

## III.4 Calculation of Results

### (a) Magnitude of the moving mass above the force sensing element

A simple series of experiments were conducted to obtain the magnitude of the mass of the force transducer above the force sensing piezo-electric crystal. A known mass and small accelerometer were screwed to the top of the force transducer, the bottom of the transducer being attached to the spindle of an electro-magnetic vibrator. The transducer was then excited sinusoidally at several known frequencies and the values of the acceleration and force transmitted to the known mass noted. This was repeated with several different known masses. From simple calculations of force equals mass times acceleration, the average effective mass of the force transducer above the force sensory element was determined. The magnitude of the total moving mass was calculated as follows:

| | Mass in grams |
|---|---|
| Aluminium centre block | 42.0 |
| Aluminium connector and washers | 6.6 |
| Accelerometer | 12.7 |
| Accelerometer screw and washer | 4.5 |
| Effective mass of rubber | 2.0 |
| Effective mass of force transducer | 28.4 |
| | 96.2 gm (0.21 lb) |

### (b) Determination of acceleration values for given strain and frequency

Thickness of rubber in shear = 0.168 cm (0.066")

Let X cm be the peak displacement amplitude of the moving mass.

Consider a shear strain of say 0.001 cm/cm.

Then shear strain = $0.001 = \frac{X}{0.168}$ i.e. $X = 0.000168$

Now peak acceleration $\ddot{X} = -X\omega^2$ where $\omega$ = frequency.

Thus $\ddot{X} = \frac{0.000168 \times 4\pi^2 \times f^2 \times g}{981}$ where f is frequency in Hz.

$= (0.00000676 \times f^2)$ g

See table III.4.1 for further details.

Examples of results and necessary calculations for the determination of $\eta$ and G' are given in tables III.4.2. and III.4.3.

III.5 Single Slug Tests

The results of the above method for obtaining shear modulus show a slightly unusual trend to the normal behaviour of viscoelastic materials. At elevated temperatures the shear modulus falls slightly with increasing frequency, whereas the usual behaviour is a slightly increasing shear modulus with increase of frequency.

To check this trend and the magnitude of previous results for shear modulus, specimens were made up in a different manner as in Fig 8. The material was tested using a resonant method as suggested by Nashif et al (60). As stated in Section II.2 this method has several limitations in that it is difficult to control the applied strain, and frequency variation is limited by a natural upper frequency limit. However of the alternative methods available for comparing results with the forced oscillation method, it was thought that this was the most attractive.

Consider the system shown in Fig. 8.

M = Total moving mass of system including effective mass of "spring".

$K'$ = Real part of complex spring stiffness.

$\eta$ = Loss factor of "spring".

$\omega$ = Base excitation frequency.

H = Height of spring.

S = Cross-sectional area of spring.

Y = Displacement of top of spring.

X = Displacement of bottom of spring.

From the equation of motion of the system the following relation results:

$$\{- M\omega^2 + K'(1 + i\eta)\} Y = K'(1 + i\eta) X$$

Thus $\frac{Y}{X} = \frac{\ddot{Y}}{\ddot{X}} = \frac{1 + i\eta}{1 + i\eta - \frac{M\omega^2}{K'}}$

Thus if A is the amplification factor $= \frac{\ddot{Y}}{\ddot{X}}$ at resonance,

Then $A = \frac{\sqrt{1 + \eta^2}}{\eta}$ and $\eta = \frac{1}{\sqrt{A^2 - 1}}$

If E is the modulus of elasticity of the "spring" material,

$$E = \frac{K'H}{S} = \frac{M\omega^2 H}{S} \quad \text{at resonance.}$$

Hence from measurements of natural frequency and resonant amplification factor, the real part of the elastic modulus and loss factor of the material can be determined. Since the Poisson's Ratio of the rubber is 0.5, the results for elastic modulus were factored by a value of $1/3$ for direct comparison with the shear results as suggested in (62). Elementary spring theory suggests that one third of the mass of the rubber should be added to the total of tuning mass and accelerometer mass and this is incorporated in the values of moving mass in Table III.5.1. Nashif (60) shows the importance of selecting the correct aspect ratio for the specimen to obtain either true Young's Modulus or true Bulk Modulus. A specimen of aspect ratio 1 (height/diameter) was chosen to give results of Young's Modulus (K) assuming a state of plane stress to exist in the specimen. If the height/diameter ratio were small, the assumption of plane strain is more accurate, and Poisson's Ratio effects have to be taken into account leading to a determination of the Bulk Modulus of the material.

During testing resonance was detected both by observing a $90^{\circ}$ phase shift between the two acceleration signals and obtaining the maximum tuning mass acceleration for a given base excitation. The level of base excitation was varied to provide a constant strain on the material consistent with obtaining reasonable signal levels. As stated in II.2 control of strain is difficult, the test values being shown in Table III.5.1.

The results for magnitude of shear modulus agree well with the previous shear tests (Fig. 9), but the frequency limitation of the system set by the minimum practical tuning mass on top of the rubber slug, as

mentioned in II.2, prevented good confirmation of the unusual trend shown by the previous shear test results. Several other writers have observed this trend (63, 64, 65), and the forced oscillation type of shear test apparatus has given results in good agreement with known material properties when P.V.C. type materials were tested (55). Hence it was concluded that this trend is a feature of the material under test.

The results for extensional loss factor are compared with those for shear loss factor in Fig. 10. As expected the values are of similar magnitude, the relatively greater scatter of the extensional results was thought to be due to the different strains applied at the various frequencies (see Table III.5.1) by the resonance method.

## III.6. Moulding of Specimens

### III.6.1 Shear Test Specimens

Details of the mould assembly are shown in Fig. 11. The end and filler blocks were permanently bolted to the base plate. The specimen "U" block was then located on four dowel pins and bolted firmly to the base. The cap screws on either side of the end block were then done up finger tight to prevent splaying of the legs of the specimen "U" block when the rubber was under pressure.

Two samples of rubber were weighed out 15-20% over the requirement for completely filling the spaces between fixed and moving specimen blocks. The two pieces of rubber were rolled to approximately 2" long and .080" thick before being placed either side of the bottom of the mould. The moving block was then placed on to it's two locating pins and pushed down into the mould until it contacted the rubber strips. The whole assembly with cover plate was then placed in an hydraulic press with platens heated to initial curing temperature. As the moving block was pushed onto its locating pins, the rubber was squeezed up from the bottom of the mould to completely fill the available space before

vulcanising. Pressure was maintained in the press for 20 mins. to allow for complete vulcanising and any excess rubber to squeeze over the top edges of the "U" block and into the run off channels.

Before moulding could take place all surfaces except those to be bonded had to be coated with a release agent of 2% Aquarex solution. The surfaces to be bonded were treated with Midland Silicones type MS 2402 primer after first being cleaned in petroleum ether.

The initial curing was done by the heated press platens as above, whilst the post-curing was carried out in a standard heat treatment oven with thermostatic control. For this curing the completed specimen was unbolted from the base plate and placed in the oven by itself.

III.6.2 Single Slug Specimen

Details of the single slug specimen are shown in Fig. 8. This shows the completed specimen with accelerometers attached and a tuning mass in place, the mould and mould base are also shown, in Plate 4.

All surfaces not to be bonded to the rubber were treated with a 2% Aquarex solution in alcohol. The mould was assembled by bolting the cylindrical mould body to the base plate with six cap screws and screwing the specimen top washer to the mould cap. A quantity of rubber was then weighed out to 15-20% over the requirement for filling the mould. This was prepared by rolling into a thick sheet about 6 mm ($\frac{1}{4}$") thick and cutting discs from this with a coring tool. Discs were then placed into the mould, after the surfaces to be bonded had been primed as before, until the top of the last disc was about 3 mm ($\frac{1}{8}$") below the top of the mould body. The mould cap complete with attached specimen top washer was then inserted into the mould body and the entire assembly placed between the heated platens of an hydraulic press. The press was then closed and opened slightly several times, to cause the rubber to flow and expel any air within the mould. Finally the press was closed firmly and the excess rubber allowed to extrude through the radial run-off channels in the top of the mould body. Pressure was maintained for one hour to allow complete vulcanising at the initial curing temperature of

140°C. The mould was then cooled in cold water and the specimen removed. Post curing was carried out as before but for 24 hours in total, gradually increasing the temperature from 100°C to 200°C in five equal increments. This was necessary owing to the greater mass and thickness of rubber used, and to avoid any significant temperature gradients within the specimen. If such temperature gradients are allowed to develop it is possible for pockets of uncured material to be surrounded by areas of material which are already cured. In this case the chemical by-products of vulcanization which it is desired to drive off by post-curing, will not be able to diffuse through the cured material to the outside. This leads to reversion of the uncured pockets eventually causing voids within the specimen. This problem did arise when it was attempted to post-cure the single slug specimens in the same manner as the shear test specimens, i.e. 8 hours at 200°C, hence the development of a longer curing technique for such specimens.

III.6.3 Beam Specimens

Details of the beam mould and samples of beams moulded from it are shown in Plates 5 and 6. The mould consisted of a base plate made from 6 mm ($\frac{1}{4}$") thick duraluminium, mould plates of varying thickness (1.22 mm to 2.57 mm, .048" to .104") and a cover plate of 6 mm ($\frac{1}{4}$") thick duraluminium. The base plate had dowel pins inserted at either end to locate the mould plate and had several more inserted in the mould region to space the several lower plates of the shear damping beam. These pins are discernable in Plate 5. A second base plate without these spacing pins but with the two mould plate locating pins was also prepared to enable continuous sandwich beams to be moulded. The mould plate had corresponding holes at each end for location on the base plate and had a 50 mm (2") wide and 454 mm (18") long rectangular hole cut in its centre. Thus when assembled to the base plate a recess the thickness of the mould plate deep was created, with sufficient space for two 25 mm (1")

wide sandwich beams to lay side by side in it.

The continuous upper and discontinuous lower constraining plates of .43 mm (.017") and .86 mm (.034") were prepared by guillotining from sheet and then made perfectly flat by pressing. The surfaces of the plates were scoured with carborundum paper taking care not to touch the scoured surface to avoid contamination with grease. The plates were carefully wahed in petroleum ether prior to coating with Midland Silicones type MS 2402 primer. These precautions were necessary to ensure good bond strength after moulding to prevent the beams delaminating when subjected to flexure. All surfaces of the mould were treated with Aquarex release agent as before.

Moulding was commenced by weighing out a sample of rubber to 10% over the required weight and rolling this in a mill until a length of 454 mm (18") by 50 mm (2") wide approximately, was achieved. This desired size using a fixed amount of rubber was achieved by varying the spacing of the rolls. The ready primed discontinuous plates were then laid face up in the bottom of the mould. The rubber sheet having been placed on a sheet of silicone coated paper was then inverted and placed on top of the lower plates in the mould. The silicone paper was removed by doubling it right back and gradually pulling off. The continuous upper plates were then pressed into place and any slight excess of rubber around the edges removed with a razor blade. The mould assembly was then placed between the heated platens of the hydraulic press and the press closed and opened several times as before to expel unwanted air. The reason for using thick base and top plates for the mould was to retard heat flow to the rubber thus ensuring the rubber did not solidify before expelling all the unwanted air. Finally pressure was maintained for 20 minutes keeping the temperature at 130$^{o}$C to allow complete vulcanization to occur within the mould. Upon completion of the initial curing the mould was removed, cooled in cold water, and the two beams removed side by side. The excess rubber which had extruded into a very

thin sheet around the beams was removed and the two beams separated using a razor blade. Post curing took place in a thermostatically controlled oven for 8 hours at 200°C. To further improve bond strength some beams were post-cured as for the single slug specimen i.e. 24 hours at 100 to 200°C. This did improve the bond slightly and was used on all beams intended for test on the integral plate. Continuous beams were moulded in the same way except that the second base plate was used and continuous constraining plates inserted in the bottom of the mould.

III.6.4 Preparation of the Rubber

The rubber is stored in a deep freeze without any catalyst added. Thus it is necessary to "work" the rubber to make it pliable and able to flow in the mould, and to mix in the small amount of catalyst required. The only practical way of doing this is to use a powered two roll mixing or compounding mill. The rollers are first cleaned by thorough washing in petroleum ether to prevent the rubber sticking. After some experiment it was found that the optimum gear ratio between the two rolls was approximately 1.1 to 1 and not 1 to 1 as at first expected. This allowed the rubber to come off the same roll each time instead of sticking to first one roll then the other. The rubber was worked until it was pliable and the catalyst dissolved in a small amount of silicone oil before rubbing this in on the rolls with a spatula. In the case of those specimens requiring additional filler, this was added at this stage by pouring measured amounts of finely divided silica powder in between the two rolls. Any spillage was collected in an aluminium tray beneath for return to the rolls. After some 15 to 20 minutes of working in this manner the rubber was ready for use.

## IV. RESULTS FROM SHEAR TEST APPARATUS

Many results were obtained from the shear test apparatus for various materials modified both chemically and by differences in the mixing process. In order to be able to put these results into some perspective, a brief description of the basic micro-structural damping mechanisms is given, followed by a discussion of the results for the various materials with attempts to describe the trends observed experimentally, in terms of these damping mechanisms. The discussion is divided into various sections, each section dealing with the variation of one of the test variables and its effect on the loss factor and dynamic shear modulus of the material under test.

In order to try and condense the information obtained at various frequencies and temperatures for the most promising specimen, an attempt was made to collapse this data onto a master curve using the method of reduced variables. This work is also described in this chapter.

### IV.1 Comparison of Materials

Before comparing the results of tests on the different materials, it is necessary to have an understanding of the damping mechanisms within the micro-structure of the material. What follows is a very brief description of the micro-mechanism intended only to give the reader an appreciation of the damping mechanisms to relate to the results. A fuller treatment of this subject can be found in (66) and (67).

It is thought that there are two main damping mechanisms within the material, filler interaction and viscous damping of the raw polymer.

The basic structure of the material is the silicone chain molecule. These are coiled up and mixed with each other in the unstrained state. As the material is strained the long chain molecules uncoil and slide over each other. Filler interaction is the blocking of movement of the chain molecules by the filler particles. When filler is introduced into the rubber it takes up vacant positions in the structure and provides

obstacles for the molecules to slide around. There is also thought to be some interaction between the filler particles themselves as they move over each other causing shearing and fracturing of the particles. Of the two materials tested, the fluoro-silicone (Specimen 1, Appendix 1) had the greater filler content, as the basic polymer was supplied containing 25% of unspecified fillers to which was added a further 20% of Aerosil filler. The methyl-vinyl rubber (Specimen 4) was supplied as a raw polymer to which was added 20% of Aerosil filler. Thus the fluoro-silicone contained over twice as much filler as the methyl-vinyl rubber.

The viscous damping of the raw polymer is caused by interactions between the surfaces of the molecule chains. These are basically strings of silicone atoms with various chemical groups attached to the unsatisfied silicone bonds. For fluoro-silicone rubber every silicone bond is satisfied by attachment to either another silicone atom or to a stable fluorine group ($CF_3$). These groups are small and since they are stable the outer surfaces of the chain molecules are smooth and relatively inert. Thus interactions between the surfaces of chains are small. Hence in this material the viscous effect is small. However, since the transition temperature of fluoro-silicone is $-70^{\circ}C$, the material was working near to its best possible range and some viscous action would have taken place. The methyl-vinyl rubber had large complicated methyl and vinyl groups attached to the unsatisfied silicone bonds. These groups themselves have unsatisfied bonds, thus interaction between molecules is high, with strong dipole type interactions. The methyl-vinyl groups are also physically large, thus the surfaces of the chain molecules are rough, causing high internal friction as with the filler. However, since the transition temperature of this material is $-120^{\circ}C$, the material was working well outside its best temperature range, and viscous effects are reduced in proportion to the difference between working and transition temperatures.

Reference to Figs. 12 and 13 shows that damping for fluoro-silicone (Specimen 1) is better over the whole frequency range, than for methyl-vinyl rubber (Specimen 4). It was thought that the doubled amount of filler in the fluoro-silicone was causing enough interaction to mask any lack of viscous effects. The overall increase in loss factor with frequency (Fig. 12) was thought to be due to the greater energy input at high frequencies causing a larger proportion of particle shearing and fracturing than at low frequencies. Hence a larger proportion of the energy input was dissipated at High frequencies. The very low damping of methyl-vinyl rubber (Specimen 4) at low frequencies (Fig. 13) was thought to be due to the lack of filler interaction at low energy inputs, the viscous effects also being small due to operation at temperatures well above the transition temperature. Cross plots to show the variation of damping with temperature (Figs. 14 and 15) demonstrate the small dependency on temperature of these materials.

The variation of shear modulus with temperature for the two materials is as expected for visco-elastic materials (Figs. 16 and 17), the modulus gradually falling with increasing temperature. The fall-off is more noticeable for the fluoro-silicone (Fig. 17) as this was nearer to its transition temperature than the methyl-vinyl rubber and in its transition region. The reduction in modulus for methyl-vinyl rubber (Fig. 16) is so small over the temperature range considered, that the material can be regarded as being completely in the "rubbery" region at these temperatures. This also explains the lower loss factor for methyl-vinyl rubber compared with the fluoro-silicone operating in the transition region (see Fig. 2). The reduction in stiffness with increasing frequency (Figs. 18 and 19) was thought to be due to the strain softening phenomenon which occurs with these materials. As the test frequency is increased, the polymer has less time between each strain peak to recover and hence becomes softer. This effect was greatest for the methyl-vinyl rubber (Fig. 19) as this relied more on the polymer than the filler for its stiffness, compared with fluoro-



→ for 6.2 →

silicone rubber which contained a higher proportion of filler.

It was concluded from these tests that the fluoro-silicone rubber had the best performance and all subsequent testing was based on this material.

IV.2 Strain Variation

Initial tests with fluoro-silicone rubber were run at strain levels between .0004 and .001. Results of these tests showed no significant variation in the dynamic shear properties with varying shear strain. It was concluded that these tests were conducted at strain levels below that of strain dependency of the dynamic shear properties. These results appear in Figs. 20 to 27 inclusive.

Further tests were conducted at strain levels of .003, .005, .01, Overall results for these tests are shown in Figs. 28, 29 and 30. The results show the strain softening phenomenon as described previously. Comparison of Figs. 28 and 29 shows an overall drop in modulus G' for increasing strain. The variation of G' with temperature (Figs. 32, 33 and 31) at these higher strain levels is as before and typical of visco-elastic behaviour as in Fig. 2. Complete details of these results are contained in Figs. 31 to 42 inclusive.

Values of loss factors were higher for higher strain levels (Fig. 30). This was thought to be due to the material being capable of dissipating more energy by filler interaction and bond disintegration at the higher strain levels. The increase of damping with increasing frequency was also thought to be due to these mechanisms as described in Section IV.1. A typical result is shown in Fig. 37. Damping was nearly constant with changes in temperature for a given frequency and strain level. A typical result is shown in Fig. 38 demonstrating the suitability of this material for use in damping treatments over this temperature range.

IV.3 Filler Variation

To determine the sensitivity of the dynamic shear properties to

material composition, two further fluoro-silicone specimens were prepared containing 3% (Specimen 2) and 6% (Specimen 3) by weight extra Aerosil filler. Overall results of tests on these specimens are shown in Figs. 43 and 44. As was expected, the addition of filler stiffened the rubber. Fig. 43 shows the slightly higher overall shear modulus for 6% filler addition over that for 3% addition. The results for modulus against temperature (Fig. 43) are as before and typical of visco-elastic behaviour (Fig. 2). Softening with increasing frequency is reduced compared with the plain rubber. This was thought to be due to the volume of polymer subject to strain softening being reduced by the addition of the extra filler.

The effect on damping is seen in Fig. 44, the overall result is a reduction in loss factor over the range considered, in direct proportion to the amount of extra filler added. It was thought that the additions increased the filler content over the optimum value for maximum damping, leaving insufficient polymer for the filler to interact with. This may also explain the low damping measured at the 200 Hz frequency. The variation of loss factor with temperature for a given frequency is small as before and the increase in the loss factor with increasing frequency is as before, compare Figs. 12 and 44. More detailed results for the effect of filler variation as shown in Figs. 45 to 52 inclusive.

IV.4 Low Temperature Tests

The results for shear modulus variation with temperature over the range 0 to -60°C are shown in Figs. 53 and 54. The stiffening with decreasing temperature was as expected for a visco-elastic material (Fig. 53) and the levelling off of the curves at the lowest temperature was caused by the proximity of the transition temperature for this material at -68°C. The strain softening phenomenon was less noticeable due to the material being more in its "glassy" state at the very low temperatures (Fig. 54).

Damping was well maintained over the temperature range to -60°C

(Fig. 55) with the same general increase in the loss factors with increasing frequency (Fig. 56). The overall levels of damping were higher than previous tests, and were thought to be due to the increased viscous damping taking place at these low temperatures close to the transition temperature of the material.

IV.5 The Method of Reduced Variables

An attempt was made to use the Ferry-Fitzgerald method of combining the data at various temperatures into one master curve detailing the damping properties at a single reference temperature covering an extended frequency range. This semi-empirical method was first described by Ferry et al in Ref. 68.

The method depends on the fact that it is possible to find the damping properties of most visco-elastic materials occurring at one of several "corresponding states". This may be stated algebraically as follows:-

$$\eta_{w,T} = \eta(w.A),\ T_o$$

where w is the test frequency

T is the test temperature

$T_o$ is the reference temperature

A is the ratio of relaxation times at temperatures $T_o$, T.

That is the loss factor at frequency w and temperature T is the same as the loss factor at frequency w times A and temperature $T_o$, since the latter is the corresponding state to the state at frequency w and temperature T. The temperature dependency of A represents the basic effect of temperature on the visco-elastic properties. Thus it is necessary to find the values of A at all the test temperatures. For values of T above the reference temperature $T_o$, the value of A is less than unity. Hence it can be seen that it is possible to extend the frequency range of the measured data down to lower frequencies than the lowest test frequency. It is also possible to confirm data higher up the frequency range by comparing it with the reduced data from other tests at different temperatures.

If logarithmic plots of the temperature corrected real parts of the shear modulus ($G' T/T_o$) against w are made for each constant temperature test, a family of similar shaped curves will result (Fig. 57). For the method of reduced variables to be accurate, these curves should be nearly parallel to each other. Then the change in the logarithm of A between each test temperature is defined as the horizontal distance between two corresponding curves. Let this be defined as $\Delta \log A$. This is also shown in Fig. 57. Obviously at temperature $T_o$, $\Delta \log A$ is zero and A is equal to unity. By successive additions of $\Delta \log A$ it is possible to obtain log A and therefore A at all the test temperatures. A plot of log A against temperature is then made to ensure a smooth curve results. This is shown in Fig. 58. Values of log A are then taken from this curve and fitted into what is known as the W.L.F. equation (see Ferry, Ref. 66 for complete details) which is defined as:-

$$\log A = -C_1 (T-T_o)/(C_2 + (T-T_o))$$

If a plot of $(T-T_o)/\log A$ versus $(T-T_o)$ is made, the result should be approximately a straight line with slope s and intercept i. Then $C_1 = 1/s$ and $C_2 = i/s$.

These values of $C_1$ and $C_2$ are replaced in the W.L.F. equation and values of log A calculated from this. The operation has the effect of smoothing the values of A before using these to predict the properties at some "corresponding state". Alternatively, the W.L.F. equation may be stated as follows:-

$$\log A = \frac{C_1 (T - T_o)}{T - T_{oo}}$$

For a wide range of materials is has been found that (69) this gives a linear plot for $T_{oo}$ as a fixed temperature. $T_{oo}$ is usually found to be about $50^oK$ below the glass to rubber transition temperature. The constants $C_1$ = slope of line and $C_2 = T_o - T_{oo}$ can then be found and values of A calculated as above. A third alternative is suggested by Snowden (70) in his book as a particular version of the W.L.F. equation

which seems to apply to a wide range of materials. This is really a modification of the above statement of the W.L.F. equation. It states that $\log A = \frac{-8.86\ (T-T_1)}{101.6 + (T - T_1)}$ where $T_1$ = glass to rubber transition temperature $T_T + (50 \pm 5)^\circ K$. Thus for fluoro-silicone rubber $T_1$ is approximately $250^\circ K$.

Values of log A were calculated using all three of these methods. Details of these calculations are shown in Table IV.5.1. It can be seen that there is some considerable variation in the values of A obtained by the three methods, but the smoothed measured values and those calculated from Snowden's equation seem the most consistent. Thus an average of these latter values was taken and used to obtain reduced data of the loss factor $\eta$. These results are shown in Fig. 59 together with measured low frequency results at the reference temperature of $21^\circ C$. It can be seen that there is considerable scatter in the reduced data and this method overestimates the values of loss factor, although the increase of loss factor with increasing frequency is confirmed quite well. The overestimates of loss factor are caused by values of A being too large. In the W.L.F. equation this means that $T_{oo}$ is too small, implying that perhaps T is only say $10^\circ K$ below the glass to rubber transition temperature $T_T$, instead of $50^\circ K$ for these materials, or that in Snowden's equation $T_1$ is too small, i.e. $T_1$ is more than $50^\circ K$ above $T_T$. These two statements are really the same implying that the empirical results found to date do not really hold for these types of material. Also it was stated previously that the basic curves for measuring values of $\Delta \log A$ from, should be parallel. Reference to Fig. 57 shows that for these materials this condition is not entirely true, hence it is not surprising to see the resultant scatter and over-estimation of the reduced data. It was concluded that since these materials contained a high proportion of filler, this was causing a deviation from true visco-elastic behaviour and that the assumption of corresponding states was invalid to some extent.

## IV.6 Conclusions

The fluorinated rubber (Specimen 1) maintained a high loss factor throughout the frequency and temperature range considered. There was only a slight drop in the value of loss factor as the temperature was increased to the maximum of 150°C. The methyl-vinyl rubber (Specimen 4) was operating well above its transition temperature in this application and has been shown to be inferior in all aspects of performance to the fluoro-silicone rubber.

The different values of strain applied to the fluorinated rubber shown that the damping performance is improved with higher strains. Tests have shown that these strains are of the same order as that encountered in practical damping mechanisms.

The variation in filler content (Specimens 2 and 3) shows a useful way of stiffening the material at the expense of a small drop in the damping performance. It was thought that the optimum filler content for maximum damping capacity may be slightly less than that contained in Specimen 1.

The results for elastic shear modulus in the shear tests agree within 10% of the results obtained from the single slug test. This was thought to be a satisfactory confirmation of the technique of shear testing described in Section II.3.

The materials as tested are those which have to be hot moulded and cured in situ. These are only suitable for those applications where the damping mechanism can be made and attached separately to the main structure. However, a modified material is available with cold curing properties which would be suitable for incorporating in a structure at the manufacturing stage, e.g. visco-elastic layers in the joints of a built-up structure.

It was concluded that fluorinated silicone rubbers are entirely suitable for use as damping treatments in the temperature range -60°C to +150°C and over the range of frequencies 200 to 1000 Hz.

## V. EXPERIMENTS ON THE INTEGRAL PANEL

An integral panel of suitable size was available from previous structural response tests as a specimen for evaluating the effects of the shear damping beams. The first tests undertaken were with the panel mounted in an acoustic siren facility. The object of these tests was to establish the shear strain levels in the damping material when the panel was subjected to a typical level of random noise corresponding to jet noise excitation or similar. When these strain levels had been obtained they were used to confirm the choice of strain test levels in the shear test apparatus described previously.

Following these tests the panel was removed and re-mounted in a convenient manner for quantitative assessments of the damping treatments. This necessitated using a single point excitation technique with a force transducer interposed between vibrator and panel. The panel was carefully suspended by thin cables to minimise energy flow to the support frames. Measurements of mode shape for both the undamped and damped panel were undertaken to observe any changes in modal characteristics and investigate whether the usual assumptions in damping calculations, that the mode shapes remain substantially unaltered by the damping treatment, were justified or not.

Two techniques were used for assessing the damping effects, the first by measurements of energy inputs, and the second by establishing the frequency response curves for constant vibrator force excitation. In addition several tests on full scale structures showing strain-gauge output reductions for the damped specimen are shown, which indicate the practicability of the damping treatment in reducing dynamic stresses due to resonant type response.

### V.1 Stringer Deflexion Tests

Preliminary checks using an accelerometer showed that the shear strains experienced by the viscoelastic core of a shear damping beam applied to a vibrating stiffened panel were of the order .001. Hence

the material testing described previously was based on strains of this magnitude. However, after the shear strain dependency of the damping materials had been determined it was thought desirable to measure the shear strains experienced by the shear damping beam core more accurately, to determine whether or not these strains would materially affect the damping material's properties. In order to calculate these shear strains it was necessary to know the horizontal displacement of the free edges of the stringers at the points of attachment of the shear damping beam. It was decided to use non-contacting cathode type displacement probes for this purpose, as the previous checks with an accelerometer had shown the inaccuracy of this method, due to the high sideways accelerations imposed on the accelerometers attached to a stringer which was vibrating in a rotational as well as transverse manner.

V.I.1 Panel Mounting Configurations

Since it was desired to simulate a panel incorporated in a real structure, the single test panel was constrained on each of its four edges by steel and aluminium clamps. On the edges parallel to the stringers a 50 mm x 50 mm (2" x 2") square section steel bar was bolted to the end stringer, the skin at these ends being clamped between the steel bar and a piece of 50 mm x 50 mm (2" x 2") square section aluminium bar using 7 mm (5/16") diameter bolts. On the edges perpendicular to the stringers the skin was clamped between a piece of 50 mm x 50 mm (2" x 2") aluminium bar, machined to be a close fit over the stringers, and pieces of 50 mm x 50 mm (2" x 2") steel angle. The clamping bars were joined to each other at the corners by bolts to produce a sturdy clamping frame. A layer of L.D. 400 unconstrained damping material which had been applied to the skin bays of the panel in previous experiments was left attached to the skin. It was thought that this would adequately simulate the additional damping effect of a real panel attached around its edges to sub-structure with rivets or bolts. Previous attempts by Cicci (31) to measure the damping of the panel with this unconstrained layer by using vector plots of the response to acoustic

excitation, had been confused by the multi-modal response of the system, but had shown the overall value of the loss factor to be of the order 0.01. This is closer to the values observed by other investigators for stiffened panels incorporated in real structures, than the measured loss factor of approximately 0.001 for the bare panel. Hence it was thought justifiable to leave the unconstrained layer in place for all future testing.

The panel system complete with edge constraints was suspended in a close fitting wooden frame by two pieces of steel shim 10 mm ($\frac{3}{8}$") wide at each of the upper corners of the panel. This whole assembly was then mounted in the wall of an acoustic tunnel and held in place by rubber bungee cord. The panel was arranged so that the stringers were vertical and the skin was subject to a horizontal propagation of plane acoustic waves impinging at grazing incidence. The sound pressure level of the impinging acoustic waves was monitored by a 12.5 mm ($\frac{1}{2}$") B. Bruel and Kjaer condenser microphone mounted in the centre of the tunnel and 150 mm (6") from the panel centre.

V.1.2 Measuring Probes

Initially a Bruel and Kjaer capacitance type displacement probe was used, mounted on an aluminium block, for measuring stringer deflexions. The block was free to slide along a 30 mm diameter (1.18") steel bar which was in turn attached to the back of the clamping frame. This system then enabled the probe to be moved along from one stringer position to the next, the sliding aluminium block being clamped to the round bar by means of two grub-screws. This system was not satisfactory as despite the low mass of the probe assembly, the round bar vibrated considerably at certain test frequencies. The system was modified by using a specially developed right-angled Wayne-Kerr capacitance probe and a much more massive support rail. This support rail was machined from a solid piece of 50 mm x 50 mm (2" x 2") section steel bar with slots for clamping bolts and special "T" section nuts running along its length. A slider of

similar section steel was clamped to this rail by two cap screws. The "T" section nuts then enabled the slider to be freed without disturbing the shear damping beam beneath the assembly with any spanner etc. The special right-angled probe was mounted in the slider with a threaded adaptor to enable the distance of the probe tip away from the skin line to be adjusted, thus enabling measurements of the stringer tip deflexion or the deflexion of any other points further down the stringer, to be measured. The threaded adapter was locked with a grub screw for absolute security under the vibration conditions to be encountered. A view of the panel with this probe mounting in place is shown in Plate 11.
With this more massive probe structure no significant structural resonances were encountered at the test frequencies. Checks made with a small (2 gram) accelerometer attached to various parts of the structure showed accelerations of less than 2% of that of the moving stringer. Some difficulty was encountered when the probe support rail was bolted to the panel edge stiffeners. During the machining operations some of the built in stresses of the steel bar were relieved resulting in distortion of the mounting feet. These were made flat again by grinding two reference surfaces in the upper surface of the rail, inverting the rail and mounting it on parallels, before grinding the feet level again. The rail was then carefully offered up to the panel system and bolted to the edge stiffeners taking care to tighten the four mounting screws evenly.
In this way it was assured that no distortion of the integrally stiffened panel took place.

V.I.3 Experimental Testing and Results

Discrete tone excitation was used at frequencies previously observed to be the major resonance frequencies of the treated panel. Narrow band filtering was used in order to eliminate any harmonics and any possibility of multi-modal response. The response of the panel was monitored with 3 semi-conductor strain gauges mounted in the centre of each of the left-hand skin bays (viewed from the rear). It was necessary

to use strain gauges of this type as with the limited excitation pressure available, the strains induced in the panel were small. An excitation level of 140 db OASPL was selected as typical of the order of level which these panels are expected to withstand. The frequency of testing was varied slightly from the previously obtained values until a maximum response was recorded on the strain-gauges. The displacement at that particular stringer position was then recorded before reducing the noise level and adjusting the probe to the next stringer position. The excitation level was then brought back up to 140 db OASPL and the displacement of that stringer position noted and so on until all the required deflexions had been measured. The convention for stringer numbering is shown in Fig. 72. The results of stringer tip deflexion and resulting shear strains in the core of the shear damping beam for the first three modes are given in Table V.1.1. The response in the higher modes was so significantly reduced by the damping treatment that no clear indications of resonance could be obtained, thus it was concluded that vibration in the first three modes would give results of maximum shear strain to be experienced by the viscoelastic core of a shear damping beam. It can be seen from Table V.1.1. that the maximum shear strain observed was about 1%, thus this value was chosen as the maximum to be used in the material tests described previously in Chapter III.

## V.2 Single Point Excitation Tests

### V.2.1 Test Panel Apparatus

During the stringer deflexion tests mentioned in the previous Section it was found very difficult to maintain a constant level of excitation in the acoustic tunnel at different frequencies. This was found to be due to inherent resonances in the tunnel system itself. These resonances combined with those of the panel under test caused some interaction and it was found that the sound pressure level could vary by as much as 4 db when the excitation oscillator drifted slightly

off frequency. Also because of the installation used it was impossible to gain access to the skin side of the panel during testing. Thus any mode shape determination would have to have been done using strain gauges previously applied to the panel. This had the great disadvantage that if a mode shape was in question, it was impossible to clarify it by taking further readings, as with a roving accelerometer. Since it was desired to take accurate measurements of response reduction after application of the damping treatment and observe any mode shape deformation resulting from such an application, it was decided to abandon the acoustic test method and revert to a method using an electro-dynamic vibrator as an exciter with a force gauge interposed between the panel and vibrator, for accurate control of excitation level. By careful design of the suspension of the panel it was hoped to repeat accurately those mode shapes observed in the acoustic test facility. Once this had been achieved, since access to both sides of the panel was easy, accurate observations of mode shape etc. could be made.

Views of the single point excitation apparatus are shown in Plates 7 to 11 inclusive. The complete panel, with attached edge constraints as used in the stringer deflexion tests, was suspended by two steel cables from a large steel girder frame. This is best shown in Plate 7. Suspension by steel cables was used to eliminate any significant energy flow from the panel system into the support frame. In this way no additional damping could be added to the panel system by the attachment to its supporting frame. Since it was already known from the stringer deflexion tests that there was no significant movement of the panel edges, it was concluded that any damping measurements would then give a true indication of the additional damping caused by the artificial treatment applied to the panel. In addition to the two suspension cables two further cables were connected between the lower corners of the panel and the large support frame. These are also shown in Plate 7. The ends of these cables were attached to eye-bolts which in turn ran

through holes in the lower frame member. For ordinary testing these eye-bolts were slackened off to allow the panel to hang freely from its susupension. However, when work was done on the panel, such as the application or removal of a damping beam, these cables were tightened up by means of the eye-bolts to hold the panel steady and prevent damage to the vibrator armature and suspension system.

The upper eye-bolts were used to adjust the height of the suspended panel so that the point of attachment of the vibrator and vibrator spindle were exactly in line. Adjustment of each eye-bolt was also made in turn until the panel hung with its stringers truly vertical. Plate 9 shows the arrangement of the attachment of the suspension wires to the upper corners of the panel system. The slotted right-angle bracket was used so that the suspension wires could be arranged exactly over the centre of gravity of the panel with various probes attached to the back of the panel. The range of adjustment was sufficient so that the panel could be hung vertically in the plane of the stringers with the capacitance displacement probe for stringer deflexion attached, or with the panel bare.

The electro-dynamic vibrator was mounted on a separate stand in the shape of a large right-angle bracket. The vibrator itself was bolted to a flat steel plate which had two slots cut in it top and bottom. This was bolted to the upright part of the right-angle stand enabling a small height adjustment to be made to the vibrator spindle. This stand can be seen in Plate 10. The line up between the panel attachment point and the vibrator spindle was made by first adjusting the heights of the panel and vibrator until the vibrator spindle could be seen concentric with the mounting hole in the panel. The vibrator frame was then moved away from the panel to allow the force gauge to be attached to the panel by a short screw. The vibrator system was then offered up to the force gauge using mallets to move the

vibrator frame across the floor. When the line up had been carefully checked for truth with squares, the vibrator frame was fixed to the floor by weighting with shot bags and steel bars. Since the force gauge was connected to the vibrator with an adjustable threaded link as on the previous material tests, it was possible to depress the vibrator spindle and connect up the link without any further movement of the vibrator frame. Thus it was possible to maintain the careful line up of the panel and vibrator system throughout the series of tests despite the necessity of occasionally removing the force gauge for calibration checks. Plate 7 shows the vibrator side of the panel and the force gauge can just be determined adjacent to the panel.

V.2.2 Mode Shape Determination

Although the panel had been adequately strain gauged with foil type resistance strain gauges, it was not possible to use these for even basic mode shape determination as the resulting signals were of too low a magnitude to be discernible from the electronic noise in the amplifiers used. Three semi-conductor type strain gauges were applied to critical areas of the panel however for control purposes. These gauges with their much greater sensitivity, enabled reasonable signals to be derived and were used to compare response with that in the acoustic tunnel. By comparing the signals obtained from these semi-conductor gauges in acoustic tunnel tests and single point excitation tests, it was found that a force input of approximately 32n (1.5 lbf) resulted in similar levels of response to those recorded when the panel was subjected to an acoustic pressure field of 140 db OASPL at the resonant frequencies of major interest (300-400 Hz).

Mode shapes were determined by attaching a small (2 gm) B & K accelerometer to various parts of the structure with wax once the correct excitation level had been set. In all cases the excitation level was adjusted to give similar levels of response to those observed using acoustic excitation with an overall sound pressure level of 140 db.

Plate 8 shows the panel test configuration for these tests with the unconstrained layer of L.D. 400 material in between the stringers in each skin bay. A Muirhead decade oscillator was used to provide the excitation signal, the frequency was varied around the values obtained in the acoustic tests until maximum response was obtained on the semi-conductor strain gauges. The roving accelerometer was then placed in the middle of each skin bay in turn on the centre line of the skin side of the panel and the resulting accelerations recorded.

V.2.3 Undamped Mode Shapes

The results of mode shape for the first five modes observed in this manner are shown in Fig. 60. In cases where the mode shape was doubtful the accelerometer was applied to several extra positions to clarify the result, see for example the fifth mode at 825 Hz. The mode shape in the direction parallel to the stringers in all the tests was a single half wave, the higher order modes with more than one half-wave in this direction were beyond the frequency range of interest (viz 200-1000 Hz). The results of these tests for basic mode shapes can be compared with those obtained in the acoustic tests (Fig. 61). In general the frequencies are slightly lower, caused it is thought by the slight added mass of the connecting link, force gauge and vibrator armature attached between the panel and the vibrator. This added mass amounted to 4.7% of the panel mass, thus the expected frequency shift downwards was 3%. All the modes were slightly distorted by the single point of application of the excitation force, the worst effect being in mode 3. The position of the point of application of the excitation force was chosen as a compromise to ensure reasonable excitation in all the first five modes. However, for mode 3, if the mode shape were perfectly symmetrical it can be seen that the vibrator attachment point would be at a nodal position, thus it was hardly surprising to observe considerable distortion in this particular mode. Referring to Fig. 61 it

can be seen that all the modes are slightly asymmetrical, the nodes being displaced to the left. This effect can also be seen in the mode shapes obtained in Fig. 60. It was thought that this was due to some slight manufacturing inaccuracy in the panel. The fact that this effect was reproduced in the single point excitation tests and the generally good agreement with the previous acoustic tests, was thought to justify any further quantitative measurements on the panel using single point excitation. It was concluded that by careful control of the edge constraints and excitation force, it would be possible to adequately simulate acoustic excitation using the single point technique.

The roving accelerometer was also applied to twelve positions on each stringer tip to confirm the expected motions of these points. The results of these tests for the first five modes are shown in Figs. 62 to 66. The stringer tip movements are shown as lines plotted using the stringer/skin attachment line as a base. The mode shape in the direction perpendicular to the stringers along the centre line of the panel is also shown, plotted with the panel centre line as base. The scales refer to the accelerometer output signal in millivolts after being passed through an amplifier with a gain of 20 db. It can be seen that some distortion occurs in the stringers adjacent to the skin bay where the excitation force is applied, but that the other stringers all behave in the expected manner with a single half wave between the top and bottom edges of the panel. The slight asymmetry can still be observed with greater displacement to the left. The edge stringers were only observed to have measurable movements in the first two modes. This movement was less than 6% of the maximum movement recorded for the other stringers, demonstrating the effectiveness of the edge constraints. All the above tests were carried out at an excitation level equivalent to an acoustic sound pressure level of 135 db. This was necessary because it was found that an equivalent excitation level of 140 db as used in the first mode shape tests for direct comparison with previous acoustic

tests, was putting an excessive load on the vibrator when used for prolonged periods.

V.2.4 Damped Mode Shapes

A further series of mode shape determinations were made with an artificial damping treatment attached to the panel. The configuration of the shear damping beam attached to the stringer tips along the centre-line of the panel is illustrated in Plate 10. In this case a shear damping beam with 0.43 mm (0.017") aluminium constraining plates, 0.76 mm (0.030) thick rubber centre layer and 25 mm (1") width, was attached to the free edges of the stringers with quick setting epoxy adhesive. This type of attachment was used since it was easy to remove old beams and replace them with new specimens without removing the panel from its carefully set up fixture. The adhesive used was a relatively heavily filled epoxy resin system which was stiff in the shearing mode. Thus the movements of the stringer tip were wholly transferred to the lower constraining plates of the shear damping beam with minimum losses in the attachment system. Due to the effectiveness of this artificial damping treatment it was only possible to positively identify the first 3 modes of resonant vibration of the panel. The mode shapes obtained are shown in Figs. 67 - 69. Since the peaks in the panel frequency response curve were broadened by the additional damping, it was not possible to use the semi-conductor strain gauge responses as a reliable means of tuning the excitation frequency to that of the panel resonant frequency. To overcome this problem an accelerometer was attached to the panel at the point where the force transducer was bolted to the skin. Measurements of phase angle between the signals from the accelerometer and the force transducer were then taken at various frequencies around the estimated resonant frequency. Plots of these measurements are shown in Figs. 70-72. From these plots the resonant frequencies were determined by observing at what frequencies the rate of change of phase angle was greatest. That

is the resonant frequencies were those at which the curves shown in Figs. 70-72 had greatest slope. Note that the phase angles at resonance need not have been exactly $90^{\circ}$, as with a simple single degree of freedom system, since the panel had a multi-modal response. The vector plot of response against frequency may have several loops within each other, thus the only criterion that can be used for accurate determination of the resonant frequencies is the maximum rate of change of phase angle and not its magnitude. Testing was carried out with increased excitation force so that the average panel displacement was the same as that observed during the undamped tests. It can be seen by comparing Figs. 67-69 with Figs. 62-64 that the mode shape along the centre line of the panel was not significantly altered by the addition of the shear damping beam. However, the stringer tip deflexions were altered in the expected manner, the centres being constrained whilst the outer portions vibrated with nearly the same magnitude as in the undamped condition. This additional constraint increased the effective flexural stiffness of the panel and resulted in an increase in the resonant frequencies. The effect was greater at the higher frequencies, for example the third modal frequency increasing from 453 Hz to 519 Hz.

V.2.5 Energy Measurements

In a general treatise on damping measurements, Mead in Ref. 10 suggests that the best technique for determining the change in loss factor caused by the addition of an artificial damping treatment, is to measure the difference in energy inputs at the system resonant frequencies. When the system is vibrating at its resonant frequency the elastic and inertia forces exactly cancel each other out leaving only the dissipation force to be balanced by the excitation force. Now the modal loss factor is defined as the ratio of energy dissipated per cycle to total energy of vibration, when the system is vibrating in one mode only. Thus if measurements of energy input to the system at each modal frequency are made in the damped and undamped conditions, and if it is assumed that

the addition of the artificial damping treatment does not significantly increase the total vibrational energy, then the modal loss factors will be in the same ratio as the measured energy inputs. This assumption is only justified for system loss factors less than about 0.1 and for widely spaced modes in the frequency domain. For harmonic excitation and response it can be shown that by integrating the applied force multiplied by the velocity of the point of application of the force over a complete cycle of vibration, the work done by the excitation force and thus the energy input to the system per cycle is equal to: $P.y. \sin \alpha$ where P is the peak excitation force, y the peak resulting displacement of the point of application of the force, and $\alpha$ is the phase lag between excitation and response. This result assumes that both the excitation and response are perfectly harmonic. If there is any harmonic distortion in one of these quantities it can be shown that (10) the energy input to the vibrating system is proportional to the D.C. output of the signal resulting from the multiplication of the electrical outputs of transducers recording excitation force and velocity of the point of application of this force. No attempts to use this latter method were made due to the lack of a suitable accurate velocity transducer. However, it is thought that the energy measurements made would be improved in accuracy if this method were adopted since with a multi-modal system some harmonic distortion is almost certain to appear in the response signal. It is important to ensure that no phase shift occurs in such systems due to longitudinal waves being set up in the vibrator to panel linkage. Assuming a moving mass equal to that of the bare panel, the first natural frequency of such longitudinal vibrations was found to be approximately twice that of the highest test frequency (i.e. 2000 Hz). Thus it was concluded that no significant phase shift would result from using this type of linkage.

Since only the first three modes of vibration of the panel in the damped condition could be positively identified, comparative energy

measurements were only made for these three modes. For these tests the panel was set up in the configurations shown in Plates 8 and 10. The same shear damping beam as used in the stringer deflexion tests was applied for the damped tests. An accelerometer was attached to the head of the bolt used to connect the panel to the force transducer. The signals from this accelerometer and from the force transducer were fed through suitable phase matched amplifiers to an ADYU phase meter. Initial testing in the undamped condition was carried out applying a constant excitation force of approximately 16n magnitude. The modal frequencies were determined as before by plotting phase shift against frequency and noting the points on these curves where the slope and hence rate of change of phase angle were greatest. The mode shapes were measured with a roving accelerometer attached with wax as in the previous section. The values of phase angle between the force and acceleration signals were then noted and are shown in Table V.2.2. The panel was then tested in the damped condition, the modal frequencies being determined in the same way. Once a modal frequency had been found the excitation oscillator was locked at that frequency and the applied force varied by adjusting the output level of the oscillator until the mode shape of the panel matched the measured mode shape in the previous undamped tests. At first the excitation force was adjusted to give the same value of acceleration of the force transducer attachment point as in the undamped tests. However, measurement of the resulting mode shape showed some variation to that obtained in the undamped condition. Hence considerable care was taken with each reading to try and match the undamped mode by measuring the damped mode at each one of several small adjustments of excitation force around the desired value. Exact matching was not achieved, but by interpolation of the above results a suitable value of excitation force was obtained. The oscillator output was then readjusted to give this value and the phase angle measured again. These

values of excitation force signal and phase angle are also given in Table V.2.2. From these results values of the energy input per cycle were calculated for the panel in its two conditions. These are shown in Table V.2.2. also, together with the increase in energy dissipated by the addition of the shear damping beam and therefore the increase in modal loss factors. Since response is approximately inversely proportional to modal loss factor, the expected ratio of damped response to undamped response is shown, together with that observed from later steady state tests. It can be seen that the predicted response reductions underestimate those obtained in practice, however the general trend is followed. The accuracy of this method is not thought to be greater than 25% due to the difficulty of matching the mode shapes. Thus the variations shown in Table V.2.2. are not outside the bounds of experimental error.

It was decided not to repeat the energy measurements for the other different shear damping beams available since it was thought that any differences in performance obtained could easily be masked by the experimental error resulting from the difficulty in matching modes. The technique of testing was also extremely time consuming and it was not thought worthwhile to obtain further results of limited accuracy. This decision was justified by later observations which showed the variation of performance of the different shear damping beams to be small.

V.2.6 Quasi-steady State Tests

In order to investigate the effect of changing the parameters of the shear beams on the damping performance, four different beams were manufactured as described in Section III.6.3. See Appendix IV for the beam details. It was thought that the most reliable definitive test to measure the effect of changing the beam parameters, would be a steady-state resonance test. To carry out such a test to a sufficient degree of accuracy by incrementing excitation frequency by say 1 Hz over the

range 200-1000 Hz and reading the values of the response transducer outputs at each frequency increment, whilst keeping excitation force constant, is a very time consuming process. In view of the number of different damping beams to be tested on the panel it was decided to use a quasi-steady state technique to save time. This type of test consists of slowly sweeping through the frequency range with a motor driven oscillator and recording the response transducer output on an XY plotter with one axis driven by the oscillator to give a displacement proportional to frequency. It is assumed that the frequency sweep is sufficiently slow to allow the system to respond with no appreciable time lag.

Initial tests were carried out using an ISVR sweep oscillator with its ramp voltage driving the X axis of an XY plotter. The response transducer was an accelerometer placed in one of two positions which were near antinodes of all the modes of vibration of interest. Details of the panel and accelerometer positions as shown in Fig. 73. It was observed that the addition of a damping beam had very little effect on response, whilst the gain of the vibrator power amplifier was kept constant. By monitoring the force applied to the panel using the force gauge in the vibrator linkage, it was discovered that the applied force was varying considerably over the frequency range of interest. Since this was to be a definitive test it was obviously important to maintain the excitation force at a constant known level. To achieve this the testing equipment was changed and a Bruel-Kjaer Beat Frequency Oscillator geared to a Level Recorder, used instead. With this system a feed-back loop was incorporated with which the excitation oscillator gain was varied to maintain a constant excitation force of approximately 16N over the frequency sweep. Plots of excitation force versus frequency in both damped and undamped conditions are shown in Fig. 74; the small reduction at the highest frequency was thought to be insignificant.

Initial sweeps were made in the undamped and damped conditions (with 25 mm (1") wide type 1 beam attached along the centre of the stringer free edges), with sweep times varying from 3 to 48 minutes over the frequency range 200 to 1000 Hz. To ensure that the response in the various frequency sweeps was not reduced by the rate of sweepings, two steady state tests were carried out for comparative purposes. These two tests, one in the undamped, and one in the damped condition as above, were made using the same accelerometer as a response transducer and placed in the same two positions to record the response in all the modes of vibration of interest. The results of the steady state tests are shown in Figs. 75 and 76 for the two accelerometer positions chosen. Comparison of these figures with those for the initial sweeps showed that the undamped response was being underestimated as expected by the quasi-steady state test. This underestimation was significant for the faster (3 min. and 6 min.) sweeps, but amounted to less than 5% for the 12 min. and slow sweeps. Hence it was decided that the 12 min. sweep time would be sufficiently accurate for the remaining tests with the different shear damping beams. Comparison of Figs. 75 and 77 and 76 and 78 shows the similarity of response for both steady state and quasi-steady state tests. Major peaks corresponding to the first two modes of vibration can readily be identified in all figures. The accelerometer position for Figs. 76 and 78 was chosen so that response in the third mode would be recorded. An additional peak corresponding to this mode is discernable when compared to Figs. 75 and 77. The higher modes are not clearly shown in any of the figures, although evidence of the existence of the fourth mode is shown by the broad peaks occurring at approximately 500 Hz in Figs. 77 and 78, and particularly in Fig. 75 at 540 Hz. Compared to the steady state test, the modal frequencies in the quasi-steady state test are lower. This was thought to be due to two factors. Firstly, the frequency scale of the automatic plots could only be determined by dividing the beginning and end of the plot suitably as the recording system possessed no method of marking the plot with intermediate

frequencies. Secondly the motor driven variable frequency oscillator was connected to the recorder by a flexible drive cable to drive the recording paper at the same speed as the frequency was swept at. Any backlash in the mechanics of this system would cause the paper drive to lag behind the true frequency. It was concluded that the automatic plots were sufficiently close to those obtained in steady state tests, for comparative purposes. Figs. 79 and 80 show the results of sweeps carried out with a 25 mm (1") wide damping beam (Type 1) applied across the centre of the stringer free edges. Peaks corresponding to the first two modes are still visible with very much smaller peaks showing the existence of the higher modes. Due to the greater modal coupling provided by the addition of damping, the peak corresponding to the third mode is now in evidence for both accelerometer positions. The appearance of extra small peaks between 500 and 600 Hz is also thought to be due to this higher modal coupling. This feature is also evident in the steady state tests - see Figs. 75 and 76.

In some of the figures relating to quasi-steady state tests two additional traces marked H and L are plotted. These correspond to the responses of the panel measured at positions above (H) and below (L) the centre line where the two main accelerometer positions were located. This was done to check repeatability of the results and confirm that only one half wave existed in the direction parallel to the stringers. If this had not been true the traces would have been dissimilar and thus readily observed. As was expected the additional traces showed exactly the same form of response but reduced in magnitude proportional to the distance from the centre line of the panel. These also show that the addition of damping in the centre of the panel reduces the displacement and hence stresses at points away from the centre line.

Figs. 80 and 81 show the responses with type 2, 3, 4 beams attached. The peaks are similar to those observed when the type 1 beam was attached

although the response reduction is not so great. The effect of increasing the core thickness of the shear damping beam is shown in Figs. 80 and 81. The general shape of the response curve is again similar for this type 2 beam as for the type 1. The levels of response are not reduced as much as with the type 1 beam. Figs 80 and 81 also show the effect of a type 4 beam. In this case the response is hardly reduced at all compared to the undamped response in Figs. 77 and 78 and confirms the theoretical predictions made in the next chapter.

The percentage reductions in the major response peaks due to the additions of shear damping beams of all types are summarised in Table V.2.3. The average percentage reduction in the response peaks for each particular beam is also shown. It can be seem that the greatest reductions occur using a type 1 beam followed by a type 2, type 3 and type 4 in that order. The difference in performance between the first 3 types is small whereas use of a type 4 beam resulted in a very small average reduction to only 87% of the undamped peak value.

An attempt was made to use a rapid sweep since excitation signal and a method of transient analysis developed by Wright (71). This involves calculating the Fourier Transforms of the response transducer output signal and the same signal with a known time delay. Measurements of the ratio of heights of corresponding peaks in the two transforms and knowledge of the time delay, enables the modal loss factors for each pair of peaks to be calculated directly. Unfortunately with the equipment available it was not possible to excite the damped panel sufficiently to obtain reasonable output signals without distortion at certain frequencies. Although no meaningful results were obtained it was thought that this method should be further investigated in future work.

## V.3 Full Scale Tests

### V.3.1 Fin Box Assembly

Measurements of response reduction due to the application of

shear damping beams to two pieces of full size aicraft structure were made to confirm the effects observed on the single experimental panel. The first tests were made on a prototype. Concorde fin-box assembly, which consisted of similar integrally machined outside skins separated by built-up frames and ribs. Each skin was made of nine identical panels in a three by three array. An access hatch was cut in the rear centre panel so that a shear damping beam of type 1 could be attached to the centre of the stringer free edges of the front centre panel. The access hatch was sealed with a cover plate attached with twenty small bolts. Initially the undamped assembly was suspended by two chains from a fixed frame in front of a bank of four loudspeakers. The fin-box was arranged so that the acoustic pressure wave impinged at grazing incidence on the front panels. The response of the centre front panel to discrete tone excitation was monitored via a strain gauge mounted in the centre skin bay. The mode shape of the assembly was then determined at each major resonant peak by scanning the surface of the fin-box with a small accelerometer attached to the structure with wax.

With the fin-box suspended on chains it was discovered that the only modes of vibration being excited were overall beam modes of the whole structure. This was thought to be due to the position of the suspension points being too close to the nodal positions of the fundamental free-free mode. The suspension system was then changed and the structure attached to the fixed frame with rubber bungee cord and plastic foam used to insulate the fin-box from the frame. In this way it was hoped to constrain the structure sufficiently to excite the local skin modes. Due to the limitations of the loudspeakers used, the maximum excitation possible corresponded to an overall sound pressure level of 123 db re. $2 \times 10^{-5}$ N/m$^2$. This was insufficient to excite the local skin modes sufficiently for the mode shapes to be positively identified with the accelerometer scan. However, the strain gauge used was a semi-conductor device with a high sensitivity and recordings of strain in the centre

skin bay at the various resonant peaks in both the damped and undamped conditions were made. These observations showed that the application of a single type 1 beam to the centre panel of the three by three array reduced the resonant peaks of response by an average of 40%. When the structure was subjected to broad-band excitation by white noise in the frequency range 200 - 2000 Hz, the r.m.s. strain level in the centre skin bay was reduced by approximately 35% due to the additional damping. These figures agree well with those obtained in the single panel tests. The fin-box skins were of a lighter construction than the single test panel and thus with the same size of damping beam attached it was expected that the damping effect would be greater for the fin-box structure. It was thought however that the other eight panels in the array contributed some vibration energy to the centre panel by coupling through the connecting frames and ribs, to cancel out this effect.

V.3.2 Curved Fuselage Specimen

The second series of full-scale tests were carried out on a typical aircraft curved fuselage panel consisting of three bays separated by two rivetted intermediate frame assemblies. The dimensions of the panel were as follows:

| | |
|---|---|
| Frame pitch | .51 m (20") |
| Stringer pitch | .135 m (5.25") |
| Stringer height | .0178 m (0.7") |
| Stringer thickness | 2.01 mm (0.079") |
| Skin thickness | 1.4 mm (0.055") |
| Radius of curvature | 1.45 m (56.7") |
| Overall size | 1.54 m long (60") |
| | 1.02 m wide (40") |

Initial tests were carried out in an acoustic siren facility with the panel mounted at grazing incidence to the plane acoustic wave. For these first tests a single type 1 damping beam was affixed to the centre of the stringer free edges in the centre bay only. Using discrete tone

excitation slowly swept over the range 200 to 700 Hz with a constant OASPL of 135 db, the response of a strain gauge mounted near to the free edge of the centre stringer at an intermediate frame position, was recorded. Comparison of the resulting traces in the undamped and damped conditions show an overall reduction in the peaks of response to approximately 60% of the undamped values. At certain individual frequencies the peaks are reduced to approximately 10% of the undamped value. When broad band excitation in the form of white noise was used, the reduction in strain spectrum level was much less, with only one region between 200 and 300 Hz showing a noticeable reduction to 60% of the undamped level. The reason for this apparent anomally was thought to be due to the characteristics of the curved panel itself. The shear damping beam relies for the major part of its effect on shear strain being transmitted to the viscoelastic core directly by rotation of the stringers. Thus the system is most effective in stringer torsion modes. With a flat panel stringer torsion modes are the first to occur as the excitation frequency is increased from that of the fundamental. In the frequency range of interest the first stringer bending modes involving very little stringer rotation are not encountered. In the case of curved panels this ordering of the modes is not retained, and depending on the panel characteristics, the stringer bending modes may occur in the same frequency range as stringer-torsion modes. In the case of the panel tested with broad band noise it may have been that the stringer torsion modes were not so strongly excited as the stringer bending modes, due to the energy distribution of the excitation spectrum. Also since the damping beams were attached to a curved panel they were themselves curved in between the stringers. Any rotation of the stringers would then cause buckling of the beams rather than direct shearing of the lower plates over the upper constraining layer. Thus the shear strain induced in the core would be indirect, caused by the flexure of the beam. This would tend to lessen the effect of the beams compared to those on a similar

flat integral panel.

A second series of tests were carried out with the same fuselage panel excited with a vibrator attached to the centre of the centre bay adjacent to the central stringer. In this case three type 1 beams were attached along the centre line of each bay between the frames. The response of the panel to a constant vibrator input current was recorded with a series of accelerometers and strain gauges, whilst the excitation frequency was swept slowly from 200 to 800 Hz. In the low frequency region between 200 and 300 Hz the average reduction of the response peaks was to approximately 30% of their undamped value. In the middle and high frequency ranges the reduction was to between 80 and 55% of the undamped values for the sharp resonant peaks only. Certain transducers exhibited large reductions at particular frequencies in this range, particularly those close to the vibrator connexion. In certain places the response was greater in the damped condition, in effect the troughs between the undamped resonant peaks were filled in to a degree in the damped condition. Further tests using type 3 beams in an attempt to reduce the buckling effect resulted in additional reductions at the previously observed points of response reduction, by a further 20 to 40%.

With most reduction occurring at the lower frequencies, it was thought that the damping strips were again being more effective in the lower modes where stringer torsion vibration is predominant. In the higher modes where stringer bending is predominant, the damping effect is lessened due to the shear strain in the core being induced by flexure only. The marked effect which the additional damping had on certain higher frequency peaks was thought to be due to those corresponding to higher order stringer torsion modes. With the damping strips attached these drops became less sharp, with very "peaky" regions becoming flattened whilst the troughs between peaks were filled with contributions from surrounding modes. This provided further evidence of the coupling effect of the

added damping and explains the points where response was apparently slightly higher in the damped condition. For one clearly defined mode that was observed (five half waves in the direction perpendicular to the stringers, one half wave beteen frames), Kennedy-Pancu type vector plots were made to estimate the modal loss factor. It was found that the amplitude of vibration had been reduced by a factor of 2 or 3 whilst the loss factor had increased by a similar amount. (From an average of .0042 undamped to .0083 damped at a frequency of 233 Hz).

From these full scale tests it was concluded that shear damping beams can be made effective on flat panels but that some optimisation of the flexural characteristics are necessary for curved panels, plus some method of eliminating the buckling effect due to damping beam curvature between stringers.

## VI. THEORETICAL MODELS OF A SHEAR DAMPING BEAM

The incorporation of significant amounts of damping in response calculations is usually difficult as the initial assumption of low damping, which many theories depend on, is violated. Thus the initial approach was to perform a very simple calculation to gain some knowledge of the trends involved and the orders of magnitude of the two major damping mechanisms attributable to the shear damping beams. A single element of a stiffened panel was modelled using an assemblage of beams and the two basic shear damping effects - those of shear strains induced by flexure of the damping beam, and those induced directly by stringer rotation, were evaluated. These calculations showed that the flexure effect was negligible compared with the direct shearing, thus the next increase in complexity of the theory using a transfer matrix analysis, incorporated only this direct effect by means of an additional complex stiffness.

The transfer matrix model itself was simplified by modelling the panel as a "wide" beam on elastic supports. The magnitude of the stiffnesses at these supports was made to correspond to the panel stiffener and shear damping beam characteristics. This model was again only intended to give a further insight into the trends of performance of the dampers used, no direct comparisons being made with the panel experimental results. Suggestions for extending this analysis to enable direct comparisons and response predictions to be made, are contained in the concluding section of this chapter.

### VI.1 Single Element Theory

For the purposes of this analysis only a single element of the plate is considered as in Fig. 82. The element consists of three beams labelled 1, 2, 3, rigidly connected together at a point. These correspond to a section of stringer, and two sections of skin of length half the width of the skin bay, respectively. The width of these beams is

assumed to be half that of the plate width to result in a beam with the same order of magnitude of vibration energy as the real panel. The shear damping beam is assumed to be of the same width as the real beam, but to exert a restoring force uniformly along the free edge of the "stringer" beam. The following assumptions are made throughout the analysis:-

a) Rotary Inertia in the beams is neglected.

b) All deflexions are due to bending, i.e. no shear deflexion.

c) Beams are rigidly connected together to maintain the stringer perpendicular to the skin line.

d) No longitudinal vibration in the stringer beam (W direction).

e) The upper constraining plate of the shear damper remains substantially stationary (for justification of this see Ref. 31, Appendix III).

VI.1.1 Flexural Mode

Assume that the ends of the damping beam are free and the ends of the skin beams are pinned. Consider the motion of one half of the shear damping beam as a cantilever built-in at the top of the stringer beam. Following the theory and notation of Grootenhuis in Ref. 72, for a type 1 beam 25 mm (1") wide we have:

$$\text{Thickness parameter} = 0.93$$

$$\text{Shear parameter} = 0.25$$

From Fig. 3 of (72) $\eta_{beam} \doteq 0.1$ for vibration in the fundamental mode. Fig. 4 of (72) shows $\eta$ beam to be approximately 0.1 also for vibration in the first three modes of vibration. Since the core of the damping beam is soft compared to the outer plates, the flexural rigidity of the sandwich beam can be shown (36) to be approximately equal to the sum of the individual flexural rigidities of the constraining plates. Hence replace the real shear damping beam by an equivalent beam having the following properties:-

$$\eta = 0.1$$

$$EI = 3.06 \times 10^{-4} \text{ n m}^2 (1 + 0.1\, i)$$

$$\mu = 8.0 \times 10^{-2} \text{ Kg/m}$$

Consider the motion of one half of the shear damping beam as a cantilever constrained to slide vertically at Y = 0 and free at Y = L (using notation of Fig. 82). By definition the tip receptance is given by:-

$$\alpha_{oo} = \frac{\text{Deflexion at Y = 0}}{\text{Force at Y = 0}} \quad \text{(See p 289 of Ref. 73)}$$

$$= X / F^{1} e^{iwt} \quad \text{say}$$

For this type of cantilever it has been found that

$$\alpha_{oo} = \frac{-1 + \cos \lambda l}{EI \lambda^3 (\cos \lambda l \sinh \lambda l + \sin \lambda l \cosh \lambda l)}$$

where $\lambda^4 = \frac{w^2 \mu}{EI}$ and w = frequency of vibration,

$$E = E' (1 + 0.1i)$$

Thus the force applied to the junction of beams 1, 2, 3 during vibration is given by:-

$$F = M_1 \ddot{X} + 2F^{1}$$

$$= -M_1 w^2 X + \frac{2X}{\alpha_{oo}} \quad \text{assuming harmonic motion and}$$

where $M_1$ equals the mass of the stringer beam plus damping beam.

For beams 2, 3

Using the notation of Fig. 82 and the definition of $\lambda$ as above with subscripts to denote the different values of $\lambda$ for the different beams we have:-

For Beam 2 using the usual solution for harmonic beam response:-

$$W_2 = A_2 \cos \lambda_2 V_2 + B_2 \sin \lambda_2 V_2 + C_2 \cosh \lambda_2 V_2 + D_2 \sinh \lambda_2 V_2$$

$$\frac{dw_2}{dv_2} = -A \lambda_2 \sin \lambda_2 V_2 + B_2 \lambda_2 \cos \lambda_2 V_2 + C_2 \lambda_2 \sinh \lambda_2 V_2 + D_2 \lambda_2 \cosh \lambda_2 V_2$$

$$\frac{d^2 w_2}{dv_2^2} = -A_2 \lambda_2^2 \cos \lambda_2 V_2 - B_2 \lambda_2^2 \sin \lambda_2 V_2 + C_2 \lambda_2^2 \cosh \lambda_2 V_2 + D_2 \lambda_2^2 \sinh \lambda_2 V_2$$

$$\frac{d^3w_2}{dv_2^3} = A_2\lambda_2^3\sin\lambda_2V_2 - B_2\lambda_2^3\cos\lambda_2V_2 + C_2\lambda_2^3\sinh\lambda_2V_2 + D_2\lambda_2^3\cosh\lambda_2V_2$$

At $V_2 = 0$, $\frac{dw_2}{dv_2} = 0$ and $w_2 = X$

Thus substituting these boundary conditions leads to:-

$$B_2 = -D_2 \text{ and } X = A_2 + C_2$$

At $V_2 = \ell$, $w_2 = 0$-(i) and $\frac{d^2w_2}{dv_2^2} = 0$-(ii)

From (i) $0 = A_2\cos\lambda_2\ell + B_2\sin\lambda_2\ell + C_2\cosh\lambda_2\ell + D_2\sinh\lambda_2\ell$

$$= A_2\cos\lambda_2\ell + C_2\cosh\lambda_2\ell + B_2(\sin\lambda_2\ell - \sinh\lambda_2\ell) - (1)$$

Similarly from (ii) $0 = -A_2\cos\lambda_2\ell + C_2\cosh\lambda_2\ell - B_2(\sin\lambda_2\ell - \sinh\lambda_2\ell)$-(2)

Addition of these two results gives $2C_2\cosh\lambda_2\ell = 0$

Since in general $\cosh\lambda_2\ell \neq 0$ then $C_2 = 0$

Substituting this result in equations 1, 2 leads to

$$B_2 = -A_2\cos\lambda_2\ell/(\sin\lambda_2\ell - \sinh\lambda_2\ell) - (3)$$

By summetry similar results are obtained for beam 3.

Consider the equilibrium of the junction of beams 1, 2 and 3. If $Pe^{iwt}$ is excitation force applied and $SF_i$ is the shear force in beams 2 and 3 at V = 0 then cancelling $e^{iwt}$ we have:-

$$P = SF_2 + SF_3 + F$$

$$+ 2SF_2 - M_1w^2X + \frac{2X}{\alpha_{oo}}$$

Now $SF_2 = E_2I_2\frac{d^3w_2}{dv_2^3}$ at $V_2 = 0$

$$= E_2I_2(-B_2\lambda_2^3 + D_2\lambda_2^3)$$

$$= E_2I_2(-2B_2\lambda_2^3)$$

$$= \frac{2E_2I_2\lambda_2^3A_2\cos\lambda_2\ell}{(\sin\lambda_2\ell - \sinh\lambda_2\ell)}$$ substituting for $B_2$ from (3)

$$\text{Thus } P = \frac{4E_2I_2\lambda_2^3 A_2 \cos\lambda_2 l}{(\sin\lambda_2 l - \sinh\lambda_2 l)} - M_1 w^2 X + \frac{2X}{\alpha_{oo}} \quad - (4)$$

Now $X = w_2$ at $v_2 = 0$, thus since $C_2 = 0$ we have $X = A_2$ from (i)
Hence substituting for $A_2$ in (4) and dividing by X will give the inverse of the total receptance at the point under consideration. For a given excitation P we want the modulus of this number to be as large as possible for minimum response.

$$\text{Hence:- } \frac{P}{X} = \frac{4\lambda_2^3 E_2 I_2 \cos\lambda_2 l}{(\sin\lambda_2 l - \sinh\lambda_2 l)} - M_1 w^2 + \frac{2}{\alpha_{oo}}$$

$$= \beta - M_1 w^2 + \frac{2}{\alpha_{oo}}$$

For a 25 mm (1") wide type damping beam the values of $\beta$, $M_1 w^2$ and $2/\alpha_{oo}$ are given in Table VI.1.1 for the frequencies of interest from the panel tests. It can be seen that the $2/\alpha_{oo}$ term is at least four orders of magnitude less than the sum of the $\beta$ and $M_1 w^2$ terms, hence its effect on the total sum is negligible. This confirms the original qualitative assessment of the shear damping beam mechanism that the shearing effect is the major contributor to reducing response. This was also found by Cicci (74) in his analysis of uniform strips of viscoelastic material suspended across the stringer tips of a beam cut from an integral panel. He found the extensional straining effect contributed several orders of magnitude more than the flexural effect, to the overall damping of the beam.

VI.1.2. Shearing Mode

Using the notation of Fig. 82 it is assumed that the "free" ends of beams 2 and 3 are able to slide in a vertical direction only. It is also assumed that the shear stress induced in the core of the damping beam by rotation of the "stringer" beam is uniform with no edge effects. The justification for this is contained in Appendix III.

Using the same symbols as previously defined in the preceding section with subscripts to indicate to which beam they refer, we have

for beam 1:-

Assuming a solution of the form:-

$$Y = A_1 \cos \lambda_1 X + B_1 \sin \lambda_1 x + C_1 \cosh \lambda_1 x + D_1 \sinh \lambda_1 x$$

where $\lambda_1^4 = w^2 \mu_1 / E_1 I_1$

Let the force exerted by the shear damping beam on the "stringer" tip be:

$F = \frac{Y \text{ at } x = 0}{\alpha_{11}}$ using the receptance definition as before.

Then the boundary conditions are as follows:

At $x = 0$, $\frac{d^2y}{dx^2} = 0$-(i) and $\frac{d^3y}{dx^3} = \frac{F}{E_1 I_1}$ -(ii)

At $x = h$ $y = 0$ (iii) and $\frac{dy}{dx} = \theta$ say (iv)

From (i) $0 = -A_1 \lambda_1^2 + C_1 \lambda_1^2$ or $A_1 = -C_1$ -(1)

Now y at $x = 0$ is given by $y_0 = A_1 + C_1$

$= 2C_1$ from (1)

Then from (ii) $D_1 \lambda_1^3 - B_1 \lambda_1^3 = \frac{2C_1}{\alpha_{11} E_1 I_1}$

Let $k_3 = \frac{1}{2 \lambda_1^3 E_1 I_1 \alpha_{11}}$ then:-

$D_1 - B_1 = 4k_3 C_1$ - (2)

From (iii) $0 = A_1 \cos \lambda_1 h + B_1 \sin \lambda_1 h + C_1 \cosh \lambda_1 h + D_1 \sinh \lambda_1 h$

substituting for $A_1$ from (1) and $D_1$ from (2) leads to:

$$B_1 = \frac{-C_1 (\cos \lambda_1 h + \cosh \lambda_1 h + 4K_3 \sin \lambda_1 h)}{(\sin \lambda_1 h + \sinh \lambda_1 h)} = K_7 C_1 \text{ say -(5)}$$

For Beam 2

Again assume a solution of the form:-

$$w_2 = A_2 \cos \lambda_2 V_2 + B_2 \sin \lambda_2 V_2 + C_2 \cosh \lambda_2 V_2 + D_2 \sinh \lambda_2 V_2$$

The boundary conditions are:-

At $v_2 = 0$, $w_2 = 0$ (i) and $\frac{dw_2}{dv_2} = \theta$ (ii)

At $v_2 = \ell$, $\frac{dw_2}{dv_2} = 0$ (iii) and $\frac{d^3 w_2}{dv_2^3} = 0$ (iv)

From (i) $0 = A_2 + C_2$ or $A_2 = - C_2$ - (6)

From (ii) $\Theta = \lambda_2 (B_2 + D_2)$

From (iii) $0 = -A_2 \sin \lambda_2 \ell + B_2 \cos \lambda_2 \ell + C_2 \sinh \lambda_2 \ell + D_2 \cosh \lambda_2 \ell$

From (iv) $0 = A_2 \sin \lambda_2 \ell - B_2 \cos \lambda_2 \ell + C_2 \sinh \lambda_2 \ell + D_2 \cosh \lambda_2 \ell$

Adding and subtracting these latter two equations gives:

$$0 = C_2 \sinh \lambda_2 \ell + D_2 \cosh \lambda_2 \ell \quad - (7)$$

$$0 = A_2 \sin \lambda_2 \ell + B_2 \cos \lambda_2 \ell \quad - (8)$$

Similarly for Beam 3 we have:-

$$0 = A_3 + C_3 \quad - (9)$$

$$-\Theta = B_3 \lambda_3 + D_3 \lambda_3 \quad - (10)$$

$$0 = C_3 \sinh \lambda_3 \ell + D_3 \cosh \lambda_3 \ell - \quad (11)$$

$$0 = A_3 \sin \lambda_3 \ell + B_3 \cos \lambda_3 \ell - (12)$$

By symmetry we can say $\lambda_2 = \lambda_3$ and $A_2 = -A_3$ etc.

Also $E_2 I_2 = E_3 I_3$

Consider the equilibrium of the point at which beams 1, 2 and 3 join. Assume that excitation is provided by a moment $He^{iwt}$ applied to this point. For equilibrium:

$$He^{iwt} = E_1 I_1 \left(\frac{d^2 y}{dx_2^2}\right)_{x = \ell} + E_2 I_2 \left(\frac{d^2 w_2}{dv_2^2}\right)_{v_2 = 0} - E_3 I_3 \left(\frac{d^2 w_3}{dv_3^2}\right)_{v_3 = 0}$$

$$= \lambda_1^2 E_1 I_1 (-A_1 \cos \lambda_1 \ell - B_1 \sin \lambda_1 \ell + C_1 \cosh \lambda_1 \ell + D_1 \sinh \lambda_1 \ell)$$
$$+ E_2 I_2 (-A_2 \lambda_2^2 + C_2 \lambda_2^2)$$
$$- E_3 I_3 (-A_3 \lambda_3^2 + C_3 \lambda_3^2)$$

$$= \lambda_1^2 E_1 I_1 (-A_1 \cos \lambda_1 \ell - B_1 \sin \lambda_1 \ell + C_1 \cosh \lambda_1 \ell + D_1 \sinh \lambda_1 \ell)$$
$$+ 4 E_2 I_2 \lambda_2^2 C_2 \quad - (13)$$

Substituting for $A_3$ in equation (12) from (9) it can be shown that

$$B_3 = \frac{C_3 \sin \lambda_3 \ell}{\cos \lambda_2 \ell} \quad \text{and from (11)} \quad D_3 = -C_3 \frac{\sinh \lambda_3 \ell}{\cosh \lambda_3 \ell}$$

Substituting for $B_3$ and $D_3$ in (10) we have:-

$$-\Theta = \lambda_3 C_3 (\tan \lambda_3 \ell - \tanh \lambda_3 \ell)$$

or $$\Theta = \lambda_2 C_2 (\tan \lambda_2 \ell - \tanh \lambda_2 \ell) \quad - \quad (14)$$

From boundary condition (iv) for beam 1 we can write:-

$$\Theta = -A_1 \lambda_1 \sin \lambda_1 h + B_1 \lambda_1 \cos \lambda_1 h + C_1 \lambda_1 \sinh \lambda_1 h + D_1 \lambda_1 \cosh \lambda_1 h$$

Consider the L.H.S. of this equation:

From (1) $A_1 = C_1$

(5) $B_1 = K_7 C_1$

(2) $D_1 = (B_1 + 4K_3 C_1)$

$= (4K_3 + K_7) C_1$

Thus $C_1 \lambda_1 (-\sin \lambda_1 h + K_7 \cos \lambda_1 h + \sinh \lambda_1 h + (4k_3 + K_7) \cos \lambda_1 h) = \Theta$

Similarly from (14) $C_2 = \Theta / \lambda_2 (\tan \lambda_2 \ell - \tanh \lambda_2 \ell)$ - (16)

Hence substituting for $A_1$, $B_1$, $D_1$ in (13) we have:-

$$He^{iwt} = C_1 \lambda_1^2 E_1 I_1 (-\cos \lambda_1 h - K_7 \sin \lambda_1 h + \cosh \lambda_1 h + (4k_3 + K_7) \sinh \lambda_1 h) + \frac{4E_2 I_2 \lambda_2}{C_2}$$

Substituting for $C_1$ and $C_2$ from (15) and (16) and dividing by $\Theta$ gives the inverse of the receptance at the point of excitation. For minimum response we want this number to be as large as possible for a fixed H.

Hence $$\frac{He^{iwt}}{\Theta} = \frac{\lambda_1 E_1 I_1 (-\cos \lambda_1 h - K_7 \sin \lambda_1 h + \cosh \lambda_1 h + (4k_3 + K_7) \sinh \lambda_1 h)}{(-\sin \lambda_1 h + K_7 \cos \lambda_1 h + \sinh \lambda_1 h + (4k_3 + K_7) \cosh \lambda_1 h)} +$$

$$\frac{4E_2 I_2 \lambda_2}{(\tan \lambda_2 \ell - \tanh \lambda_2 \ell)}$$

Where $k_3 = 1/2 \lambda_1^3 E_1 I_1 \alpha_{11}$

$$K_7 = \frac{\cos \lambda_1 h + \cosh \lambda_1 h + 4k_3 \sinh \lambda_1 h}{\sin \lambda_1 h + \sinh \lambda_1 h}$$

$$\frac{1}{\alpha_{11}} = \frac{AG'}{t} - Mw^2 + \frac{i G' \eta A}{t}$$

Derivation of $\alpha_{11}$

Let the horizontal displacement of the stringer tip be $y_0$

Then if M is the moving mass = mass of lower constraining plate + 1/3 mass of viscoelastic core.

A is the area of core being sheared.

$G = G'(1 + i\eta)$ is the complex shear modulus of the core.

t is the thickness of the core.

For equilibrium assuming a uniform shear stress induced in the core (see Appendix III) we have:

$$F = \frac{AG}{t} y_o + M\ddot{y}_o$$

$$= \frac{AG'}{t}(1 + i\eta) y_o - Mw^2 y_o$$

Now by definition $\alpha_{11} = y_o/F$

Thus $1/\alpha_{11} = F/Y_o = \frac{AG'}{t} - Mw^2 + \frac{iG'\eta A}{t}$

Analysis for undamped element

The analysis closely follows from that of the damped element, the only change is that the boundary conditions for the free end of beam 1 are different:

At $x = 0$, $\frac{d^2y}{dx^2} = 0$ (i) and $\frac{d^3y}{dx^3} = 0$ (ii)

From (i) $0 = -A_1 + C_1$ or $A_1 = C_1$ (1)

from (ii) $0 = -B_1 + D_1$ or $B_1 = D_1$

At $x = h$, $y = 0$ (iii) and $\frac{dy}{dx} = \theta$ (iv)

From (iii) and substituting for $A_1$ and $D_1$ from above,

$$0 = C_1(\cos \lambda_1 h + \cosh \lambda_1 h) + B_1(\sin \lambda_1 h + \sinh \lambda_1 H)$$

i.e. $$B_1 = \frac{C_1(\cos \lambda_1 h + \cosh \lambda_1 h)}{(\sin \lambda_1 h + \sinh \lambda_1 h)} \quad - (2)$$

$$= D_1$$

From (iv) $\theta = -A_1\lambda_1 \sin \lambda_1 h + B_1\lambda_1 \cos \lambda_1 h + C_1\lambda_1 \sinh \lambda_1 h + D_1\lambda_1 \cosh \lambda_1 h$

Substituting for $A_1$, $B_1$ and $D_1$ in terms of $C_1$ from (1) and (2):

$$\theta = C_1\left\{\lambda_1(\sinh \lambda_1 h - \sin \lambda_1 h) - \frac{\lambda_1(\cos \lambda_1 h + \cosh \lambda_1 h)^2}{(\sin \lambda_1 h + \sinh \lambda_1 h)}\right\}$$

$$= \frac{-2C_1\lambda_1(1 + \cos \lambda_1 h \cosh \lambda_1 h)}{(\sin \lambda_1 h + \sinh \lambda_1 h)} \quad - (3)$$

Equation (14) of the previous section remains unaltered viz:

$$\Theta = C_2 \lambda_2 (\tan \lambda_2 \ell - \tanh \lambda_2 \ell) \quad - \quad (14)$$

The equation for equilibrium at the junction of the three beams after substituting for $A_1$, $B_1$ and $D_1$ from equations (1) and (2) becomes:

$$He^{iwt} = C_1 \lambda_1^2 E_1 I_1 \left\{ (\cosh \lambda_1 h - \cos \lambda_1 h) - \frac{(\sinh \lambda_1 h - \sin \lambda_1 h)(\cos \lambda_1 h + \cosh \lambda_1 h)}{(\sin \lambda_1 h + \sinh \lambda_1 h)} \right\}$$

$$+ 4 E_2 I_2 \lambda_2^2 C_2$$

Substituting for $C_1$ and $C_2$ in terms of $\Theta$ from (3) and (14) and dividing by $\Theta$ gives the inverse receptance as before:

$$\frac{He^{iwt}}{\Theta} = \frac{-(\sin \lambda_1 h + \sinh \lambda_1 h)}{2(1 + \cos \lambda_1 h \cosh \lambda_1 h)} \lambda_1^2 E_1 I_1 \left\{ (\cosh \lambda_1 h - \cos \lambda_1 h) - \frac{(\sinh \lambda_1 h - \sin \lambda_1 h)(\cos \lambda_1 h + \cosh \lambda_1 h)}{(\sin \lambda_1 h + \sinh \lambda_1 h)} \right\}$$

$$+ \frac{4 E_2 I_2 \lambda_2}{(\tan \lambda_2 \ell - \tanh \lambda_2 \ell)}$$

$$= - \frac{\lambda_1 E_1 I_1 (\cosh \lambda_1 h \sin \lambda_1 h - \cos \lambda_1 h \sinh \lambda_1 h)}{(1 + \cos \lambda_1 h \cosh \lambda_1 h)} +$$

$$\frac{4 E_2 I_2 \lambda_2}{(\tan \lambda_2 \ell - \tanh \lambda_2 \ell)}$$

VI.1.3 Numerical Results

The two equations derived from the inverse receptance in the damped and undamped conditions were programmed for a digital computer. For any particular data input the ratio of the undamped over the damped inverse receptance was calculated, thus giving a measure of the response ratio. Data input corresponding to all the different beams moulded was used, plus some extra parametric variations to investigate the effect of changing the thickness and loss factor of the viscoelastic core. The results are summarised in Table VI.1.3. It can be seen that the differences in performance between the various damping beams is small. It was thought that this was reasonable as this first analysis had given an order of magnitude type result only, requiring further sophistication of the mathematical model to yield more meaningful results. This approach was taken and is described in the subsequent sections, a transfer

matrix method being the model chosen as the one in which significant additive damping could be incorporated.

An attempt was made to model the shear damping mechanism on two adjacent stringers by setting up an analogue of two similar single degree of freedom damped oscillators coupled via a spring and damper in parallel. Equations were developed and scaled for an EIA 580 Analogue Computer. It was proposed to use a forced oscillation type analogue circuit with non-linear elements to represent the behaviour of the real dampers, corresponding to the material tests that had been undertaken previously. Unfortunately with the limited number of operational amplifiers available with this equipment it was not possible to obtain sufficient dynamic range to satisfy the scaling of the equations required. This was essentially a limitation of the equipment and not the method, which is still attractive owing to the ease with which non-linear stiffness and damping elements can be incorporated in the analogue using integrated circuit elements.

## VI.2 Transfer Matrix Method

### VI.2.1 Transfer Matrix of a Single Element

The transfer matrix method is now a well established way of analysing structures to obtain natural frequencies and mode shapes (75). In the present analysis the conventional concepts of field and point transfer matrices will be used as defined in Ref. (76). To simplify the problem the structure considered is as in the previous section, that is a wide beam of width half that of the real panel, with a single one inch wide shear damping beam attached to the centre of the stringer free edges. Lin (77) has shown that the behaviour of beams on suitable elastic supports, which represent the real panel stringer bending and torsional stiffnesses, is close to the behaviour of a real panel, thus in this analysis the bending and torsional stiffnesses of the integral panel stringers are included in the point transfer matrices used.

The single element for which a transfer matrix will be developed consists of a full width skin bay on the left hand side of which is attached a full size stiffener. The base of the stiffener is assumed to be attached to an elastic support possessing both longitudinal and rotational stiffnesses. At the top of the stiffener a portion of shear damping beam of length equal to that of a single lower constraining plate is assumed to be attached. This configuration is shown diagramatically in Fig. 83. At the frequencies of interest it can be assumed that the stringer acts as a rigid body possessing only mass and inertia. Using the notation of Fig. 83 and assuming small angles, if the stringer rotates clockwise by an angle $\Theta$ causing the stringer tip to move to the right a distance $\epsilon$, then for the angle $\Theta$ measured in radians

$$\Theta \doteq \epsilon / h$$

Shear strain on rubber = $\epsilon/t$ assuming no movement of upper constraining plate as in previous section. Thus force applied to stringer tip by damping layer of area A is given by:-

Shear stress x A = $\frac{\epsilon}{t} G' (1 + i\eta) A$

Moment at O = $\frac{\epsilon}{t} G' (1 + i\eta) A h$

Contribution to rotational stiffness at O moment/radian = $\frac{\epsilon}{t} G'(1+i\eta)\frac{Ah}{\Theta}$

$$= \frac{G'}{t}(1+i\eta)Ah^2$$

a) Point Transfer Matrix

Considering the state vector on either side of a stringer, it is assumed that there is continuity of slope and deflexion, but that the effect of the stringer is to cause an abrupt change in the values of bending moment and shear force in the skin at the point of attachment. Using suffices $r$ and $\ell$ to indicate the values of state vector to the right and left of a stringer and the notation of Fig. 83 we have:-

$$X_r = X_\ell$$

$$\Theta_r = \Theta_\ell$$

$$M_r = M_\ell + \theta_\ell \left( R - Iw^2 + \frac{G' (1 + i\eta)\, Ah^2}{t} \right)$$

$$V_r = V_\ell - x_\ell (K - Mw^2)$$

Where I = moment of inertia of stringer about skin line.

M = mass of stringer

w = frequency of vibration.

The flexural vibration of the shear damping beam and its associated effect on the change in shear has been omitted as this mechanism was shown in the previous section to have a secondary effect only compared to the shearing mechanism. Thus the point transfer matrix for a plain rectangular section integral stringer with a portion of shear damping beam attached to its tip may be written as:-

$$P = \begin{bmatrix} 1 & 0 & 0 & 0 \\ 0 & 1 & 0 & 0 \\ 0 & C & 1 & 0 \\ Q & 0 & 0 & 1 \end{bmatrix}$$

Where $C = \left(R - Iw^2 + \frac{G' (1 + i\eta)\, Ah^2}{t}\right)$ (written as K in computer program, see Appendix V).

$Q = -(K - Mw^2)$

Note the stiffnesses R and K should be made complex to account for the inherent structural damping of the panel material. Measurements of this inherent structural damping in both flat and curved integral panels using the Kennedy-Pancu technique have shown that a reasonable figure for the damping ratio is..005.

In calculating the bending stiffness of the stringer K, it is not sufficient to assume that the bending takes place about an axis through the skin. From experimental data it has been established that the neutral axis lies some distance above the skin line though not so far away as the plain stringer neutral axis. Timoshenko (78) shows that a portion of the skin on either side of the stringer should be taken into account in calculating the position of the neutral axis and the second moment of

area of the bending section. It is shown that a portion of skin of width 0.09×a should be included on either side of the stringer where 'a' equals the distance between stringer supports or frame pitch. In the case of the experimental panel this width was more than half the skin bay width, thus in calculating the bending stiffness only half the skin bay width was included on each side of a stringer. (see Appendix V for further details). With the clamping system used in the experiments, the stringer ends were not completely fixed to the clamping frame by means of cleats etc. Instead a piece of aluminium bar was machined with six slots to drop over the stringer ends and clamp the skin. Hence in the bending stiffness calculations the stringers were assumed to be simply supported at the ends. The calculations for rotational stiffness were straight-forward assuming rotation about the point of attachment of the skin and using the St. Venant torsion constant for thin sections.

b) Field Transfer Matrix

The field transfer matrix relates the state vectors at the left and right hand sides of a skin bay. With the usual notation define:

$$\lambda^4 = \frac{\mu w^2}{EI}$$

$$f_0 = \tfrac{1}{2}(\cosh\lambda\ell + \cos\lambda\ell)$$

$$f_1 = \tfrac{1}{2}(\sinh\lambda\ell + \sin\lambda\ell)$$

$$f_2 = \tfrac{1}{2}(\cosh\lambda\ell - \cos\lambda\ell)$$

$$f_3 = \tfrac{1}{2}(\sinh\lambda\ell - \sin\lambda\ell)$$

Where $\ell$ is width of skin bay.

Then the field transfer matrix F is given by (Ref. 79) as:

$$F = \begin{bmatrix} f_0 & f_1/\lambda & f_2/\lambda^2 EI & f_3/\lambda^3 EI \\ \lambda f_3 & f_0 & f_1/\lambda EI & f_2/\lambda^2 EI \\ \lambda^2 EI f_2 & \lambda EI f_3 & f_0 & f_1/\lambda \\ \lambda^3 EI f_1 & \lambda^2 EI f_2 & \lambda f_3 & f_0 \end{bmatrix}$$

Note that once again the inherent structural damping of the skin material may be included by introducing a complex flexural stiffness EI =

$E'I(1 + i\delta)$ where $E'$ is the real part of the complex elastic modulus and $\delta$ is the structural damping ratio.

c) Transfer Matrix of a Single Beam Element

Fig. 84 shows the left hand half of the beam under consideration. This is built up of three beam elements, each consisting of a skin bay attached to a stringer. Hence the transfer matrix A for one such element is given by:

$$A = F.P$$

The elements of A are shown below:

$$a_{11} = f_0 + f_3 Q/\lambda^3 EI \qquad a_{21} = \lambda f_3 + Q f_2/\lambda^2 EI$$

$$a_{12} = f_1/\lambda + C f_2/\lambda^2 EI \qquad a_{22} = f_0 + C f_1/\lambda EI$$

$$a_{13} = f_2/\lambda^2 EI \qquad a_{23} = f_1/\lambda EI$$

$$a_{14} = f_3/\lambda^3 EI \qquad a_{24} = f_2/\lambda^2 EI$$

$$a_{31} = \lambda^2 EI f_2 + Q f_1/\lambda \qquad a_{41} = \lambda^3 EI f_1 + Q f_0$$

$$a_{32} = \lambda EI f_3 + C f_0 \qquad a_{42} = \lambda^2 EI f_2 + C\lambda f_3$$

$$a_{33} = f_0 \qquad a_{43} = \lambda f_3$$

$$a_{34} = f_1/\lambda \qquad a_{44} = f_0$$

The foregoing transfer matrix for a single beam element is applicable to any structure with an odd number of stiffeners and equal width skin bays. Another commonly occuring configuration is that with an even number of stiffeners and half width skin bays at the edges. For this type of structure is it convenient to use a transfer matrix describing a single element which consists of a full stiffener with damper, on either side of which is attached a half skin bay width piece of skin, i.e. $A' = F^{\frac{1}{2}} P F^{\frac{1}{2}}$. The transfer matrix $A'$ of this element is more complex than the previous matrix A, but using the same definitions as before the elements $a'_{ij}$ are as follows:

$$a'_{11} = \frac{f_0 f_3 Q}{\lambda^3 EI} + \frac{f_2 f_3 C}{\lambda EI} + (f_0^2 + 2 f_1 f_3 + f_2^2)$$

$$a'_{12} = \frac{f_1 f_3 Q}{\lambda^4 EI} + \frac{f_0 f_2 C}{\lambda^2 EI} + \frac{2}{\lambda}(f_0 f_1 + f_2 f_3)$$

$$a'_{13} = \frac{f_2 f_3 Q}{\lambda^5 E^2 I^2} + \frac{f_1 f_2 C}{\lambda^3 E^2 I^2} + \frac{1}{\lambda^2 EI}(2 f_0 f_2 + f_1^2 + f_3^2)$$

$$a'_{14} = \frac{f_3^2 Q}{\lambda^6 E^2 I^2} + \frac{f_2^2 C}{\lambda^4 E^2 I^2} + \frac{2}{\lambda^3 EI}(f_0 f_3 + f_1 f_2)$$

$$a'_{21} = \frac{f_0 f_2 Q}{\lambda^2 EI} + \frac{f_1 f_3 C}{EI} + 2\lambda(f_0 f_3 + f_1 f_2)$$

$$a'_{22} = \frac{f_1 f_2 Q}{\lambda^3 EI} + \frac{f_0 f_1 C}{\lambda EI} + (2 f_1 f_3 + f_0^2 + f_2^2)$$

$$a'_{23} = \frac{f_2^2 Q}{\lambda^4 E^2 I^2} + \frac{f_1^2 C}{\lambda^2 E^2 I^2} + \frac{2}{\lambda EI}(f_2 f_3 + f_0 f_1)$$

$$a'_{24} = \frac{f_2 f_3 Q}{\lambda^5 E^2 I^2} + \frac{f_1 f_2 C}{\lambda^3 E^2 I^2} + \frac{1}{\lambda^2 EI}(f_3^2 + 2 f_0 f_2 + f_1^2)$$

$$a'_{31} = \frac{f_0 f_1 Q}{\lambda} + \lambda f_0 f_3 C + \lambda^2 EI (2 f_0 f_2 + f_3^2 + f_1^2)$$

$$a'_{32} = \frac{f_1^2 Q}{\lambda^2} + f_0^2 C + 2\lambda EI (f_1 f_2 + f_0 f_3)$$

$$a'_{33} = \frac{f_1 f_2 Q}{\lambda^3 EI} + \frac{f_0 f_1 C}{\lambda EI} + (f_2^2 + 2 f_1 f_3 + f_0^2)$$

$$a'_{34} = \frac{f_1 f_3 Q}{\lambda^4 EI} + \frac{f_0 f_2 C}{\lambda^2 EI} + \frac{2}{\lambda}(f_2 f_3 + f_0 f_1)$$

$$a'_{41} = f_0^2 Q + \lambda^2 f_3^2 C + 2\lambda^3 EI (f_0 f_1 + f_2 f_3)$$

$$a'_{42} = \frac{f_0 f_1 Q}{\lambda} + \lambda f_0 f_3 C + \lambda^2 EI (f_1^2 + 2 f_0 f_2 + f_3^2)$$

$$a'_{43} = \frac{f_0 f_2 Q}{\lambda^2 EI} + \frac{f_1 f_3 C}{EI} + 2\lambda(f_1 f_2 + f_0 f_3)$$

$$a'_{43} = \frac{f_0 f_3 Q}{\lambda^3 EI} + \frac{f_2 f_3 C}{\lambda EI} + (2 f_1 f_3 + f_2^2 + f_0^2)$$

Note that all the fi functions in the above should be determined using a value of $\ell = \ell/2$ for this case. Also it can be seen that the constant

term (not involving Q or C) may be more easily written, in terms of the FF functions defined in Appendix V. Since the element described by the above transfer matrix is symmetrical and transfers from left to right are the same as those from right to left, the matrix is cross-symmetric e.g. $a_{11} = a_{44}$ etc. This can be used as a monitor on any computations performed to produce the matrix numerically, and is an easy way of checking the accuracy of the machine used for computations of larger transfer matrices for systems consisting of several such elements connected together, describing multi-span systems.

VI.2.2 Development of Frequency Response Functions

The response of a structure subject to excitation either deterministic or random, can be described by using one of the following two basic functions (Ref. 80):

the impulse response function $h_{pq}(w)$

the frequency response function $H_{pq}(w)$

Considering the latter of these two, the meaning of the function is as follows. Assuming the structure to be damped and subject to a unit sinusoidally varying load ($e^{iwt}$) applied at a point on the structure q, then the response at a point p, is $Hpq\ (w)\ e^{iwt}$. For an aribitrary forcing function Pq(t) at q it can be shown that the response Rp(t) at p can be expressed in terms of Hpq(w) and a spectral analysis of Pq(t):

$$Rp\ (t) = \int_{-\infty}^{\infty} \overline{Pq}(w)\ Hpq(w) e^{iwt} dw$$

where $$\overline{Pq}(w) = \frac{1}{2\pi} \int_{-\infty}^{\infty} P_q(t) e^{-iwt} dt$$

Thus the response of a structure excited by a unit harmonic force can be directly related to the response of the same structure subject to an arbitrary forcing function. Hence the study of the effect of an artificial damping treatment on the response of structures forced by unit harmonic excitation gives a direct indication of the damping effect under conditions of arbitrary excitation. Note that for a quantitative comparison of different damping treatments suitable criteria have to be

formed in accordance with the type of motion involved, as suggested by Mead (81).

In order to develop the frequency response functions for the particular beam under consideration it is necessary to define a clear notation system for the matrices and state vectors used in the theory. Basically transfer matrices are indicated in general by the letter T enclosed in parenthesis e.g. (T) and state vectors are enclosed in square brackets with the general letter $[Z]$. Superscripts refer to the direction of transfer matrices whilst subscripts refer to the points between which a transfer takes place.

The superscripts and subscripts are read in a clockwise direction starting at the upper left hand corner of the array. For example ${}^{l}_{k}(A)^{r}_{j}$ is interpreted as a field transfer matrix A transfering the state vector from the left of point j to the right of point k. The term $[Z]^{r}_{k}$ is interpreted as the state vector at a position just to the right of k.

Consider unit harmonic inputs of shear force and bending moment at the point j in Fig. 84. By specifying suitable boundary conditions at the point N and utilising the symmetry of the beam it is possible to obtain all the symmetric and anti-symmetric modes of response for the six bay beam from consideration of the three bays shown in Fig. 84.

Then
$$[Z]^{l}_{j} = {}^{l}_{j}(T)^{l}_{o} \; [Z]^{r}_{o}$$

$$[Z]^{r}_{j} = [Z]^{l}_{j} + \begin{bmatrix} 0 \\ 0 \\ 1 \\ 1 \end{bmatrix}$$

$$= {}^{l}_{j}(T)^{l}_{o} \; [Z]^{r}_{o} + \begin{bmatrix} 0 \\ 0 \\ 1 \\ 1 \end{bmatrix} \quad - \quad (1)$$

Now
$$[Z]^{r}_{k} = {}^{r}_{k}(T)^{r}_{j} \; [Z]^{r}_{j}$$

$$= {}^{r}_{k}(T)^{r}_{o} \; [Z]^{r}_{o} + {}^{r}_{k}(T)^{r}_{j} \begin{bmatrix} 0 \\ 0 \\ 1 \\ 1 \end{bmatrix} \quad \text{from (1)}$$

Substituting for the boundary conditions at the point O:-

$$[Z]^{r}_{k} = {}^{r}_{k}(T)^{r}_{o} \begin{bmatrix} 0 \\ 0 \\ M \\ V \end{bmatrix}^{r}_{o} + {}^{r}_{K}(T)^{r}_{j} \begin{bmatrix} 0 \\ 0 \\ 1 \\ 1 \end{bmatrix} \quad - \quad (2)$$

The overall transfer matrix equation is:-

$$[Z]^{r}_{\eta} = {}^{1}_{n}(T)^{r}_{o} [Z]^{r}_{o} + {}^{1}_{n}(T)^{r}_{j} \begin{bmatrix} 0 \\ 0 \\ 1 \\ 1 \end{bmatrix}$$

Substituting for the boundary conditions at N in $[Z]^{r}_{n}$ for the symmetric modes leads to:

$$\begin{bmatrix} X \\ 0 \\ M \\ 0 \end{bmatrix}^{r}_{n} = {}^{1}_{n}(T)^{r}_{o} \begin{bmatrix} 0 \\ 0 \\ M \\ V \end{bmatrix}^{r}_{o} + {}^{1}_{n}(T)^{r}_{j} \begin{bmatrix} 0 \\ 0 \\ 1 \\ 1 \end{bmatrix} \quad - \quad (3)$$

Using $t_{ij}$ as the individual elements of the transfer matrices, the following equations can be extracted:

$$\begin{bmatrix} 0 \\ 0 \end{bmatrix} = {}^{1}_{n}\begin{bmatrix} t_{23} & t_{24} \\ t_{43} & t_{44} \end{bmatrix}^{r}_{o} \begin{bmatrix} M \\ V \end{bmatrix}^{r}_{o} + {}^{1}_{n}\begin{bmatrix} t_{23} & t_{24} \\ t_{43} & t_{44} \end{bmatrix}^{r}_{j} \begin{bmatrix} 1 \\ 1 \end{bmatrix}$$

Thus $$\begin{bmatrix} M \\ V \end{bmatrix}^{r}_{o} = - {}^{1}_{n}\begin{bmatrix} t_{23} & t_{24} \\ t_{43} & t_{44} \end{bmatrix}^{r-1}_{o} {}^{1}_{n}\begin{bmatrix} t_{23} & t_{24} \\ t_{43} & t_{44} \end{bmatrix}^{r}_{j} \begin{bmatrix} 1 \\ 1 \end{bmatrix}$$

Now substitute for $\begin{bmatrix} M \\ V \end{bmatrix}^{r}_{o}$ in (2)

from this equation:

$$[Z]^{r}_{k} = -{}^{r}_{k}(T)^{r}_{o} {}^{1}_{n}\begin{bmatrix} t_{23} & t_{24} \\ t_{43} & t_{44} \end{bmatrix}^{r-1}_{o} {}^{1}_{n}\begin{bmatrix} t_{23} & t_{24} \\ t_{43} & t_{44} \end{bmatrix}^{r}_{j} \begin{bmatrix} 1 \\ 1 \end{bmatrix}$$

$$+ {}^{r}_{k}(T)^{r}_{j} \begin{bmatrix} 0 \\ 0 \\ 1 \\ 1 \end{bmatrix} \quad - \quad (4)$$

A similar equation can be produced for the case of antisymmetric modes by altering the boundary conditions in (3). This leads to the same

equation as above with $t_{13}$, $t_{14}$, $t_{33}$, $t_{34}$ replacing $t_{23}$, $t_{24}$, $t_{43}$, $t_{44}$ respectively.

From consideration of Fig. 84 it can be seen that the transfer matrices in the above equation are given by:

$$ {}^{r}_{k}(T)^{r}_{o} = (A)^{2} = (B) \text{ say with elements } b_{ij} $$

$$ {}^{1}_{n}(T)^{r}_{o} = (A)^{3} = (C) \text{ say with elements } C_{ij} $$

$$ {}^{r}_{k}(T)^{r}_{j} = (A) $$

It can also be shown that ${}^{1}_{n}(T)^{r}_{j} = (A)^{2} = (B)$

In order to avoid some of the numerical difficulties encountered when evaluating transfer matrices, (see for example Ref. 82) it was decided to develop the elements of the above matrices directly by algebraic methods, rather than evaluate the (A) matrix numerically and then relying on the accuracy of a matrix multiplication routine. The elements of (B) are given in Appendix V. The four elements of (C) required for the calculation of the displacement response at k due to a unit shear force at j were calculated numerically from values of $b_{ij}$. This particular frequency response function was chosen as being the closest in similarity to the single point excitation tests carried out on the panel with the various shear damping beams attached. Referring to equation (4) and considering a zero applied moment and unit applied shear:

$$ [Z]^{r}_{k} = -(B) \begin{bmatrix} C_{23} & C_{24} \\ C_{43} & C_{44} \end{bmatrix}^{-1} \begin{bmatrix} b_{23} & b_{24} \\ b_{43} & b_{44} \end{bmatrix} \begin{bmatrix} 0 \\ 1 \end{bmatrix} + (A) \begin{bmatrix} 0 \\ 0 \\ 0 \\ 1 \end{bmatrix} $$

$$ = -(B) \frac{\begin{bmatrix} -C_{44} & C_{24} \\ C_{43} & -C_{23} \end{bmatrix}}{\left(C_{43}\,C_{24} - C_{23}\,C_{44}\right)} \begin{bmatrix} b_{24} \\ b_{44} \end{bmatrix} + \begin{bmatrix} a_{14} \\ a_{24} \\ a_{34} \\ a_{44} \end{bmatrix} $$

From equation (2) it can be seen that only the third and fourth columns of ${}^{r}_{k}(T)^{r}_{o}$ are significant, thus (B) in the above equation reduces to to a 4 x 2 matrix consisting of the third and fourth columns of (B).

Hence we have:

$$[Z]^r_k = - \begin{bmatrix} b_{13} & b_{14} \\ b_{23} & b_{24} \\ b_{33} & b_{34} \\ b_{43} & b_{44} \end{bmatrix} \frac{\begin{bmatrix} -C_{44} & b_{24} + C_{24} & b_{44} \\ C_{43} & b_{24} - C_{23} & b_{44} \end{bmatrix}}{(C_{23}\, C_{24} - C_{23}\, C_{44})} + \begin{bmatrix} a_{14} \\ a_{24} \\ a_{34} \\ a_{44} \end{bmatrix}$$

This 4 x 1 matrix equation gives the value of the state vector just to the right of k. We desire only the displacement at k, thus only the first element of $[Z]^r_k$ has to be calculated. The displacement $X^r_k$ for a sliding support at the centre of the beam is given by:

$$X^r_k \ (SL) = \frac{b_{13}\,(C_{44}\, b_{24} - C_{24}\, b_{44}) - b_{14}\,(C_{43}\, b_{24} + C_{23}\, b_{44})}{(C_{43}\, C_{24} - C_{23}\, C_{44})} + a_{14}$$

Similarly for the case of a simple support at the centre of the beam we have:

$$X^r_k \ (S\ S) = \frac{b_{13}\,(C_{34}\, b_{14} - C_{14}\, b_{34}) - b_{14}\,(C_{33}\, b_{14} + C_{13}\, b_{34})}{(C_{33}\, C_{14} - C_{13}\, C_{34})} + a_{14}$$

VI.2.3 Numerical Results

The above equations were programmed on a digital computer (I.C.L. 1907 and later I.B.M. 360) for numerical evaluation. A listing of this computer program is given in the back of Appendix V together with an explanation of the data input required and the symbols used to represent the various structural parameters.

The results of the numerical computation are plotted in Figs. 85 and 86. These show the displacement response due to a unit shear force over a frequency range 100 - 1000 Hz. The two figures 85 and 86 show the response in the symmetric and anti-symmetric type modes respectively. The untreated response, calculated assuming a structural damping ratio of .005, shows the expected multi-modal behaviour with peaks corresponding to modes 1 and 3 in Fig. 85 and peaks corresponding to modes 2 and 4 in Fig. 86. The usual order of occurrence of modes with increasing frequency is seen to occur. The calculated response of the structure with various shear damping beam additions shows a complex pattern, only

recognizable by studying the effect of very small damping additions. Initially the damping parameters for a 25 mm (1") wide shear damping beam with a viscoelastic core of thickness 0.711 mm (.028"), were used. Damping material properties were approximated to those found in the previous shear damping tests, VIz $G' = 2.07 \times 10^6$ n/m$^2$ (300 lb/in$^2$), $\eta = 0.00051w + 0.240$, where w is excitation frequency in Hz. The result for this case is shown by the line labelled D in the two figures. Both cases of anti-symmetric and symmetric modes show no real evidence of resonant behaviour for this amount of additive damping. However the response levels are considerably reduced compared to the untreated resonant peaks. From previous experience of beams cut from integral panels (31) where it was found necessary to reduce the damping additive to very small dimensions to obtain a recognizable resonant response, it was decided to simulate shear damping beams of reduced width (actually 6.25 mm - $\frac{1}{4}$" and 3.125 mm - $\frac{1}{8}$" wide) in order to obtain a damped resonant type response. These results are shown in Figs. 85 and 86 by the curves labelled $\frac{1}{4}$ D and $\frac{1}{8}$ D, being the results of applying shear damping beams of a quarter and one eighth the width of the "standard" beam.

It can be seen that reducing the beam width does indeed result in the familiar damped multi-modal type response. The resonant frequencies of all modes are increased due to the stiffening effect of the shear damping mechanism whilst the peak amplitudes are increased with the lesser damping. The overall effect of increasing the artificial damping seems to be to reduce the resonant peaks whilst "filling in" the troughs between them. In the case of the "D" line the resonant peaks are completely removed whilst trough filling is so great that the response is actually increased in many cases. This effect has been observed in the full scale tests of Section V.3 involving a curved aircraft skin panel. Two further curves labelled $\frac{1}{2}\eta$, $2\eta$ are plotted in Figs. 85 and 86. These correspond to beams of width 3.125 mm ($\frac{1}{8}$") having visco-elastic cores with loss factors half and twice that of the "standard"

beam, respectively. These curves show the expected effect that increased loss factor leads to reduced response over the whole frequency range with no additional trough filling, ignoring frequency shifting effects.

Comparison of Figs. 85 and 86 shows that the damping mechanism is more effective in antisymmetric modes than symmetric modes. This is as expected since there is greater stringer rotation in the anti-symmetric type modes and the assumed damping mechanism relies entirely on such rotation to transmit shear strains to the viscoelastic core of the damper. The difference in performance of the shear damper in the two different types of modes is such that the optimum damper will probably have to be chosen to suit the user. If overall damping is required in all modes, a compromise will have to be made, whereas if it is necessary only to damp one mode in particular, then the computer program can be used to obtain the largest response reduction at a particular frequency. In conclusion, the shear damping beam has such a complex effect that it is suggested that a range of possibilities are tried for any particular structural response problem and the best compromise configuration chosen for the practical application. For example, for the structural response illustrated in Figs. 85 and 86, if it is desired to damp out all the modes, then the optimum damper configuration would be $\frac{1}{3}$ D. It should also be noted that quite large changes in the damping parameters have relatively little change on the response. Thus slight inaccuracies in the manufacture, or selection of a non-optimum beam, will not drastically affect the response.

No attempt was made to compare directly the results of this theory with the measured experimental response reductions following the application of a shear damping beam. There were several reasons for this, the major one being the lack of information regarding the loss factor of the bare panel. Some attempts were made to measure this using the Kennedy-Pancu technique, but were unsuccessful due to the lack of suitable phase matched amplifiers for the transducer signals. Later experiments

on the full scale three bay specimen described in Section V.3 were more successful and the overall panel loss factor was measured in a number of modes from several different transducers. Despite the considerable precautions taken to eliminate experimental error, the scatter in the results was considerable. However an overall mean value of approximately .005 was obtained, and since the type of construction of the full-scale and laboratory test panel was similar, it was decided to use this value as being the most typical and reliable yet obtained. With this low level of damping, small changes in loss factor lead to substantial changes in response. Thus due to the uncertainty of the value of the real loss factor of the laboratory experimental panel, it was felt that any comparisons could be considerably in error. The reductions in the resonant peaks for a three fold increase in beam material structural damping are shown by the points for SI = .0015 in Figs. 85 and 86 to illustrate this. It can be seen that the resonant response is reduced to approximately 1/3 of the previous response for SI. = .005.

The damping modelled by this theory consists essentially of an additional complex rotational stiffness acting on the base of the stringers. Referring to Fig. 83, the real and imaginary parts of this stiffness are:- $\frac{h^2 A.G'}{t}$ and $\frac{h^2 A.G'\eta}{t}$ respectively. In Figs. 85 and 86 the curve D corresponds to values of these quantities arising from the application of a "standard" 25 mm (1") wide shear damping beam. Previously it was stated that the curves $\frac{1}{4}$D, $\frac{1}{8}$D etc. corresponded to beams of a quarter and one eighth the width of a "standard" beam. Consideration of the damping in terms of the equivalent complex rotational stiffness as above shows that these curves are also applicable to beams with cores 4 times and 8 times as thick as a standard one. There are other combinations of damping properties which will give the same result.

Essentially the D value is proportional to:

the height of the stringers squared

the area of the lower constraining plate attached to the stringer

the real part of the viscoelastic core's shear modulus

and inversely proportional to the core thickness.

Since any combination of the above properties can be used to obtain the optimum D value, and since a higher loss factor always results in an overall response reduction, it pays to choose a material for its high loss factor in preference to its other properties, in order to obtain the largest response reduction over the whole frequency range. It is interesting to note from the shear damping tests that the loss factor of the silicone rubber used as a viscoelastic core, increases with rising temperatures. Thus the performance of such a shear damping beam in a real aircraft environment should be improved in the major high temperature portion of the flight envelope.

VI.2.4. Comments on the Transfer Matrix Model

It has been stated previously that the beam transfer matrix analysis was not intended to give accurate response predictions due to the relative simplicity of the model used. The disadvantages and inaccuracies of the model can be summarised as follows:

a) In order to reduce the complexity of the problem to a minimum, use was made of the symmetry of the system by considering only the left-hand half of the beam. Appropriate boundary conditions (sliding and pinned) were applied at the centre of the panel to give the results for symmetric and anti-symmetric modes respectively. Hence the calculated responses could only be considered accurate close to a resonant peak, the intermediate response being inaccurate due to incorrect boundary conditions at the centre. To obtain the off-resonance or intermediate response it would be necessary to combine the two calculated responses in such a way as to give the appropriate boundary condition at the centre. This would be very difficult and the only real way to obtain an accurate total response would be to model the whole beam from frame to frame.

b) Also associated with the use of symmetry is the fact that the portion of beam considered was not exactly half that of the whole beam. In order

to use the elemental transfer matrix only, it was necessary to omit a full width stringer and shear damper at the centre of the six span array. For perfect symmetry there should have been a half width stringer and damper at the centre; however to use this would have involved the development of another transfer matrix, a complication not thought worthwhile at this stage.

c) In any calculation of responses the effect of the boundary conditions at the frames is very important. In the beam analysis the only possible conditions where those involving zeros of either displacement, slope, bending moment or shear force and combinations of these with zero values. It is very doubtful whether the real boundary conditions could be adequately described by these means, hence the calculated response could be in considerable error due to insufficient accuracy in specifying the boundary conditions.

The transfer matrices of two basic damped beam elements have been developed which cover the two most commonly occuring cases of stiffened structures, i.e. even numbers of stringers with a full width skin bay at the panel edge and odd number of stringers with a half width skin bay at the panel edge. Frequency response functions have only been developed for the even number of stringers case, as this corresponded to the experiments performed on the real panel. It would be interesting to see if the computed behaviour of the damped system for the odd numbers of stringers case is similar to the behaviour of the case already computed, and if experimental evidence were made available by further tests on a different test panel, whether the correlation between experimental and theoretical behaviour patterns is similar to that obtained for the even number of stringers case.

In all the above theory only the direct shearing component of damping has been included in the point transfer matrices since the flexural component has been shown to be small (see Section VI.1.1.). However if it was desired to include the flexural component, (as in a

curved panel analysis perhaps) this could easily be achieved by adding the component of shear force necessary to drive the damped beam, to the Q term in the point transfer matrix.

# VII. CONCLUSIONS

## VII.1 Discussion and Suggestions for Further Work

### VII.1.1 Material Properties

The shear damping tests to determine basic material properties were somewhat difficult to carry out at sub-ambient temperatures due to the rather basic cooling system used. Since the over-pressure required to force the liquid nitrogen coolant around the copper coil was only of the order .14 x $10^4 n/m^2$ (2 $lb/in^2$), this was mostly achieved by the natural boiling off of the coolant in the resevoir. The small additional pressure required was also difficult to control as the smallest regulator available was a 0 - 2 x $10^5 n/m^2$ (0-30 $lb/in^2$) unit. Hence the control of temperature was a rather difficult task, the ability to repeat an identical temperature being virtually impossible. To avoid these difficulties in any future tests, serious thought should be given to the construction of a better quality environmental chamber with a thermostatically controlled flow of coolant. This would be more expensive than the system used previously, but if tests on several materials are planned, would more than pay for itself in time saving and the ability to accurately repeat test conditions.

From the shear damping tests at room temperature, showing the frequency dependence of the loss factor and shear modulus, linear approximations were formed for incorporation in the theoretical analyses. Due to the simplicity of the theoretical models of the structure used, it was not thought worthwhile to increase the accuracy of these mathematical models for loss factor and shear modulus as suggested by Ref. (83). However it is thought that a valuable extension to the work could be made by forming simple mathematical models for the temperature dependences of the dynamic material properties and incorporating these into the theoretical structural response calculations. The behaviour

of the damped system could then be evaluated in a more realistic environment than one of standard room temperature.

VII.1.2 Panel Response Experiments

Transducers

In most of the panel response tests accelerometers were used in preference to strain gauges for monitoring the response. The main reason for this was that the accelerometers could be easily moved to a different part of the panel since they were only attached by a thin layer of wax. The disadvantage of using accelerometers in this way is that the resulting signals are proportional to both the panel displacement and the square of the excitation frequency. When plotting mode shapes where all signals are of the same frequency, then acceleration is only proportional to the displacement and the accelerometer signals can be used directly without modification in plotting the mode shapes as in Figs. (62-69). However when comparing undamped and damped responses where the resonant frequencies are increased by the addition of a shear damping beam, a correction must be applied. Since the main interest is in reducing the resonant displacement and hence stress peaks, the correction can be made by inclining the frequency axis of the acceleration plot upwards at 6db/octave. Measurement of the height of peaks above this axis will then give a direct indication of the magnitude of the displacement at that frequency. Alternatively, this can be stated in the following manner:- If corresponding undamped and damped acceleration resonant peaks of magnitude $R_{ud}$ and $R_d$ respectively, occur at frequencies $W_{ud}$ and $W_d$ where $W_d > W_{ud}$, then to calculate the displacement or stress reduction due to the addition of the damper it is not sufficient to use the ratio $R_d/R_{ud}$. This ratio must be modified to correct for the frequency shift by a factor of $(W_{ud}/W_d)^2$. Thus displacement reduction

$$= \frac{R_d}{R_{ud}} \left(\frac{W_{ud}}{W_d}\right)^2 .$$

Reference to the final column of Table V.2.3 gives the estimated stress reduction using this type of correction.

Choice of measured parameters

It will be noted that the emphasis has been placed on predicting or measuring the response reductions rather than the increase in values of loss factor due to the application of an artificial damping treatment. There are two main reasons for this. Firstly it was thought that in a real engineering application the designer would prefer to have information on the direct response reduction resulting from the application of a particular size damper rather than have some estimate of the change in loss factor which would then have to be used in a further calculation to obtain response levels. Secondly the measurement and interpretation of loss factor is made very difficult by the presence of even small non-linearity. Newman et al (Ref. 84) have shown that for a small stiffness non-linearity composed of a cubic hardening spring, where the natural frequency of a single degree of freedom system is increased by 2% due to the stiffness non-linearity, the apparent loss factor, as measured from a vector response plot, is reduced to 80% of its true value. Thus any measured loss factors for correlation with theory could be considerably in error. In addition most theoretical estimates of damped response make the assumption that damping is small and certain terms in the equations can be ignored. This is inadequate when artificial damping is added as the desire is to increase the loss factor to the maximum possible value. Measurements of loss factor made by measuring the width of resonant peaks are also likely to be considerably in error as even the smallest non-linearity affects the symmetry of resonant peaks. If values of loss factor are required for use in other theoretical estimates, the technique developed by Wright (71) may be use ful as it avoids the difficulties encountered with vector plots and width of peaks measurement, by relying on a logarithmic decrement approach. This is obviously more closely related

to direct response reduction type measurements and consists of performing two successive Fourier transforms on the digitised response signal when the structure is excited by a rapid sine sweep signal. The Fourier transforms are performed at times t = 0 and t = $\Delta$t. By measuring the height of corresponding peaks in the two Fourier transform curves and knowing the time delay between the transforms, the damping of that particular mode can be estimated. This is particularly useful for multi-modal response as the individual modal loss factors can be determined from a single test.

Application to curved panels

Almost all the experiments and all the theoretical analyses performed have been for the case of flat panels. The only exception was in one of the full scale tests on a three bay curved fuselage panel. In this case the response reductions obtained were not as great as was expected. A possible explanation for this has been suggested to the effect that since the shear damping beam was curved to fit onto the curved panel specimen, buckling rather than direct core shearing may have taken place. It is thought that more work on this aspect would be valuable to determine whether or not the basic damping mechanism is changed for the case of curved panels. Also although the flexural effects of the shear damping beam have been shown to be small compared to the direct shearing effect, if direct shearing is no longer possible for curved panels, the possibility of optimising the flexural effects by correct choice of shear parameter etc. (see Ref. 72) should be investigated.

VII.1.3 Transfer Matrix Method

The transfer matrix analysis described previously utilised the similarity that had been observed between the behaviour of a beam on many elastic supports and a stiffened panel, to give an insight into the effect of added damping. This model of the plate is a fairly crude one only chosen to give an idea of the effects involved and not to result in

accurate response predictions. However, having shown that the artificial added damping of a shear damping beam can be successfully incorporated in a transfer matrix analysis and give sensible response values, the analysis could be fairly easily extended to the full plate case. The transfer matrices for skin bays and stringers have already been developed by Mercer and Seavey (76), the additional complex terms due to the artificial damping are easily added to the appropriate elements of the stringer point transfer matrix. Certain assumptions would have to be made to make the computation feasible however. The usual boundary condition of simple supports at the frames would have to be applied to allow separation of variables and subsequent development of the skin field transfer matrix. The damping force would have to be assumed to act uniformly over the length of the stringer free edge rather than over a small length in the centre of the panel as occurs in practice. This may not be too drastic a change if the application of two beams is used, (one above and one below the panel centre line, to reduce local stringer distortion yet still achieve significant shear strain in the viscoelastic cores and give more uniform response reductions over the whole area of the plate). The resulting computation would involve considerable complex arithmetic with the usual requirement in transfer matrix analysis of a high degree of accuracy to overcome the problems of ill conditioning of the matrices involved. This facility of double precision complex arithmetic is available increasingly on computers and should not be too difficult a problem to overcome. Associated with the complex arithmetic is the fact that the value of the frequency determinant will no longer be a real number which changes sign at the points where a resonant frequency occurs. Instead the value will be a complex one and the resonant frequencies will be associated with minima of the modulus of this number. In order to calculate the values of the resonant frequencies accurately enough for subsequent back-substitution to obtain mode shapes and resonant responses, it will be necessary to develop a stable routine

for locating these minima to a good degree of accuracy. Experience shows that location of the positions of the minima has to be within 0.1Hz of the natural frequency for reasonable mode shape results.

## VII.2 Conclusion

### VII.2.1 Shear Damping Tests

The shear damping measurement technique which has been developed has been shown to be a reliable method of determining the dynamic properties of various viscoelastic materials. The method overcomes the problem of true separation of the relevant variables and accurately demonstrates the true frequency, temperature and strain dependencies of the dynamic properties of the materials. Repeatable results were easily obtainable for most values of the relevant variables. The only exceptions to this were for high strain levels which were limited by the maximum force available from the vibrator, and for sub-ambient temperatures where accurate control of temperature and hence repeatability of environmental conditions was difficult,due to the simple cooling system used. Suggestions are made to improve on the basic system used by incorporating a coolant pump. Although all the shear damping tests described were carried out with the rubber material of the specimen moulded in situ, it is possible to use a similar type of specimen for materials which require a separate adhesive bond. Bolted up specimen 'U' blocks were made to confirm the viability of the method for sheets of viscoelastic material attached to the various parts of the block with cold curing adhesive. Apart from the effect of the adhesive these tests proved that this system was equally effective, and thus could be used for the wide range of pre-vulcanized materials available.

Of the materials tested, the flourinated silicone rubber seems to have the best properties for a general aircraft application. From the results of tests on this material with varying amounts of additional filler, it appears that the optimum volume for maximum loss factor may

be slightly less than the basic +20% Aerosil used in the initial tests. With further additions of filler the shear modulus is increased whilst the loss factor drops slightly. This may however prove a useful technique in optimising the material properties for sandwich beam applications where it is desired to maximise the flexural effects by the correct choice of shear parameter (as in the curved panel case mentioned in the previous section). Some experimentation was undertaken varying the curing technique and choice of catalyst when moulding the specimens. However this was mainly done to obtain a good bond between the rubber and aluminium after initial failures and it is thought that further investigation along these lines may result in improved dynamic properties also.

VII.2.2 Shear Damping Beams

The method of attachment of the shear damping beams to the stringer tips would certainly have to be improved in a real application. In all the experiments the lower constraining plates of the shear damping beams were simply bonded to the stringer free edges with an epoxy resin compound. Although no problems with these joints were encountered in any of the experiments, it is thought that they would prove inadequeate in a prolonged vibration environment. Hence it is suggested that in any future application the lower constraining plate should incorporate a stringer cap consisting of an inverted "U" shaped slot cut from the centre of a small block attached securely to the lower constraining plate. The whole assembly including lower constraining plate would be best made from a single piece of aluminium either by extrusion or by machining from solid if small quantities were required. The cap would fit snugly over the stringer tip and the adhesive used would only be subject to direct compressive stresses, which should prevent premature failure.

Theoretical investigations on a single beam type element model of the panel have shown that the direct shear damping effect is the major

mechanism contributing to the reduction of response. The effects due to shear strains induced in the viscoelastic core by flexure of the damping beam have been shown to be small in comparison to the direct shearing mechanism. Using this information it has been shown to be theoretically possible to incorporate both significant amounts of inherent structural damping and the effects of direct shear damping due to an artificial treatment in a transfer matrix analysis of the panel. This was achieved by using a complex number notation system in a periodically supported beam transfer matrix analysis of the panel. This relatively simple model demonstrated that the shear damping system can be optimised for a particular panel. Thus in any future applications of the system this optimisation should be performed to obtain the best performance for a particular case. No detailed comparisons were made between theory and experiment for reasons stated previously in VI.2.4. However the trends predicted by the theory are followed by the experimental results. The best performance was obtained from a beam having the smallest core thickness, although the variation in performance with differing shear damping beam parameters was small. This was confirmed by the theory where quite large changes in data input were required to significantly affect the response curves.

VII.2.3 Fatigue and Crack Propagation

Some fatigue data is available for integral panels and it is thought that a panel with a shear damping beam attached should be subjected to a similar test. This would confirm whether or not the resulting improvement in life corresponds to the reduction in stress measured in response tests and to see if the same S/N curve can be used for damped as well as undamped panels. This knowledge is essential for a deeper understanding of the mechanisms of acoustic fatigue and possible means of alleviating the problem. In addition a fatigue test on a damped integral panel would prove the fatigue resistance of the attachment system for the shear damping beam. There is evidence to suggest that the failures caused by acoustic fatigue in integral panels

start with initial cracking at the free edges of the stringers. Looking at the mode shapes obtained with a single shear damping beam attached along the centre line of the panel, it can be seen that the extra restraint on the stringer causes additional lateral bending at the free edge. This bending combined with the stringer bending associated with normal plate vibration may increase the principal stresses at the free edge compared to a undistorted mode with the same normal panel displacement. To avoid this and obtain a less distorted mode to prevent premature failure, it is suggested that two shear damping beams could be applied either side of the panel centre line with the distance between them equal to their distance from the frames or panel edges (as in Section VII.1.3). To maintain a similar weight addition these two beams could be made only 12.5 mm ($\frac{1}{2}$ in) wide. The overall damping effect would be changed very little whilst a more uniform stress reduction over the whole panel would be achieved.

The reduction in stress achieved by the application of an artificial damping treatment is important not only in prolonging fatigue life, but also by reducing crack propagation rates. Recent work has shown that crack propagation rate is proportional to the applied dynamic stress raised to the power of four approximately. Thus even a small reduction in stress results in a considerable reduction in crack length growth. In the case of aircraft structures this is important since for air-worthiness requirements the structure is required to be fail safe for the period between inspections. Thus if crack propagation rates can be slowed down the period between inspections can be lengthened and costs reduced in proportion.

VII.2.4 Final Comments

Finally in conclusion from the work described, it has been shown practically that the shear damping beam using a fluorinated rubber viscoelastic core, when applied to typical integrally machined panels, is capable of reducing dynamic stresses by some 50% for a weight addition

of only 2%. The system is effective in all the lower order modes tested and the core material has been shown to have a satisfactory performance in a wide range of environments. It has been shown that the effects of inherent structural damping and additional artificial damping can be successfully incorporated in theoretical analyses of the response of panel systems. It is concluded that the method of shear damping beams should be particularly useful in improving the life of structures subjected to acoustic fatigue as well as being useful in more conventional fatigue and vibration situations.

APPENDIX I

List of Specimen Compsositions

Specimen 1 - Flourinated Silicone Rubber

Type LS 63 U Midland Silicone Polymer

2.6% by weight catalyst (Perkadox PD5 50) in silicone oil, active constituent.1.3% by weight Dichlorobenzoylperoxide, 20% by weight Aerosil 380 silicone filler.

Specimen 2 - Flourinated silicone rubber as above but with 23% by weight Aerosil 380 filler.

Specimen 3 - Flourinated silicone rubber as above but with 26% by weight Aerosil 380 filler.

Specimen 4 - Methyl-vinyl silicone rubber.

I.C.I. E302 Polymer

3% by weight Varox catalyst,

20% by weight Aerosil 380 silica filler.

## APPENDIX II

### Curing techniques for Specimens

Specimens 1, 2, 3.

Initial cure (moulding) 20 min. at 130°C

Post cure 8 hr. at 200°C

Specific gravity 1.46

Specimen 4

Initial cure (moulding) 1 hr. at 160°C

Post cure 8 hr. at 200°C

Single Slug

Initial cure (moulding) 40 min. at 130°C

Post cure 8 hr. at 100°C

8 hr. at 150°C

8 hr. at 200°C

All Shear Damping Beams

Initial cure (moulding) 20 min. at 130°C

Post cure 8 hr. increasing hourly from 40°C to 180°C in 20°C steps followed by 8 hr. at 200°C.

APPENDIX III

Consider the free body diagram of a single element of a shear damping beam as shown in the upper part of Fig. A.III, subscripts t, c, b, refer to the upper face plate, core and lower face plate respectively. Let the force applied to this element by the stringer tip be F. Then for overall equilibrium:-

$$2P_t + 2P_b + F = 0 \quad - \quad (1)$$

Consider the equilibrium of a small length of the upper constraining plate shown in the lower part of Fig. A.III. For internal equilibrium:-

$$\delta P_t = \tau \delta x \quad \text{thus} \quad \tau = \frac{dP_t}{dx} \qquad (2)$$

Also for small strains:

$$\gamma = \frac{U_t - U_b}{h_c} \quad \text{and} \quad \tau = G\gamma \text{ where G is}$$

the shear modulus of the core.

Hence $$\tau = \frac{G}{h_c} (U_t - U_b) \quad - \quad (3)$$

Define $\sigma_i$ and $\epsilon_i$ as the stresses and strains in the face plates and core. Then:

$$\frac{P_t}{h_t} = \sigma_t = E\epsilon_t = E\frac{du_t}{dx} \quad - \quad (4a)$$

$$\frac{P_b}{h_b} = \sigma_b = E\epsilon_b = \frac{E\,du_b}{dx} \quad - \quad (4b)$$

Where E is Young's Modulus for the face plates.

From (2) and (3), $$\frac{dP_t}{dx} = \frac{G}{h_c} (U_t - U_b)$$

Differentiating with respect to x:-

$$\frac{d^2P_t}{dx^2} = \frac{G}{h_c} \left( \frac{du_t}{dx} - \frac{du_b}{dx} \right)$$

From (4a) and (4b) :-

$$\frac{d^2P_t}{dx^2} = \frac{G}{h_c}\left(\frac{P_t}{Eh_t} - \frac{P_b}{Eh_b}\right), \text{using (1) to estimate } P_b \left(= \frac{-F}{2} - P_t\right),$$

$$\frac{d^2P_t}{dx^2} = \frac{G}{h_c}\left[P_t\left(\frac{1}{Eh_t} + \frac{1}{Eh_b}\right) + \frac{F}{2Eh_b}\right]$$

or $$\frac{d^2P_t}{dx^2} - \frac{G(h_t + h_b)}{E\,h_c h_t h_b} Pt = \frac{G.F}{2Eh_t h_b}$$

This has a solution of the form:-

$$P_t = A\cosh\beta x + B\sinh\beta x - \left(\frac{h_t}{h_t + h_b}\right)\cdot\frac{F}{2}$$

where $$\beta^2 = \frac{G(h_b + h_t)}{E\,h_c h_t h_b}$$

Boundary conditions:-

At $x = 0$, $P_t = 0$ (i)

At $x = \frac{L}{2}$, $P_t = -F/2$ (ii)

From (i) $$0 = A - \frac{h_t}{h_t + h_b}\cdot F/2 \text{ or } A = \frac{h_t}{h_t+h_b}\cdot F/2$$

From (ii) $$-F/2 = \frac{h_t}{h_t+h_b}\cdot F/2\cosh\beta\frac{L}{2} + B\sinh\beta\frac{L}{2} - \frac{h_t}{h_t+h_b}\cdot F/2$$

Thus $$B = F/2\left[\frac{h_t}{h_t + h_b} - 1 - \frac{h_t}{h_t + h_b}\cosh\beta\frac{L}{2}\right]\operatorname{cosech}\beta\frac{L}{2}$$

$$= F/2\left[\frac{h_t}{h_t + h_b}\left(1 - \cosh\beta\frac{L}{2}\right) - 1\right]\operatorname{cosech}\frac{\beta L}{2}$$

Thus we have as a solution:-

$$P_t = - \frac{h_t}{h_t + h_b} \cdot F/2 \left[ 1 - \cosh \beta x + \left( \cosh \frac{\beta L}{2} + \frac{h_b}{h_t} \right) x \right.$$

$$\left. \operatorname{cosech} \frac{\beta L}{2} \sinh \beta x \right]$$

If $\frac{\beta L}{2}$ is small, $\cosh \frac{\beta L}{2} \doteq 1$ and $\cosh \beta x \doteq 1$ since $x < L/2$

Then we have, $P_t = - \frac{h_t}{h_t + h_b} \cdot F/2 \left[ \frac{h_t + h_b}{h_t} \cdot \frac{2}{\beta L} \cdot \beta x \right]$

$$= - \frac{Fx}{L}$$

$$= - F/2 \text{ when } x = L/2$$

Thus if $\beta L/2$ is small the assumption of uniform shear stress over the lower constraining plate is justified. For a type 1 shear damping beam the parameters have the following values:-

$G = 300 \text{ lb/in}^2$

$E = 10 \times 10^6 \text{ lb/in}^2$

$h_t = h_b = .017 \text{ in}$

$h_c = .030 \text{ in}$

$L/2 = 1.4 \text{ in}$

Thus $\frac{\beta L}{2} = \frac{300}{10^7} \cdot \frac{0.034}{0.017^2 .0.030} \quad 1.4$

$$= 0.48$$

Thus $\cosh \frac{\beta L}{2} \doteq 1.11$

Hence the stress distribution varies by no more than approximately 5% between $x = 0$ and $x = L/2$

APPENDIX IV

Details of shear damping beams.

Face plates - light alloy equal thickness top and bottom.

Core - type LS 63U polymer + 20% Aerosil Filler.

| Beam Type | Face Plate Thickness | Core Thickness | Comments |
|---|---|---|---|
| 1 | 0.43 mm (.017in) | 0.76 mm (.030in) | Discontinuous lower plates |
| 2 | 0.43 mm (.017in) | 2.03 mm (.080in) | " " |
| 3 | 0.89 mm (.035in) | 1.02 mm (.040in) | " " |
| 4 | 0.43 mm (.017in) | 0.76 mm (.030in) | Continuous lower plates |

APPENDIX V

Before writing the elements of (B) it is convenient to define the following FF functions in terms of $f_0$, $f_1$, $f_2$, $f_3$ as stated in VI.2.1 (b):-

$$FF2 = f_0^2 + 2 f_1 f_3 + f_2^2 = \tfrac{1}{2} (\cosh 2\lambda\ell + \cos 2\lambda\ell)$$

$$FF4 = f_0 f_1 + f_2 f_3 = \tfrac{1}{4} (\sinh 2\lambda\ell + \sin 2\lambda\ell)$$

$$FF5 = f_1^2 + 2 f_0 f_2 + f_3^2 = \tfrac{1}{2} (\cosh 2\lambda\ell - \cosh 2\lambda\ell)$$

$$FF6 = f_0 f_3 + f_1 f_2 = \tfrac{1}{4} (\sinh 2\lambda\ell - \sin 2\lambda\ell)$$

$$FF1 = 2.FF6 + f_0 f_3$$

$$FF3 = FF5 + f_0 f_2$$

$$FF7 = 2.FF4 + f_0 f_1$$

$$FF8 = FF2 + f_0^2$$

Then the elements of $b_{ij}$ of (B) are:-

$$b_{11} = \frac{Q^2 f_3^2}{\lambda^6 EI} + \frac{CQ f_2^2}{\lambda^4 E^2 I^2} + \frac{Q}{\lambda^3 EI} \cdot FF1 + \frac{C f_2 f_3}{\lambda EI} + FF2$$

$$b_{12} = \frac{C^2 f_1 f_2}{\lambda^3 E^2 I^2} + \frac{CQ f_2 f_3}{\lambda^5 EI} + \frac{K}{\lambda^2 EI} FF3 + \frac{Q f_1 f_3}{\lambda^4 EI} + \frac{2.FF4}{\lambda}$$

$$b_{13} = \frac{Q f_2 f_3}{\lambda^5 E^2 I^2} + \frac{C f_1 f_2}{\lambda^3 E^2 I^2} + \frac{FF5}{\lambda^2 EI}$$

$$b_{14} = \frac{Q f_3^2}{\lambda^6 E^2 I^2} + \frac{C f_2^2}{\lambda^4 E^2 I^2} + \frac{2.FF6}{\lambda^3 EI}$$

$$b_{21} = \frac{Q^2 f_2 f_3}{\lambda^5 E^2 I^2} + \frac{CQ f_1 f_2}{\lambda^3 E^2 I^2} + \frac{Q FF3}{\lambda^2 EI} + \frac{C f_1 f_3}{EI} + 2\lambda FF6$$

$$b_{22} = \frac{C^2 f_1^2}{\lambda^2 E^2 I^2} + \frac{CQ f_2^2}{\lambda^4 E^2 I^2} + \frac{C.FF7}{\lambda EI} + \frac{Q f_1 f_2}{\lambda^3 EI} + FF2$$

$$b_{23} = \frac{Q f_2^2}{\lambda^4 E^2 I^2} + \frac{C f_1^2}{\lambda^2 E^2 I^2} + \frac{2.FF4}{\lambda EI}$$

$$b_{24} = \frac{Q f_2 f_3}{\lambda^5 E^2 I^2} + \frac{C f_1 f_2}{\lambda^3 E^2 I^2} + \frac{FF5}{\lambda^2 EI}$$

$$b_{31} = \frac{Q^2 f_1 f_3}{\lambda^4 EI} + \frac{CQ f_0 f_2}{\lambda^2 EI} + \frac{Q}{\lambda} FF7 + C\lambda f_0 f_3 + \lambda^2 EI.FF5$$

$$b_{32} = \frac{C^2 f_0 f_1}{\lambda EI} + \frac{CQ f_1 f_2}{\lambda^3 EI} + C.FF2 + \frac{Q f_1^2}{\lambda^2} + 2\lambda EI.FF6$$

$$b_{33} = \frac{Q f_1 f_2}{\lambda^3 EI} + \frac{C f_0 f_1}{\lambda EI} + FF2$$

$$b_{34} = \frac{Q f_1 f_3}{\lambda^4 EI} + \frac{C f_0 f_2}{\lambda^2 EI} + \frac{2}{\lambda} . FF4$$

$$b_{41} = \frac{Q^2 f_0 f_3}{\lambda^3 EI} + \frac{CQ f_2 f_3}{\lambda EI} + Q.FF8 + C\lambda^2 f_3^2 + 2\lambda^3 EI.FF4$$

$$b_{42} = \frac{C^2 f_1 f_3}{\lambda EI} + \frac{CQ f_0 f_2}{\lambda^2 EI} + \frac{Q f_0 f_1}{\lambda} + C\lambda.FF1 + \lambda^2 EI.FF5$$

$$b_{43} = \frac{Q f_0 f_2}{\lambda^2 EI} + \frac{C f_1 f_3}{EI} + 2\lambda.FF6$$

$$b_{44} = \frac{Q f_0 f_3}{\lambda^3 EI} + \frac{C f_2 f_3}{\lambda EI} + FF2$$

The Fortran program listing shown is that of the program used on an IBM 360 machine with a GI level compiler and is therefore not entirely written in I.S.O. Fortran.

Explanation of symbols used in computer program:

Referring to Figs. 83 and 84 and using the notation of the figures the symbols are as follows:-

INPUT

T - thickness of viscoelastic core of shear damper = $t_c$ in Fig. 83.

A - area of lower constraining plate attached to a stringer free edge.

G1 - real part of complex shear modulus of core material (G').

AMASS - magnitude of moving mass at stringer tip including 1/3 mass of core.

FLEC - real part of flexural rigidity of skin material (EI).

H - height of stringer tip above inside skin line.

AL - stringer pitch.

AM - mass of one stringer section = $\frac{\rho}{g}$ H.c. $\frac{a}{2}$

AI - moment of inertia of stringer section about point O = AM x $H^2/4$

RT - rotational stiffness of stringer (equivalent to R in Fig. 83) about point O = $\frac{E}{3} \times \frac{I_p}{a}$

where $I_p = 1/3\ Hc^3$

SI - structural loss factor of beam material (typically .005 to .015).

BS - bending stiffness of stringer and associated skin about N.A. In Fig. 83 width of associated skin on side of stringer is X = .09a or AL/2, whichever is the least, where a is frame pitch. To include cross-sectional area effect of fillet radii and skin under stringer add $2t_s$ to H, i.e. $h = (H + 2t_s)$,

Then $\bar{y} = \left(\frac{ch^2}{2} + X_m t_s^2\right) / (2t_s X_m + ch)$

$$I_{na} = \frac{ch^3}{12} + X_m t_s^3 + ch\left(\frac{h}{2} - \bar{y}\right) + X_m t_s \left(\bar{y} - \frac{t_s}{2}\right)^2$$

Then BS = $\frac{E.I_{na}}{a^3}$ equivalent to K in Fig. 83

ETAK - coeffecient of $\eta$, the viscoelastic material loss factor, to enable parametric variations to be made by simple changes in the data allowing the frequency dependence of $\eta$ to be maintained.

<u>All the above in free format</u>

N1 - starting frequency in Hz of range to be covered by frequency response function.

N2 - final frequency in Hz of range covered.

N3 - increment of frequency used in covering the range.

<u>The above in 3I4 format</u>

OUTPUT

XRKSLM - complex displacement frequency response at point k due to unit input shear force at j for symmetric modes, (referring to Fig. 84).

XRKSSM - as above for assymmetric modes.

```
IMPLICIT REAL*8 (A-H,O-Z)
REAL*8 KR,KI
COMPLEX*16 K,Q,B13,B14,B21,B22,B23,B24,B41,B42,B43,B44,D24,D44,BA2
3,BA24,BA43,BA44,XRKSL,B11,D12,B31,B32,B33,B34,XRKSS
,BA13,BA14,BA33,BA34,A13,A23,A14,A24,FLEX
 ,ALAM,A43,A34,Z,S,C,SH,CH,F0,F1,F2,F3,Z2,S2,C2,SH2,CH2,
FF1,FF2,FF3,FF4,FF5,FF6,FF7,FF8,A33,A44
READ(5,*)T,A,C1,AMASS,FLEC,H,AL,AM,AI,RT,SI,BS,ETAK
READ(5,10)N1,N2,N3
FORMAT(3I4)
WRITE(6,20)T,A,C1,AMASS,FLEC,H,AL,AM,AI,RT,SI,BS,ETAK
FORMAT(2X,13D8.3)
DO 30 I30=N1,N2,N3
W=I30*0.0284D1
ETA=(0.00051D0*I30+0.240D0)*ETAK
ALAMR=DSQRT(W/0.0284D1)*0.1313D1
ALAMI=-ALAMR*0.25D0*SI
ALAM=DCMPLX(ALAMR,ALAMI)
KR=-AI*W*W+(AL*AL*A*C1)/T+RT-AMASS*H**4*W*W
KI=(AL*AL*A*C1*ETA)/T+SI*RT
K=DCMPLX(KR,KI)
QI=-SI*BS
QR=AI*W*W-BS
Q=DCMPLX(QR,QI)
FLECI=FLEC*SI
FLEX=DCMPLX(FLEC,FLECI)
Z=ALAM*AL
S=DSIN(Z)
C=DCOS(Z)
SH=0.5D0*(DEXP(Z)-DEXP(-Z))
CH=0.5D0*(DEXP(Z)+DEXP(-Z))
F0=(CH+C)/2D0
F1=(SH+S)/2D0
F2=(CH-C)/2D0
F3=(SH-S)/2D0
Z2=2D0*Z
S2=DSIN(Z2)
C2=DCOS(Z2)
SH2=0.5D0*(DEXP(Z2)-DEXP(-Z2))
CH2=0.5D0*(DEXP(Z2)+DEXP(-Z2))
FF1=3D0*F0*F3+2D0*F1*F2
FF2=(CH2+C2)/2D0
FF5=(CH2-C2)/2D0
FF3=FF5+F0*F2
FF4=(SH2+S2)/4D0
FF6=(SH2-S2)/4D0
FF7=2D0*FF4+F0*F1
FF8=FF2+F0*F0
MATRIX ELEMENTS
A13=F2/(ALAM*ALAM*FLEX)
A23=F1/(ALAM*FLEX)
A33=F0
A43=F3*ALAM
A14=F3/(ALAM**3  *FLEX)
A24=F2/(ALAM*ALAM*FLEX)
A34=F1/ALAM
A44=F0
```

```
B13=Q*F2*F3/(ALAM**5  *FLEX*FLEX)+K*F1*F2/(ALAM**3  *FLEX*FLEX)
-FF5/(ALAM*ALAM*FLEX)
B14=Q*F3*F3/(ALAM**6  *FLEX*FLEX)+K*F2*F2/(ALAM**4  *FLEX*FLEX)
+FF6*2D0/(ALAM**3  *FLEX)
B21=Q*Q*F2*F3/(ALAM**5  *FLEX*FLEX)+K*Q*F1*F2/(ALAM**3  *FLEX*FLEX
)+Q*FF3/(ALAM*ALAM*FLEX)+K*F1*F3/FLEX+2D0*ALAM*FF6
B22=K*K*F1*F1/(ALAM*ALAM*FLEX*FLEX)+K*Q*F2*F2/(ALAM**4  *FLEX*FLEX
)+K*FF7/(ALAM*FLEX)+Q*F1*F2/(ALAM**3  *FLEX)+FF2
B23=Q*F2*F2/(ALAM**4  *FLEX*FLEX)+K*F1*F1/(ALAM*ALAM*FLEX*FLEX)
+2D0*FF4/(ALAM*FLEX)
B24=Q*F2*F3/(ALAM**5  *FLEX*FLEX)+K*F1*F2/(ALAM**3  *FLEX*FLEX)
+FF5/(ALAM*ALAM*FLEX)
B41=Q*Q*F0*F3/(ALAM**3  *FLEX)+K*Q*F2*F3/(ALAM*FLEX)+Q*FF8+K*ALAM*
ALAM*F3*F3+2D0*ALAM**3  *FLEX*FF4
B42=K*K*F1*F3/(ALAM*FLEX)+Q*K*F0*F2/(ALAM*ALAM*FLEX)+Q*F0*F1/ALAM+
K*FF1*ALAM+FF5*ALAM*ALAM*FLEX
B43=Q*F0*F2/(ALAM*ALAM*FLEX)+K*F1*F3/FLEX+2D0*FF0*ALAM
B44=Q*F0*F3/(ALAM**3  *FLEX)+K*F2*F3/(ALAM*FLEX)+FF2
D24=B24
D44=B44
BA23=B21*A13+B22*A23+B23*A33+B24*A43
BA24=B21*A14+B22*A24+B23*A34+B24*A44
BA43=B41*A13+B42*A23+B43*A33+B44*A43
BA44=B41*A14+B42*A24+B43*A34+B44*A44
XRKSL=(B13*(BA44*D24-BA24*D44)-B14*(BA43*D24+BA23*D44))/(BA43*BA24
-BA23*BA44)+A14
B11=Q*Q*F3*F3/(ALAM**6  *FLEX)+K*Q*F2*F2/(ALAM**4  *FLEX*FLEX)+Q*F
F1/(ALAM**5  *FLEX)+K*F2*F3/(ALAM*FLEX)+FF2
B12=K*K*F1*F2/(ALAM**3  *FLEX*FLEX)+K*Q*F2*F3/(ALAM**5  *FLEX)+K*F
F3/(ALAM*ALAM*FLEX)+Q*F1*F3/(ALAM**4  *FLEX)+2D0*FF4/ALAM
B31=Q*Q*F1*F3/(ALAM**4  *FLEX)+K*Q*F0*F2/(ALAM*ALAM*FLEX)+Q*FF7/AL
AM+K*F0*F3*ALAM+ALAM*ALAM*FLEX*FF5
B32=K*K*F0*F1/(ALAM*FLEX)+Q*K*F1*F2/(ALAM**3  *FLEX)+K*FF2+Q*F1*F1
/(ALAM*ALAM)+2D0*ALAM*FLEX*FF6
B33=Q*F1*F2/(ALAM**3  *FLEX)+K*F0*F1/(ALAM*FLEX)+FF2
B34=Q*F1*F3/(ALAM**4  *FLEX)+K*F0*F2/(ALAM*ALAM*FLEX)+2D0*FF4/ALAM
BA34=B31*A14+B32*A24+B33*A34+B34*A44
BA14=B11*A14+B12*A24+B13*A34+B14*A44
BA33=B31*A13+B32*A23+B33*A33+B34*A43
BA13=B11*A13+B12*A23+B13*A33+B14*A43
XRKSS=(B13*(BA34*B14-BA14*B34)-B14*(BA33*B14+BA13*B34))/(BA33*BA14
-BA13*BA34)+A14
WRITE(6,40)I3C
FORMAT(2X,I4)
XRKSLM=CDABS(XRKSL)
XRKSSM=CDABS(XRKSS)
WRITE(6,50)XRKSLM,XRKSSM
FORMAT(10X,D20.13,24X,D20.13)
CONTINUE
STOP
END
  DATA
```

## REFERENCES


1. Y.K. Lin, I.D. Brown, P.C. Deutschle, 1964, J. Sound Vib. Vol. 1, No. 14. "Free vibration of a finite row of continuous skin-stringer panels."

2. D.J. Mead and T.G. Pearce, 1964, ML-TDR-64-51. "The optimum use of unconstrained layer damping treatments."

3. B.L. Clarkson and F. Cicci, 1969, ASME 69-Vibr-26. "Methods of reducing the response of integrally stiffened structures to random pressures." Paper presented at Vibrations Conference, Philadelphia, March 30 - April 2, 1969.

4. Y.K. Lin, 1960, J. Appl. Mech., 27, p 669. "Free vibration of continuous skin-stringer panels."

5. Y.K. Lin et al, 1965, AFML-TR-64-347, "Free vibration of continuous skin-stringer panels, with non-uniform stringer spacing and panel thickness."

6. M.D. Olsen and G.M. Lindberg, National Aero Establishment, Canada, NAE LR-544. "Free vibrations and random response of an integrally stiffened plate."

7. B.L. Clarkson, 1968, Journal Royal Aero Soc., Vol. 72, No. 665. "Stresses in skin panels subjected to random acoustic loading."

8. B.L. Clarkson, R.D. Ford, 1962, Journal Royal Aero Soc., Vol. 66, 31. "The response of a typical aircraft structure to jet noise."

9. F.C. Nelson, 1966, Shock & Vibration Bulletin, 35, Part 7. "Effect of structural damping on the modal response of a resonant beam."

10. D.J. Mead, 1958, Aeronautical Research Council Report ARL 19, 870 Strut 2043 0-1389. "Internal Damping due to Structural Joints and Techniques for General Damping Measurement."

11. D.J. Mead, 1961, WADC TR59-676, pp 235-261. "The damping, stiffness and fatigue properties of joints and configurations representative of aircraft structures."

12. C.C. Kennedy and C.P. Pancu , 1947, Journal of Aeronautical Sciences, Nov. 1947. "Uses of vectors in vibration measurement and analysis."

13. F. Cicci, 1971, J. Sound Vibration, Vo. 17, 1. "Damping of integrally stiffened structures."

14. B.J. Lazan, Oxford Pergammon Press. "Damping of materials and members in structural mechanics."

15. D.I.G. Jones and W.J. Trapp, 1971, J. Sound and Vibration, Vol. 17, 2. "Influence of additive damping on resonance fatigue of structures."

16. G.E. Warnaka et al, 1966. Shock & Vibration Bulletin, 35, part 7 (April). "Simplified approach to structural damping design."

17. D.I.G. Jones, 1970, Shock & Vibration Bulletin, 41, part 2. "Effect of free layer damping on response of stiffened plate structures."

18. S. Lyon, 1968, M.Sc. Dissertation, ISVR, University of Southampton. "The vibration of integrally stiffened panels and possible means of reducing the stresses induced in them."

19. E. Ungar & M. Kerwin, 1962, JASA, Vol. 34, No. 8, pp 1082-1084. "Loss factors of viscoelastic damped beam structures."

20. L. Lamarce and La Barge, 1970, Shock & Vibration Bulletin, 40, part 5. "Sonic fatigue resistance of structures incorporating a constrained viscoelastic core."

21. D.I.G. Jones et al, 1970, Shock & Vibration Bulletin, 40, part 5. "Damping and isolation."

22. J.L. Potter, 1970, Shock & Vibration Bulletin, 41, part 2. "Improving reliability and eliminating maintenance with elastomeric dampers for rotor systems."

23. E.M. Kerwin, 1959, JASA, Vol. 31, No. 7 (July), pp 952-962. "Damping of flexural waves by a constrained viscoelastic layer."

24. E. Ungar, Ross and Kerwin, 1959, WADC TR 59-509 (Nov.). "Damping of flexural vibrations by alternate viscoelastic and elastic layers."

25. B.J. Lazan et al, 1965, AFML-TR-65-269. "Multiple band surface treatments for high damping."

26. P.J. Torvik and B.J. Lazan, 1965, AFML-TR-64-373. "A corrugated addition for increasing damping in flexure."

27. D.R. Simmons et al, 1969, Shock and Vibration Bulletin, 39, part 4, (April). "Multi-layer alternately anchored treatment for damping of skin-stringer structures."

28. J.P. Henderson, 1966, Shock & Vibration Bulletin, 35, part 7, (April). "Energy dissipation in a vibration damper using viscoelastic suspension."

29. D.I.G. Jones et al, 1967, AFML-TR-67-307. "Development of a tuned damper to reduce vibration damage in aircraft radar antenna."

30. D.I.G. Jones, 1968, Shock & Vibration Bulletin, 38, part 3, pp 139. "Damping of multispan structures by means of viscoelastic links."

31. F. Cicci, 1970, Ph.D. thesis, University of Southampton. "The reduction of resonant vibrations in integrally stiffened skin-stringer panels using viscoelastic materials."

32. G.H. Bruns, 1967, Shock & Vibration Bulletin, 36, Part 4 (Jan). "Effect of tuned viscoelastic dampers on response of multi-span structures."

33. E. Ungar, 1963, Machine Design, Vol. 35, No. 4, pp 162-168. "A guide to designing highly damped structures using layers of viscoelastic material."

34. P. Grootenhuis, 1970, Shock & Vibration Bulletin, 40, part 5. "Control of vibrations with viscoelastic materials."

35. D.I.G. Jones et al, 1965, AFML-TR-65-151 (Dec.). "Some aspects of the analysis of damping and vibrations in simple structures."

36. J.E. Ruzika et al, 1967, NASA, CR 742 (March). "Damping of structural composites with viscoelastic shear damping mechanisms."

37. D.I.G. Jones, 1968, NASA, Damping Conference (Nov.). "Material Damping."

38. A.D. Nashif, 1968, Shock & Vibration Bulletin, 38, part 3, pp 57. "Development of practical tuned dampers to operate over a wide temperature range."

39. J.E. Ruzika, 1961, J. Engineering for Industry (Nov.). "Damping structural resonances using viscoelastic shear mechanisms."

40. F.S. Owens, 1967, Shock & Vibration Bulletin, 36, part 4. "Elastomers for damping over wide temperature ranges."

41. A.E. Turner, 1971, Environmental Engineering (June), pp 13-16. "Development of viscoelastic damping materials for applications involving large temperature fluctuations."

42. D.R. Blenner and T.J. Dudek, 1968, Shock & Vibration Bulletin, 38, part 3. "Broadband extensional damping materials."

43. R.E.D. Bishop, 1955, J. Royal Aero Soc., Vol. 59, No. 539, pp 738-742. "The treatment of damping forces in vibration theory."

44. Ungar & Kerwin, 1962, JASA, Vol. 34, No. 7, pp 954-957. "Loss factors of viscoelastic systems in terms of energy concepts."

45. S.H. Crandall, 1970, J. Sound and Vibration, Vol. 11, No. 1, pp 3-18. "The role of damping in vibration theory."

46. E. Ungar and D.K. Hatch, 1961, Prod. Eng., Vol. 32, No. 16, pp 44-56. "High damping materials."

47. D.I.G. Jones and J.P. Henderson, 1969, Shock & Vibration Bulletin, 40, part 5. "Reduction of vibrations in aerospace structures by additive damping."

48. A.D. Nashif and T. Nicholas, 1969, Shock & Vibration Bulletin, 40, part 5. "Vibration control by a multiple layered damping treatment."

49. S.D. Gehman, 1957, Rubber, Chemistry and Technology, Vol. 30, p 1203. "Dynamic properties of elastomers."

50. A.R. Payne and J.R. Scott, 1960, Maclaren and Sons Ltd. "Engineering design with rubber."

51. Kainradl and Handler, 1958, Kautshuh und Gummi, II, p 193. "Messung der dynamische eigenschaften von vulkanisation."

52. M.V. Venediktov et al, 1971, Soviet Phisics-Acoustics, Vol. 17, No. 2, (Oct-Dec). "Viscoelastic properties of filled plasticised P.V.C."

53. A.R. Payne, 1965, Maclaren & Sons Ltd. "Use of rubber in engineering." Chapter 2.

54. Journal Sci. Instruments, 1966, Vol. 42, p 65, and 1967, Vol. 44, p 169. "Damping measurements with a maintained torsional pendulum."

55. P. Grootenhuis, 1967. Paper presented at Leuven Conference of Belgian Acoustical Society. "Measurement of dynamic properties of damping materials."

56. H. Oberst, 1952, Acustica Vol. 2, No. 4. "Über die dampfung der biegeschwingungen dunner bleche durch fest heftende belÄge."

57. R.L. Adkins, 1966, Experimental Mechanics (July). "Design considerations and analysis of a complex modulus apparatus."

58. F. Abdulhadi, 1970, Shock & Vibration Bulletin, 41, part 2. "Determination of damping properties of soft viscoelastic materials."

59. K.G. McConnell, 1969, Shock & Vibration Bulletin, 39. "A proposed experimental method for accurate measurement of the dynamic properties of viscoelastic materials."

60. A.D. Nashif and C.M. Cannon, Shock & Vibration Bulletin, 38, part 3. "Damping measurements on soft viscoelastic materials using a tuned damper technique."

61. D.J.G. Jones, 1967, AFML-TR-67-363. "Multi-frequency response of viscoelastic dampers."

62. S. Timashanko and J.N. Goodier, McGraw Hill. "Theory of elasticity." Chapter 1.

63. G. Buker, 1955, Kolloid Zeit, Vol. 140. "Mechanical relaxation in unplasticized high polymers."

64. E. Fitzgerald, J. Fitzgerald and A.Woodward, 1957, Navy Contract Report NS-034-045. "Dynamic mechanical properties of plastic materials."

65. K. Yamato and Y. Wade, 1957, Journal of Physical Society of Japan, vol. 12. "An investigation of dynamic mechanical properties of glassy polymers by a composite oscillation method."

66. J.D. Ferry, 1961, John Wiley. "Viscoelastic properties of polymers."

67. J.M. Ohno, 1968, Shock & Vibration Bulletin, 38, part 3. "Effect of temperature on viscoelastic high polymer materials."

68. J.D. Ferry, R.F. Landal, M.L. Williams, 1955, J. American Chem. Soc., Vol. 77, p 3701. "Method of reduced variables."

69. T.P. Lin, 1962, Gordon Research Conferences, U.S.A. - Elastomers (July 16). "The frequency-temperature dependence of the damping characteristics of several elastomers."

70. J. Snowden, 1968, Wiley & Son Ltd. "Vibration and shock in damped mechanical systems."

71. G. Wright, 1973, University of Southampton. Private communication.

72. P. Grootenhuis, 1970, Journal of Sound and Vibration, Vol. 11 No. 4. "The control of vibrations with viscoelastic materials."

73. R.E.D. Bishop and D.C. Johnson, 1960, Cambridge University Press. "The mechanics of vibration."

74. F. Cicci, 1970. Paper presented at University of Southampton Conference - Current Developments in Sonic Fatigue, entitled "Damping in integrally stiffened structures."

75. Y.K. Lin and B.K. Donaldson, 1969, J. Sound and Vibration, Vol. 10, No. 1, pp 103-143. "A brief survey of transfer matrix techniques with special reference to aircraft panels."

76. C.A. Mercer and C. Seavey, 1967, J. Sound and Vibration. "Prediction of natural frequencies and normal modes of skin-stringer panel rows."

77. Y.K. Lin and T.J. McDaniel, 1969, ASME-69-Vibr-17. "Dynamics of beam type periodic structures."

78. S. Timashenko and J.N. Goodier, 1951, McGraw Hill, "Theory of elasticity" particularly Chapter 6, Section 52.

79. E.C. Pestel and F.A. Leckie, 1963, McGraw Hill, "Matrix methods in elastomechanics."

80. Y.K. Lin, 1967, McGraw Hill. "Probabilities theory of structural dynamics."

81. D.J. Mead, 1961, WADD-TR-61-25. "Criteria for comparing the effectiveness of damping treatments."

82. C.A. Mercer, 1965, R. Francaise Mechanique, 13, 15. "On the application of transfer matrices."

83. S.R. Robertson, 1971, J. Sound & Vibration, Vol. 19, No. 1, (Nov), pp 95-109. "Using measured material parameters in solving forced motion problems in viscoelasticity."

84. K.W. Newman et al, 1971, R.A.E. TR-71119. "Effect of a stiffness non linearity on vector response loci."

TABLE III.4.1

| Frequency (Hz) | Acceleration (g) |
|---|---|
| 200 | 0.271 |
| 400 | 1.082 |
| 600 | 2.435 |
| 800 | 4.333 |
| 1000 | 6.760 |

TABLE III.4.2

Specimen 2
Strain .0007 Tests on 20.7.70

| | g | Force | Phase |
|---|---|---|---|
| TEMP 17.5°C | | | |
| 200 | 3.87 | 43.6 | 13.2 |
| 400 | 15.5 | 49.6 | 26 |
| 600 | 34.7 | 39.2 | 39.5 |
| 800 | 61.8 | 30 | 55.5 |
| 1000 | 96.5 | 25.5 | 103 |
| TEMP 45°C | | | |
| 200 | 3.87 | 32.8 | 8.0 |
| 400 | 15.5 | 33.3 | 26.2 |
| 600 | 34.7 | 24.5 | 45.2 |
| 800 | 61.8 | 17 | 85.1 |
| 1000 | 96.5 | 26.4 | 141.5 |
| TEMP 81°C | | | |
| 200 | 3.87 | 24.3 | 7.4 |
| 400 | 15.5 | 21.8 | 26.2 |
| 600 | 34.7 | 13.2 | 58.7 |
| 800 | 61.8 | 14.9 | 135 |
| 1000 | 96.5 | 33.3 | 164 |
| TEMP 114°C | | | |
| 200 | 3.87 | 20.2 | 8.2 |
| 400 | 15.5 | 16.3 | 26.6 |
| 600 | 34.7 | 8.4 | 80.2 |
| 800 | 61.8 | 17.7 | 156 |
| 1000 | 96.5 | 37.4 | 169.8 |
| TEMP 153°C | | | |
| 200 | 3.87 | 17.2 | 7.2 |
| 400 | 15.5 | 12.3 | 26.4 |
| 600 | 34.7 | 5.94 | 111 |
| 800 | 61.8 | 20 | 164.2 |
| 1000 | 96.5 | 39.6 | 173 |

Specimen 2
Strain .0004 Tests on 20.7.70

| | g | Force | Phase |
|---|---|---|---|
| TEMP 17.5°C | | | |
| 200 | 2.21 | 24.7 | 10.2 |
| 400 | 8.84 | 27.3 | 25.3 |
| 600 | 19.8 | 22.5 | 39.0 |
| 800 | 35.3 | 17.3 | 55 |
| 1000 | 55.2 | 14.7 | 102.8 |
| TEMP 45°C | | | |
| 200 | 2.21 | 19 | 8.3 |
| 400 | 8.84 | 19.4 | 25.8 |
| 600 | 19.8 | 14.4 | 45 |
| 800 | 35.3 | 9.4 | 84 |
| 1000 | 55.2 | 15.1 | 141 |
| TEMP 81°C | | | |
| 200 | 2.21 | 12 | 8.1 |
| 400 | 8.84 | 13 | 25.7 |
| 600 | 19.8 | 7.4 | 58 |
| 800 | 35.3 | 8.2 | 134 |
| 1000 | 55.2 | 18.7 | 164 |
| TEMP 114°C | | | |
| 200 | 2.21 | 11.7 | 8.7 |
| 400 | 8.84 | 9.4 | 26.2 |
| 600 | 19.8 | 4.67 | 78.5 |
| 800 | 35.3 | 10.2 | 156 |
| 1000 | 55.2 | 21.3 | 169 |
| TEMP 153°C | | | |
| 200 | 2.21 | 9.85 | 8.4 |
| 400 | 8.84 | 7.3 | 25.9 |
| 600 | 19.8 | 3.72 | 113 |
| 800 | 35.3 | 11.4 | 161 |
| 1000 | 55.2 | 22.5 | 173.3 |

TABLE III.4.3

Specimen 2
Strain .0004 Tests on 20.7.70

| w | g | Force (lb) | Phase° | cos ø | sin ø | P cos ø | P sin ø | $M_x''$ | P cos ø + $M_x''$ | | G' |
|---|---|---|---|---|---|---|---|---|---|---|---|
| TEMP 17.5°C | | | | | | | | | | | |
| 200 | .108 | .515 | 10.2 | .9842 | .1771 | .506 | .0912 | .0227 | .5287 | .173 | 330 |
| 400 | .433 | .590 | 25.3 | .9041 | .4274 | .533 | .252 | .091 | .624 | .404 | 390 |
| 600 | .973 | .469 | 39.0 | .7771 | .6293 | .365 | .295 | .204 | .569 | .520 | 356 |
| 800 | 1.73 | .361 | 55 | .5736 | .8192 | .207 | .296 | .363 | .570 | .520 | 357 |
| 1000 | 2.70 | .306 | 102.8 | .2215 | .9751 | -.0677 | .298 | .567 | .4993 | .597 | 313 |
| TEMP 45°C | | | | | | | | | | | |
| 200 | .108 | .396 | 8.3 | .9895 | .1444 | .392 | .0572 | .0227 | .4147 | .183 | 258 |
| 400 | .433 | .404 | 25.8 | .9003 | .4352 | .364 | .176 | .091 | .455 | .387 | 284 |
| 600 | .973 | .300 | 45 | .7071 | .7071 | .212 | .212 | .204 | .416 | .510 | 260 |
| 800 | 1.73 | .196 | 84 | .1045 | .9945 | .020 | .195 | .363 | .383 | .510 | 239 |
| 1000 | 2.70 | .315 | 141 | -.7986 | .6293 | -.252 | .198 | .567 | .315 | .628 | 197 |
| TEMP 81°C | | | | | | | | | | | |
| 200 | .108 | .250 | 8.1 | .9900 | .1409 | .248 | .0352 | .0227 | .2707 | .13 | 169 |
| 400 | .433 | .291 | 25.7 | .9011 | .4337 | .244 | .117 | .091 | .335 | .349 | 209 |
| 600 | .973 | .154 | 58 | .5299 | .8480 | .0815 | .131 | .204 | .2855 | .459 | 178 |
| 800 | 1.73 | .171 | 134 | .6947 | .7193 | -.119 | .123 | .363 | .244 | .504 | 152 |
| 1000 | 2.70 | .390 | 164 | -.9613 | .2756 | -.375 | .107 | .567 | .192 | .557 | 120 |
| TEMP 114°C | | | | | | | | | | | |
| 200 | .108 | .244 | 8.7 | .9885 | .1513 | .241 | .0369 | .0227 | .264 | .14 | 165 |
| 400 | .433 | .196 | 26.2 | .8973 | .4415 | .176 | .0865 | .091 | .267 | .267 | 167 |
| 600 | .973 | .097 | 78.5 | .1994 | .9799 | .0193 | .095 | .204 | .223 | .426 | 139 |
| 800 | 1.73 | .213 | 156 | -.9135 | .4067 | -.194 | .0865 | .363 | .169 | .512 | 106 |
| 1000 | 2.70 | .444 | 169 | -.9816 | .1908 | -.436 | .0846 | .567 | .131 | .646 | 82 |
| TEMP 153°C | | | | | | | | | | | |
| 200 | .108 | .205 | 8.4 | .9893 | .1461 | .203 | .030 | .0227 | .2257 | .133 | 141 |
| 400 | .433 | .152 | 25.9 | .8996 | .4368 | .137 | .066 | .091 | .228 | .289 | 142 |
| 600 | .973 | .0775 | 103 | .2250 | .9744 | .0174 | .0755 | .204 | .1866 | .405 | 116 |
| 800 | 1.73 | .238 | 161 | .9455 | .3256 | -.225 | .077 | .363 | .138 | .558 | 86 |
| 1000 | 2.70 | .469 | 173.3 | .9932 | .1167 | -.466 | .055 | .567 | .101 | .545 | 63 |

TABLE III.5.1

| Freq(w) | Acc$^{n}$ base(g) | A | $\eta$ | M(gm) | K(mn/m$^{2}$) | K/3=G' | Strain % |
|---|---|---|---|---|---|---|---|
| 604 | 4.9 | 3.82 | .272 | 11.1 | 6.34 | 2.18 | 0.038 |
| 520 | 3.68 | 3.88 | .267 | 17 | 7.26 | 2.42 | 0.19 |
| 421 | 2.45 | 2.53 | .431 | 23.5 | 6.55 | 2.18 | 0.18 |
| 318 | 1.23 | 2.94 | .362 | 39.9 | 6.48 | 2.16 | 0.43 |
| 259 | 0.74 | 3.16 | .333 | 57.4 | 6.09 | 2.03 | 0.44 |
| 162 | 0.49 | 3.41 | .363 | 139.3 | 5.77 | 1.92 | 1.26 |

$$M = Tm + Am + Sm + Wm + Rm$$

Tm = Tuning mass (3.89 gm to 126.2 gm)

Am = Mass of accelerometer (2 gm)

Sm = Mass of fixing screw and washer (2 gm)

Wm = Mass of specimen top washer (2.21 gm)

Rm = Effective mass of rubber slug (6.9 gm)

TABLE IV.5.1

| TEMP $^{o}$K | $T_o/T$ | log A (measured) | A (measured) | A from W.L.F. equ. | A from Snowden's W.L.F. equ. |
|---|---|---|---|---|---|
| 294 | 1.0 | 0 | 0 | 0 | 0 |
| 327 | 0.9 | - .256 | .528 | .422 | .415 |
| 354 | 0.83 | - .437 | .394 | .277 | .355 |
| 379 | 0.766 | - .501 | .327 | .211 | .320 |
| 425 | 0.692 | -.565 | .260 | .151 | .274 |

TABLE V.1.1

| | Stringer Number | | | | |
|---|---|---|---|---|---|
| | 2 | 3 | 4 | 5 | 6 |
| Frequency 320 Hz | | | | | |
| Stringer Tip Deflexion (mm) | .0047 | .0042 | .0015 | .0038 | .0043 |
| Core Shear Strain % | 0.62 | 0.55 | 0.20 | 0.50 | 0.57 |
| Frequency 406 Hz | | | | | |
| Stringer Tip Deflexion (mm) | .0046 | .0031 | .0084 | .0034 | .0047 |
| Core Shear Strain % | 0.60 | 0.41 | 1.1 | 0.44 | 0.62 |
| Frequency 450 Hz | | | | | |
| Stringer Tip Deflexion (mm) | .0024 | .0022 | .0018 | .0023 | .0023 |
| Core Shear Strain % | 0.31 | 0.29 | 0.24 | 0.30 | 0.30 |

TABLE V.2.2

| Undamped | | | | Damped | | | |
|---|---|---|---|---|---|---|---|
| Freq(Hz) | Force(mv) | Acc$^{n}$(mv) | Phase$^{o}$ | Freq(Hz) | Force(mv) | Acc$^{n}$(mv) | Phase$^{o}$ |
| 296 | 15 | 95 | 102 | 316 | 20 | 96.0 | 107 |
| 367 | 15 | 30 | 84.5 | 400 | 36 | 30.3 | 102 |
| 453 | 15 | 20.8 | 89 | 519 | 32 | 21.1 | 114 |

| Energy absorbed/cycle(J) | | Energy absorbed/ cycle | Response Ratio | |
|---|---|---|---|---|
| | | | Expected | Measured |
| Mode 1 | .00532 | .00655 | 81% | 60% |
| Mode 2 | .00116 | .00238 | 49% | 53% |
| Mode 3 | .00059 | .000833 | 91% | 58% |

TABLE V.2.3

% Response Reductions $\frac{\text{Response damped}}{\text{Response undamped}}$ R%

| Damp Freq (Hz) | Undamp Freq (Hz) | Accelerometer Positions | | | | | | AV.R% | AV.R% Corrected |
|---|---|---|---|---|---|---|---|---|---|
| | | 3 | 3L | 3H | 5 | 5L | 5H | | |
| TYPE 1 BEAM OVERALL AV.R (CORRECTED FOR FREQ SHIFT) = 61.5% | | | | | | | | | |
| 250 | 255 | 76 | 84 | 80 | 78 | 73 | 79 | 78.3 | 79.8 |
| 300 | 300 | 69 | 73 | 72 | 70 | 69 | 72 | 71 | 71.0 |
| 377 | 358 | 54 | 59 | 59 | 87 | 93 | 93 | 74 | 66.6 |
| 475 | 394 | - | - | - | 53 | 67 | 64 | 61 | 42.1 |
| 550 | 480 | 48 | 72 | 70 | - | - | - | 63.3 | 48.1 |
| TYPE 2 BEAM OVERALL AV.R = 59.8% | | | | | | | | | |
| 264 | 255 | 79 | 84 | 86 | 81 | 85 | 83 | 83 | 77.5 |
| 316 | 300 | 79 | 81 | 83 | 81 | 86 | 87 | 83 | 74.6 |
| 390 | 358 | 32 | 38 | 39 | 84 | 81 | 78 | 58.6 | 49.4 |
| 508 | 394 | - | - | - | 68 | 81 | 77 | 75 | 45.0 |
| 590 | 480 | 57 | 100 | 80 | - | - | - | 79 | 52.4 |
| TYPE 3 BEAM OVERALL AV.R = 66.3% | | | | | | | | | |
| 251 | 255 | 70 | 74 | 75 | 72 | 73 | 79 | 74 | 75.0 |
| 309 | 300 | 88 | 88 | 88 | 85 | 94 | 92 | 89 | 83.8 |
| 392 | 358 | 61 | 67 | 63 | 74 | 73 | 70 | 68 | 56.8 |
| 490 | 394 | - | - | - | 88 | 110 | 104 | 101 | 65.4 |
| 590 | 480 | 54 | 80 | 80 | - | - | - | 71.3 | 50.6 |
| TYPE 4 BEAM OVERALL AV.R = 70.7% | | | | | | | | | |
| 263 | 255 | 100 | 71 | 107 | 106 | 105 | 105 | 99 | 93.0 |
| 318 | 300 | 90 | 47 | 93 | 98 | 103 | 102 | 89 | 79.3 |
| 396 | 358 | 50 | 125 | 65 | 110 | 116 | 114 | 97 | 79.0 |
| 500 | 394 | - | - | - | 82 | 105 | 100 | 96 | 59.5 |
| 580 | 480 | 58 | 40 | 90 | - | - | - | 63 | 42.9 |

TABLE VI.1.1.

| Freq (hz) | $\lambda_1 \ell$ | $\lambda_2 \ell$ | $\beta \times 10^{-5}$ | $-M_1 w^2 \times 10^{-5}$ | $\lvert 2/\alpha_{00} \rvert$ |
|---|---|---|---|---|---|
| 320 | .402 | .866 | - 37.9 | - 5.21 | + 24.4 |
| 406 | .451 | .976 | - 33.1 | - 8.37 | + 38.4 |
| 450 | .477 | 1.03 | - 34.3 | - 10.4 | + 48.8 |
| 550 | .528 | 1.14 | - 24.6 | - 15.4 | + 72.0 |
| 830 | .648 | 1.40 | - 9.05 | - 35.0 | + 164 |
| 950 | .694 | 1.494 | - 4.5 | - 45.9 | + 219 |

TABLE VI.2.1

Response Reductions calculated using 3 beam model.

| Freq (Hz) | Eta | Response Ratio % | Comments |
|---|---|---|---|
| 250 | 0.368 | 89 | Type 1 shear damping beam |
| 300 | 0.398 | 84.5 | |
| 377 | 0.440 | 75.0 | |
| 475 | 0.490 | 60.5 | |
| 550 | 0.531 | 54.5 | |
| 830 | 0.661 | 14.0 | |
| 250 | 0.368 | 92 | Type 2 beam |
| 300 | 0.398 | 89 | |
| 377 | 0.440 | 84.5 | |
| 475 | 0.490 | 89.5 | |
| 550 | 0.531 | 69.0 | |
| 830 | 0.661 | 14.0 | |
| 250 | 0.368 | 88 | Type 3 beam |
| 300 | 0.398 | 87 | |
| 377 | 0.440 | 84 | |
| 475 | 0.490 | 86 | |
| 550 | 0.531 | 67 | |
| 830 | 0.661 | 14 | |
| 250 | 0.740 | 89 | Type 1 beam, loss factor doubled |
| 300 | 0.786 | 84.5 | |
| 377 | 0.845 | 73.5 | |
| 475 | 0.882 | 62.5 | |
| 550 | 0.970 | 49.5 | |
| 830 | 1.325 | 14 | |
| 250 | 0.368 | 94 | Type 1 beam but core thickness |
| 300 | 0.398 | 90 | increased to 2.5 mm (0.1 in) |
| 377 | 0.440 | 85 | |
| 475 | 0.490 | 90 | |
| 550 | 0.531 | 70 | |
| 830 | 0.661 | 14 | |

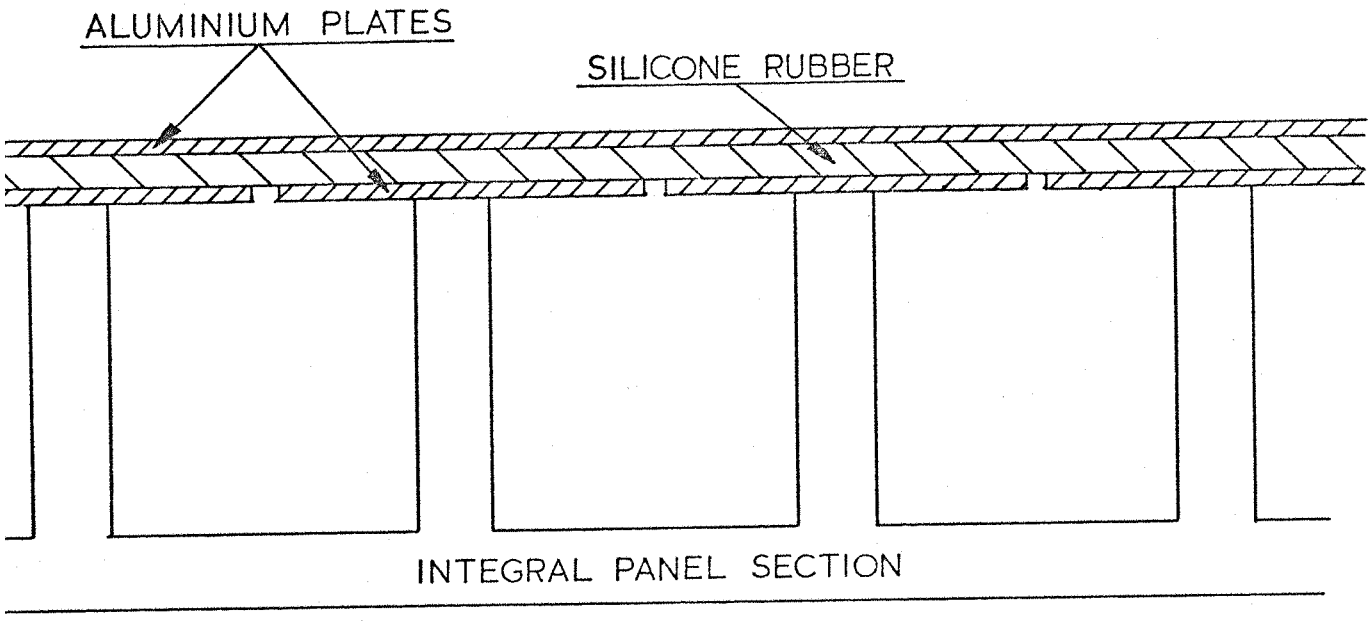


FIG. 1 Shear Damping Beam Configuration

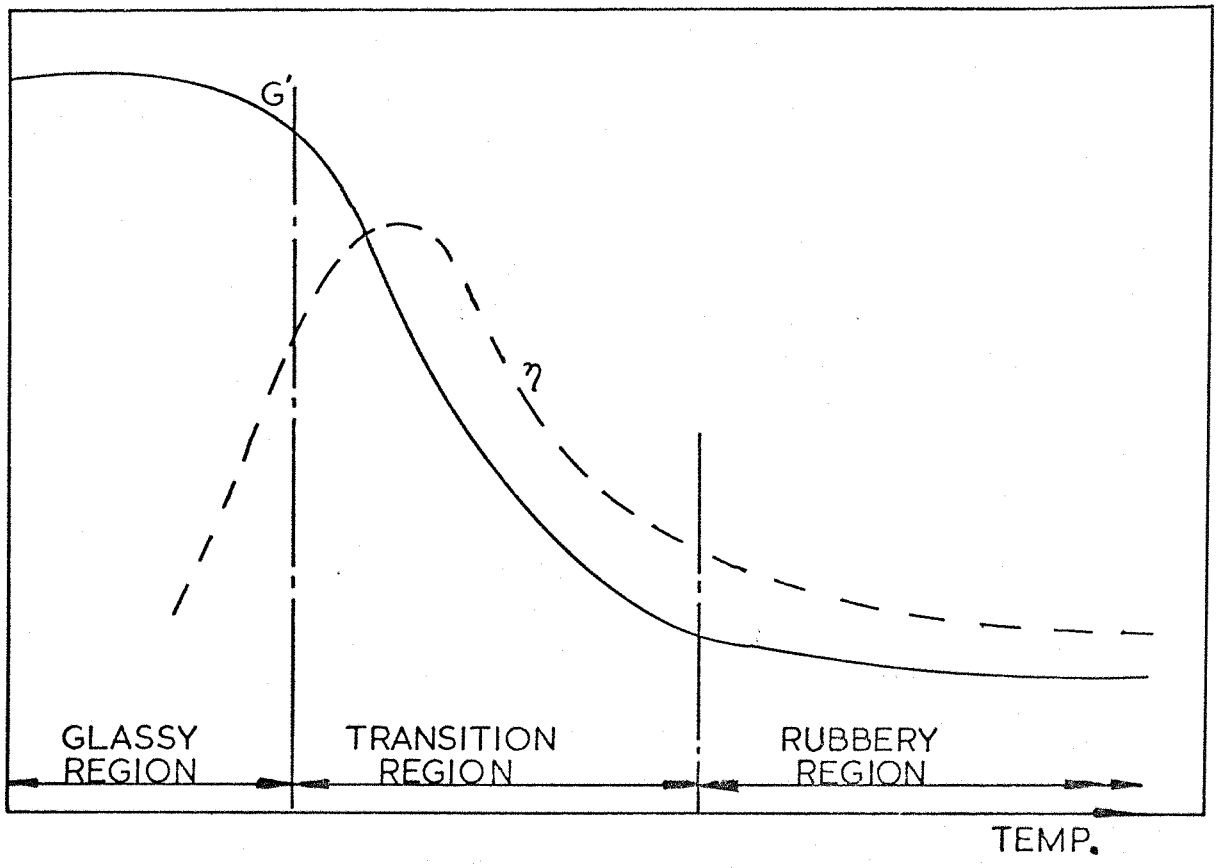


FIG. 2 Typical Dynamic Shear Properties of viscoelastic materials

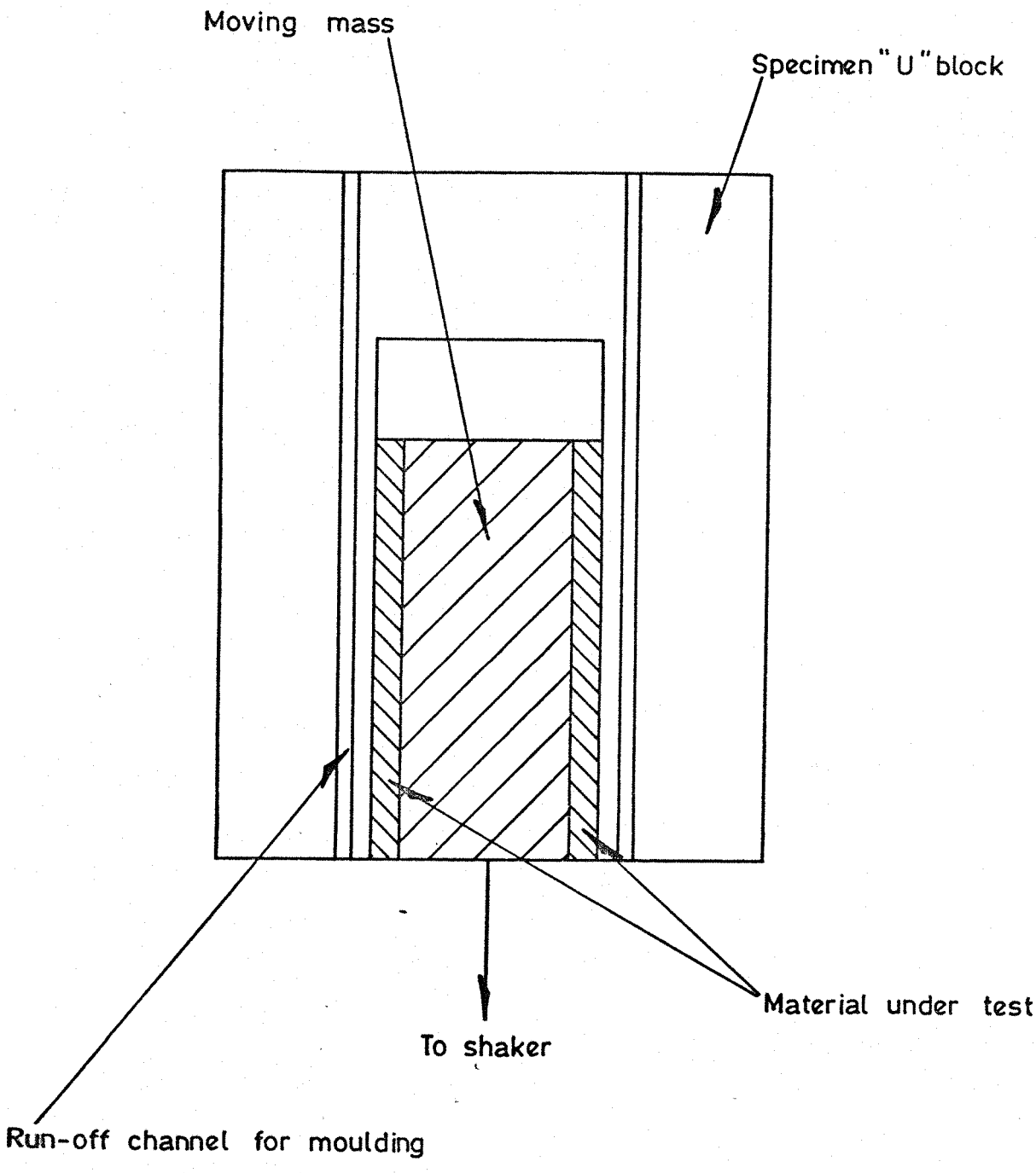


Fig. 3 Details of specimen

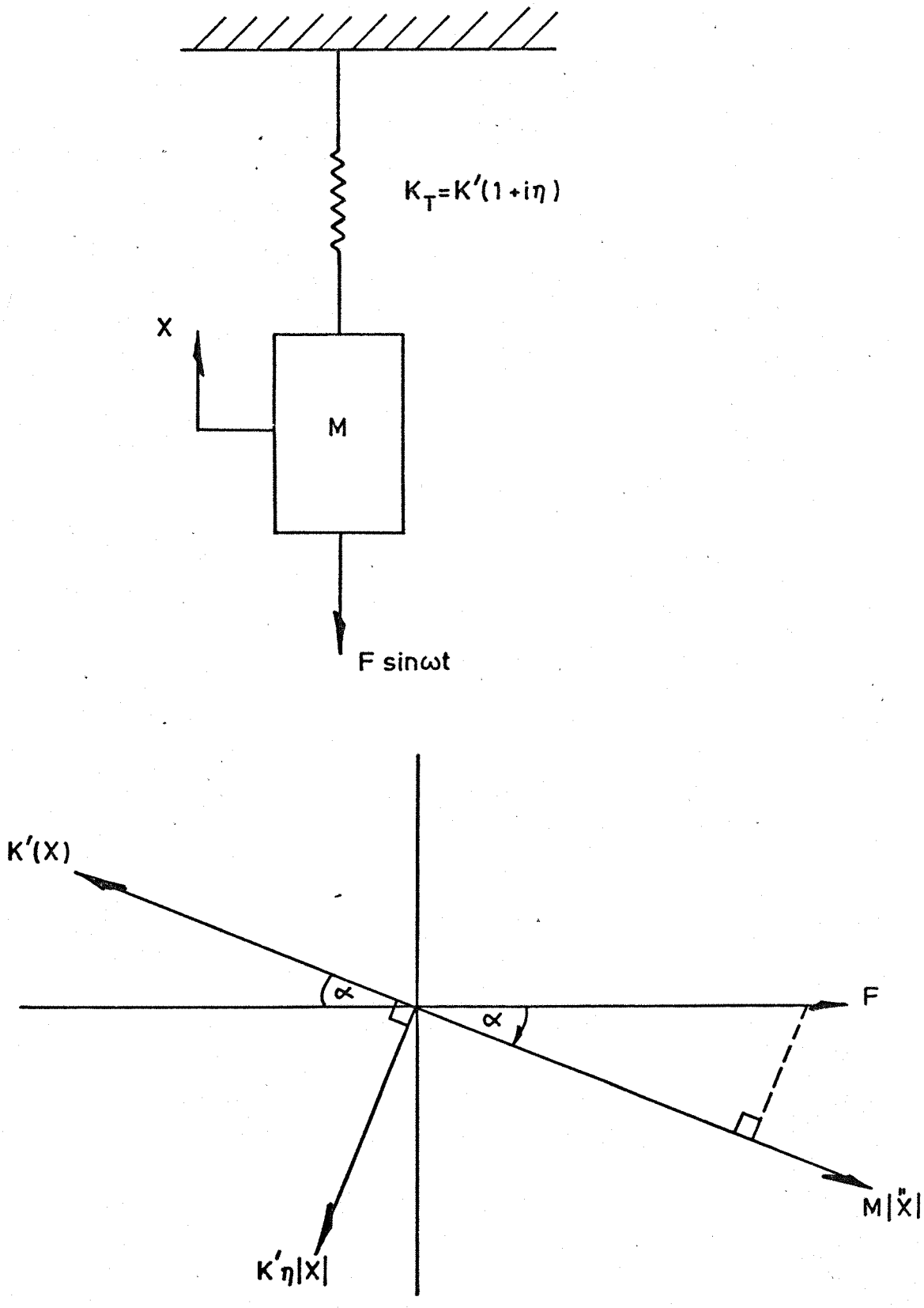


Fig. 4 Idealisation of shear test apparatus and vector diagram of forces

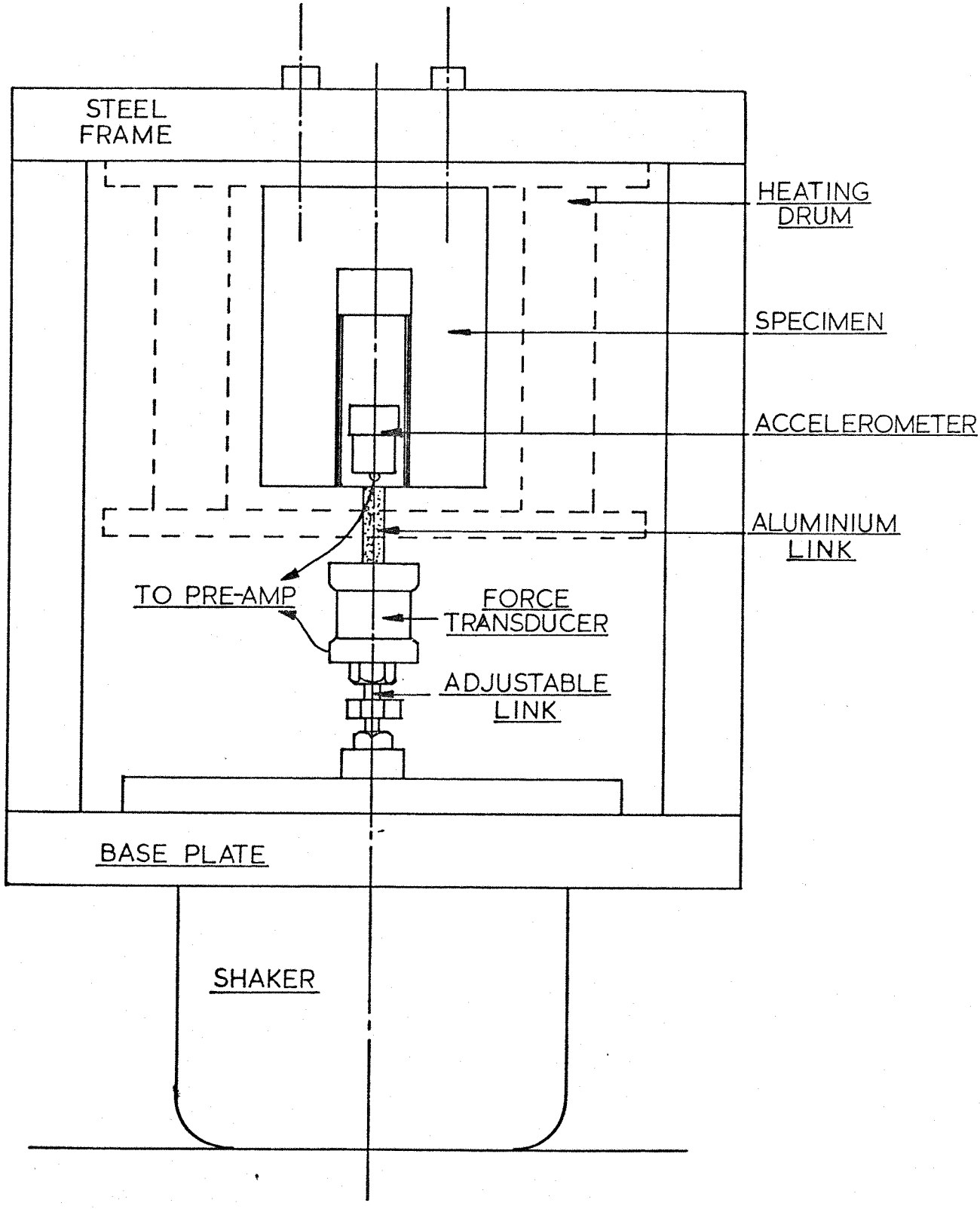


FIG. 5 Details of shear test apparatus

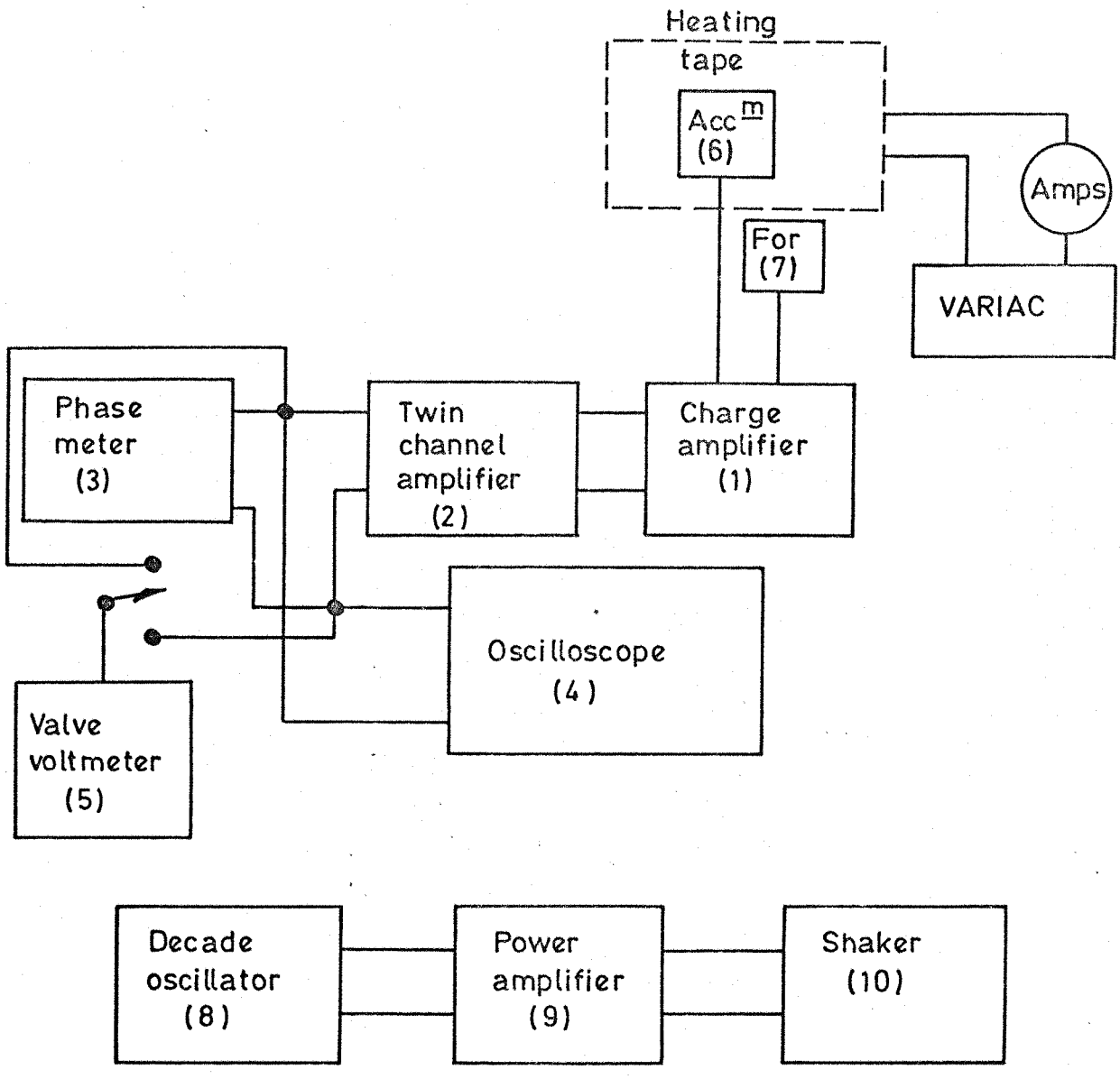


.IST OF EQUIPMENT

B and K type 2262 B accelerometer pre amplifier.
Variable gain phase matched amplifier.
Adyu type 406L phase meter.
Tektronix type 502 double beam oscilloscope.
B and K type 2417 random noise voltmeter.
B and K type 4335 accelerometer.
Endevco type 2103-500 force transducer.
Muirhead type D880B decade oscillator
Beam-echo power amplifier.
Goodmans type V390A vibration generator.

Fig. 6. Block diagram of instrumentation for shear testing

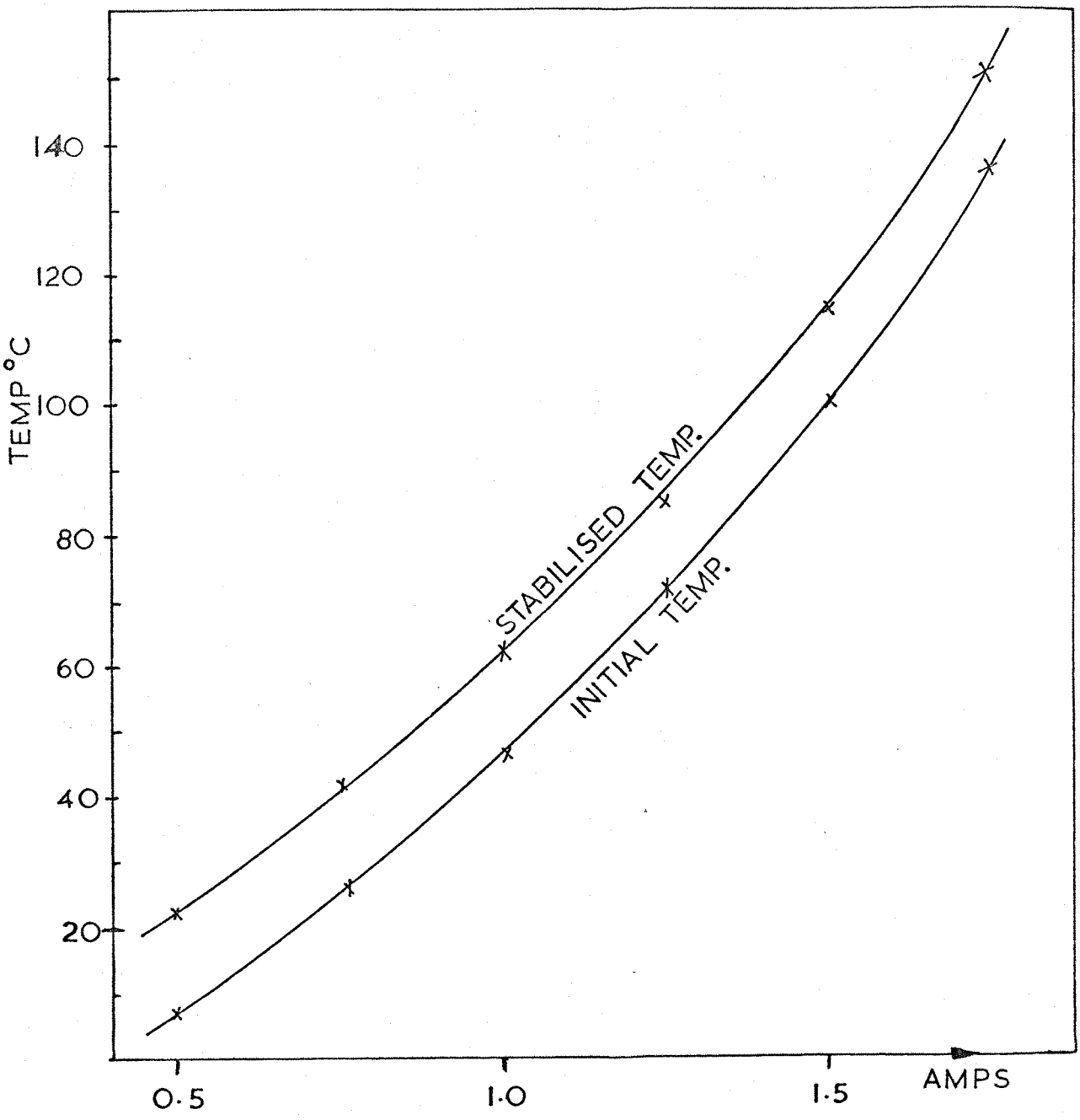


FIG. 7 Temperature rise versus current for heating tape

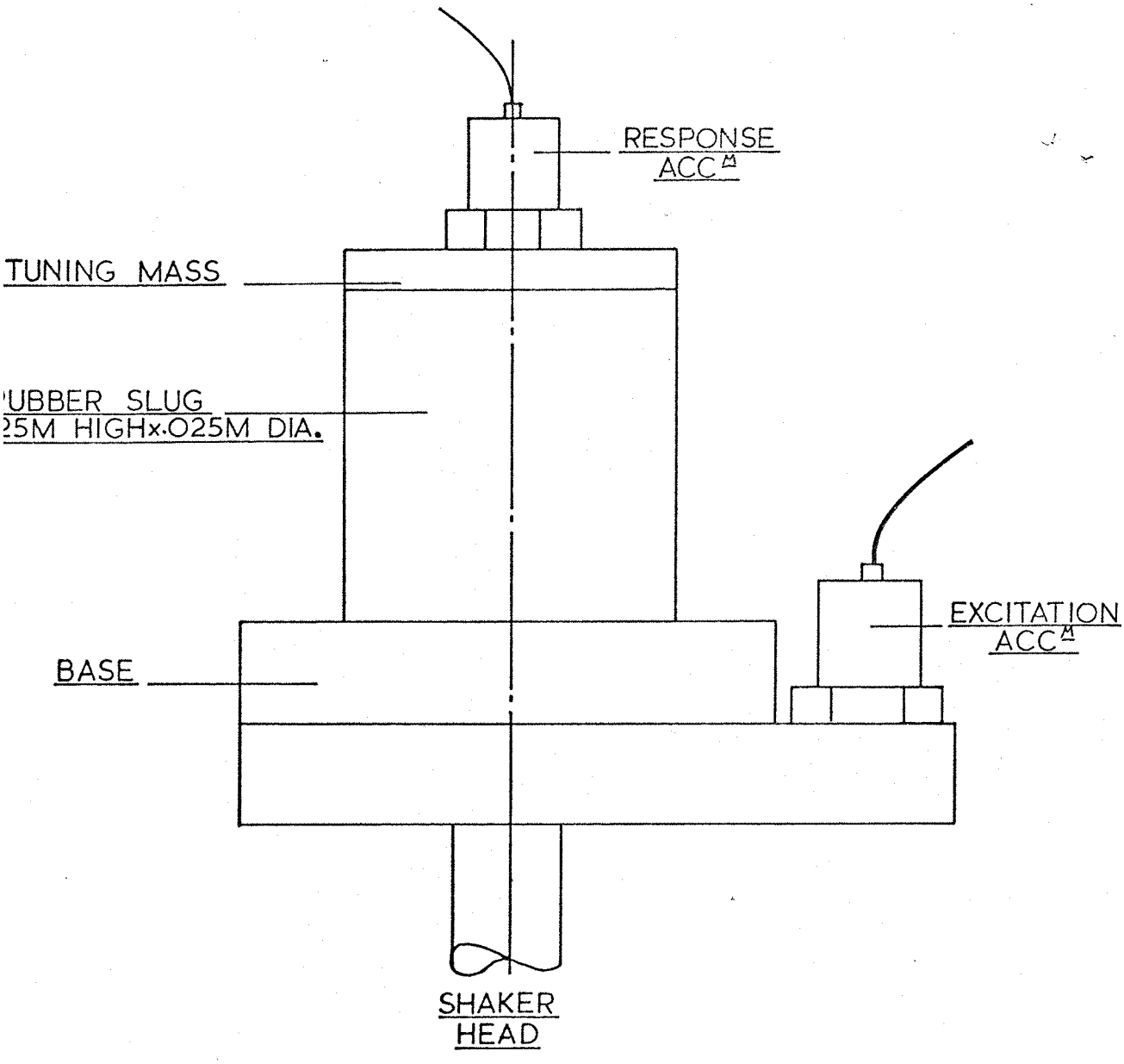


FIG. 8 Details of single slug specimen

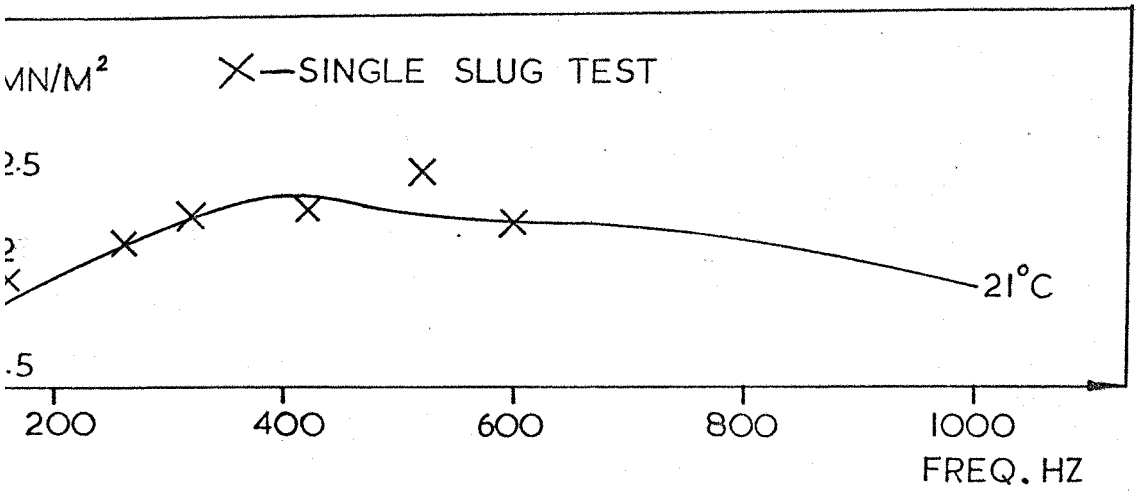


FIG. 9 Comparison of dynamic shear moduli results from single slug and shear tests

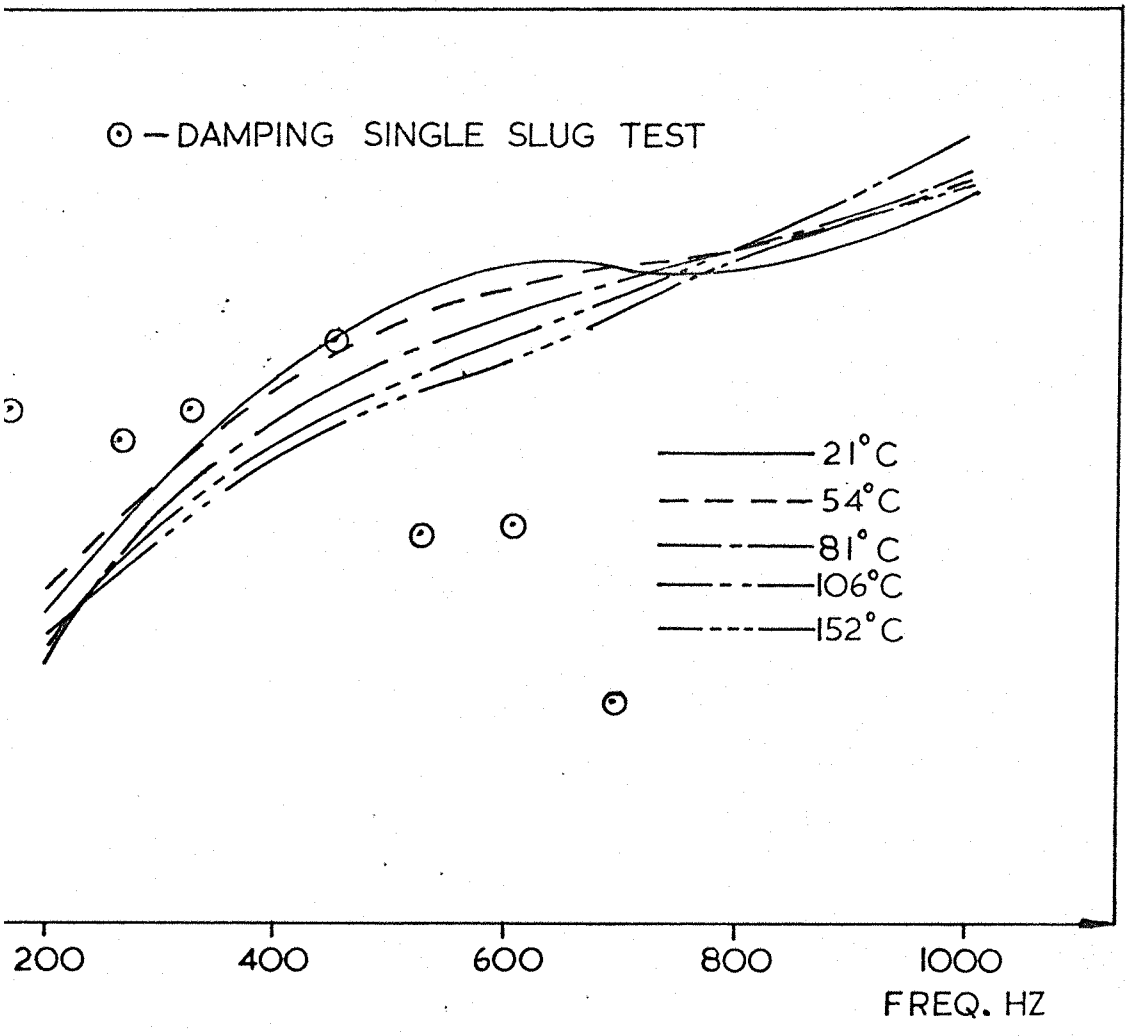


FIG. 10 Comparison of loss factor results from single slug and shear tests

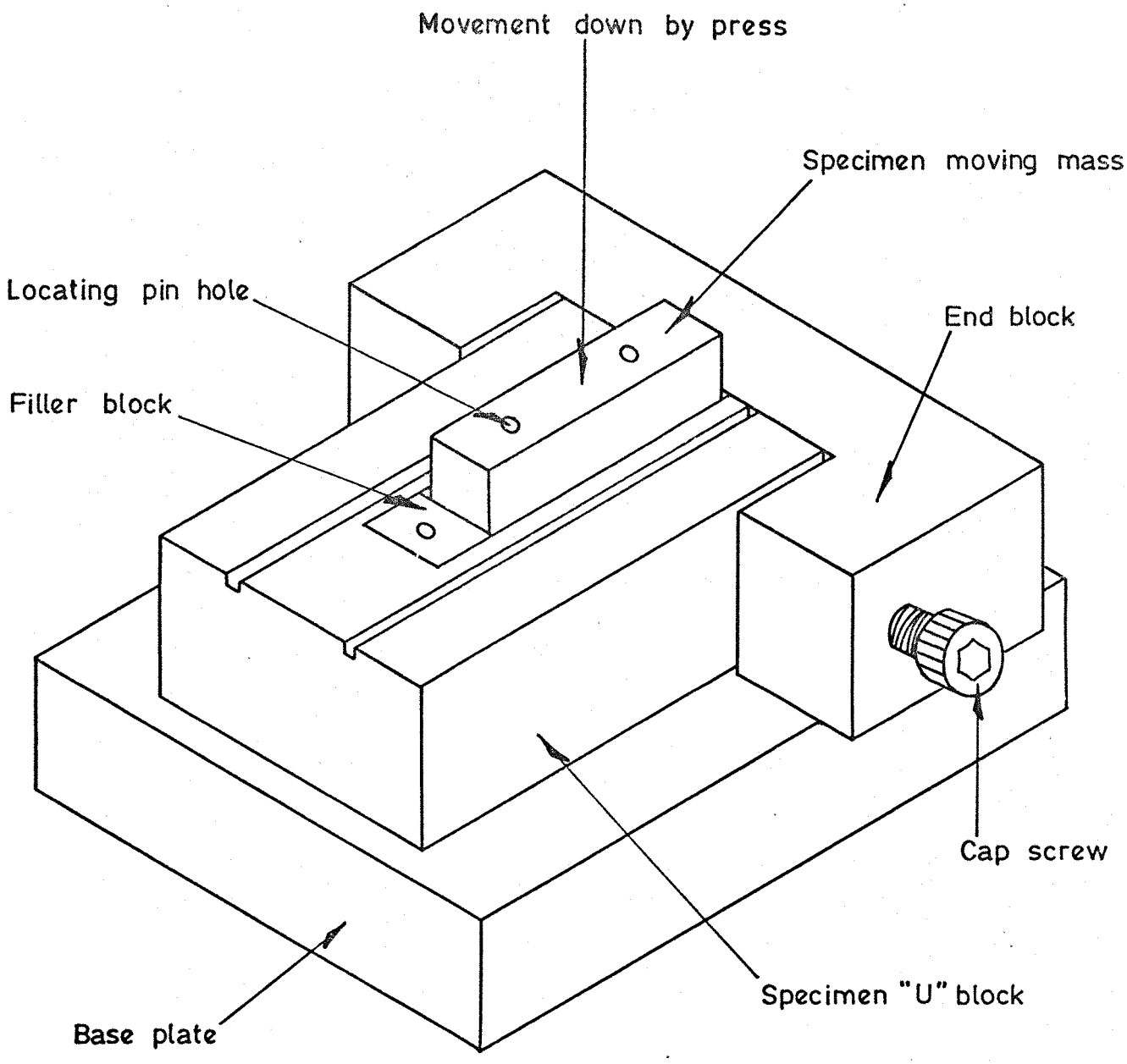


Fig. 11 Details of specimen mould.

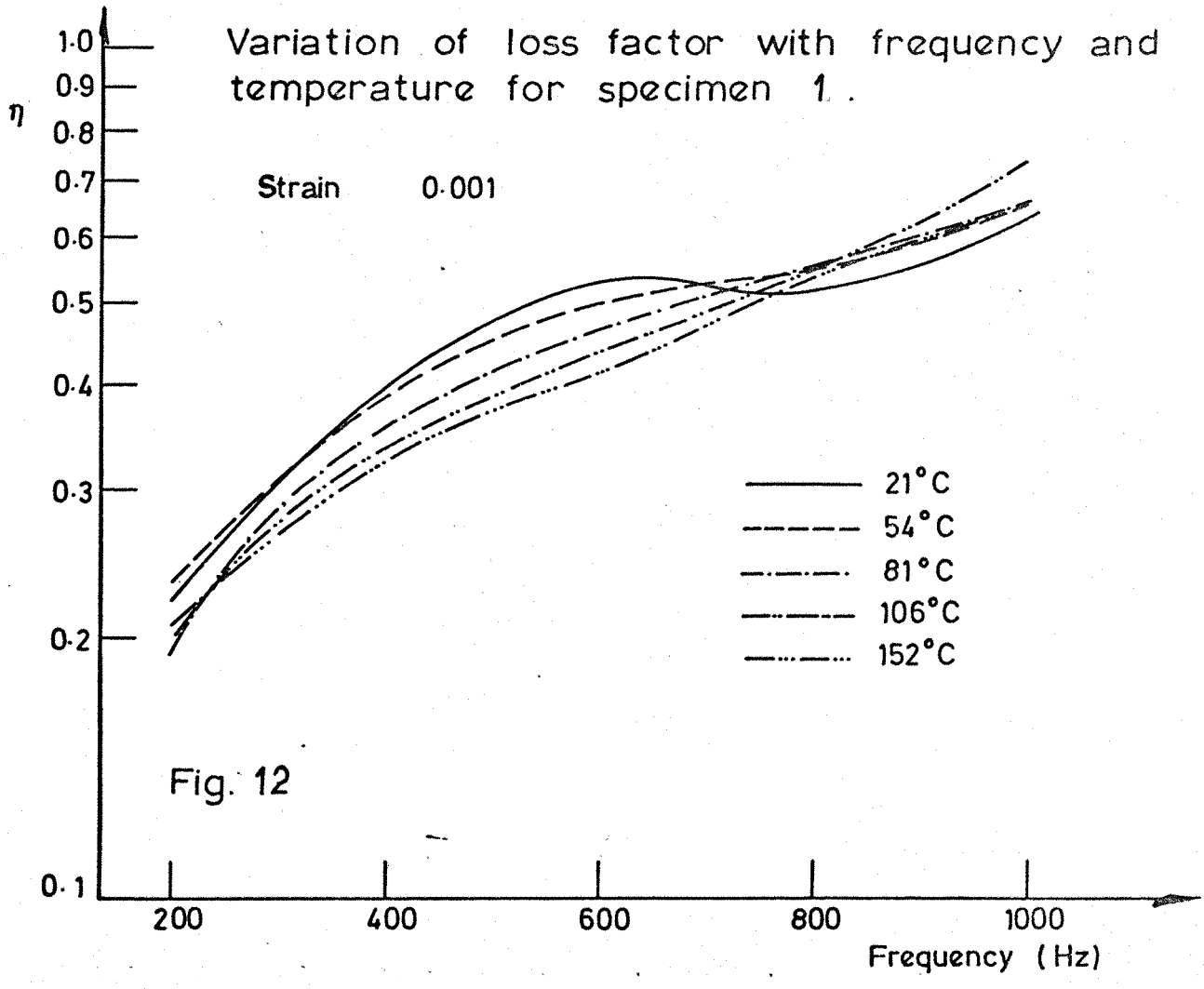
Variation of loss factor with frequency and temperature for specimen 1.
Strain 0·001
η
1·0
0·9
0·8
0·7
0·6
0·5
0·4
0·3
0·2
0·1
21°C
54°C
81°C
106°C
152°C
200
400
600
800
1000
Frequency (Hz)

Fig. 12

Variation of loss factor with frequency and temperature for specimen 4.

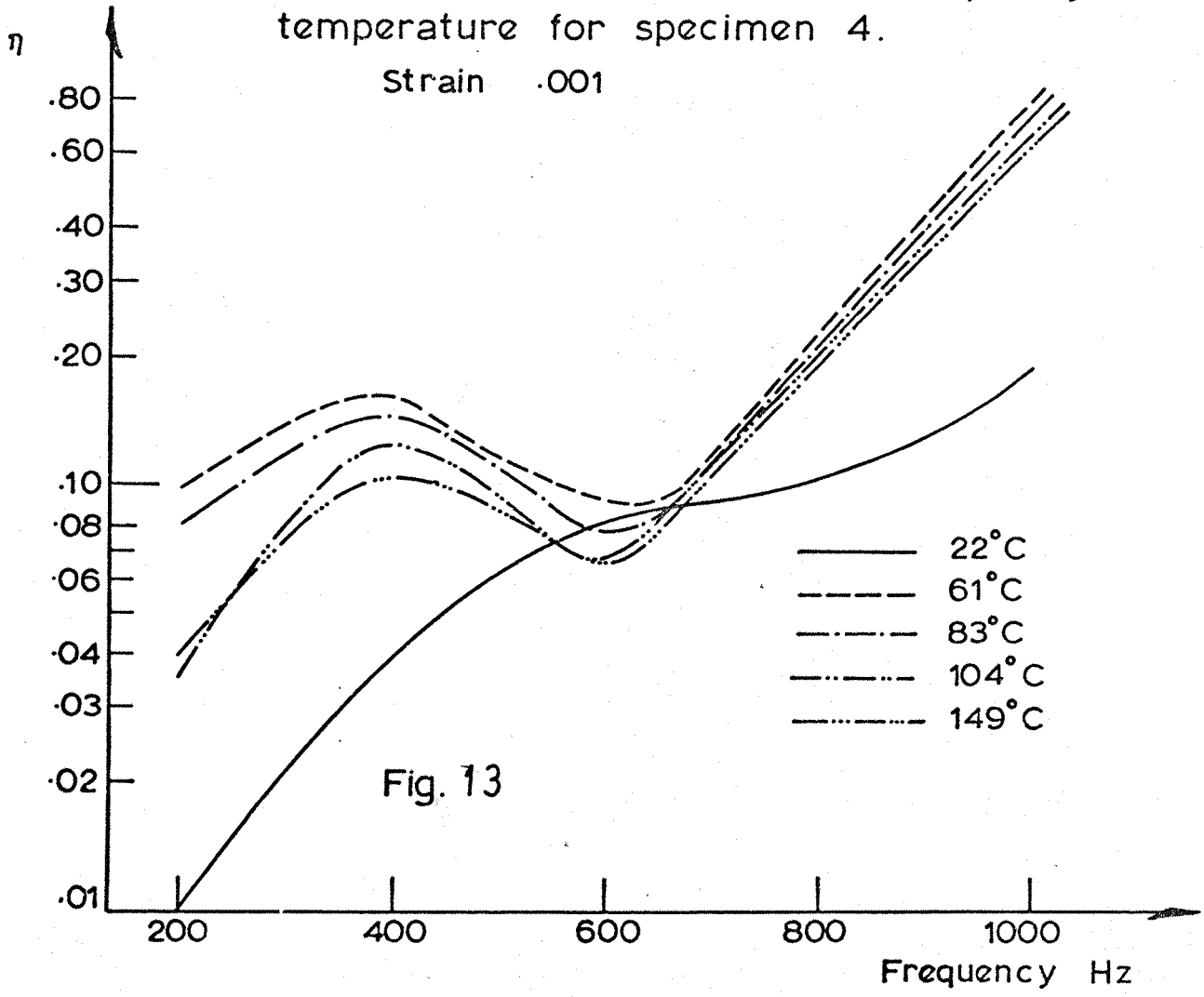


Fig. 13

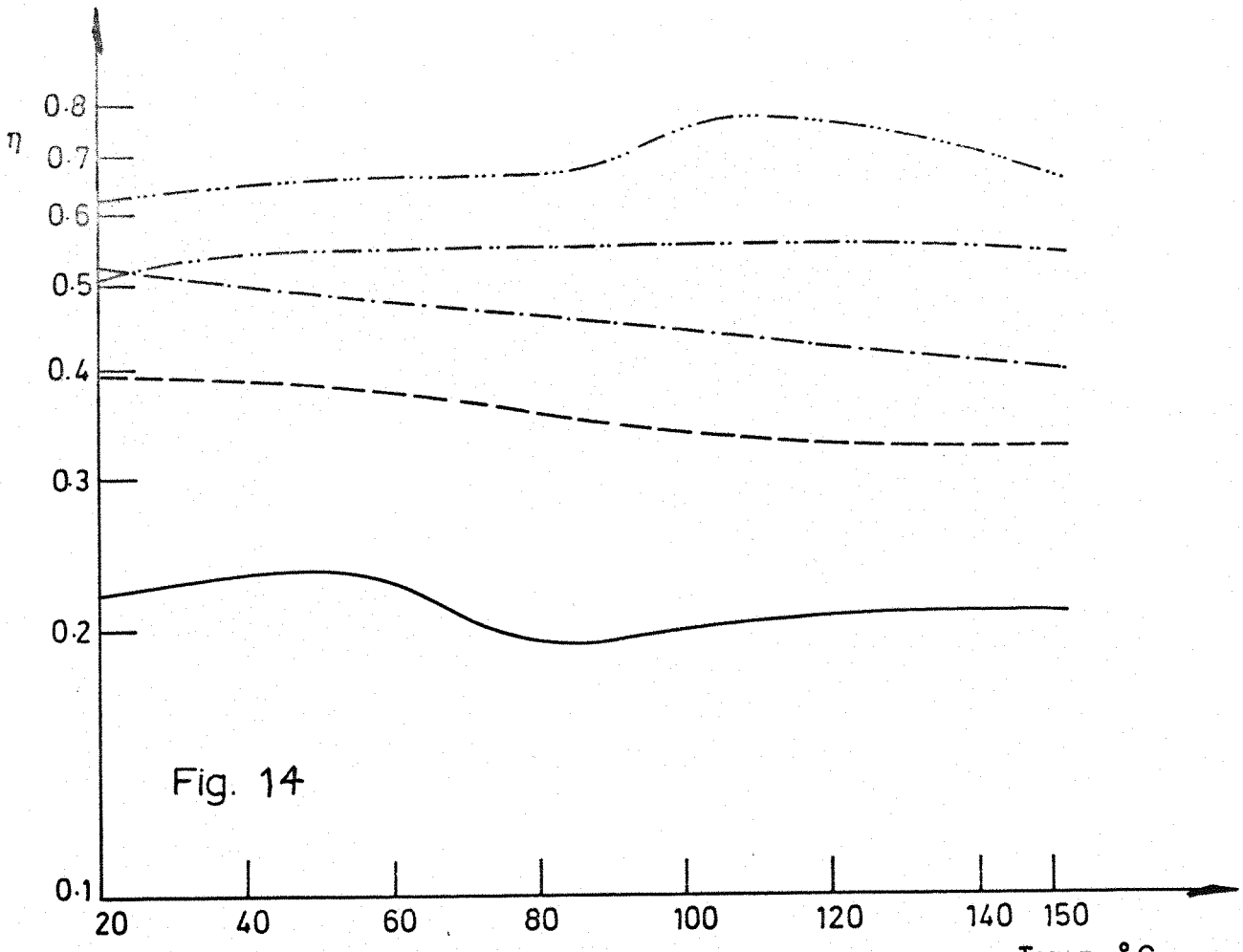


Fig. 14

Variation of Loss Factor with Temperature, Specimen 1, Strain .001

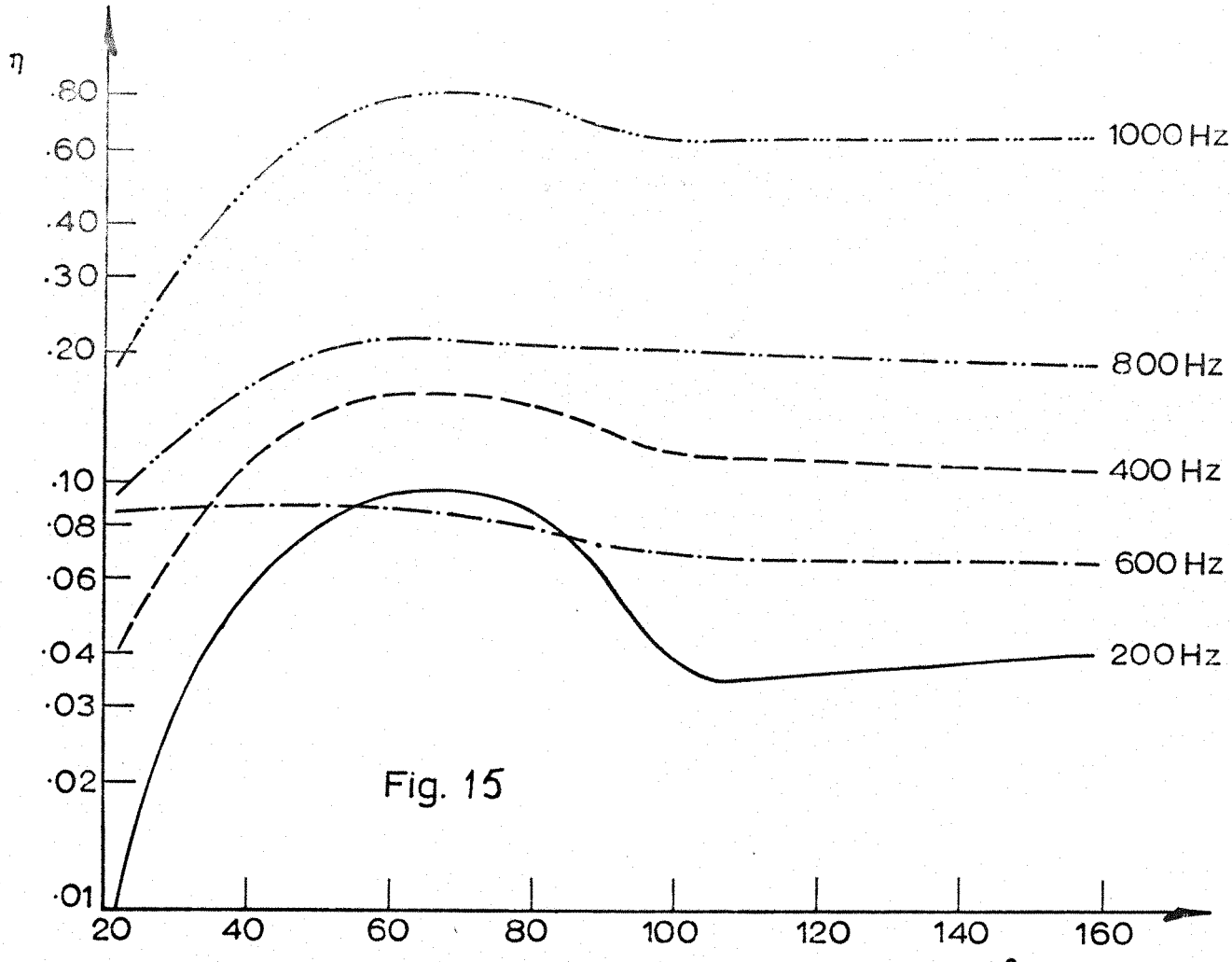


Fig. 15

Variation of Loss Factor with Temperature, Specimen 4, Strain .001

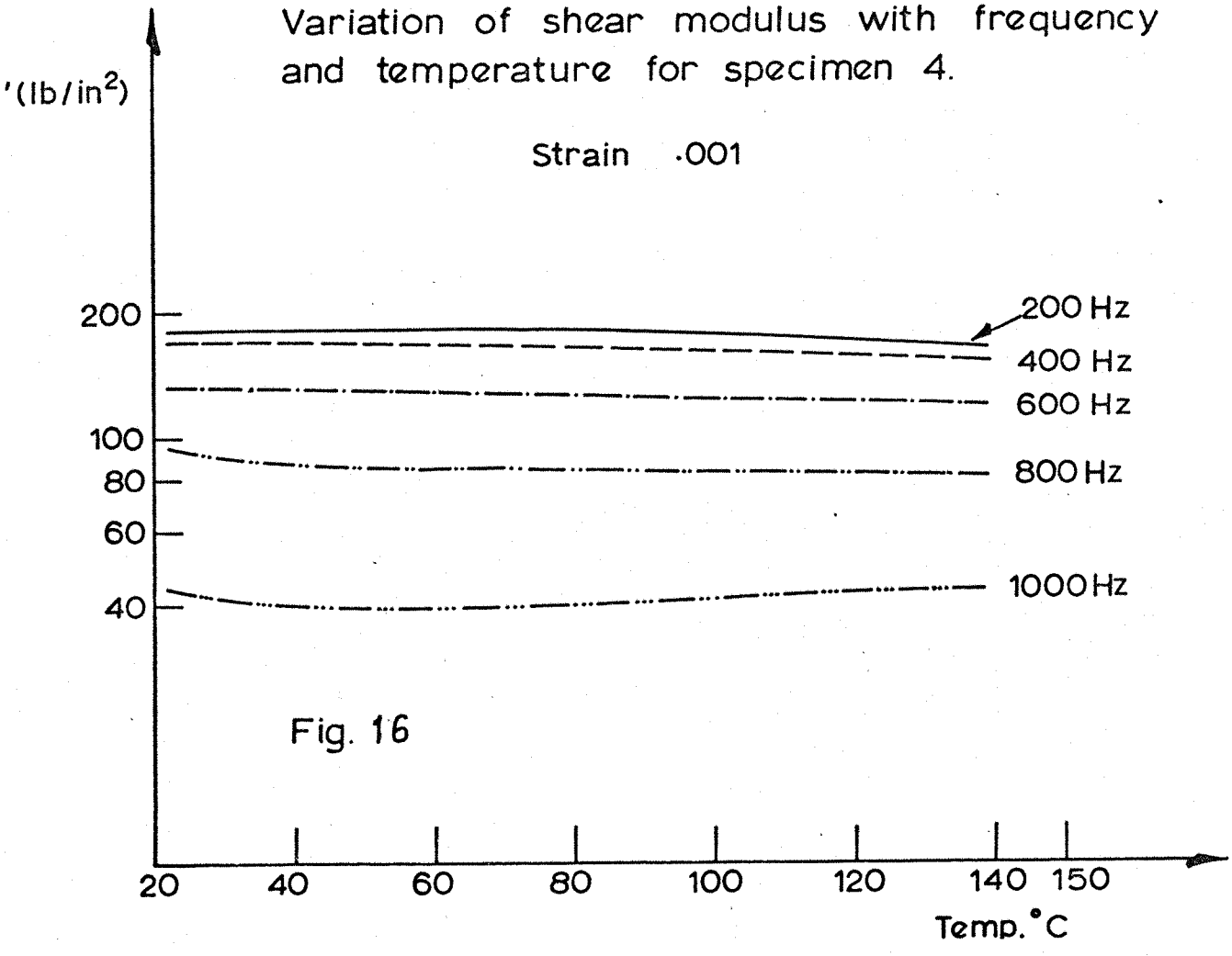
Variation of shear modulus with frequency and temperature for specimen 4.
Strain .001
'(lb/in²)
200
100
80
60
40
200 Hz
400 Hz
600 Hz
800 Hz
1000 Hz
20
40
60
80
100
120
140
150
Temp. °C

Fig. 16

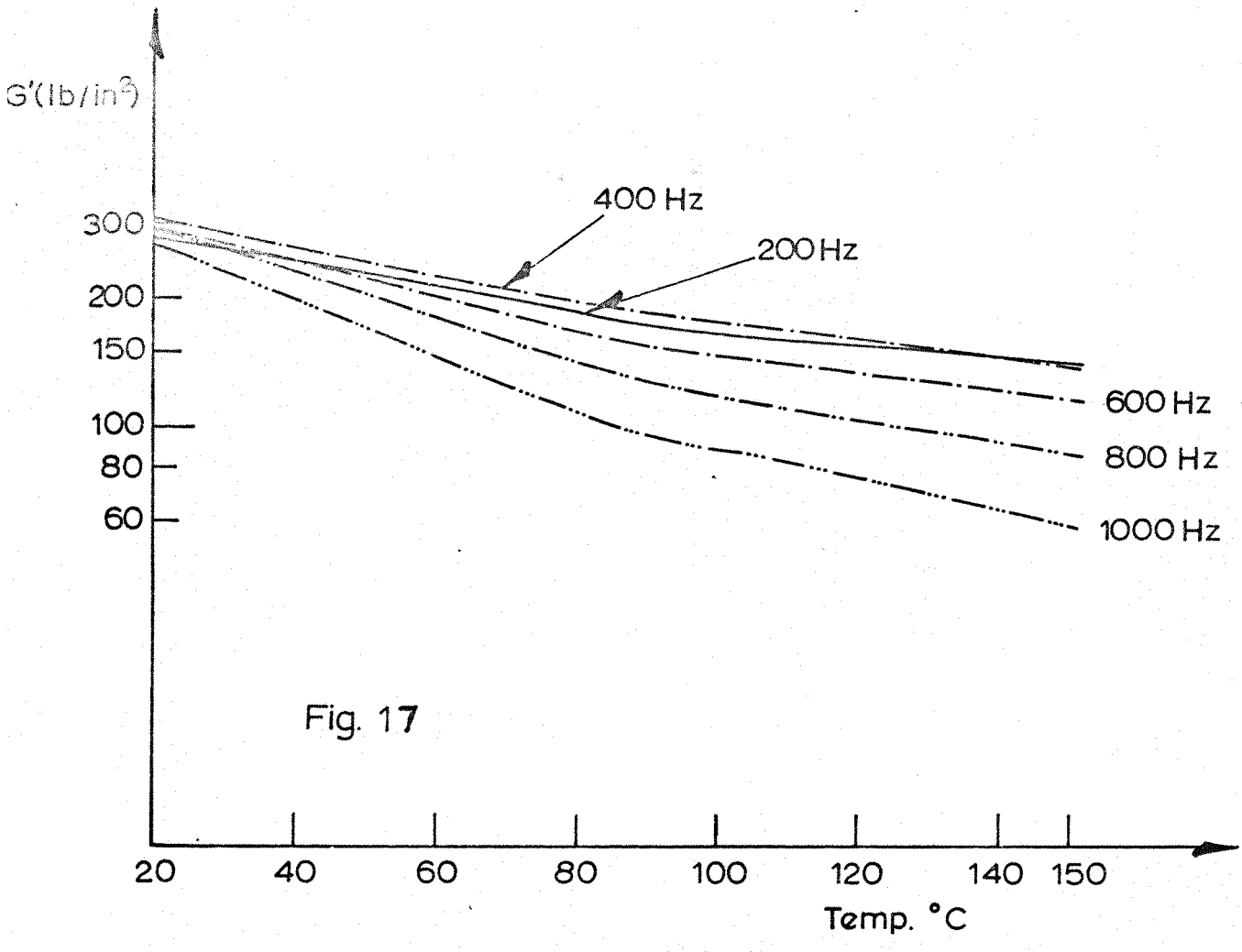


Fig. 17

Variation of Shear Modulus with Temperature for Specimen 1, Strain .001

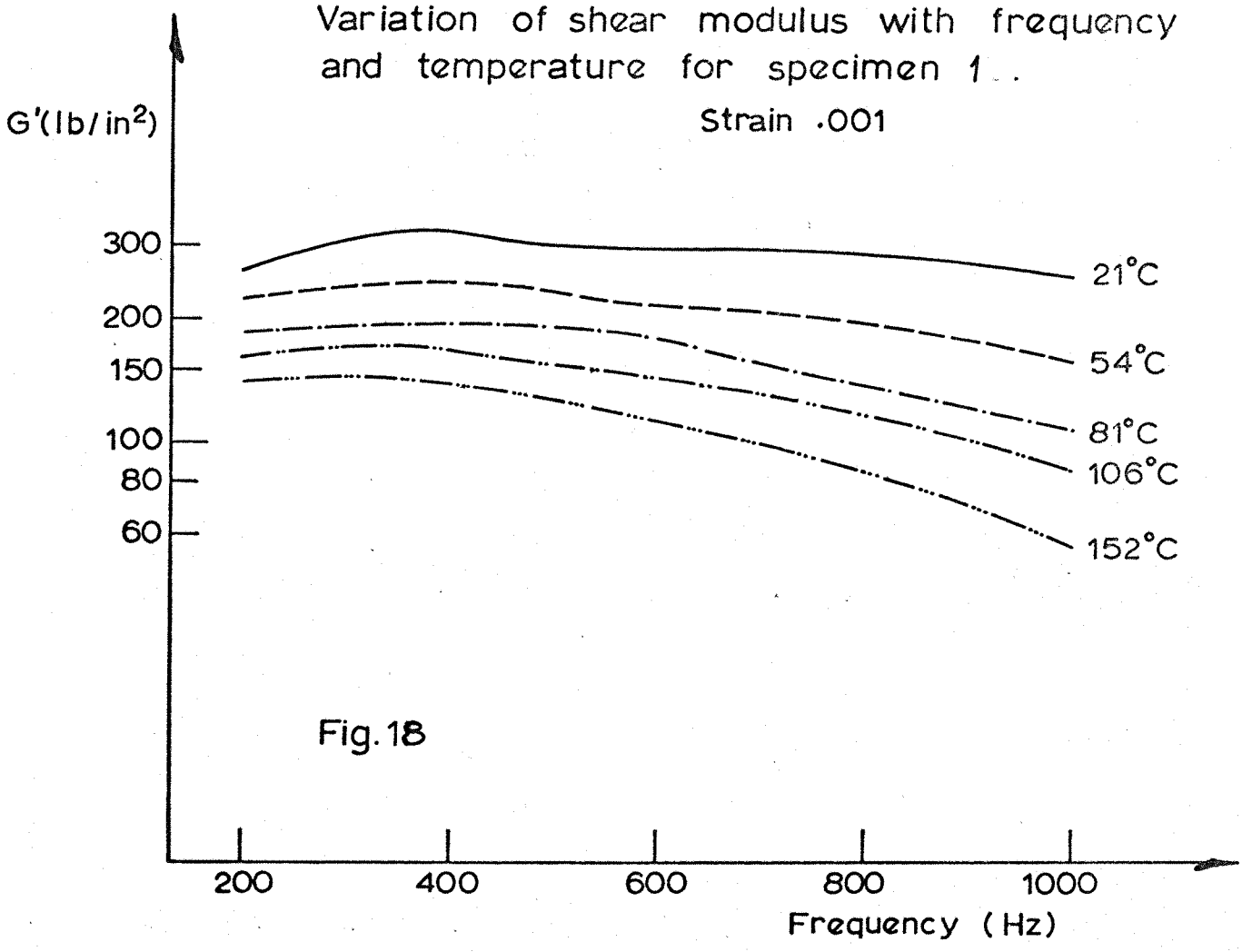
Variation of shear modulus with frequency and temperature for specimen 1 .
Strain .001
G'(lb/in²)
300
200
150
100
80
60
21°C
54°C
81°C
106°C
152°C
200
400
600
800
1000
Frequency (Hz)

Fig. 18

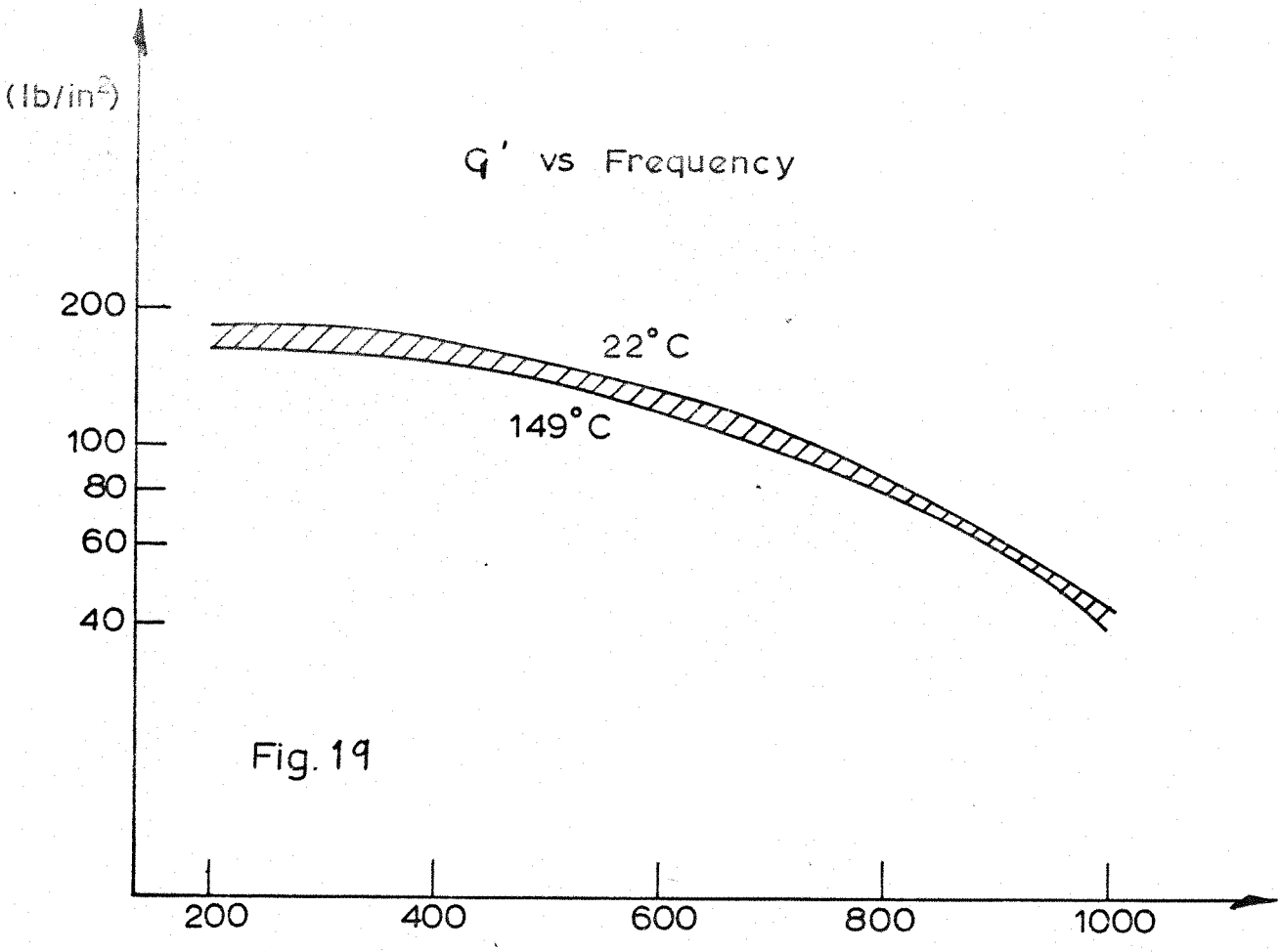


Fig. 19

Variation of Shear Modulus with Frequency for Specimen 4, Strain .001

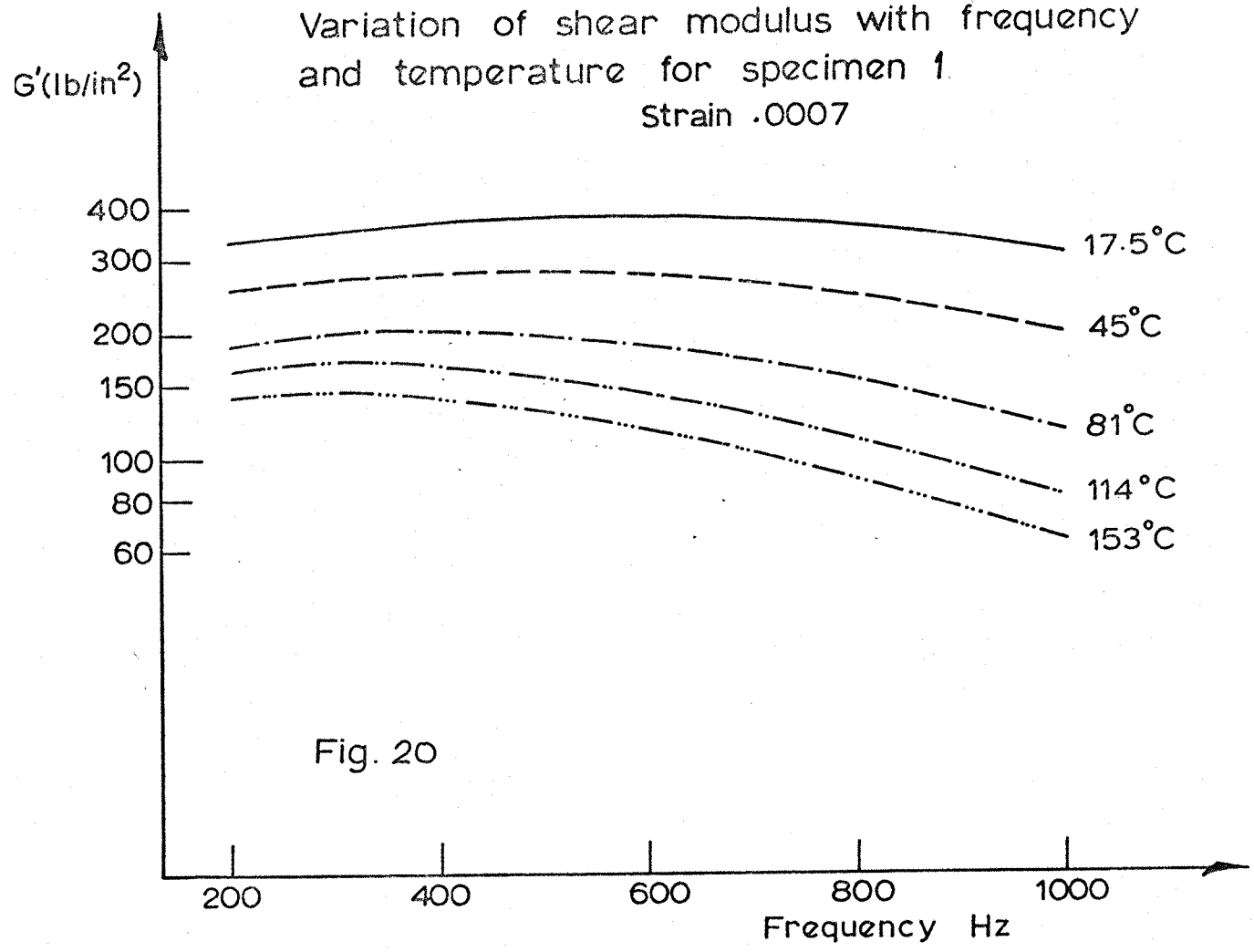
Variation of shear modulus with frequency and temperature for specimen 1
Strain .0007
G'(lb/in²)
400
300
200
150
100
80
60
17.5°C
45°C
81°C
114°C
153°C
200
400
600
800
1000
Frequency Hz

Fig. 20

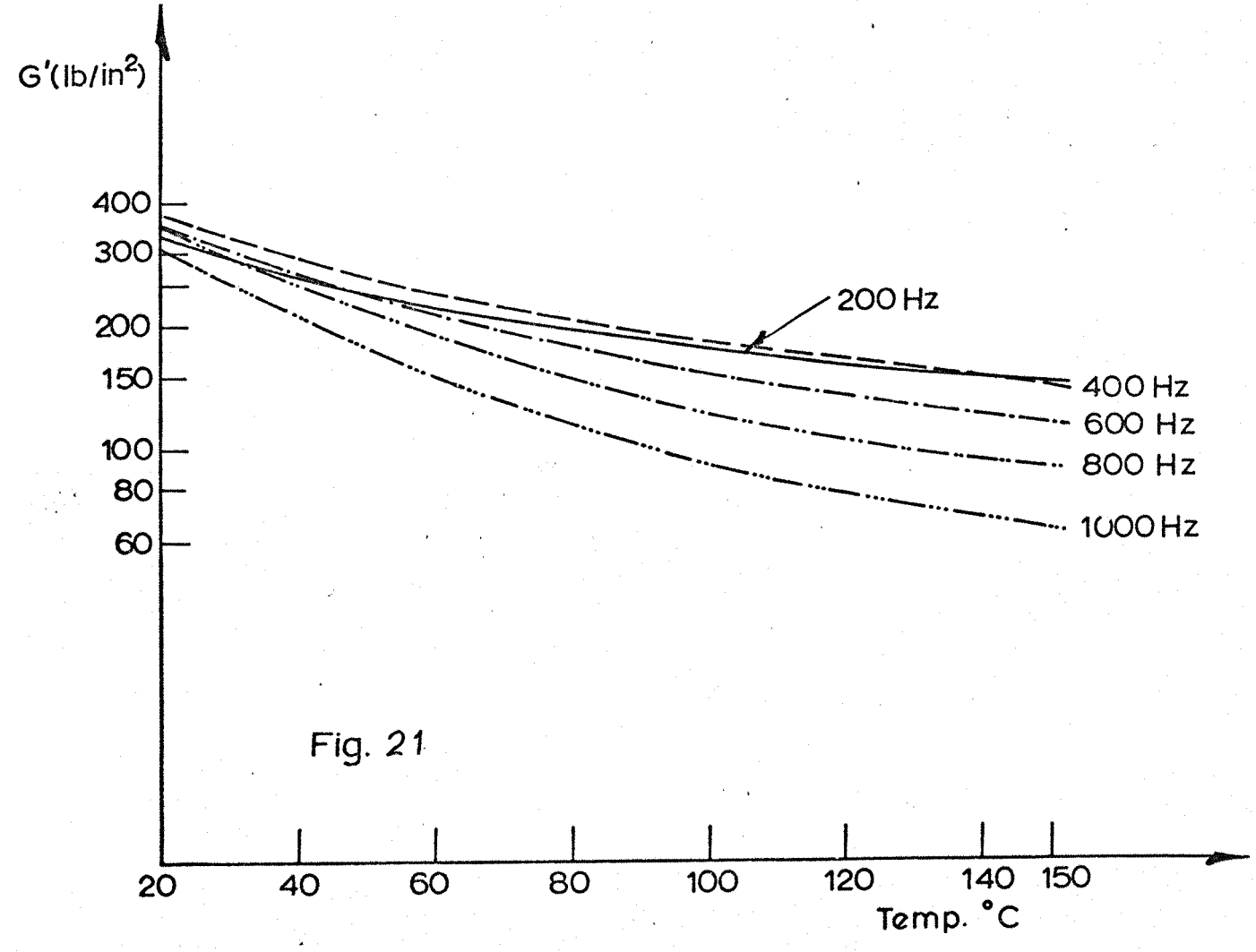
G'(lb/in²)
400
300
200
150
100
80
60
200 Hz
400 Hz
600 Hz
800 Hz
1000 Hz
20
40
60
80
100
120
140
150
Temp. °C

Fig. 21

Variation of shear modulus with frequency and temperature for specimen 1.

Strain .0004

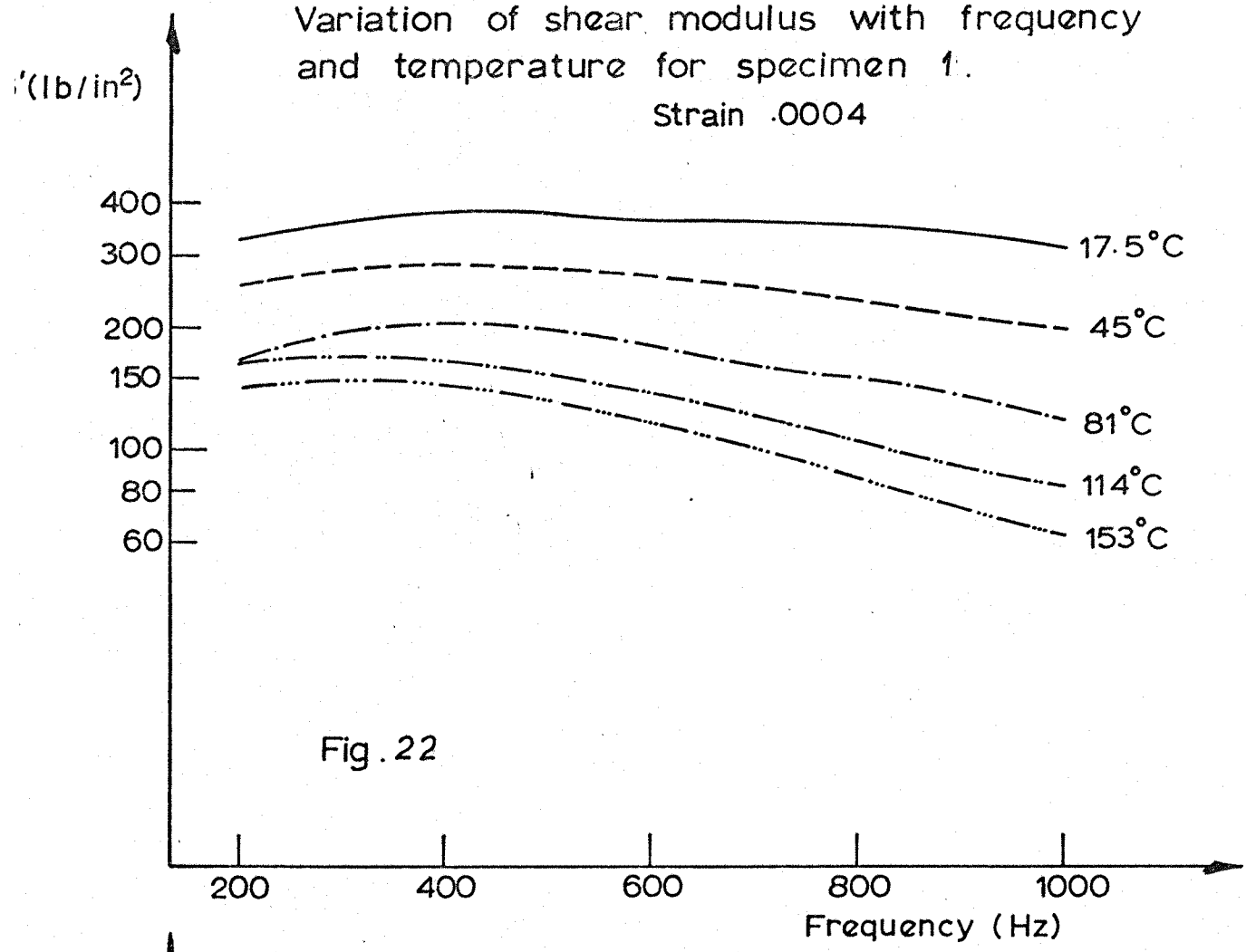


Fig. 22

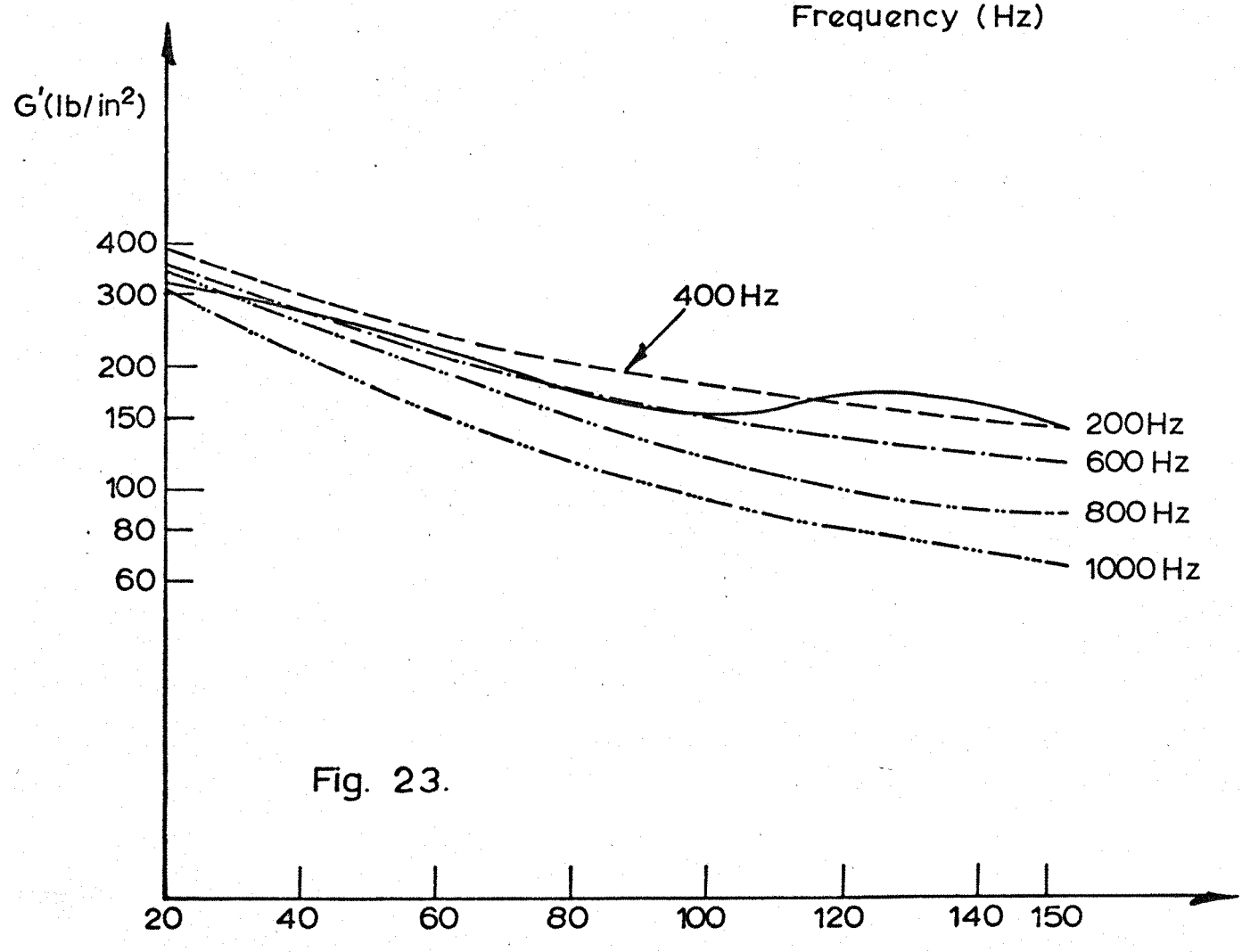


Fig. 23.

Variation of loss factor with frequency and temperature for specimen 1.

Strain 0.0007

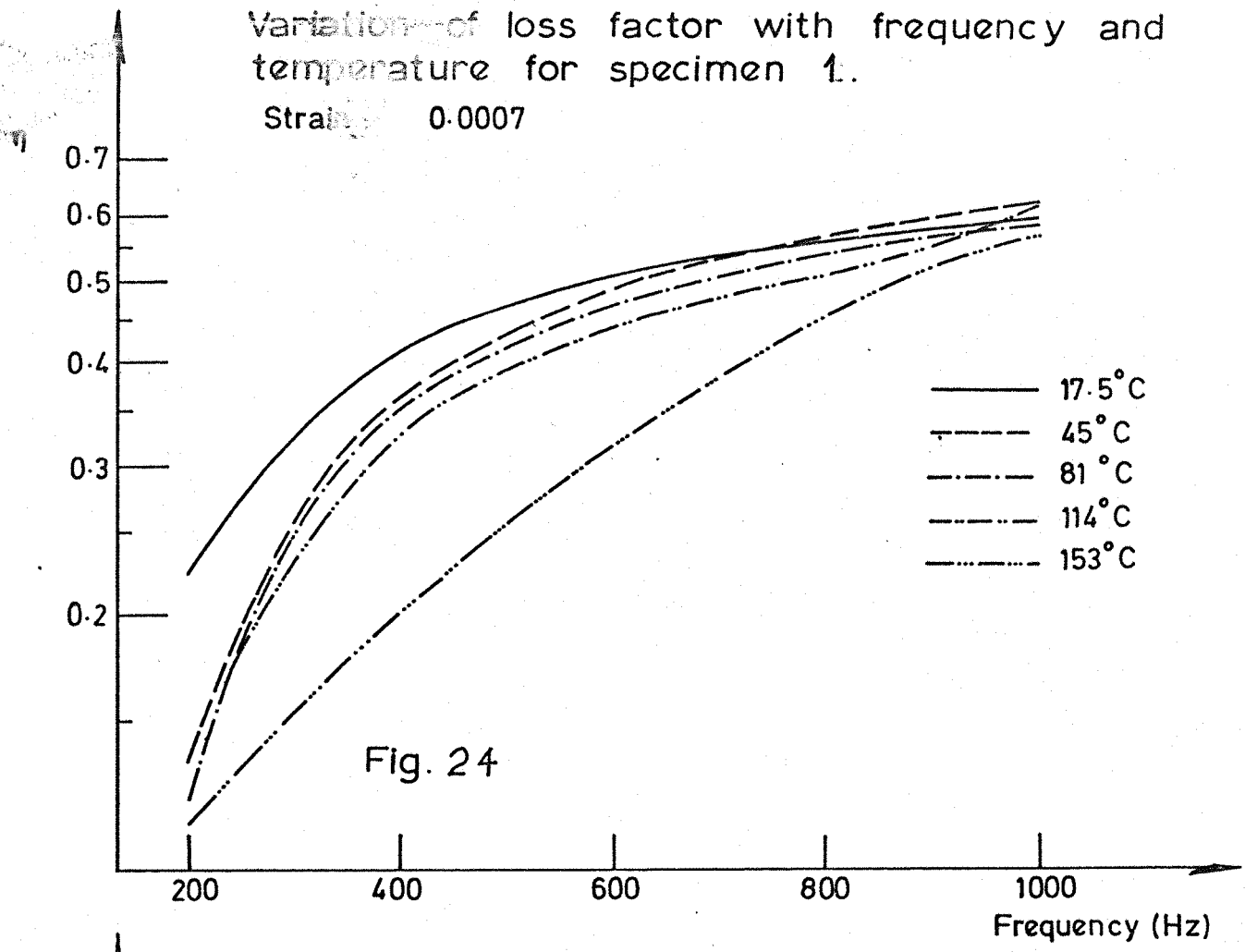


Fig. 24

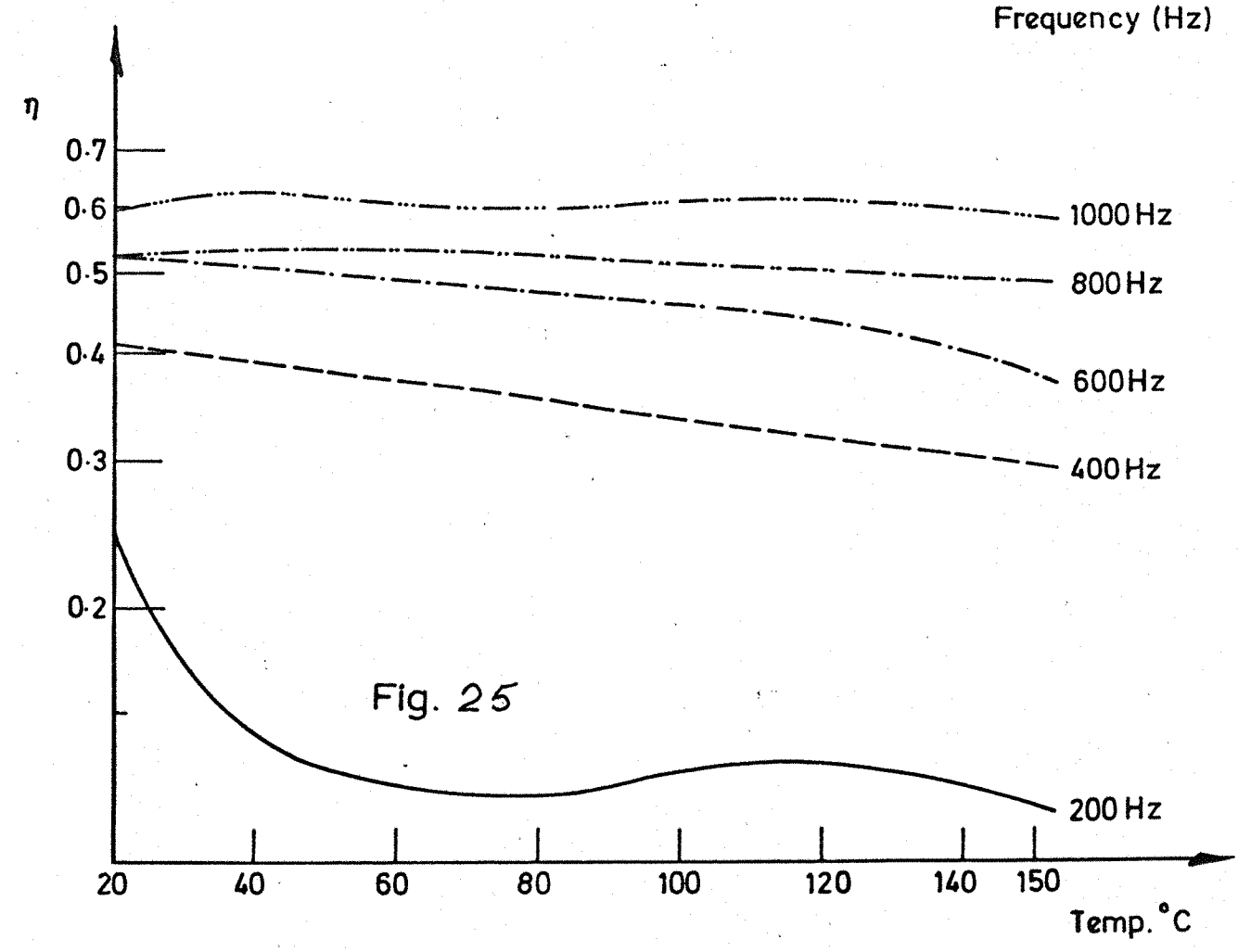


Fig. 25

Variation of loss factor with frequency and temperature for specimen 1..

Strain 0·0004

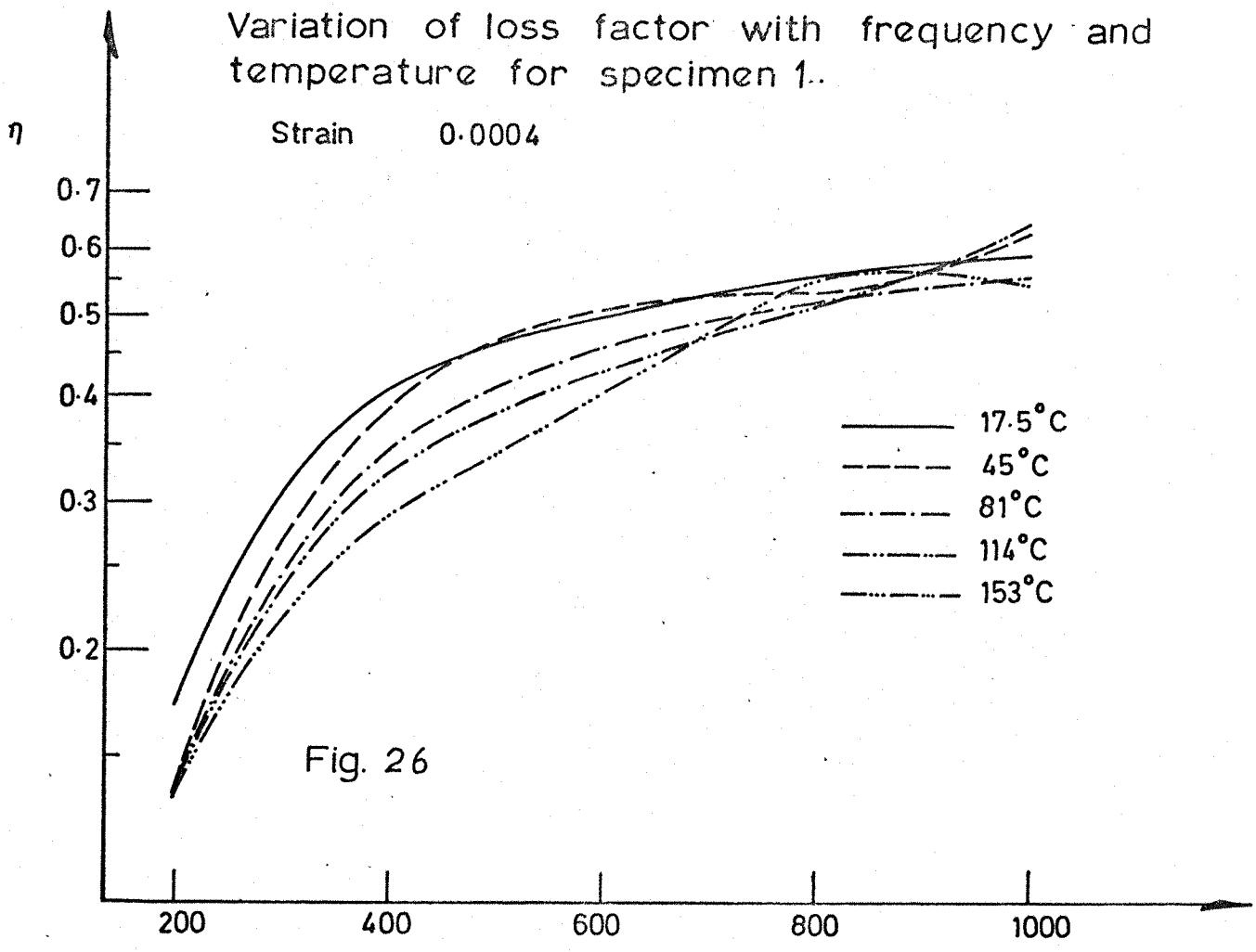


Fig. 26

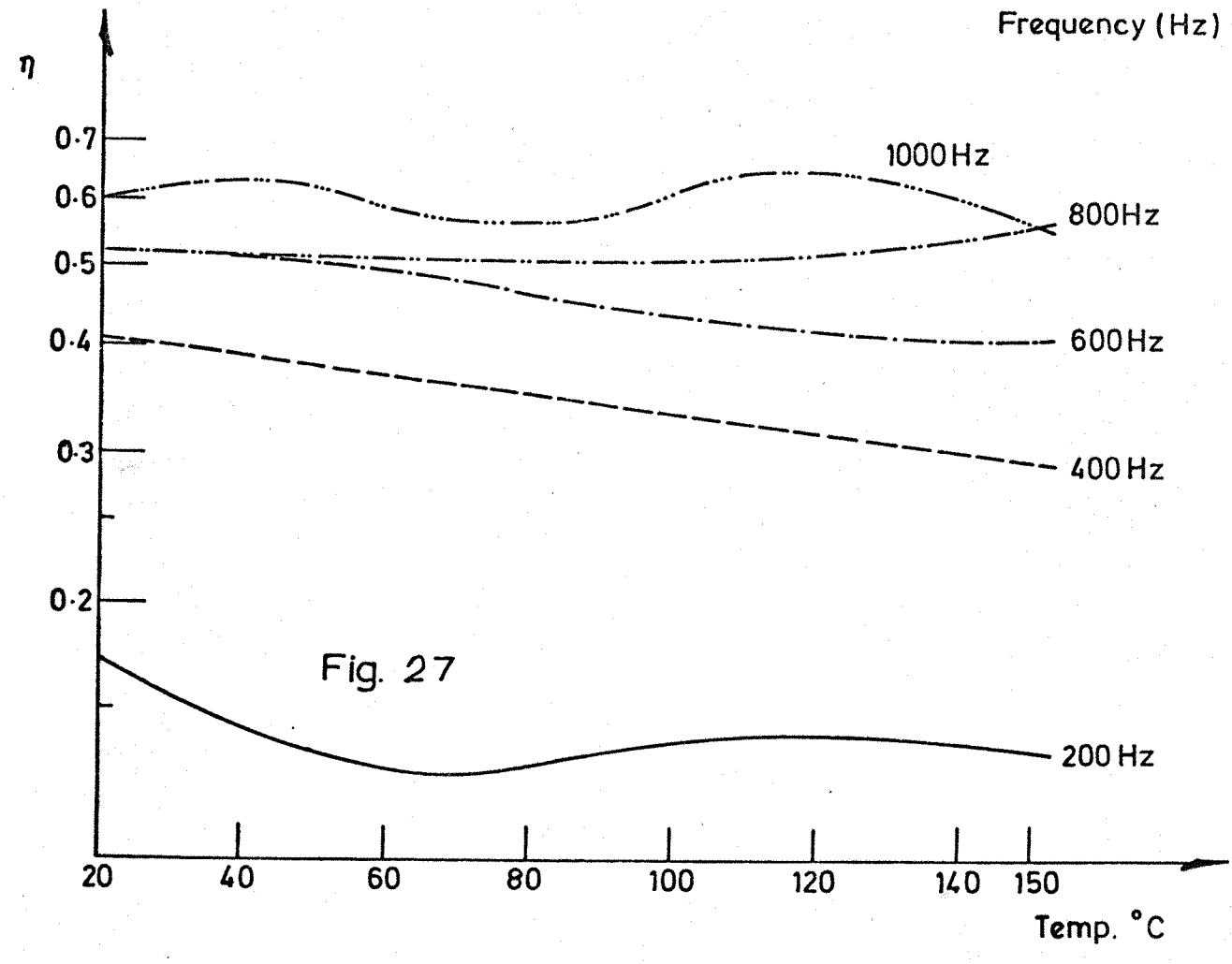


Fig. 27

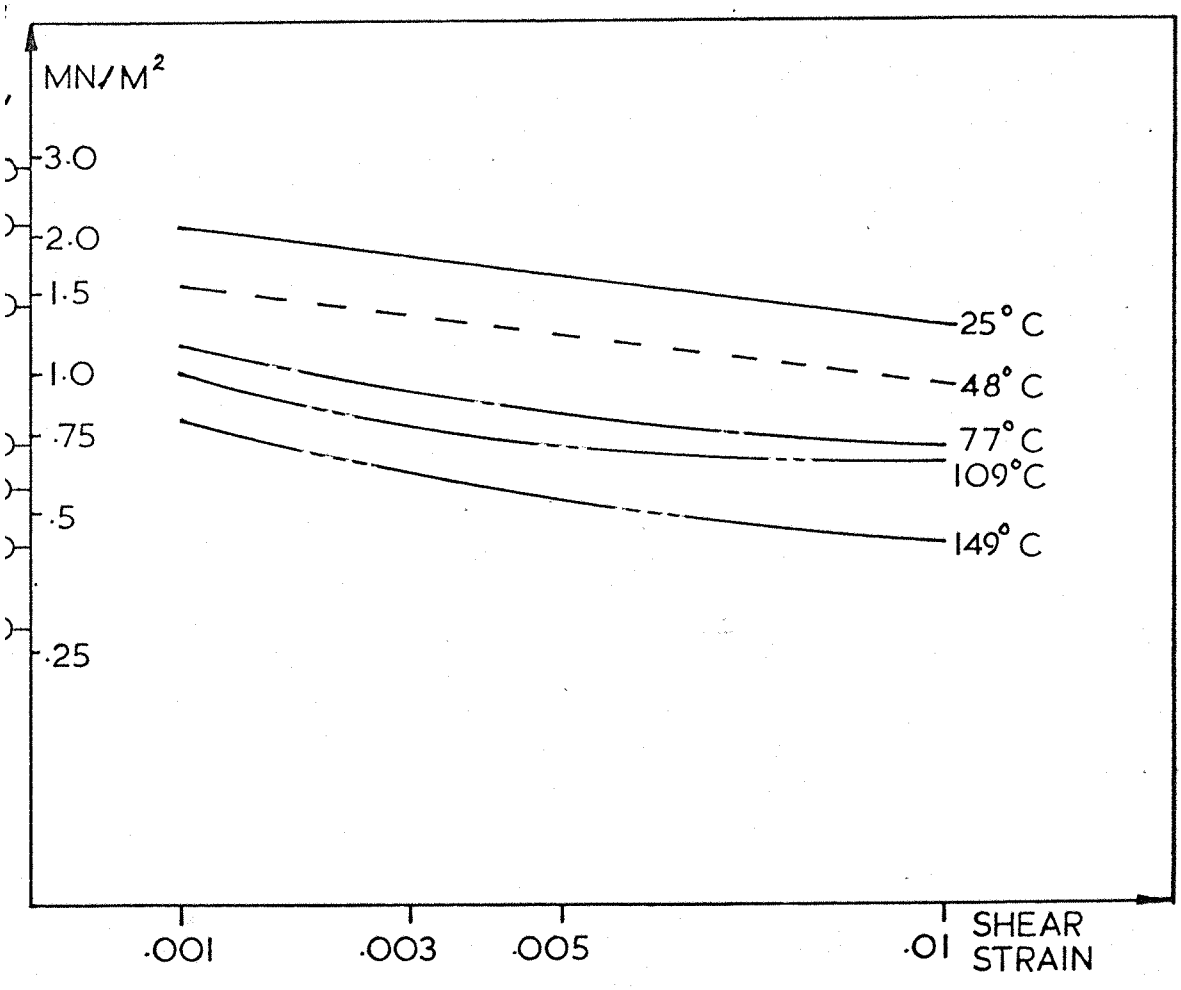


FIG. 28 Shear modulus versus shear strain and temperature for Specimen 1 at 600 Hz

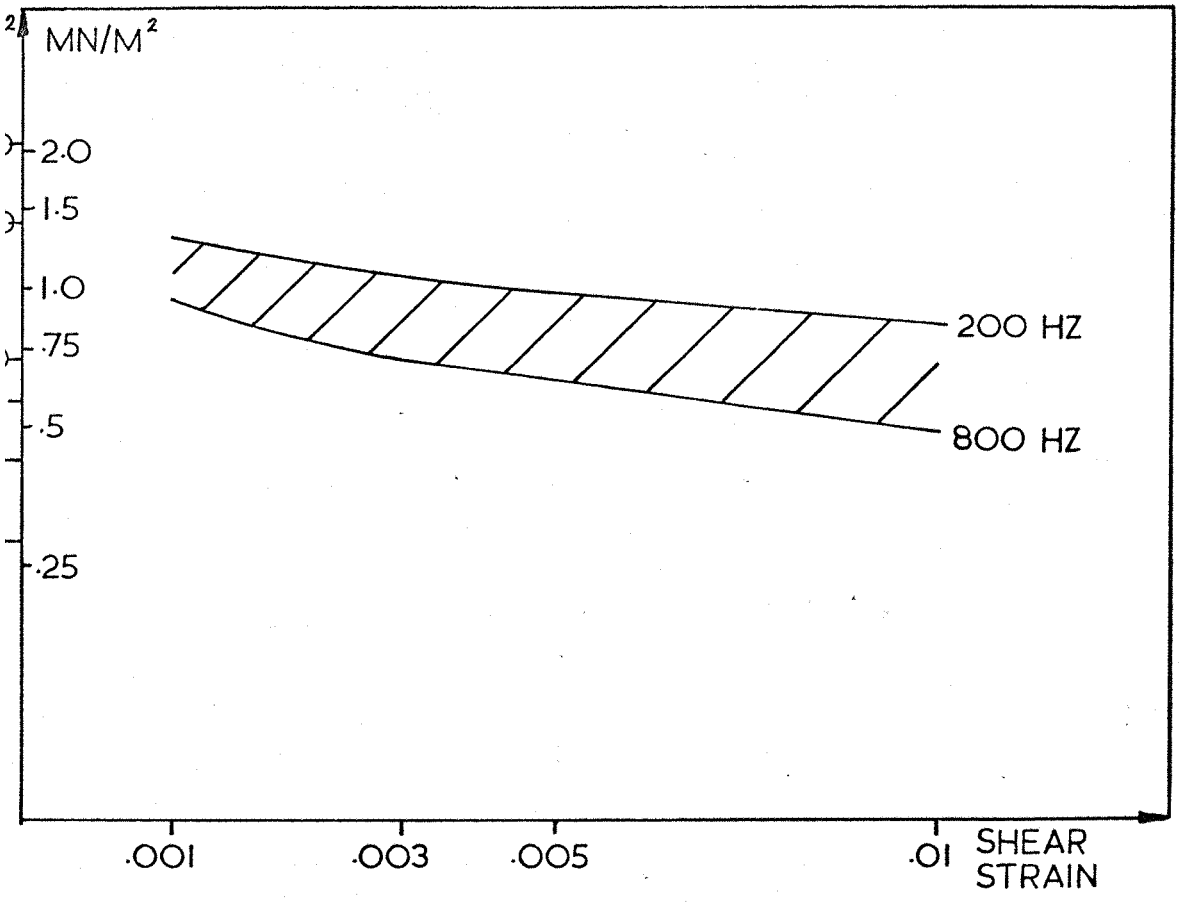


FIG. 29 Shear modulus versus shear strain and frequency for Specimen 1 at 77°C

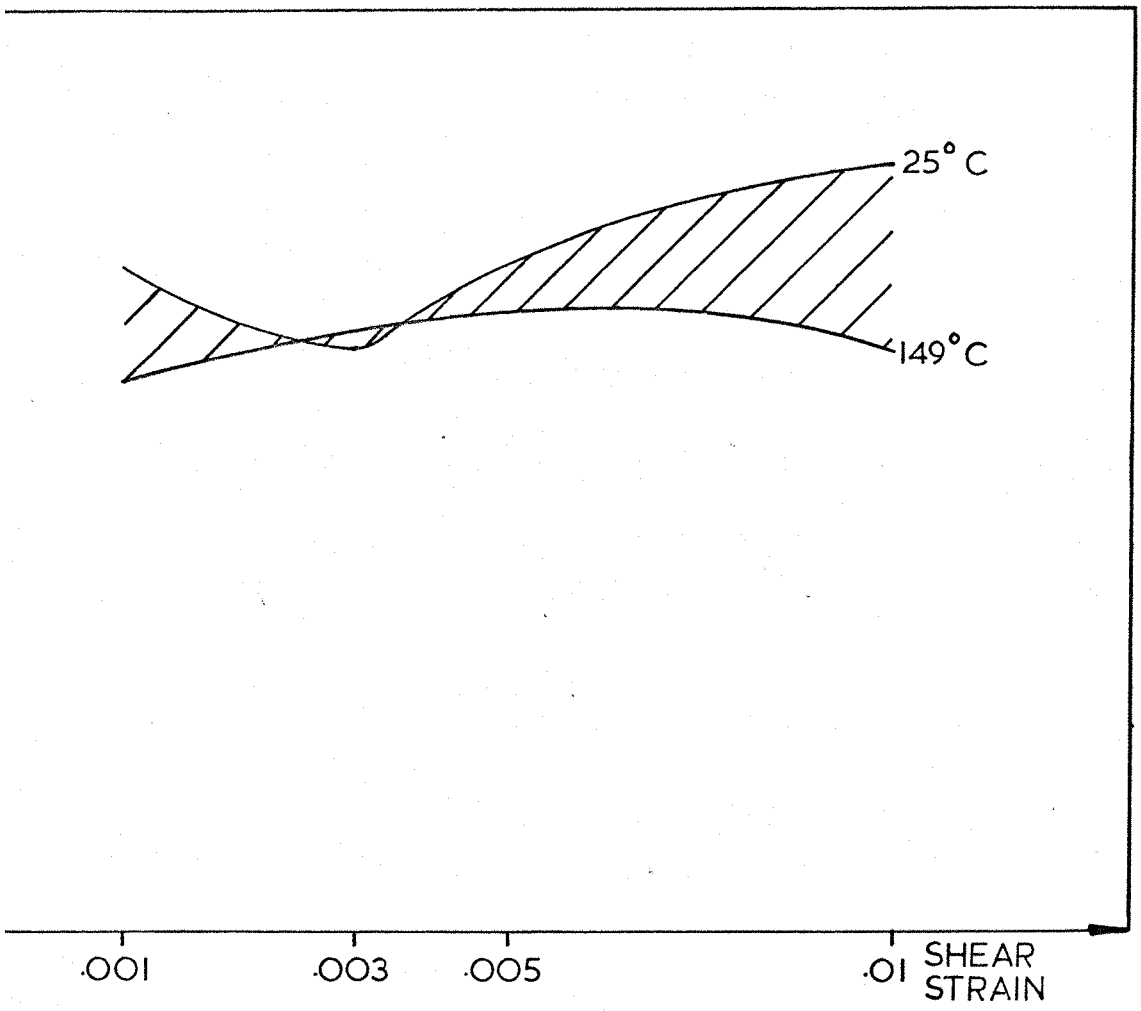


FIG. 30 Loss factor versus shear strain for Specimen 1 at 600 Hz

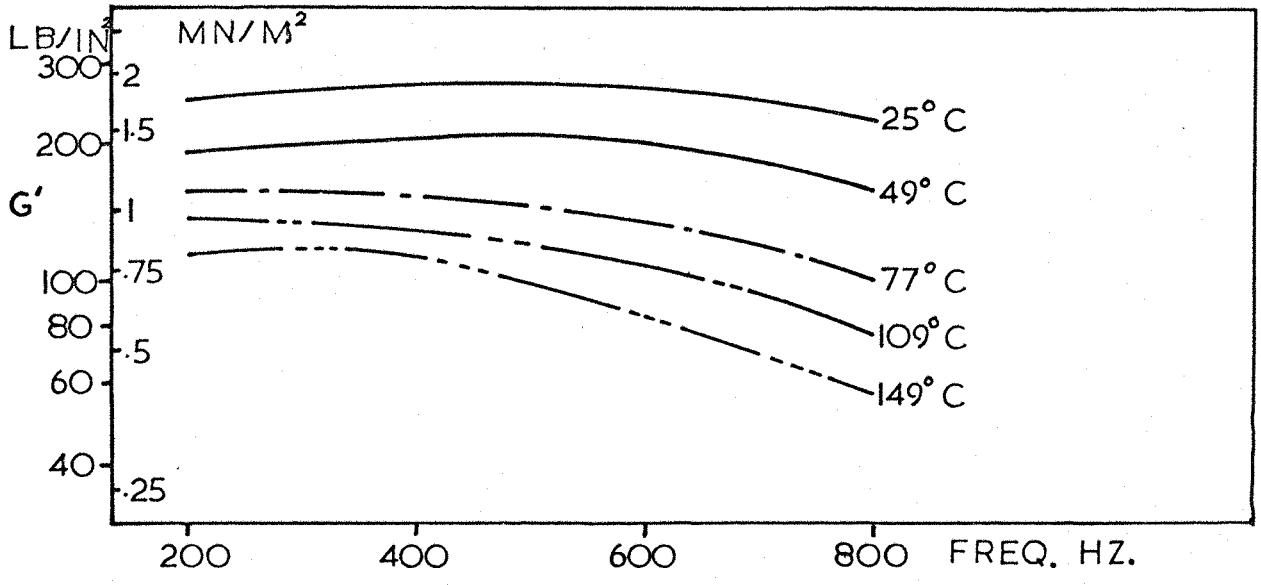


FIG. 31

Shear modulus versus frequency for Specimen 1, strain .003

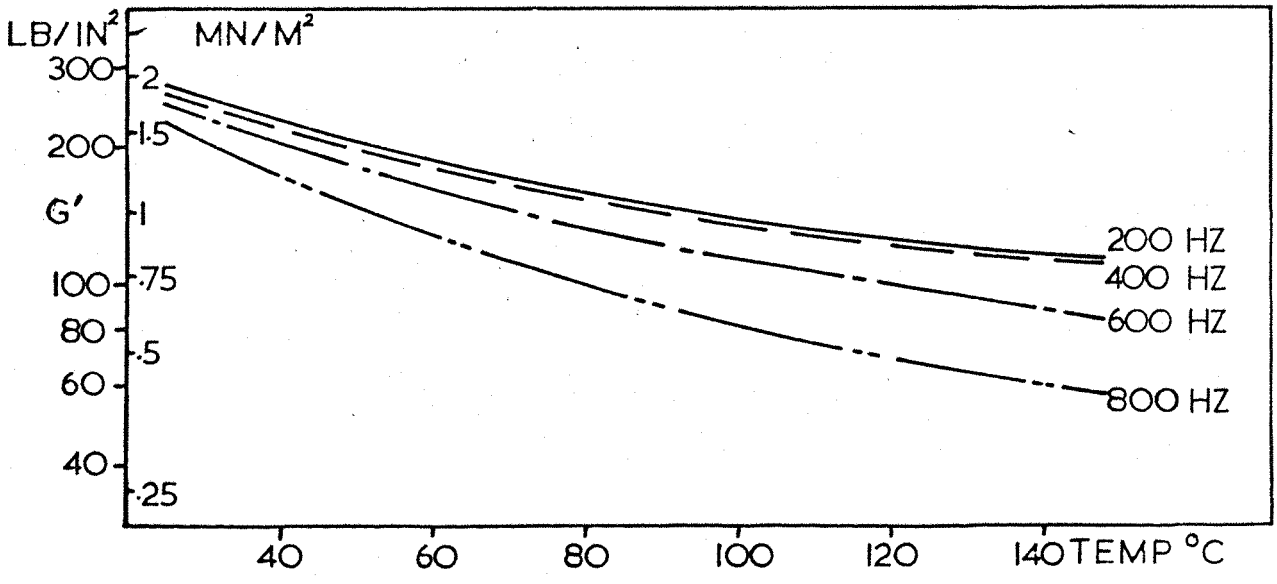


FIG. 32

Shear modulus versus temperature for Specimen 1, strain .003

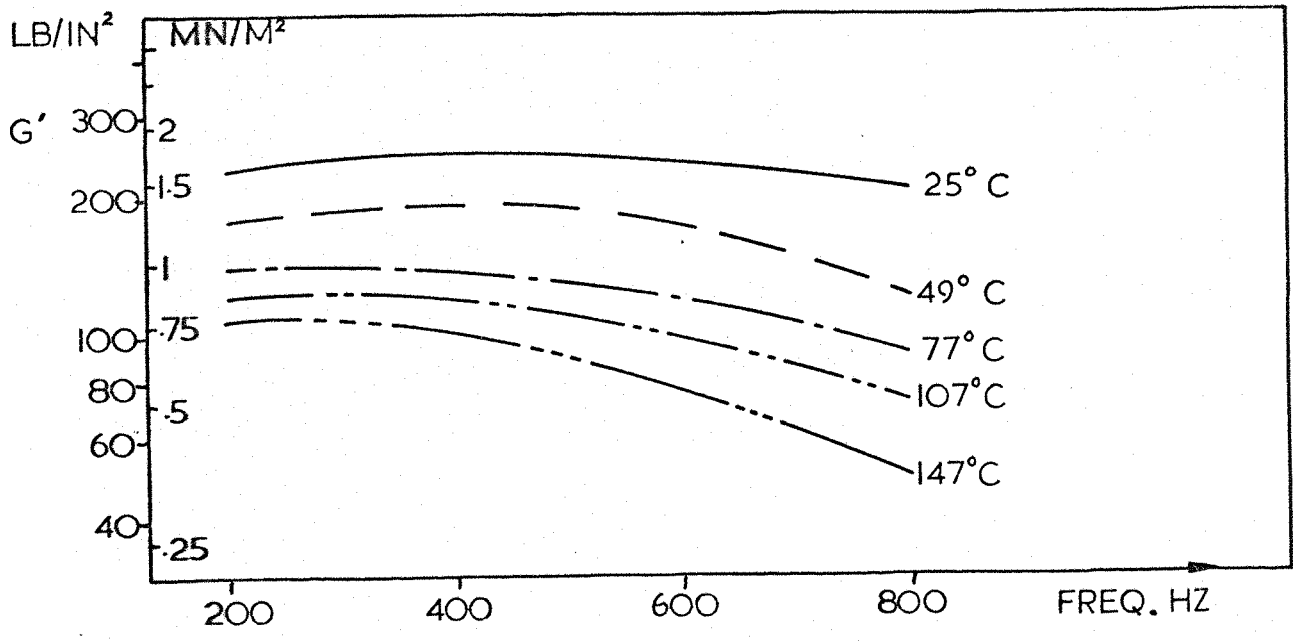


FIG. 33

Shear modulus versus frequency for Specimen 1, strain .005

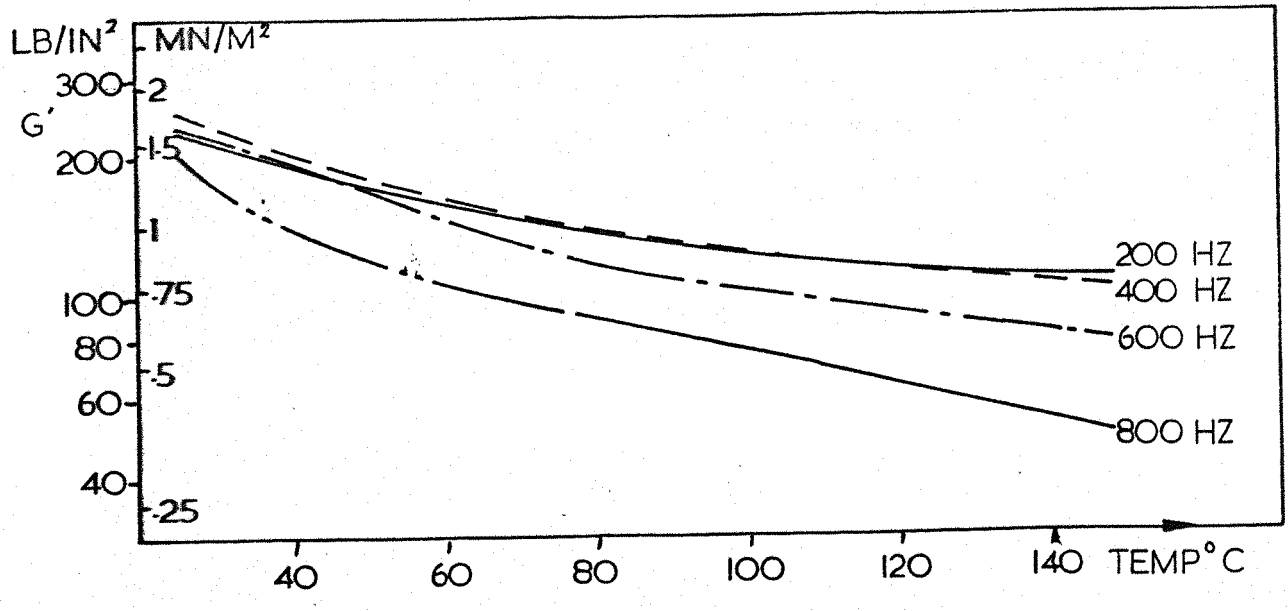


FIG. 34

Shear modulus versus temperature for Specimen 1, strain .005

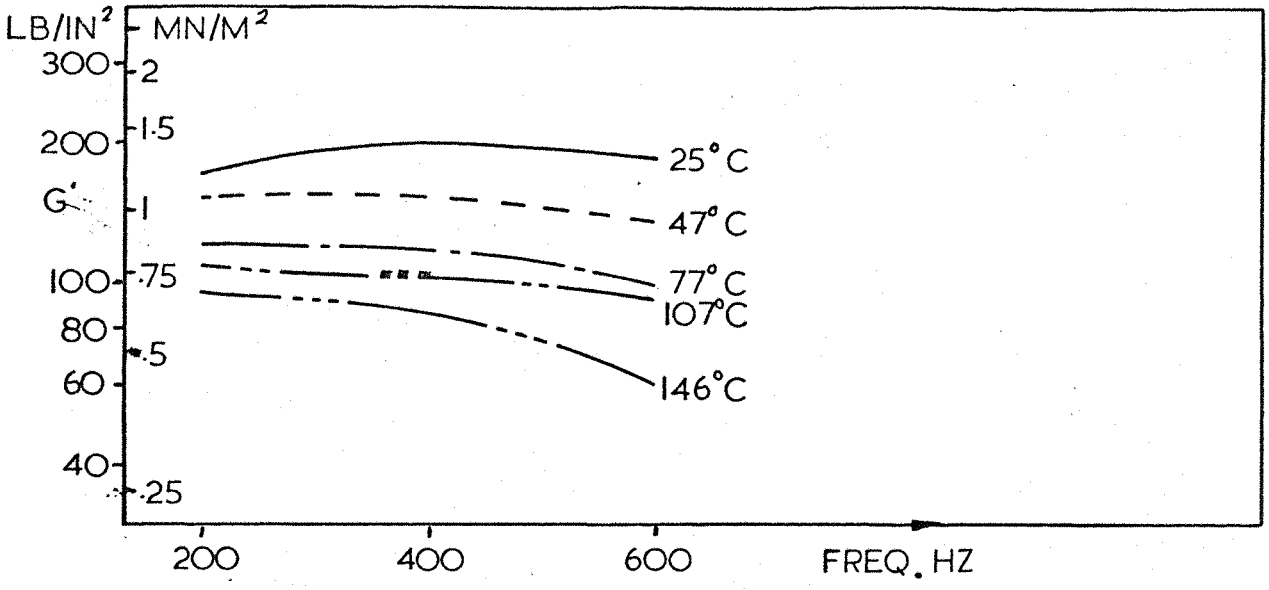


FIG 35

Shear modulus versus frequency for Specimen 1, strain .01

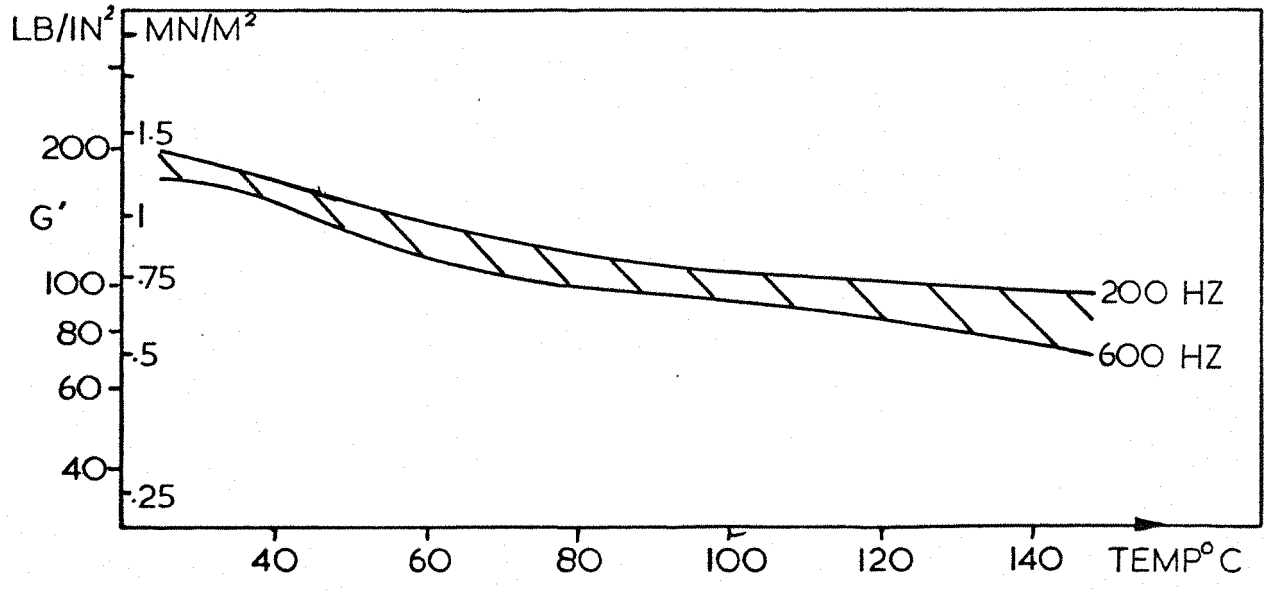


FIG 36

Shear modulus versus temperature for Specimen 1, strain .01

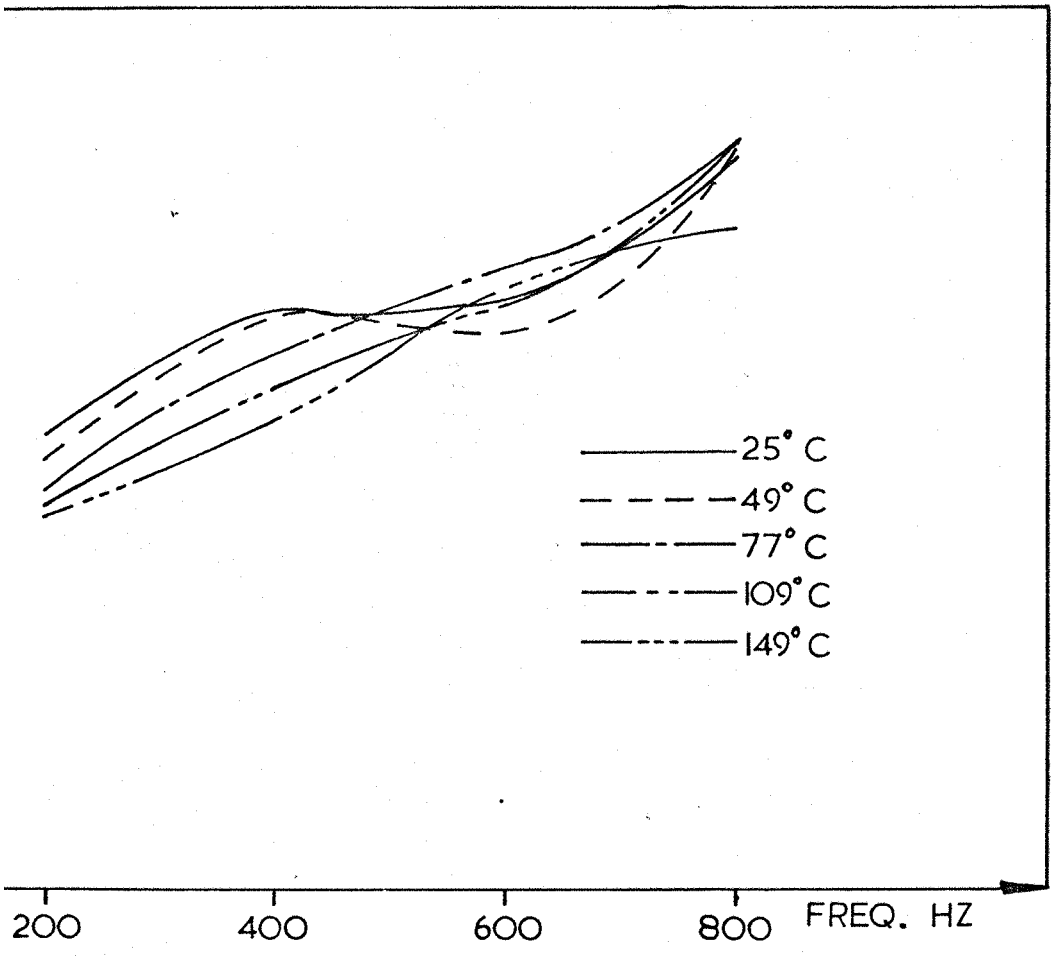


FIG. 37 Loss factor versus frequency for Specimen 1, strain .003

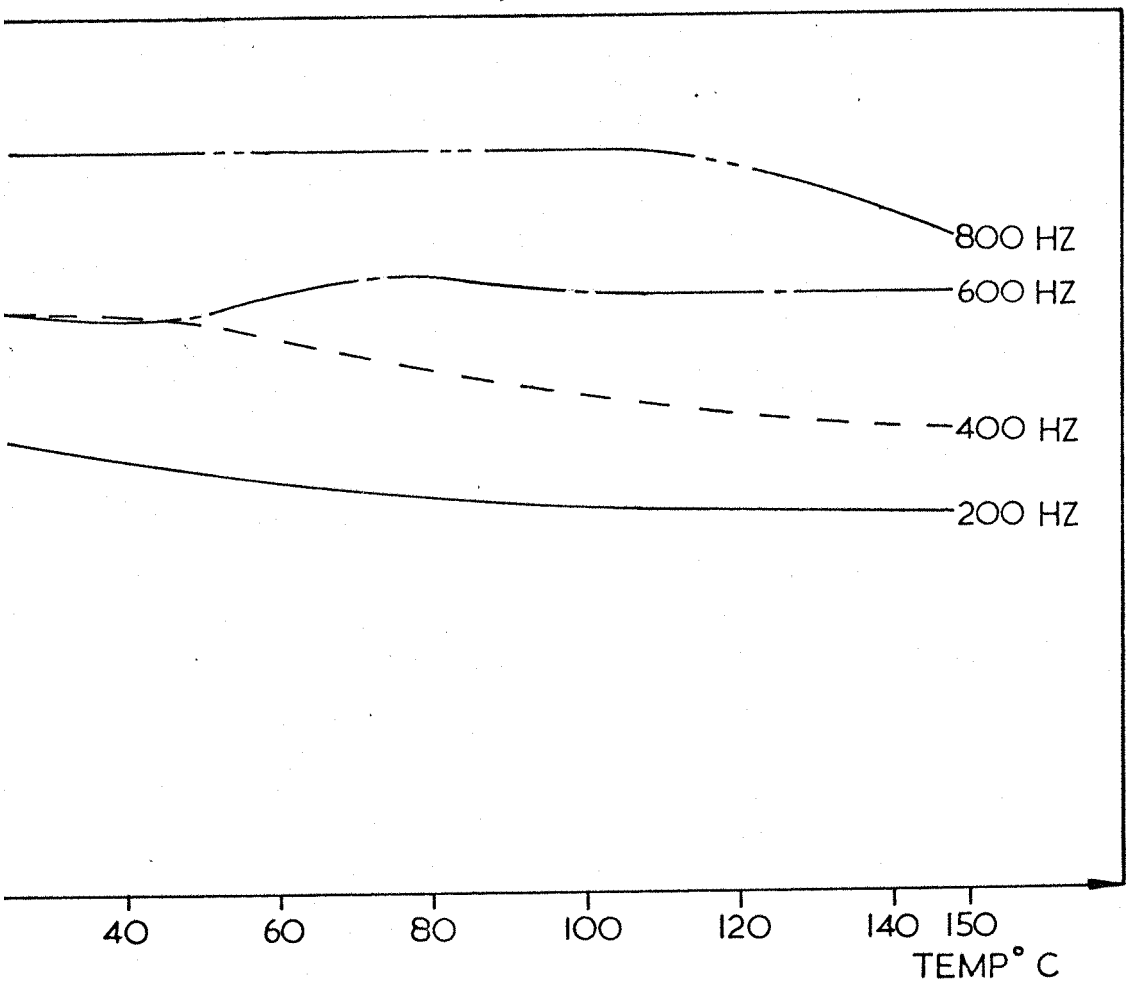


FIG. 38 Loss factor versus temperature for Specimen 1, strain .003

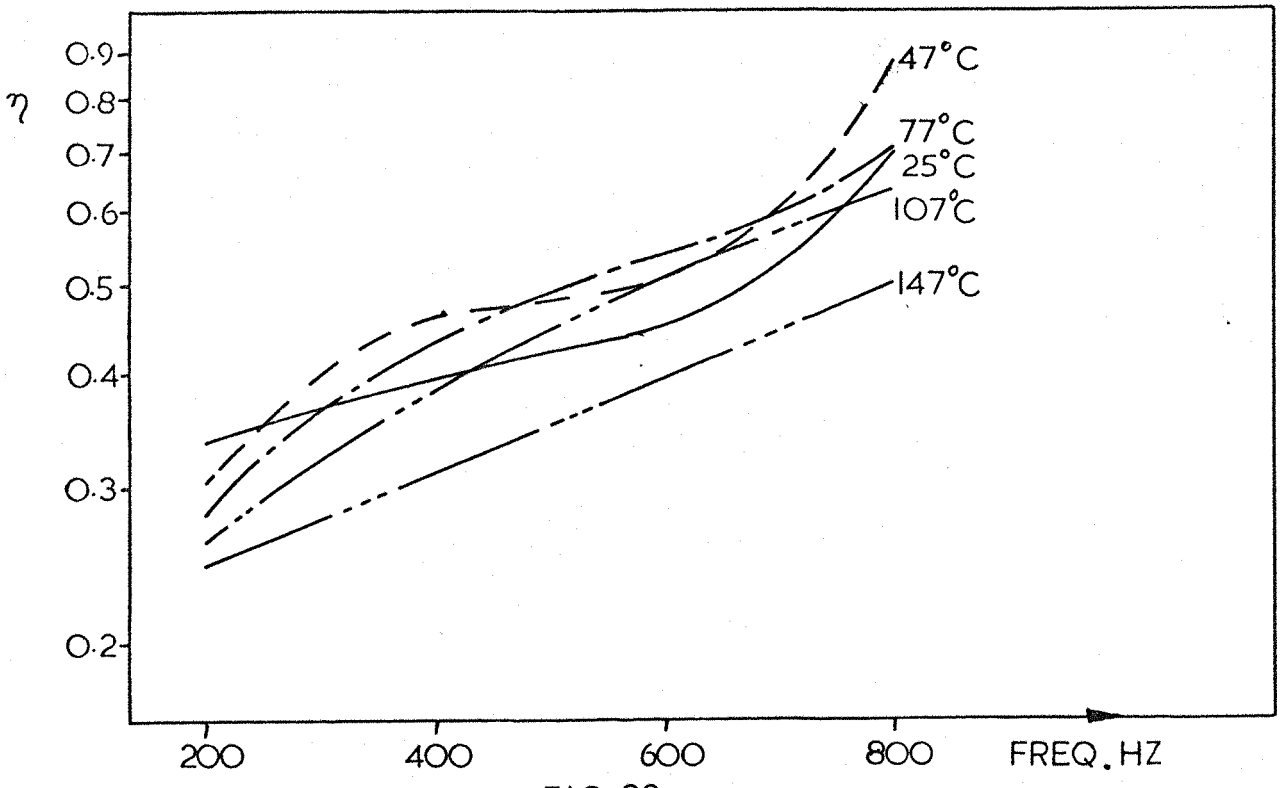


FIG. 39

Loss factor versus frequency for Specimen 1, strain .005

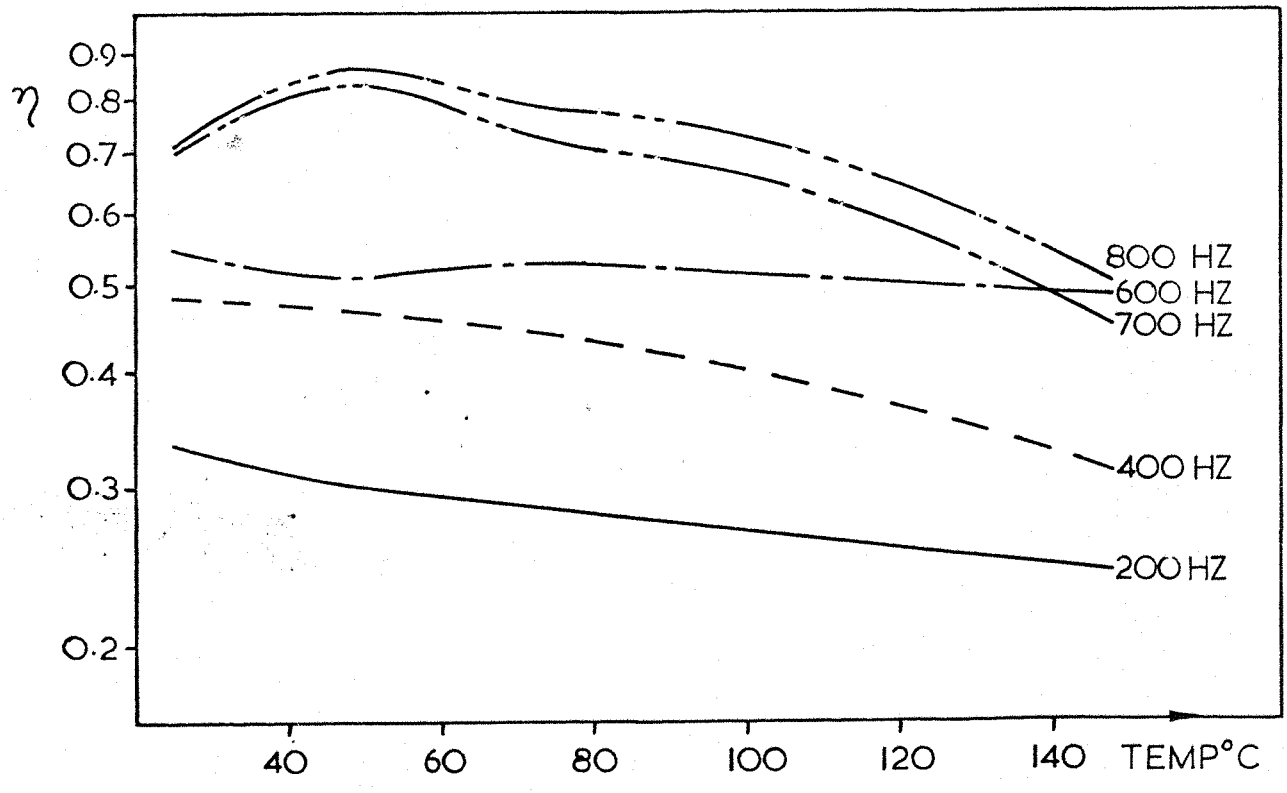


FIG. 40

Loss factor versus temperature for Specimen 1, strain .005

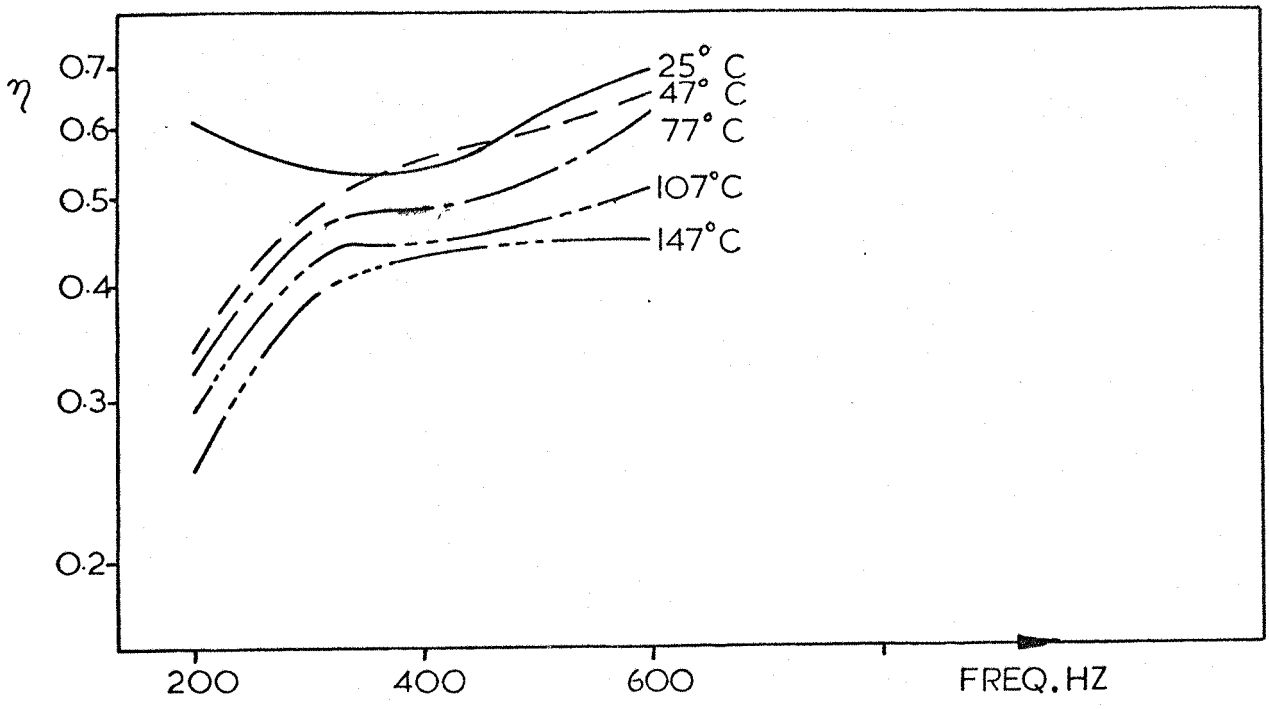


FIG. 41

Loss factor versus frequency for Specimen 1, strain .01

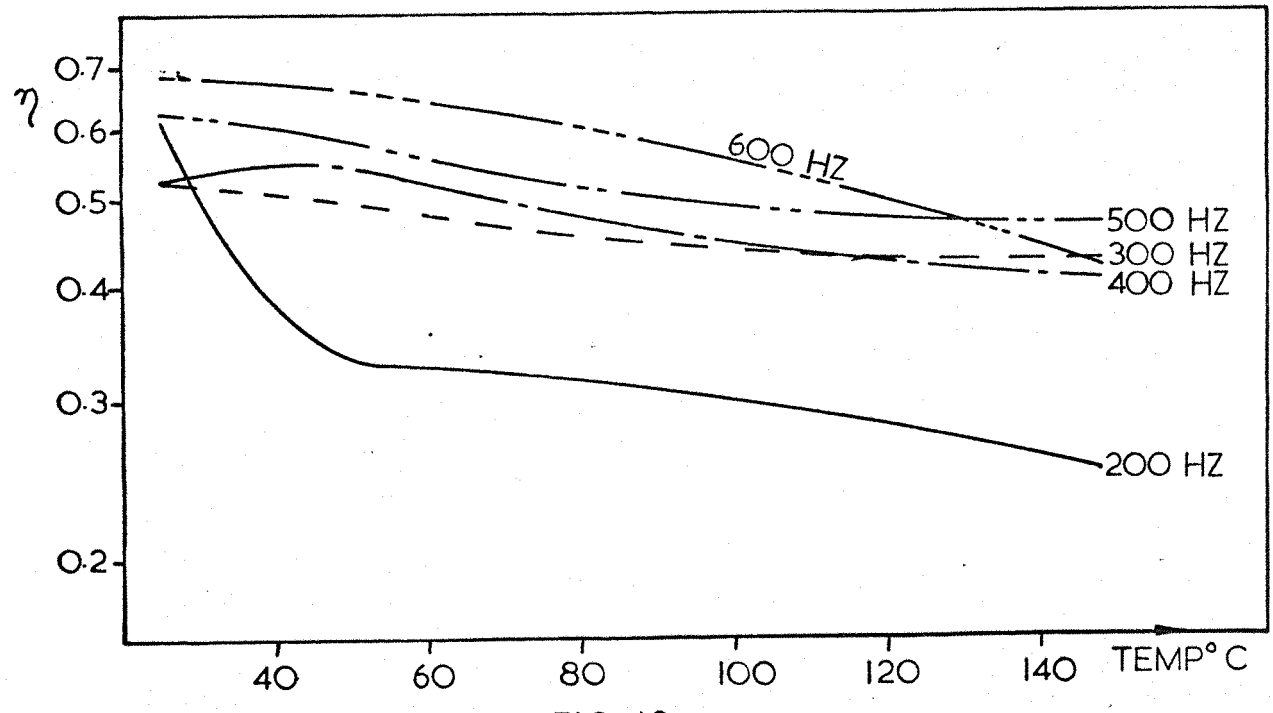


FIG. 42

Loss factor versus temperature for Specimen 1, strain .01

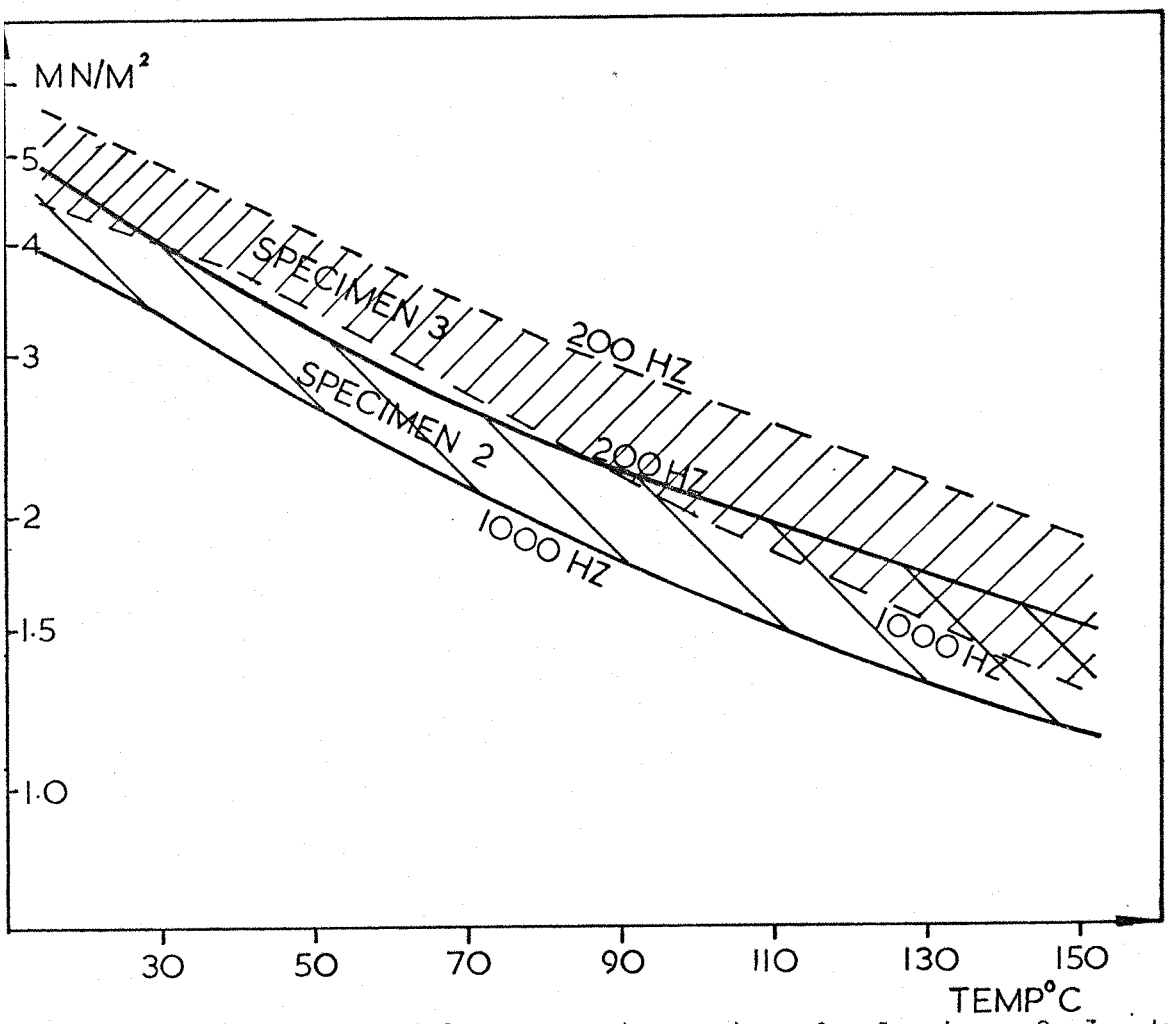


FIG. 43 Shear modulus versus temperature for Specimens 2, 3, strain .001

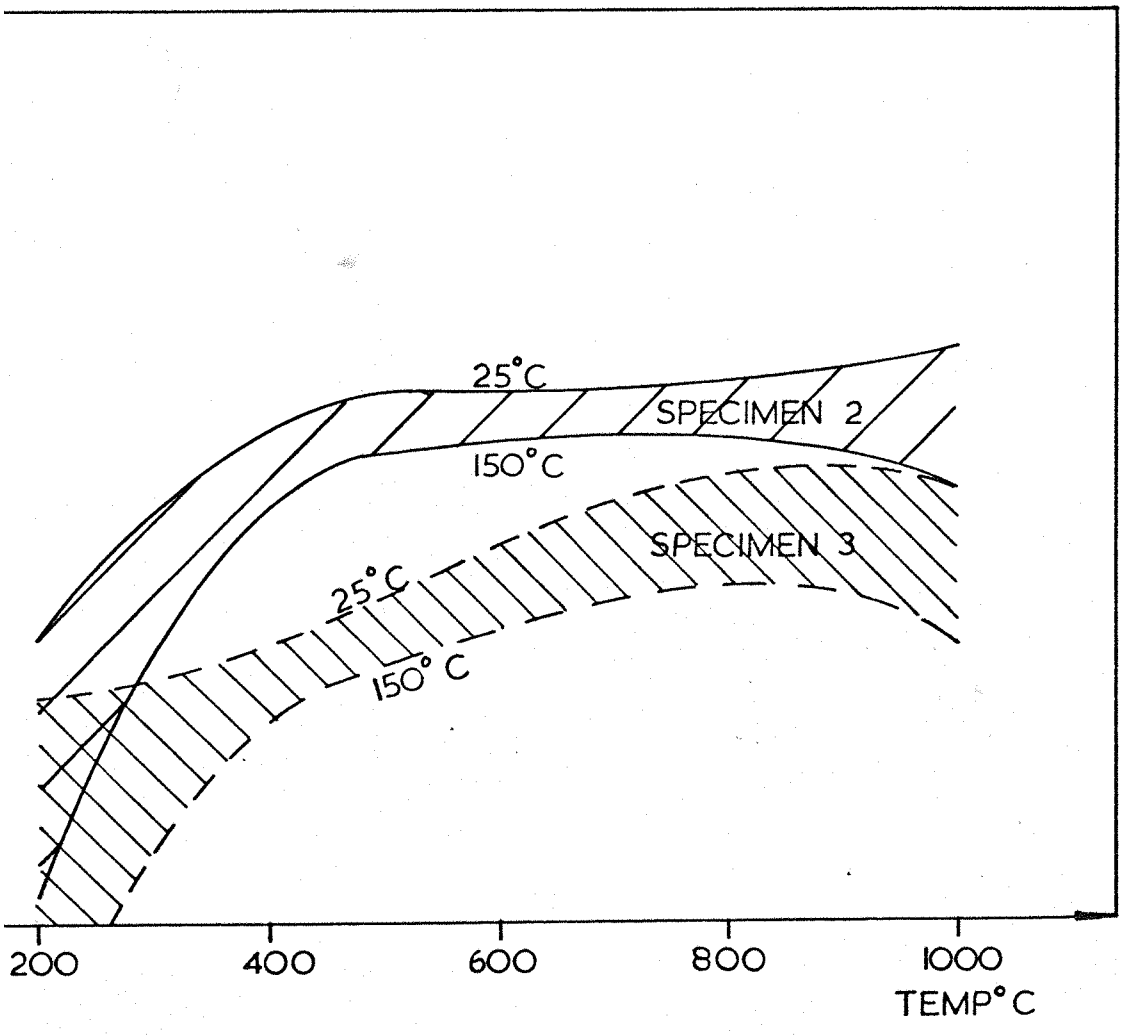


FIG. 44 Loss factor versus frequency for Specimens 2, 3, strain .001

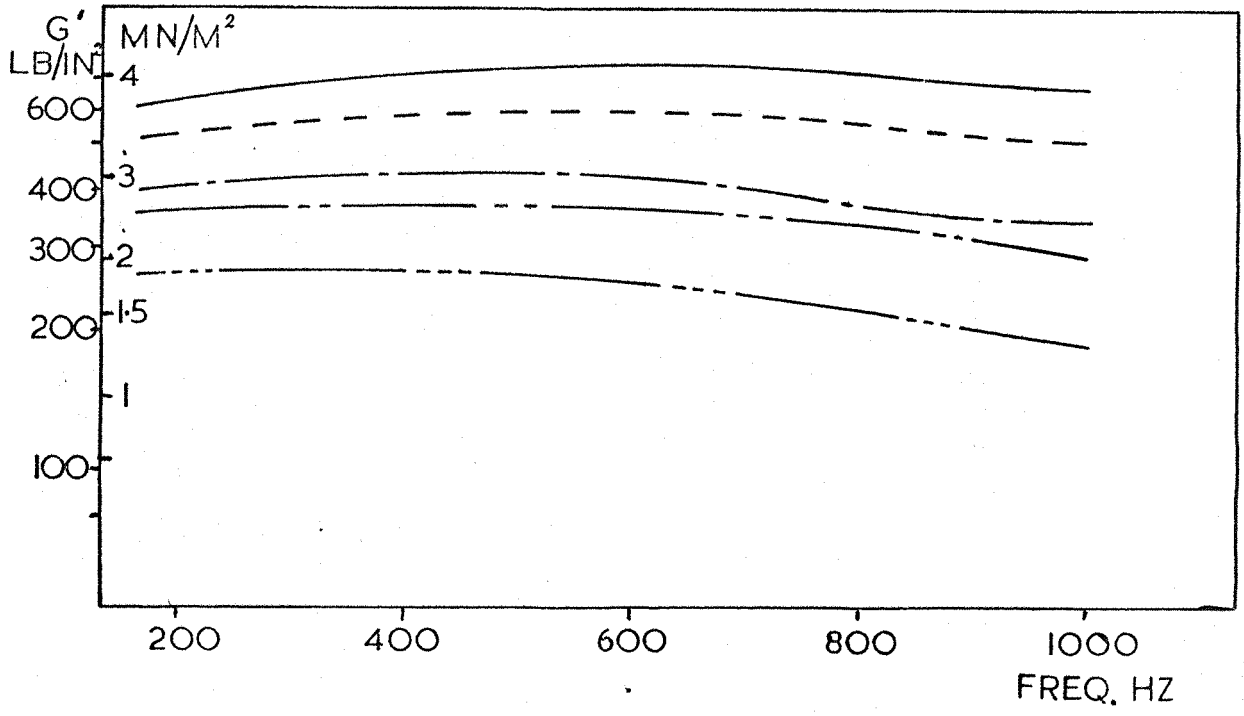


FIG. 45 Shear modulus versus frequency for Specimen 3, strain .001

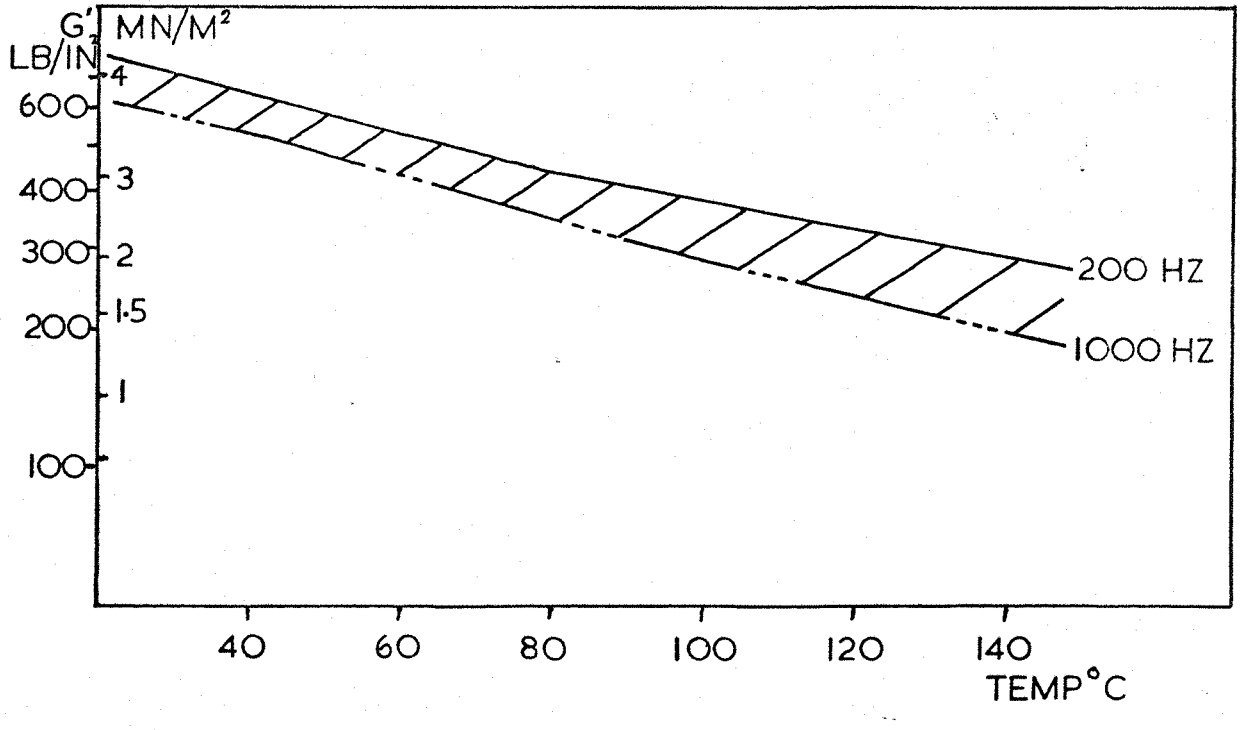


FIG. 46 Shear modulus versus temperature for Specimen 3, strain .001

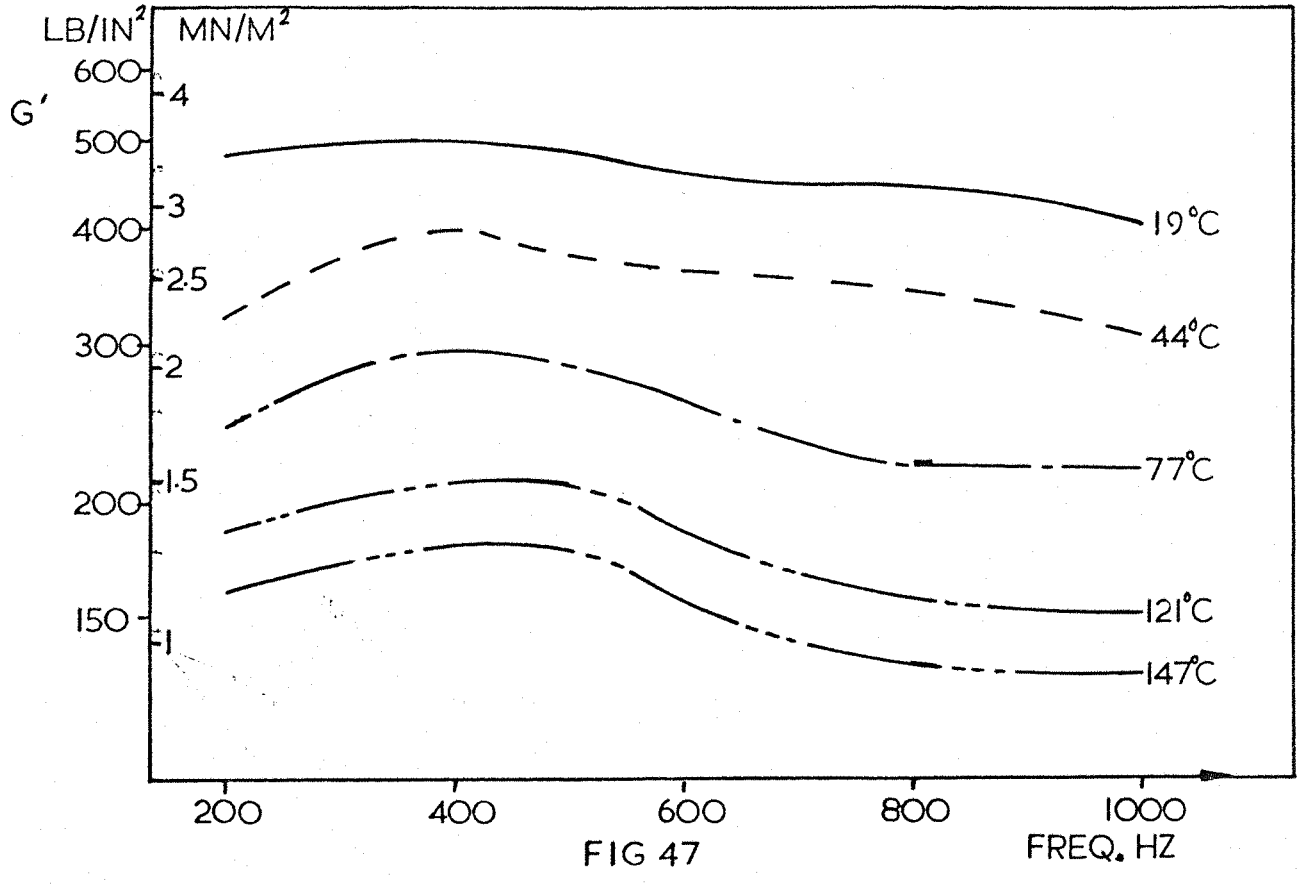


FIG 47

Shear modulus versus frequency for Specimen 2, strain .001

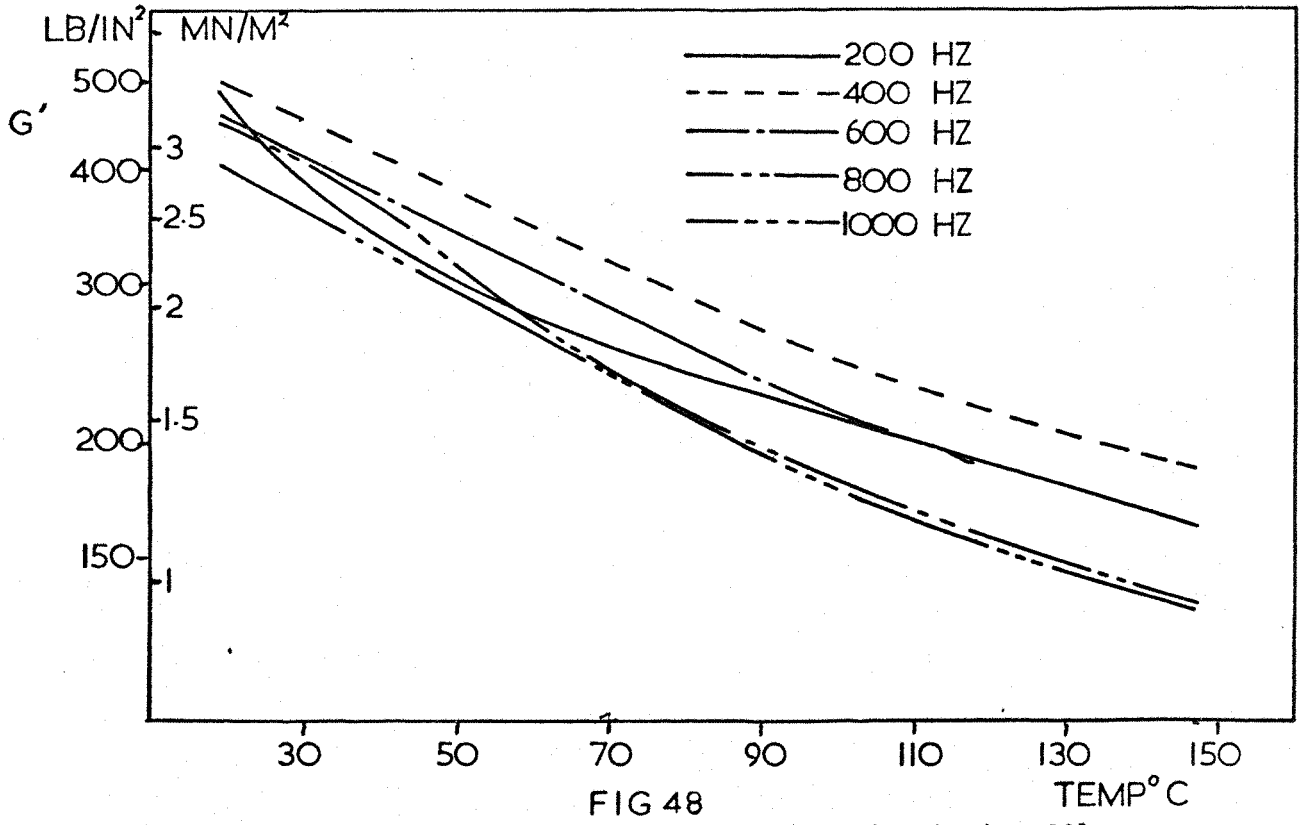


FIG 48

Shear modulus versus temperature for Specimen 2, strain .001

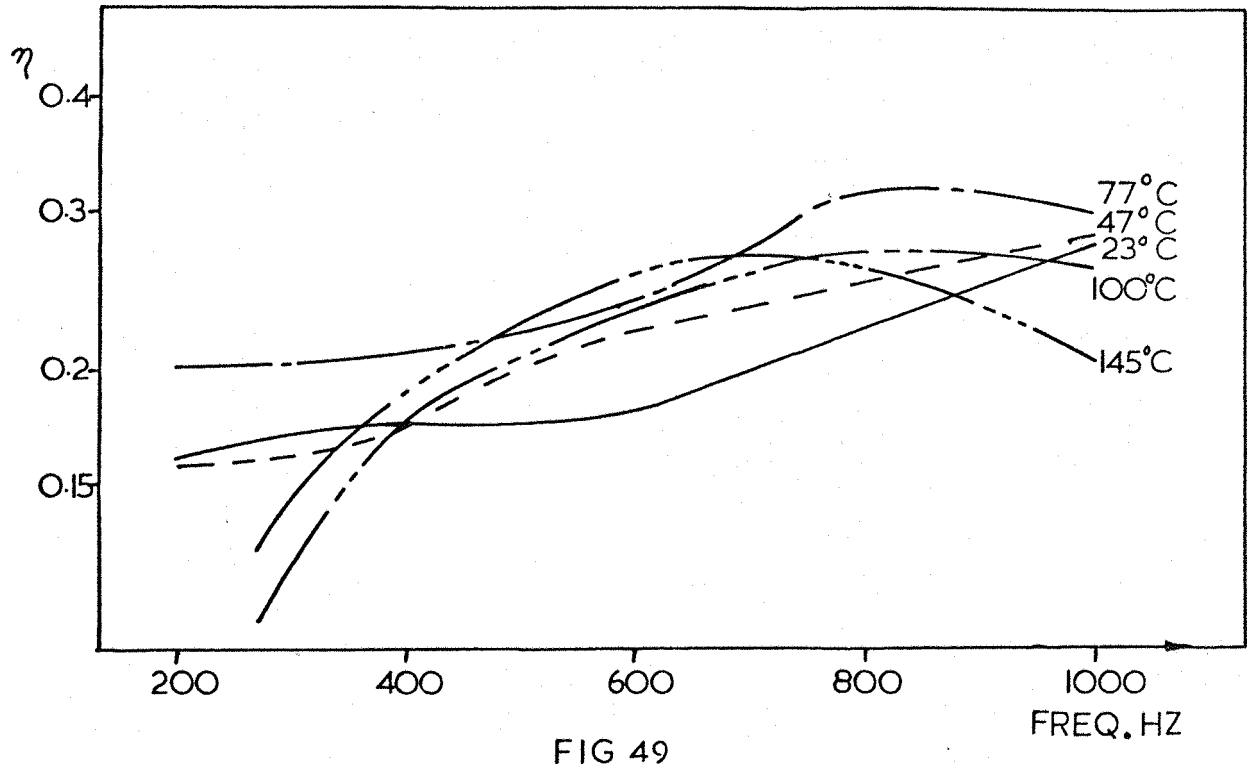


FIG 49

Loss factor versus frequency for Specimen 3, strain .001

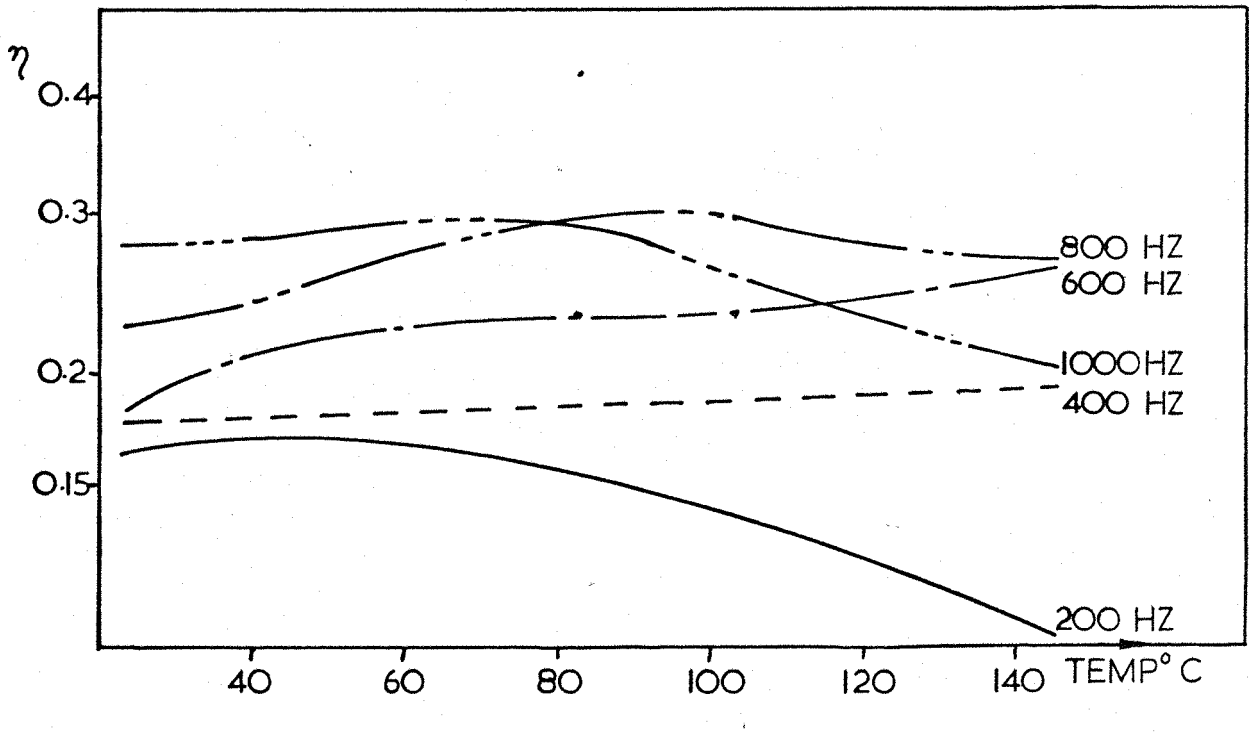


FIG 50

Loss factor versus temperature for Specimen 3, strain .001

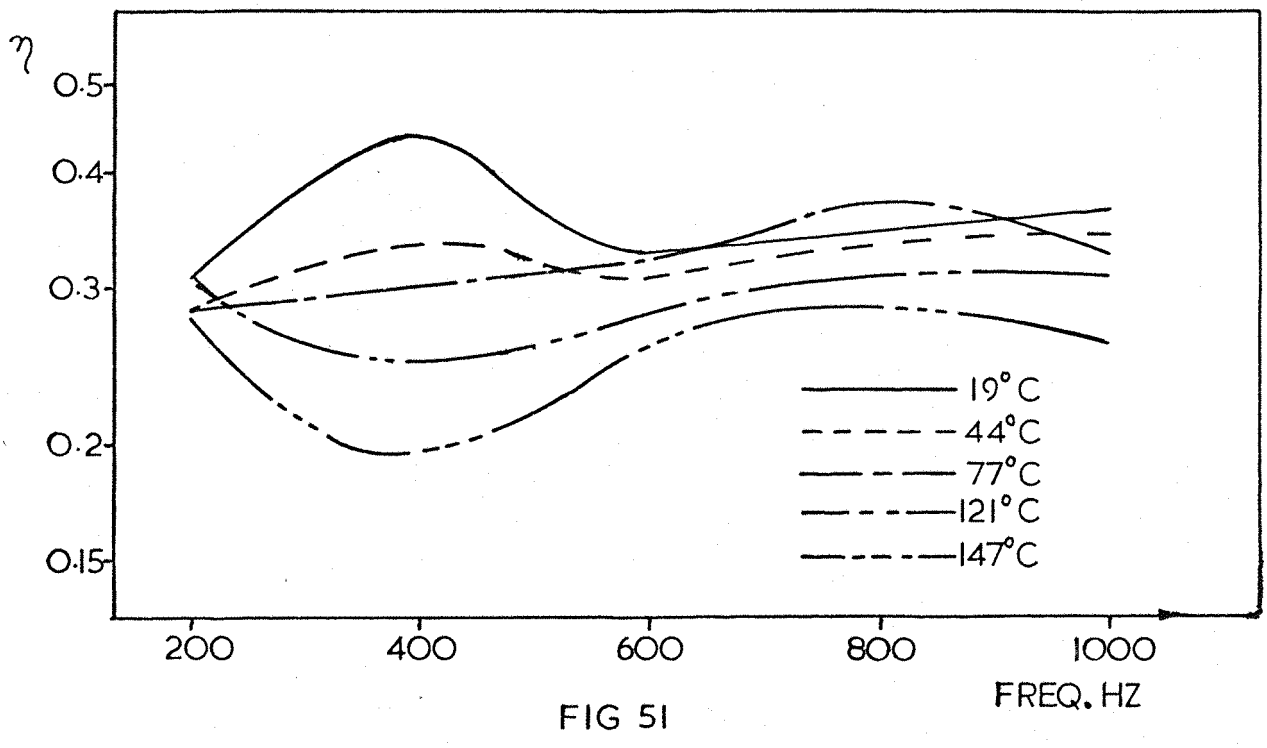


FIG 51

Loss factor versus frequency for Specimen 2, strain .001

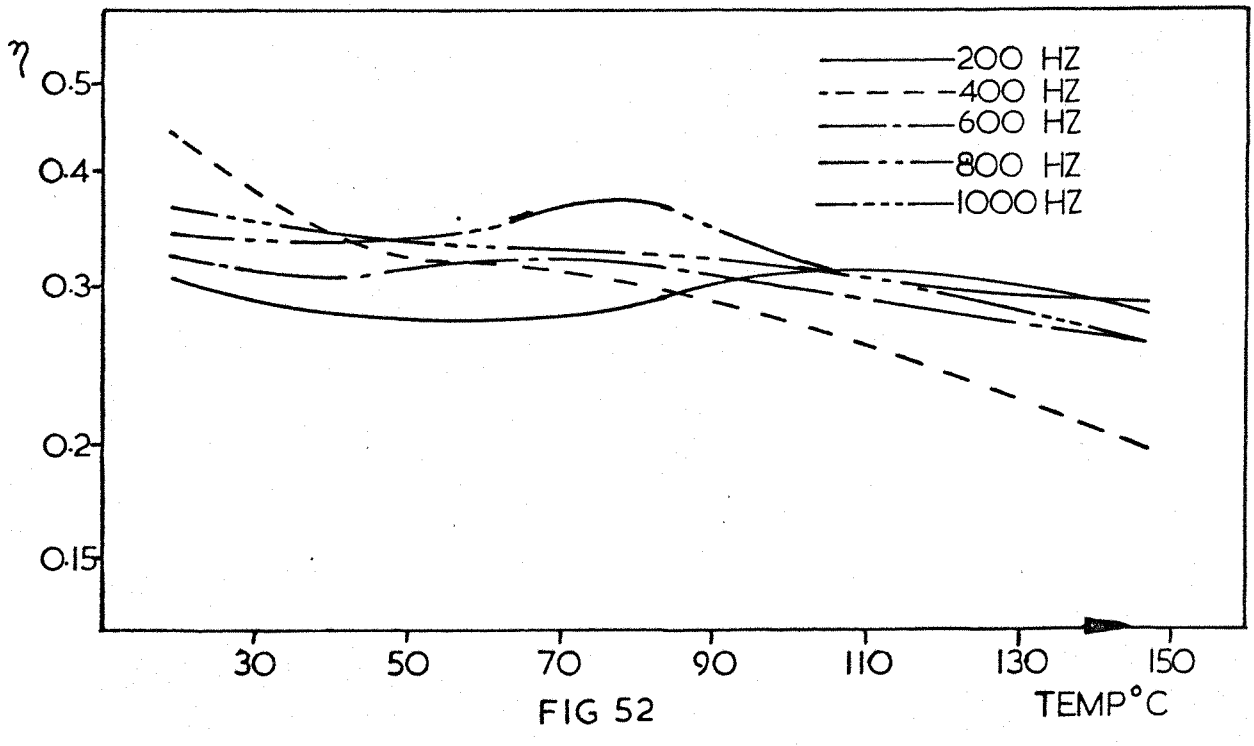


FIG 52

Loss factor versus temperature for Specimen 2, strain .001

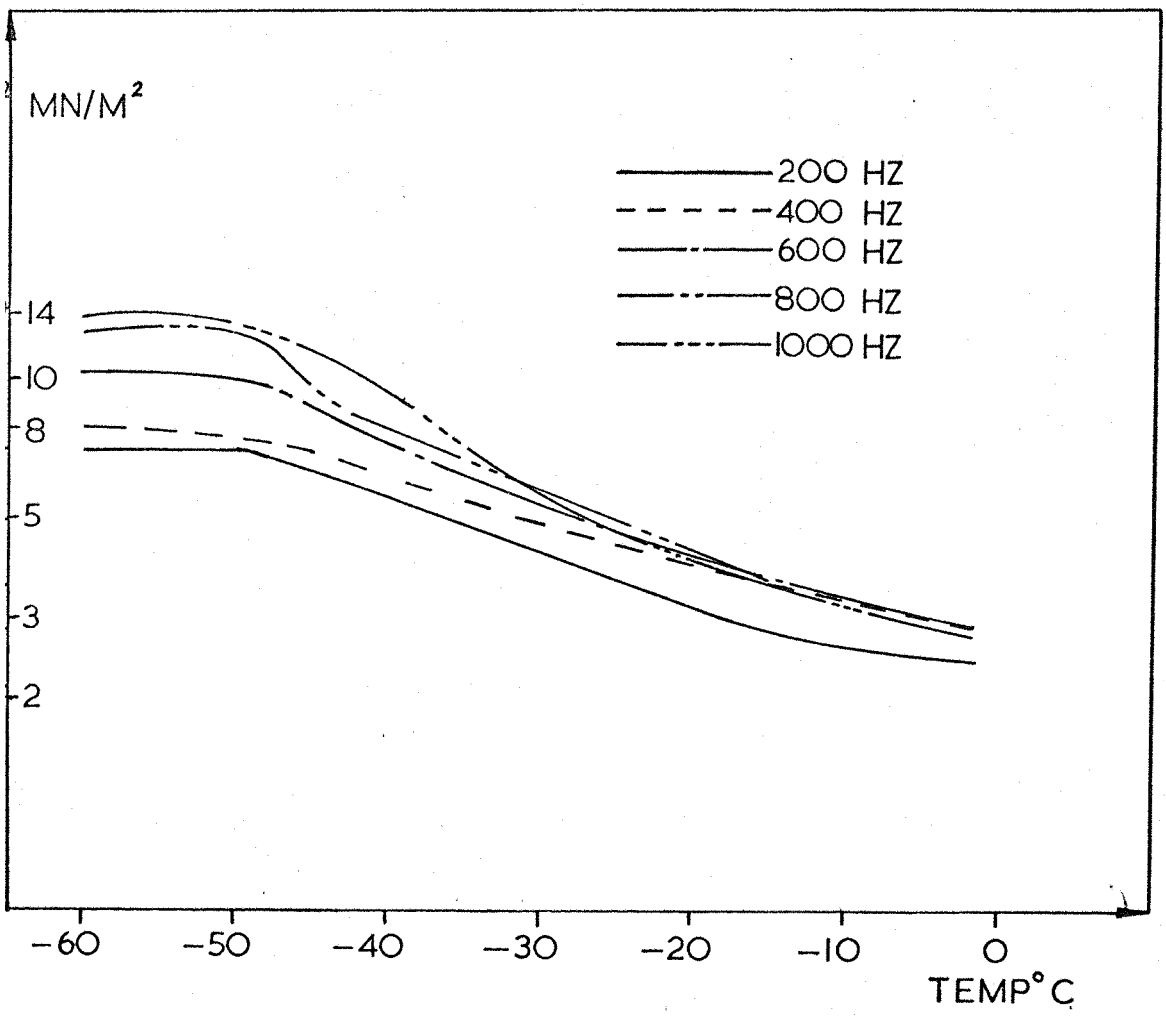


FIG. 53 Shear modulus versus sub-ambient temperatures for Specimen 1, strain .001

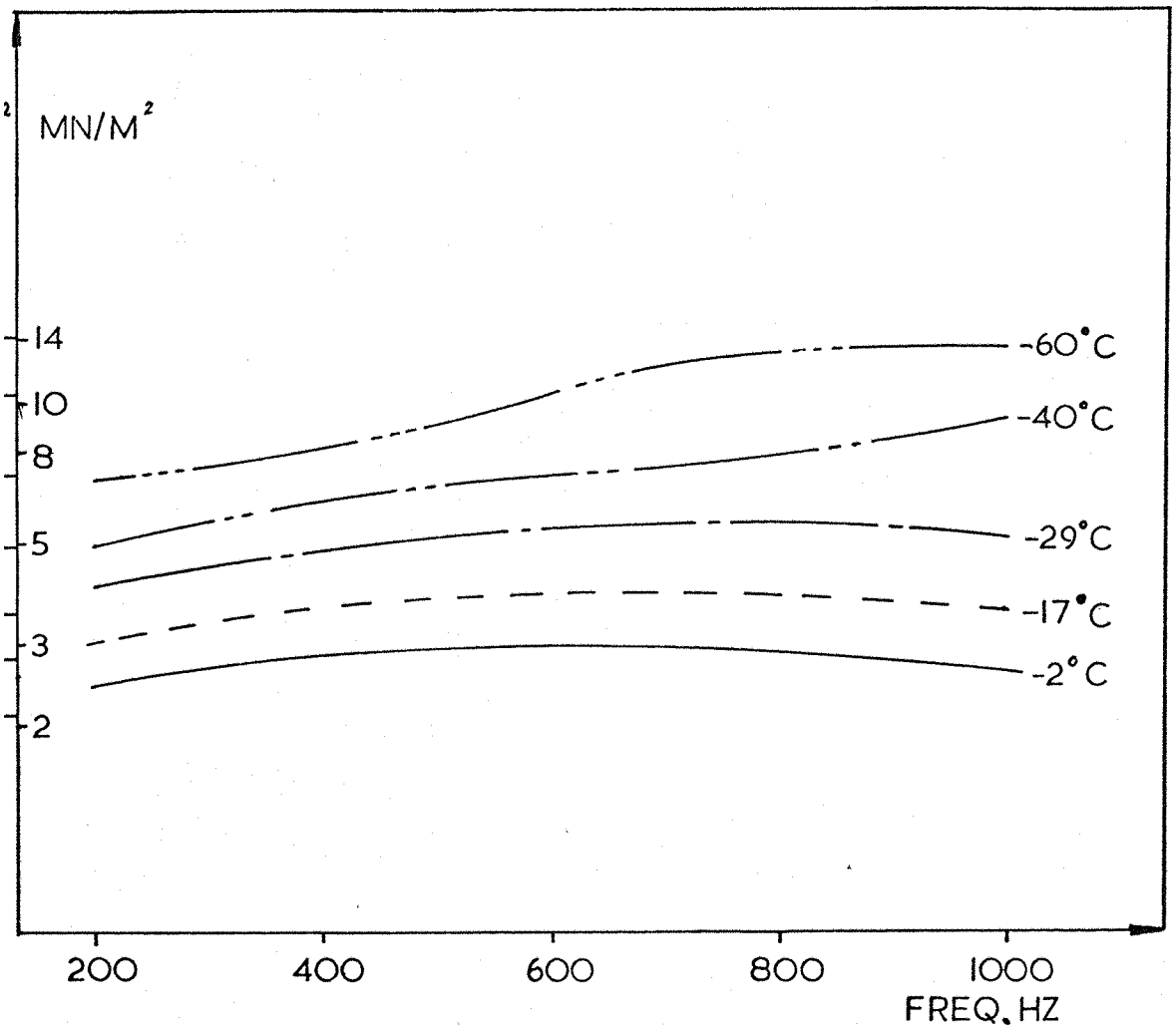


FIG. 54 Shear modulus versus frequency at sub-ambient temperatures for Specimen 1, strain .001

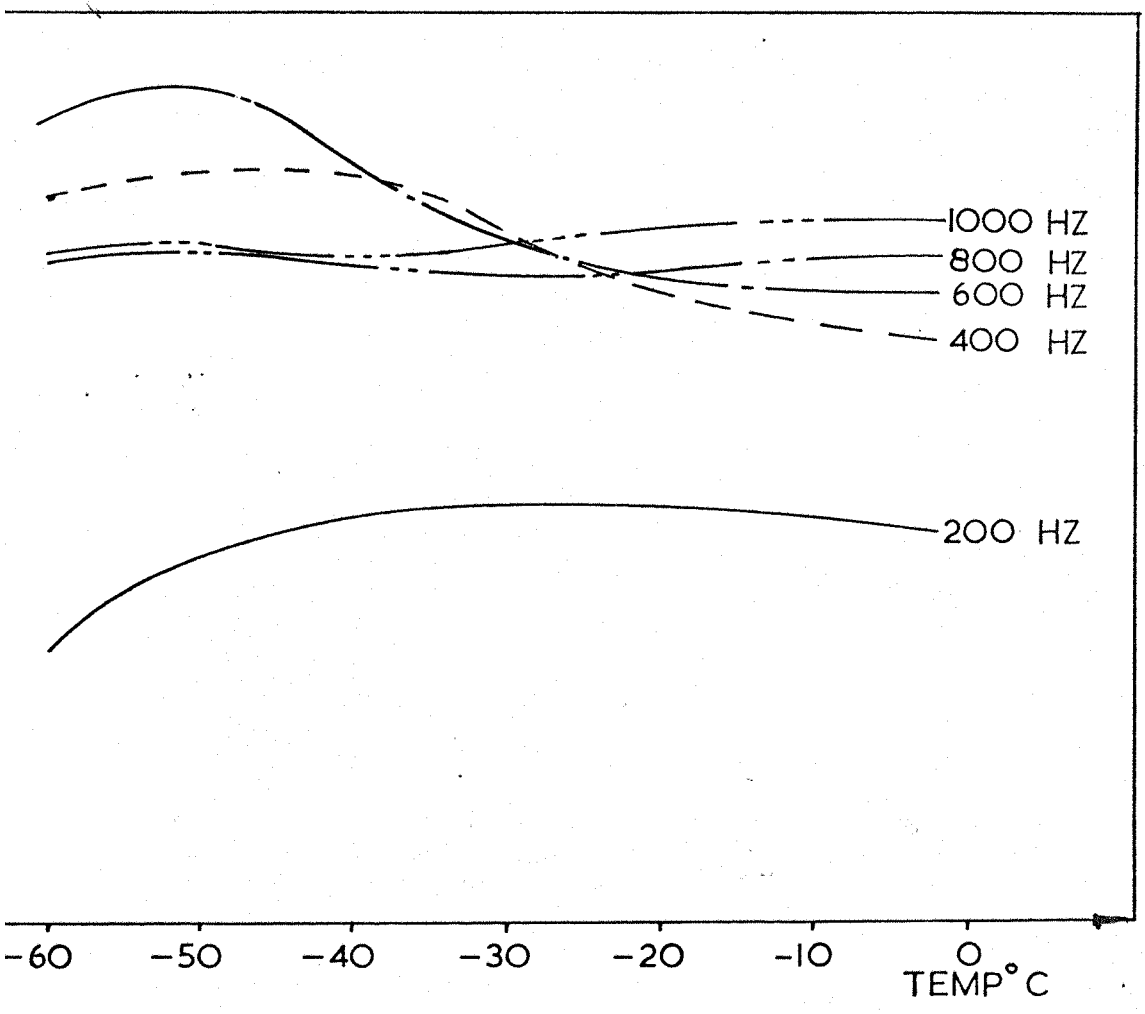


FIG. 55 Loss factor versus sub-ambient temperature for Specimen 1, strain .001

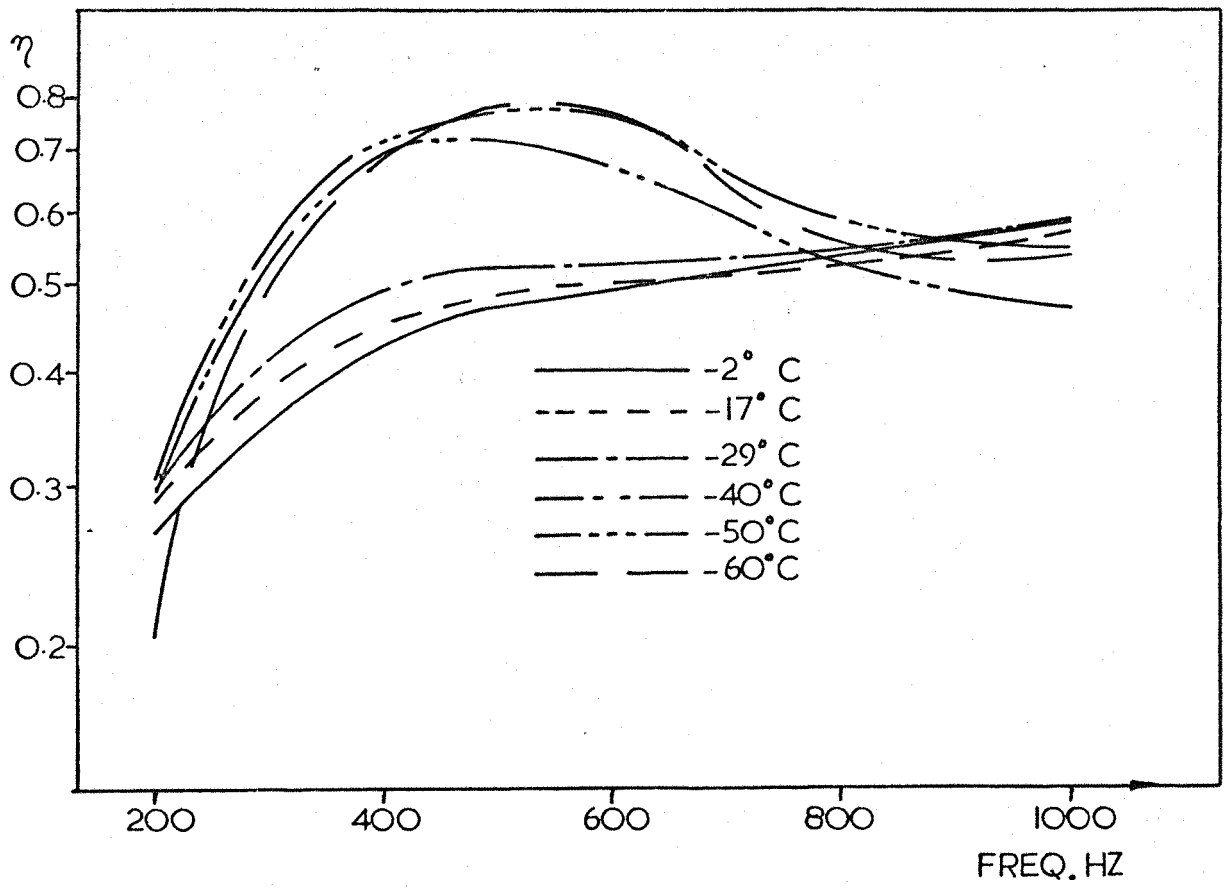


FIG. 56 Loss factor versus frequency at sub-ambient temperatures for Specimen 1, strain .001

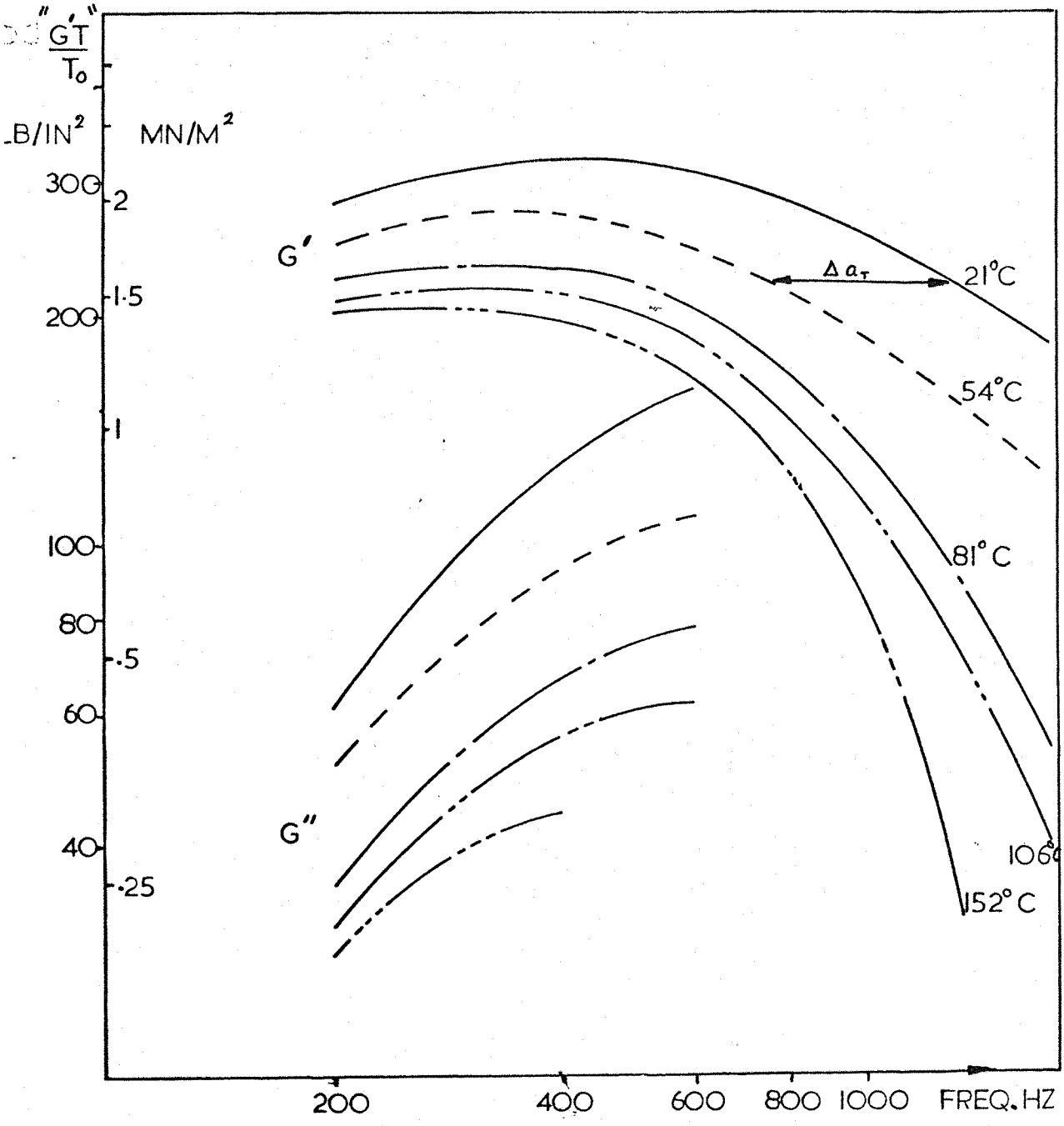


FIG. 57 Logarithmic plot of shear modulus versus frequency at various temperatures for determination of $a_t$

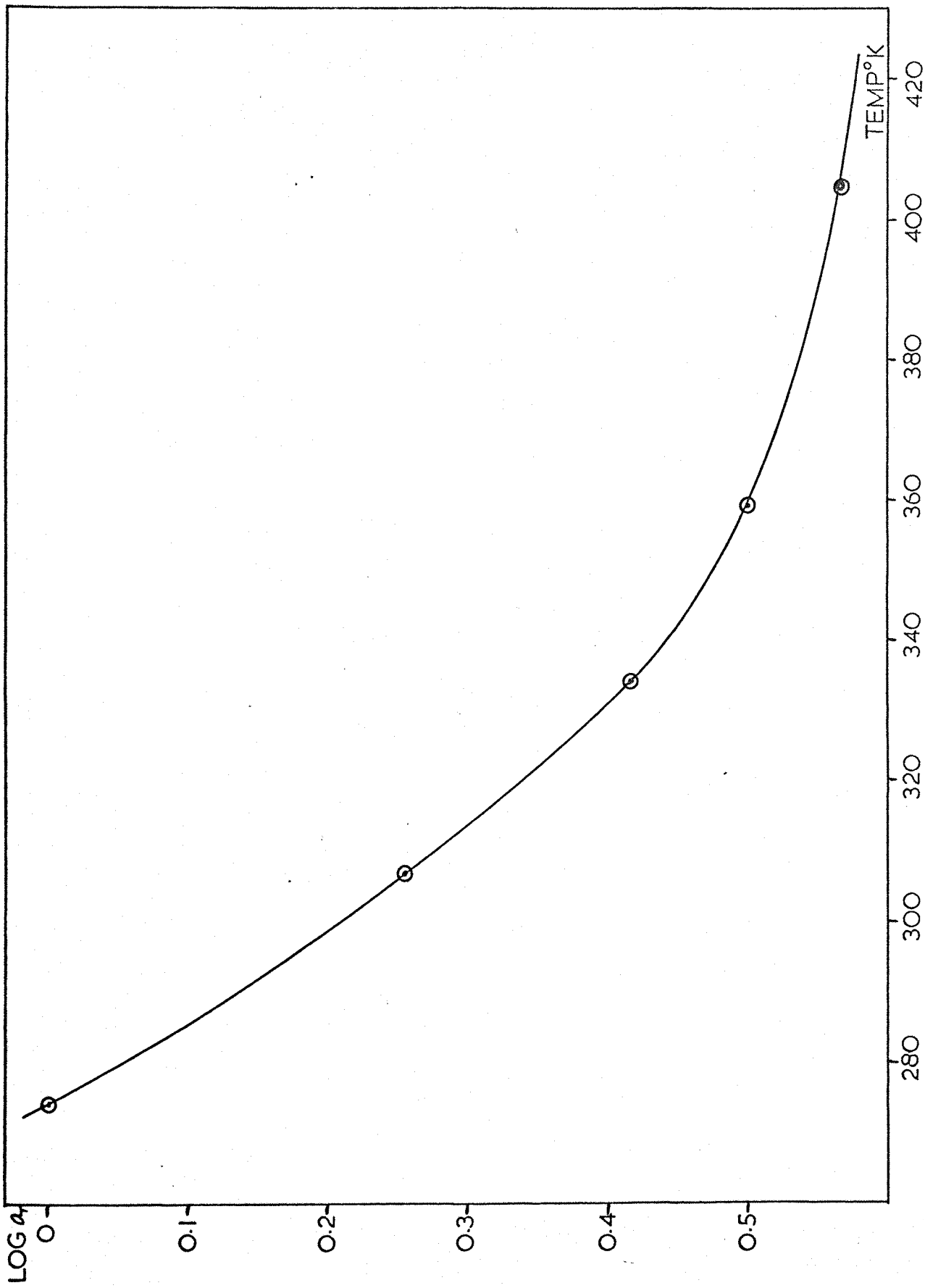


FIG. 58 Log $a_t$ versus temperature for smooth curve

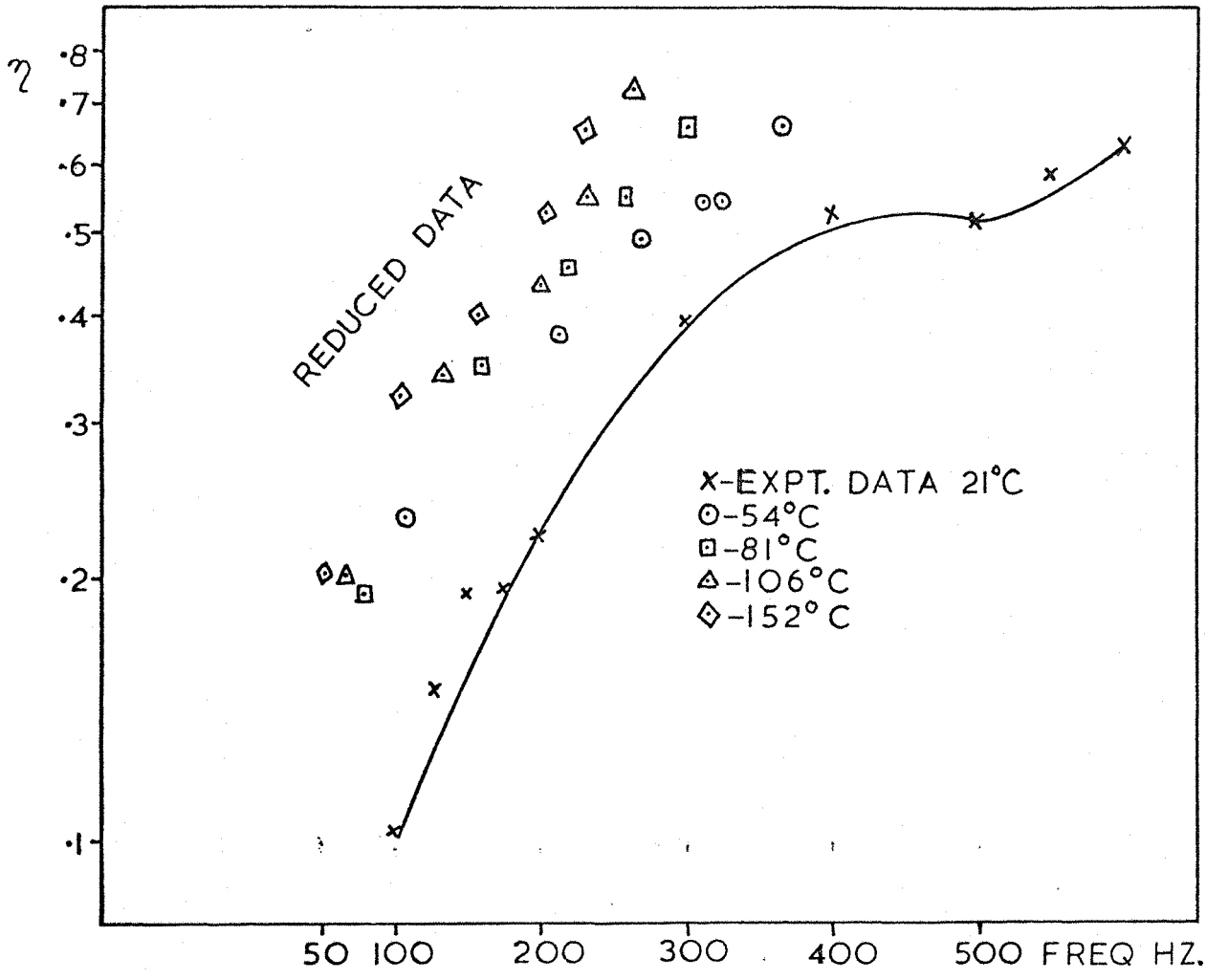


FIG. 59 Loss factor versus frequency from "reduced" data compared with shear test

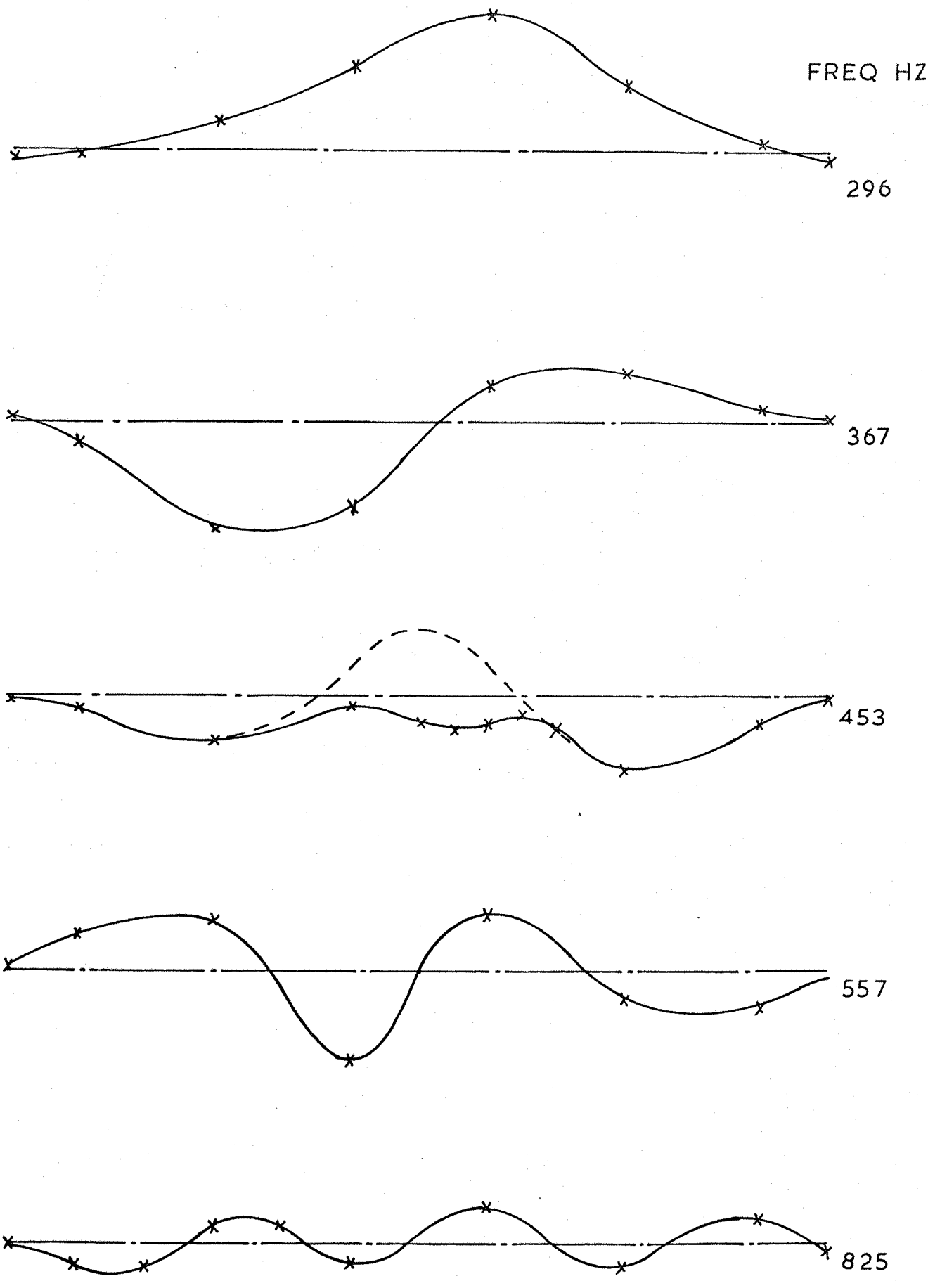


FIG. 60 Measured panel mode shapes from single point excitation tests at frequencies of peak response

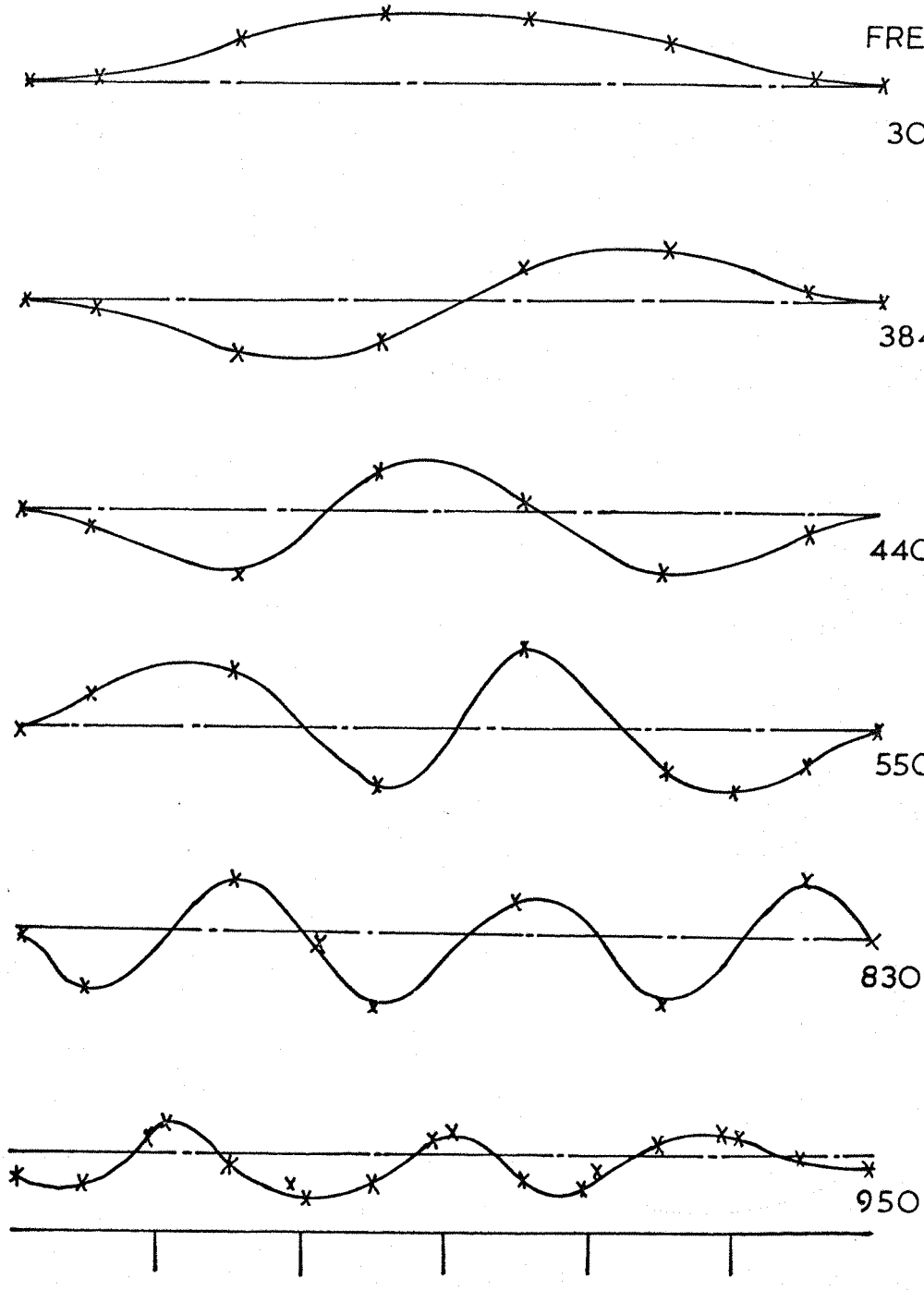


FIG. 61 Measured panel mode shapes at frequencies of peak response to acoustic excitation

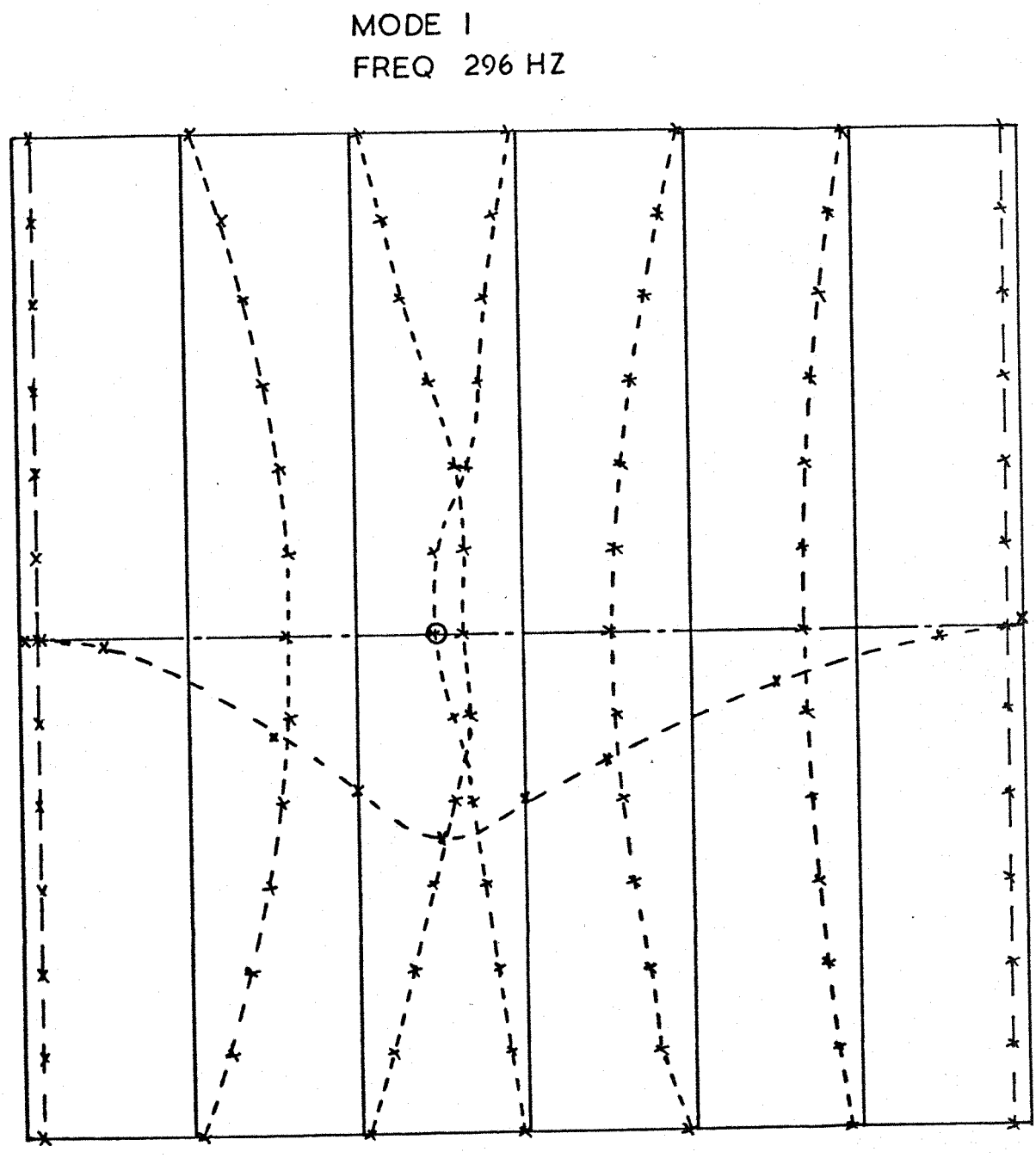


FIG. 62 First undamped panel mode with shaker excitation

MODE 2
FREQ 367 HZ

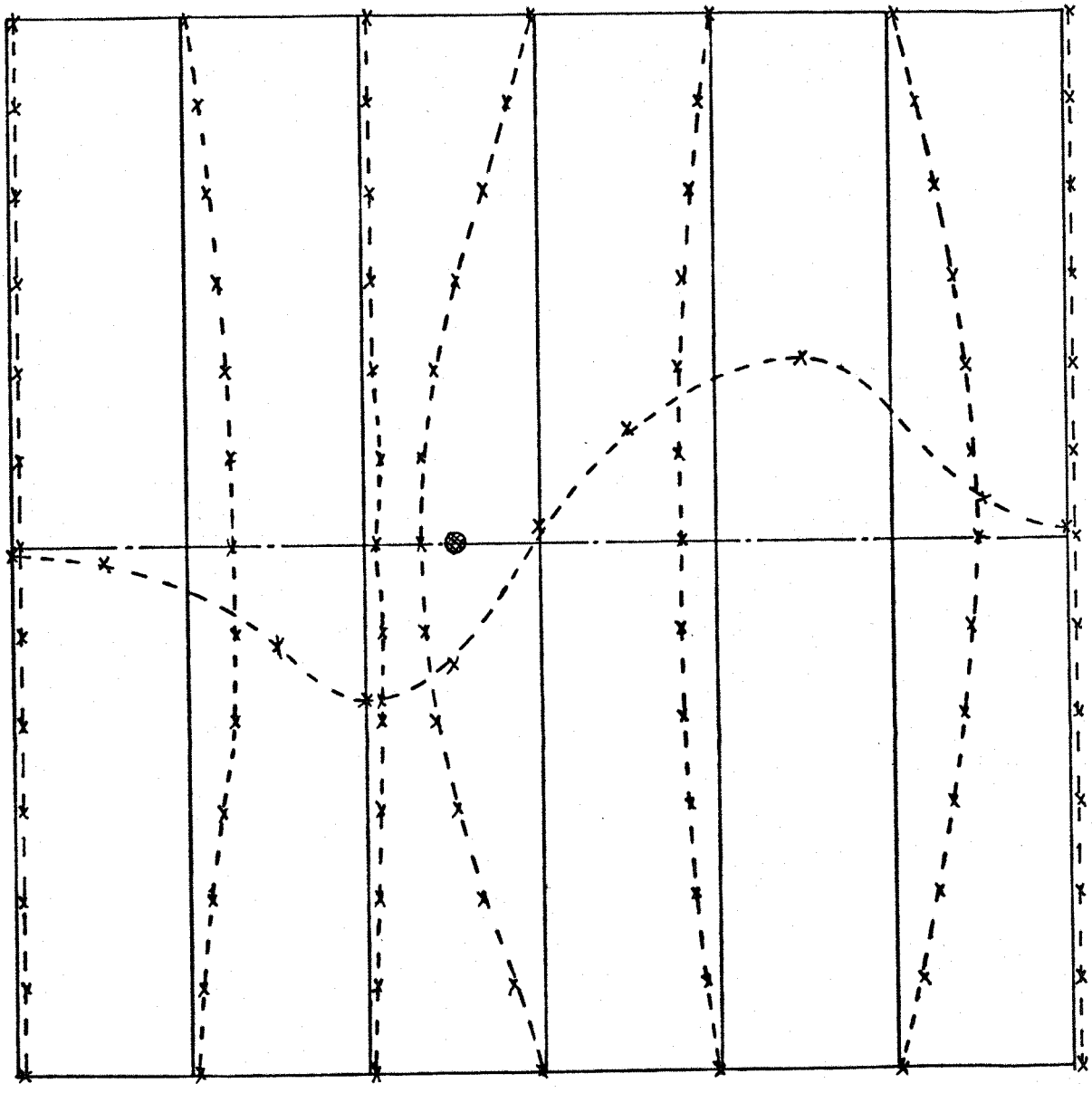

FIG. 63 Second undamped panel mode with shaker excitation

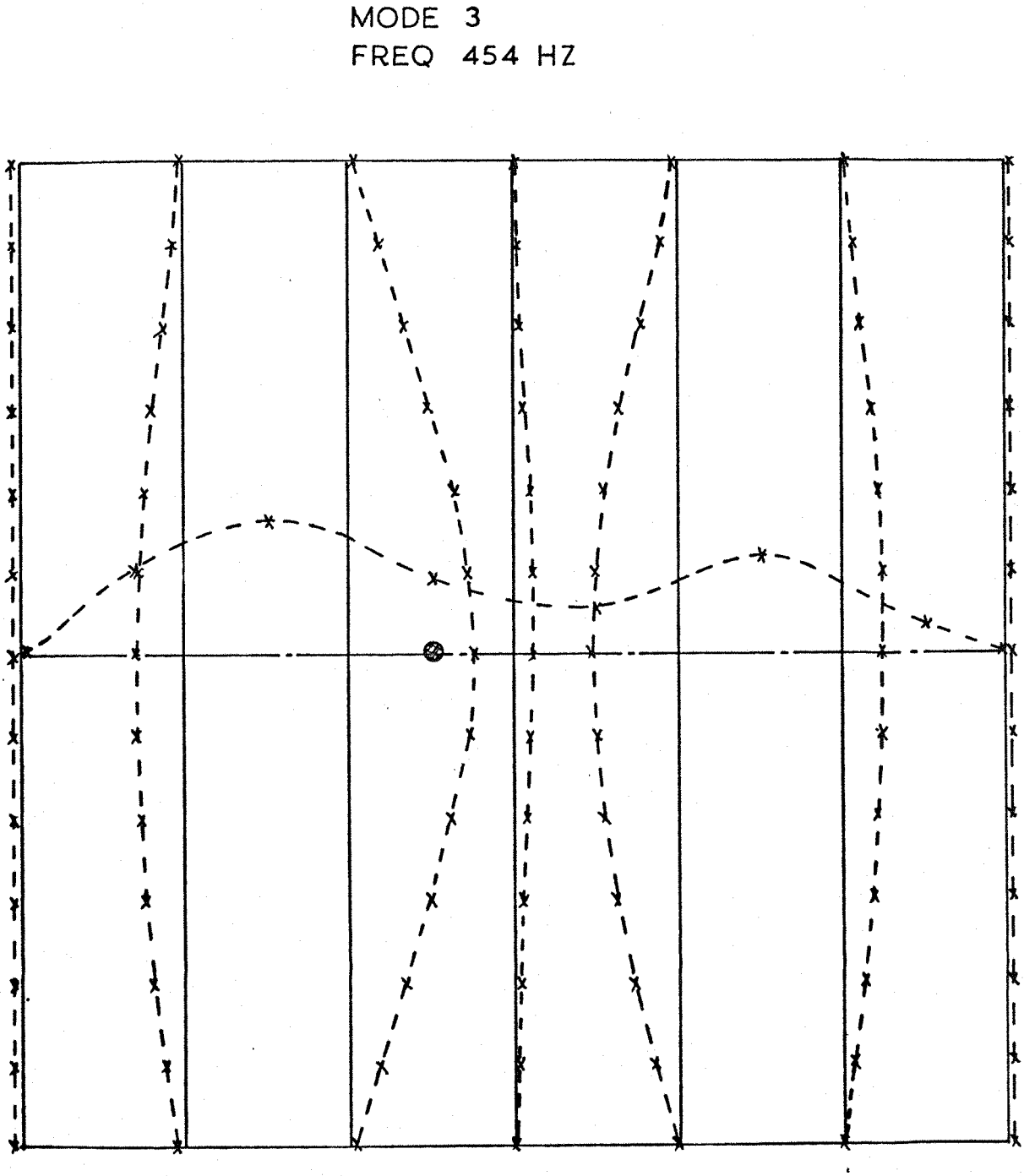


FIG. 64 Third undamped panel mode with shaker excitation

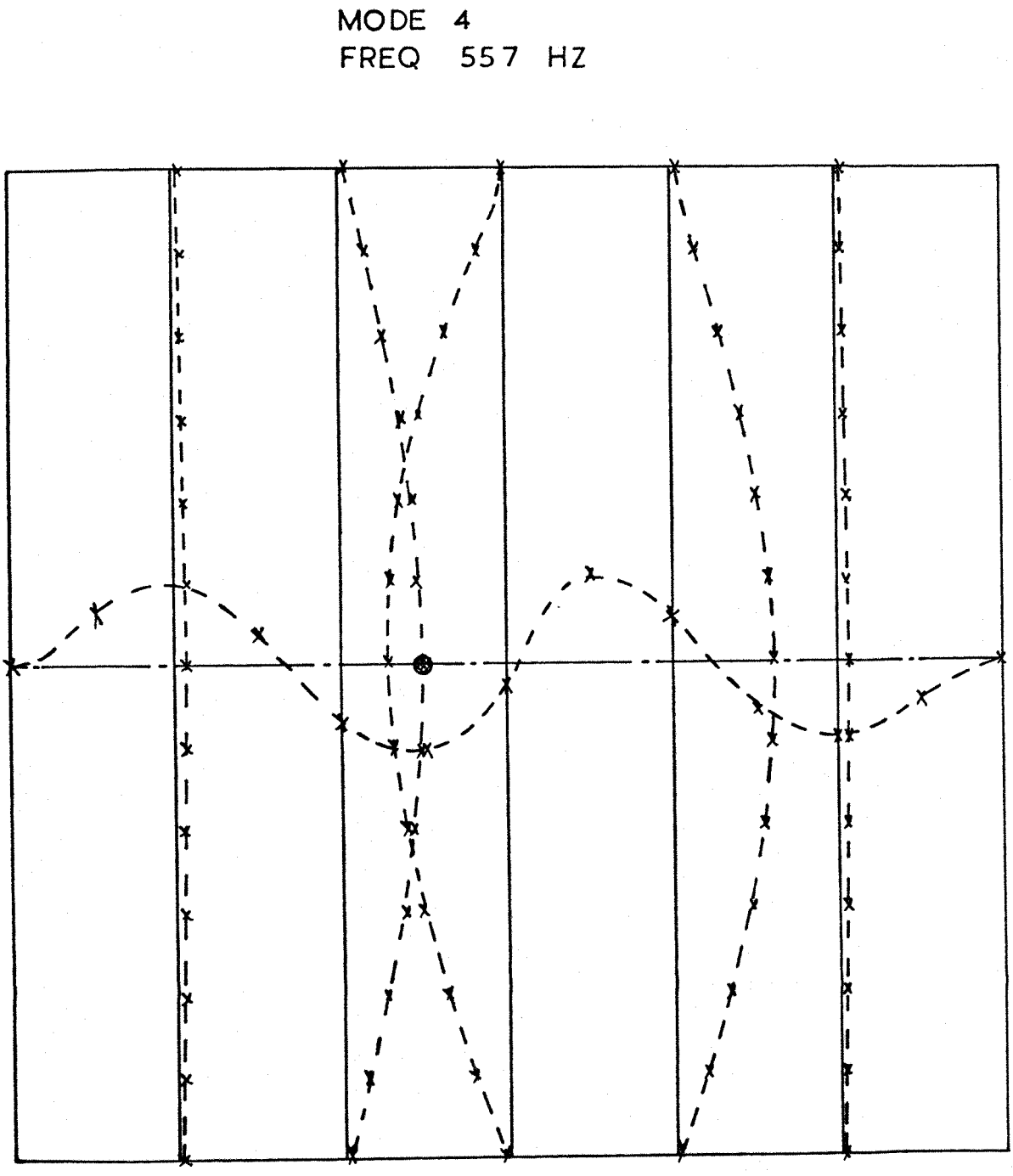


FIG. 65 Fourth undamped panel mode with shaker excitation

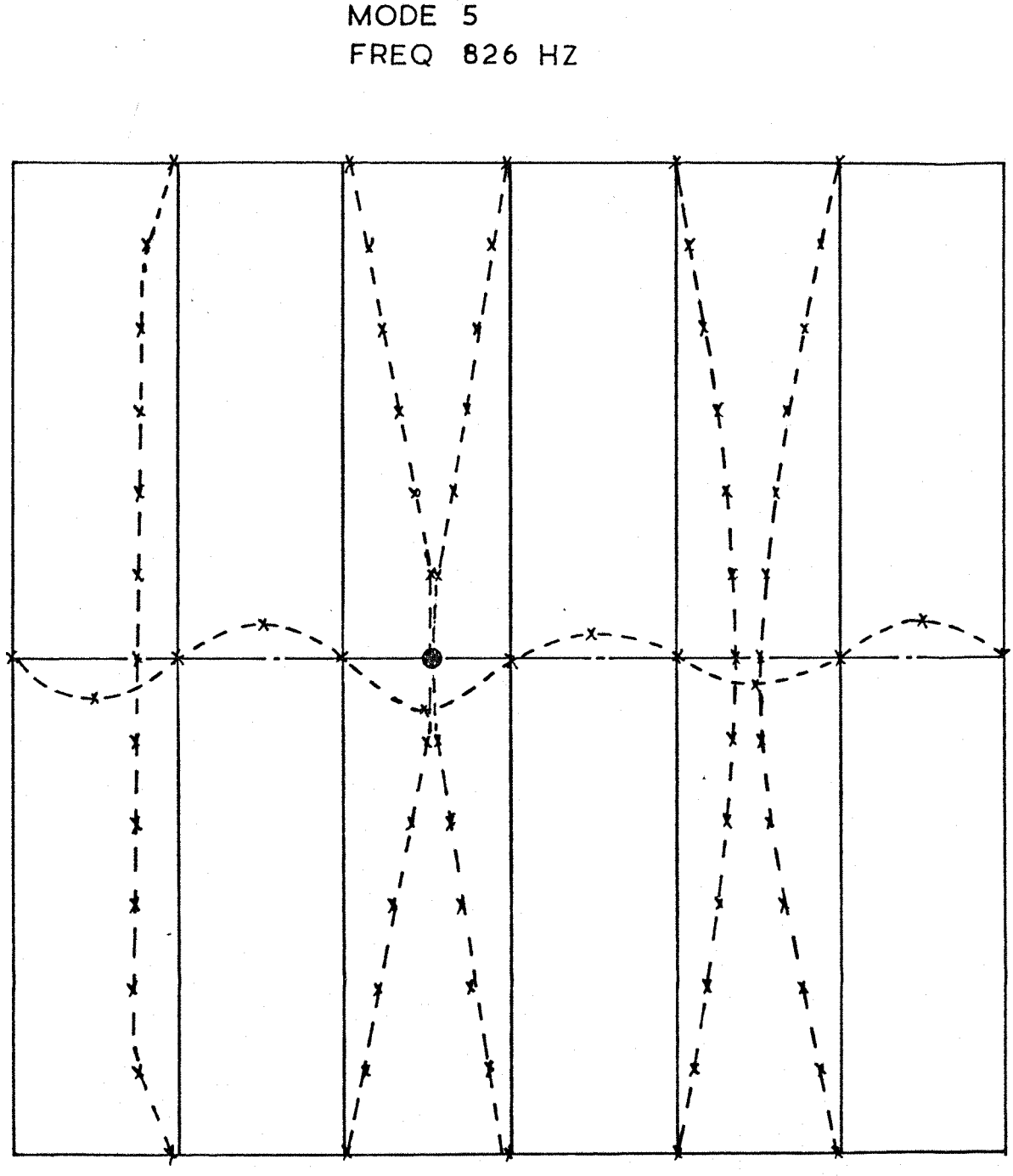


FIG. 66 Fifth undamped panel mode with shaker excitation

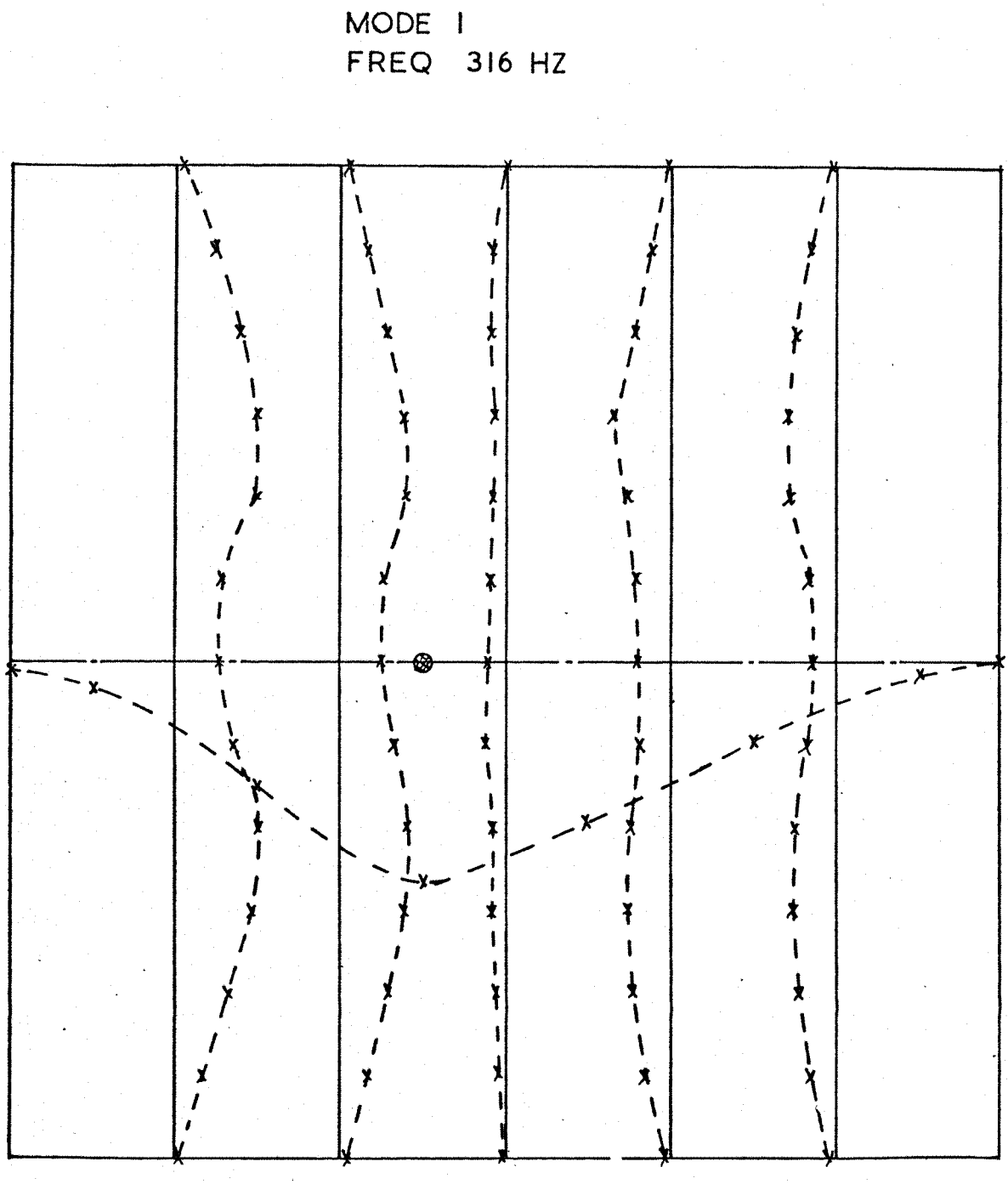


FIG. 67 First damped panel mode with Type 1 shear damping beam attached

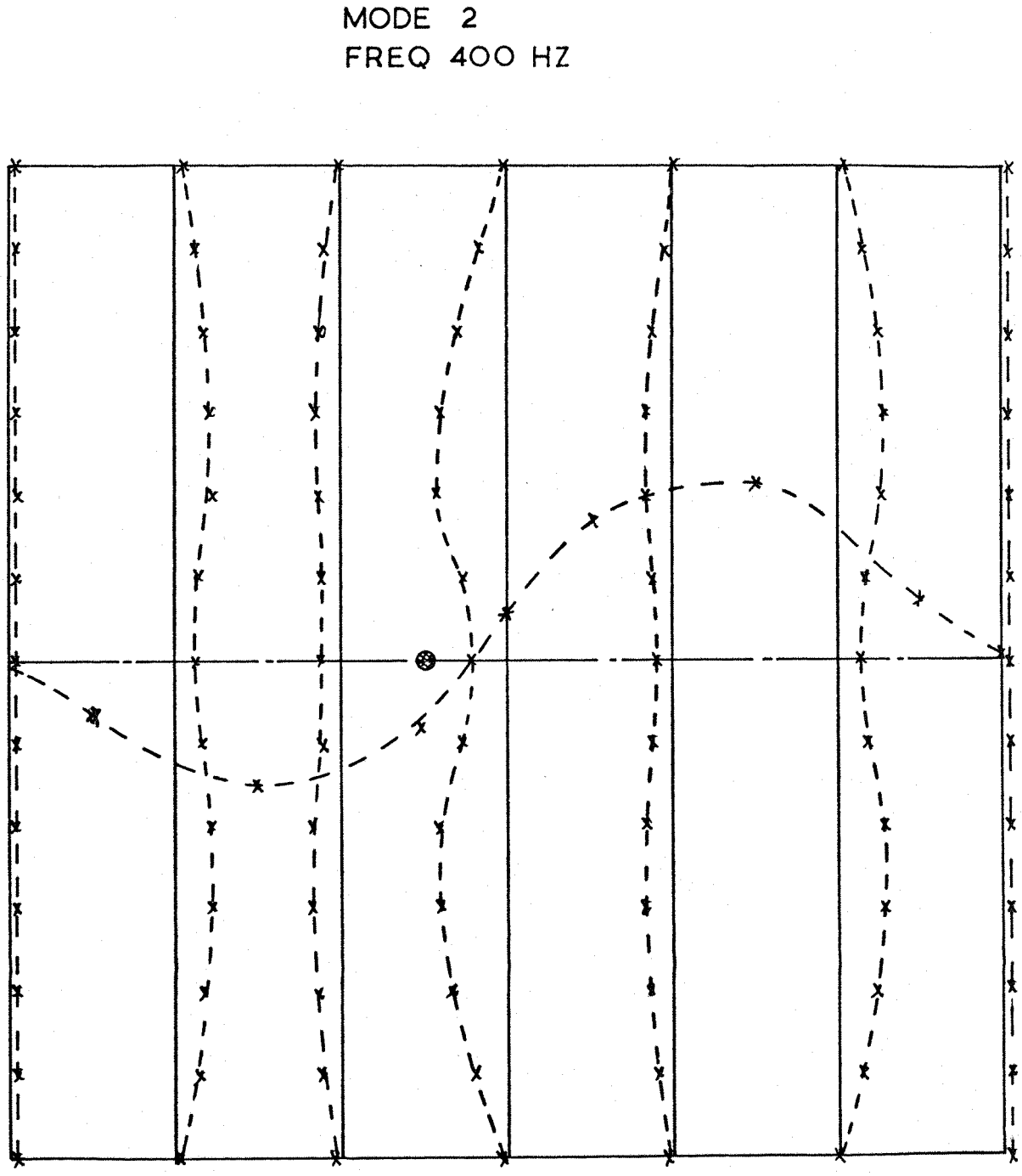


FIG. 68 Second damped panel mode with Type 1 shear damping beam attached

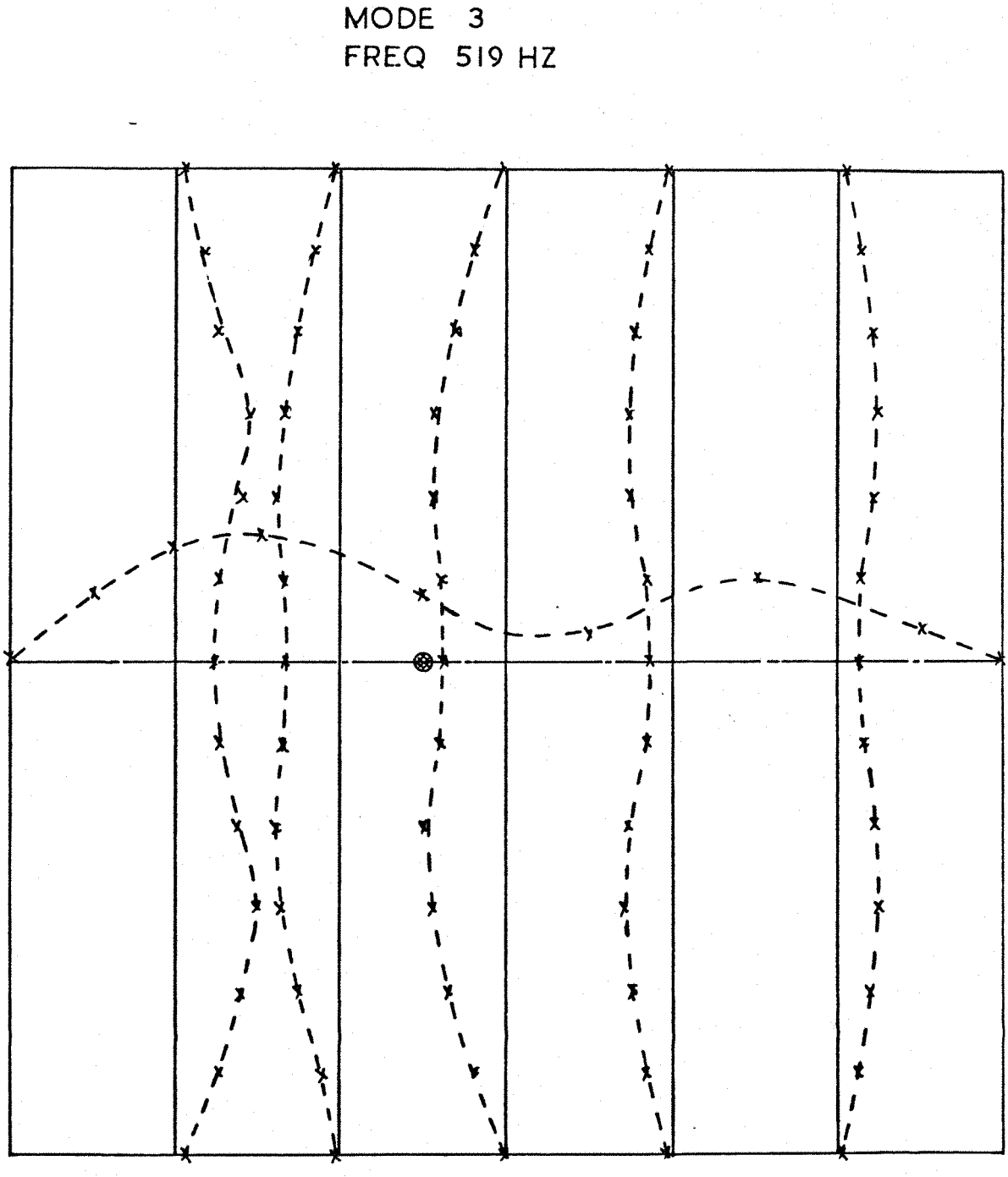


FIG. 69 Third damped panel mode with Type 1 shear damping beam attached

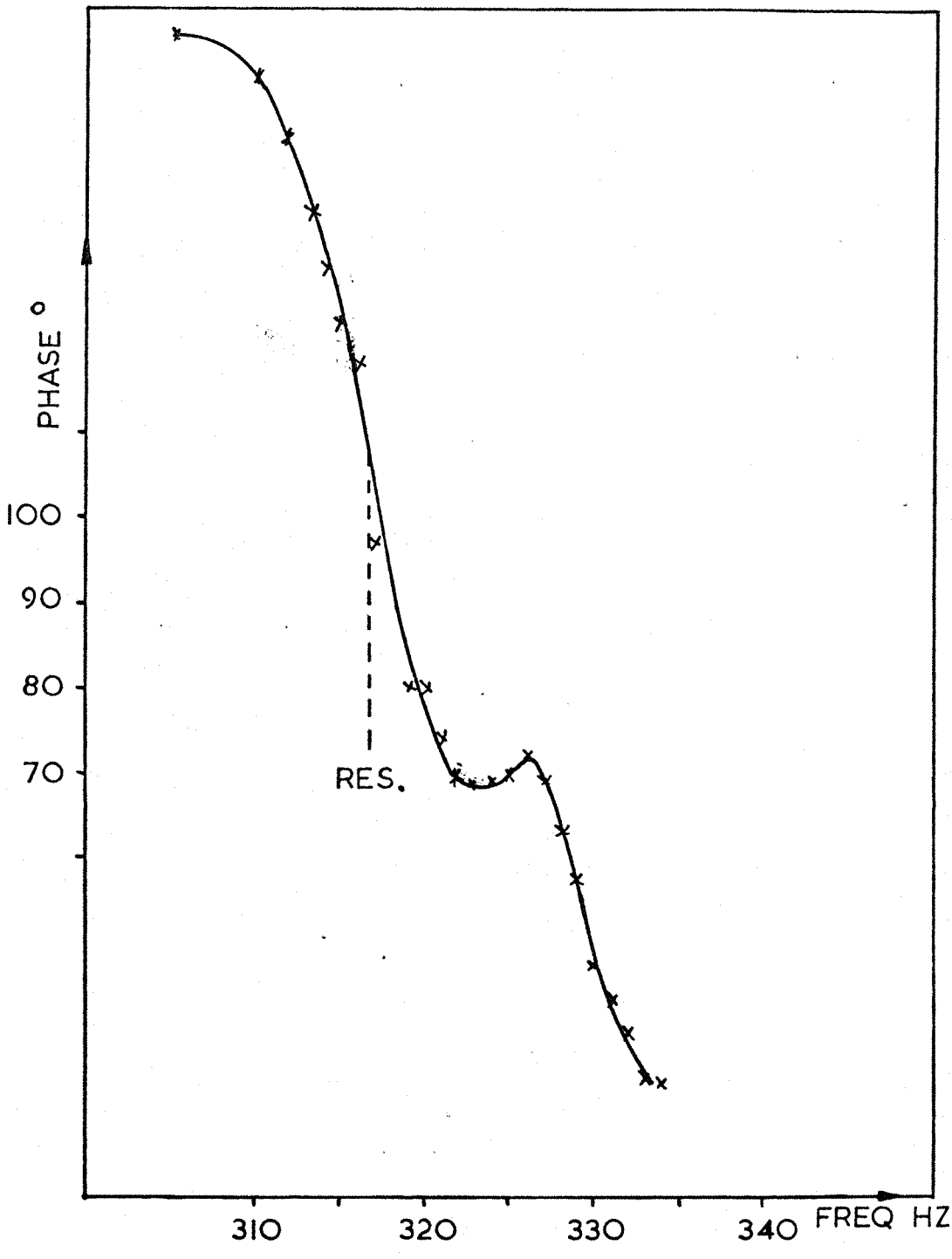


FIG. 70 Phase angle between excitation and response versus frequency for first damped mode

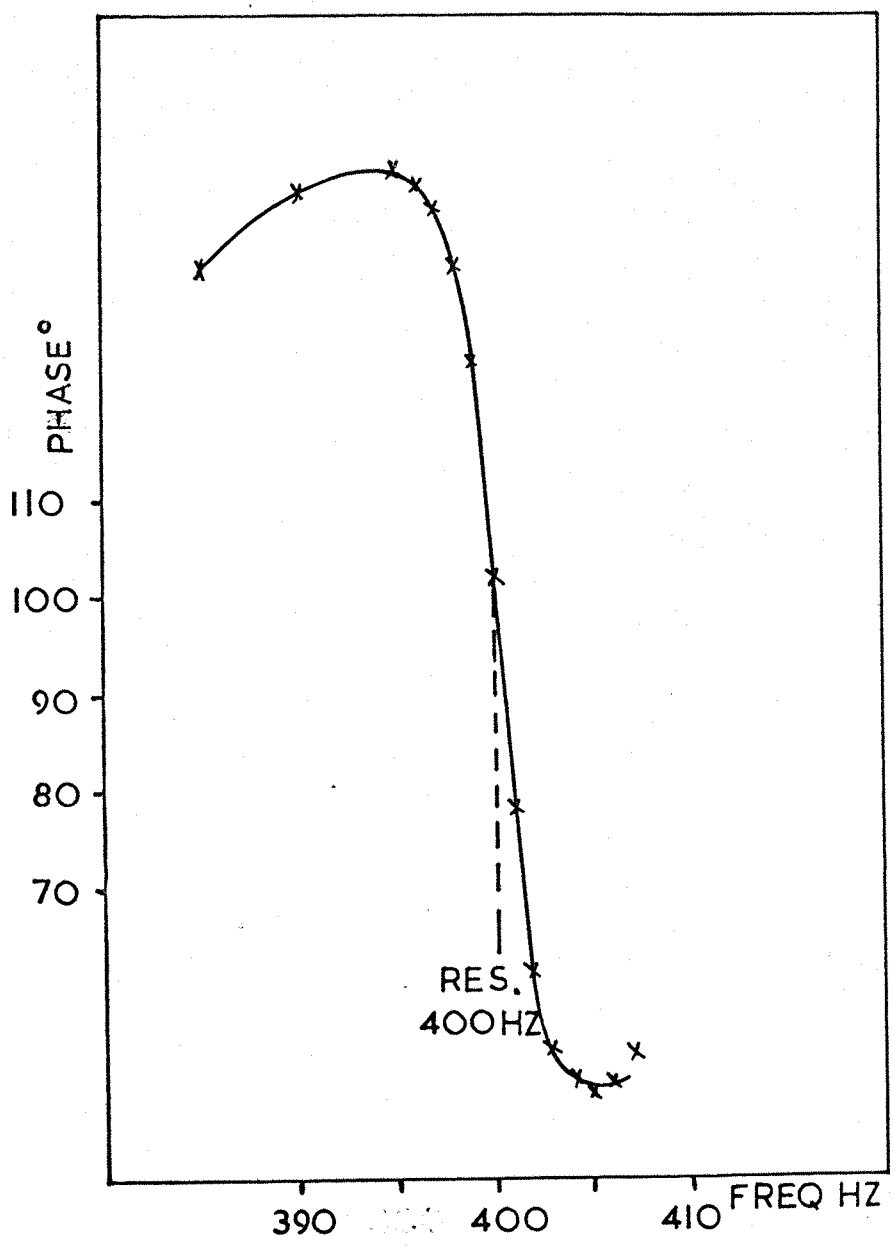


FIG. 71 Phase angle between excitation and response versus frequency for second damped mode

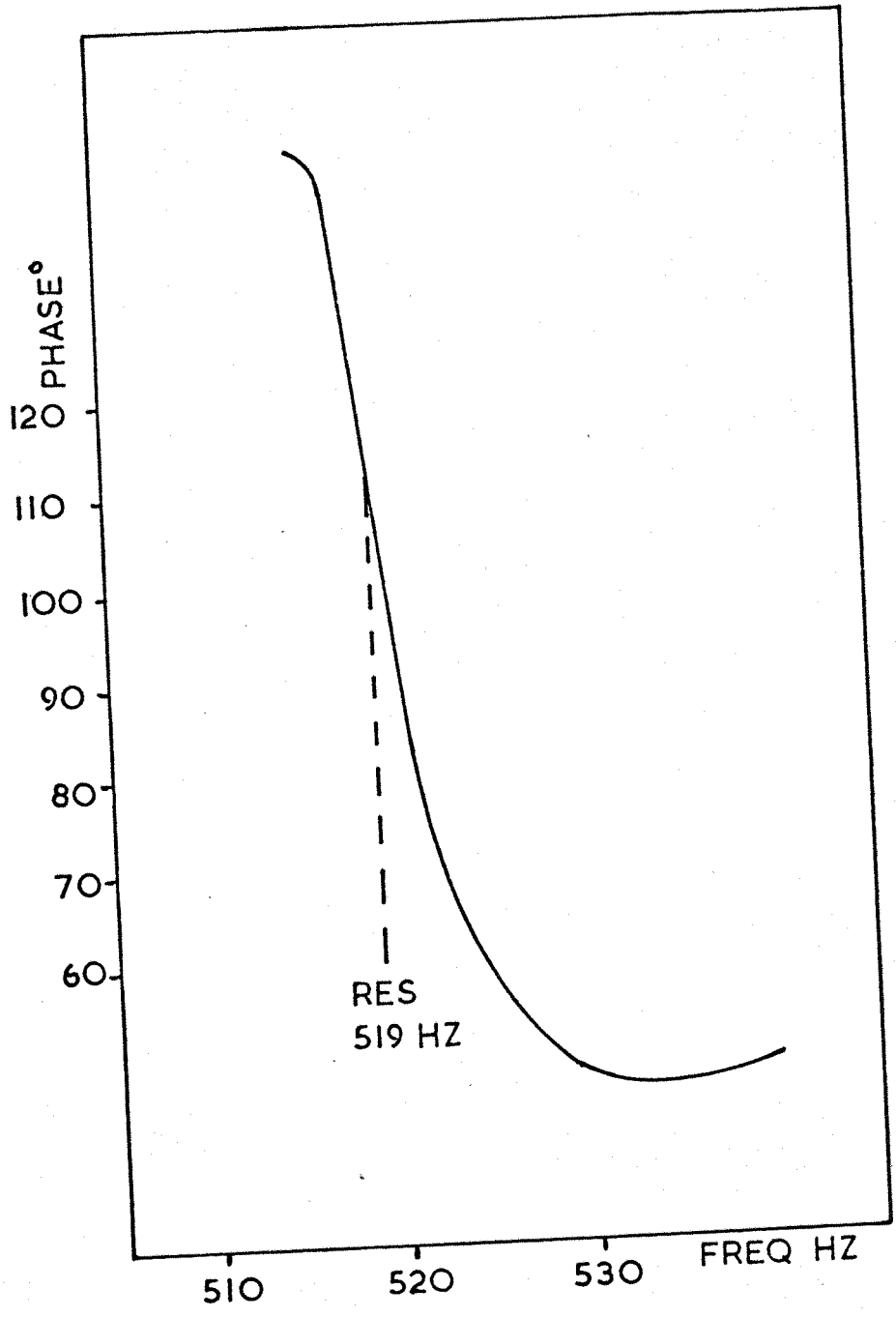


FIG. 72 Phase angle between excitation and response versus frequency for third damped mode

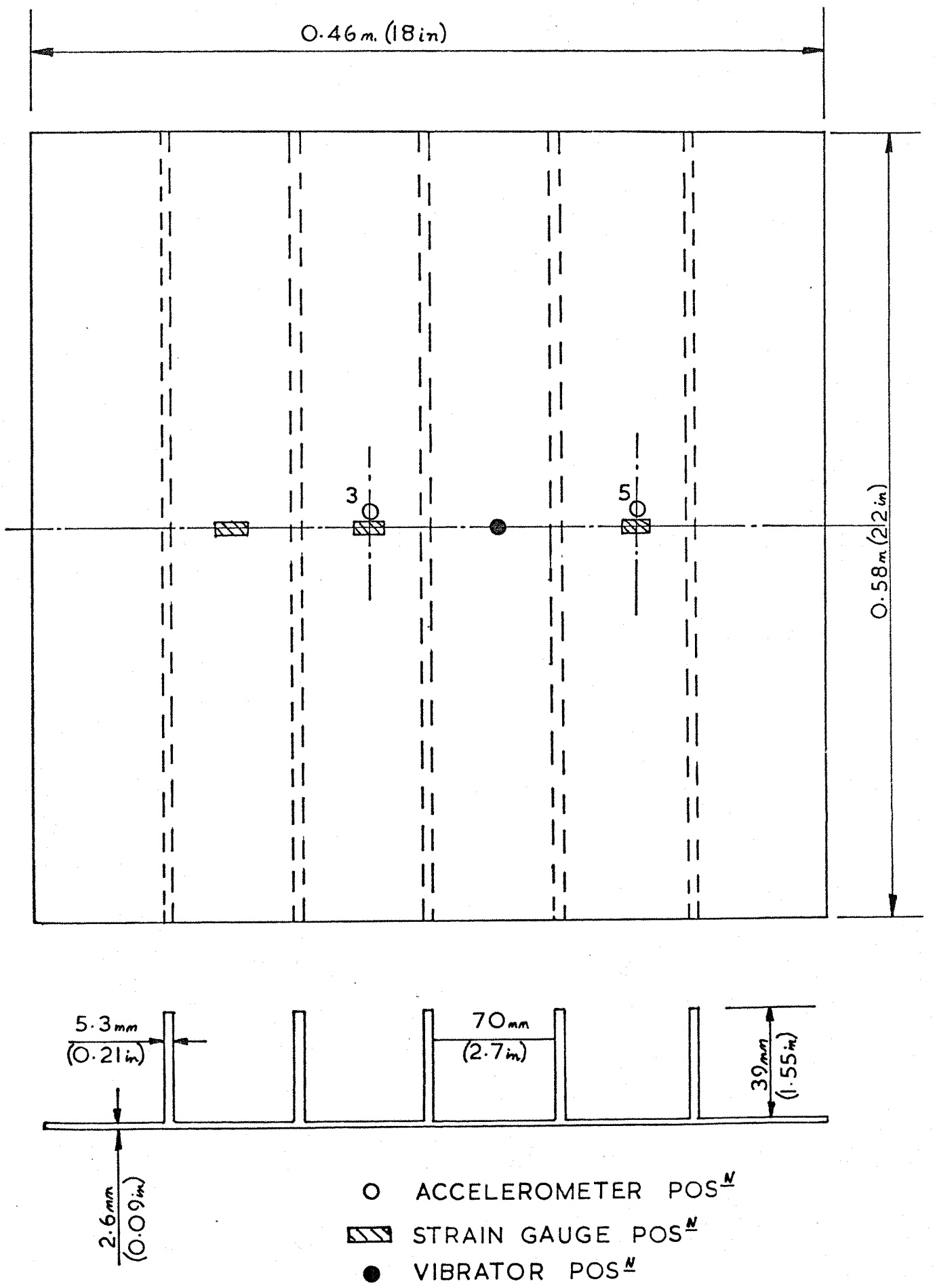


FIG. 73 Test panel details and response transducer positions

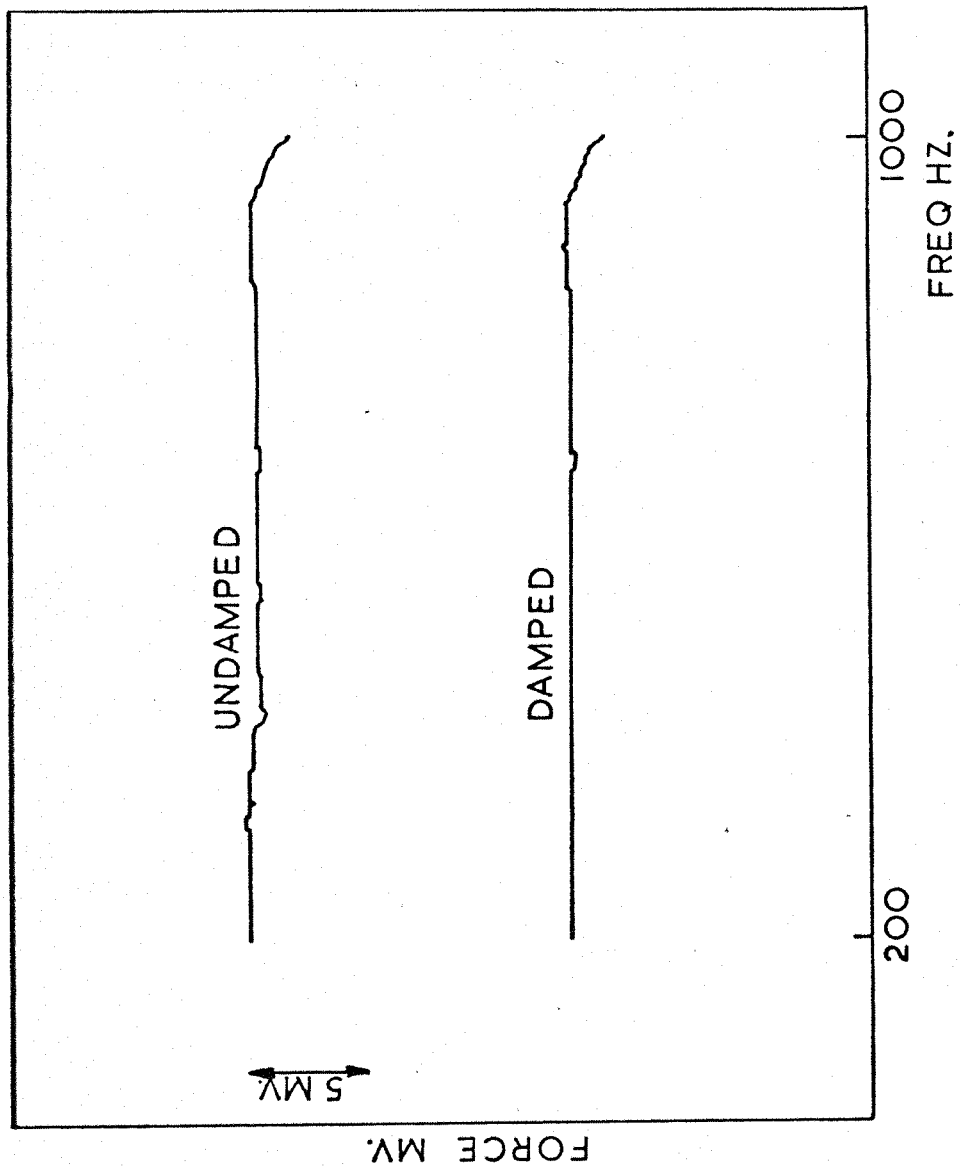


FIG. 74 Variation of panel excitation force with frequency

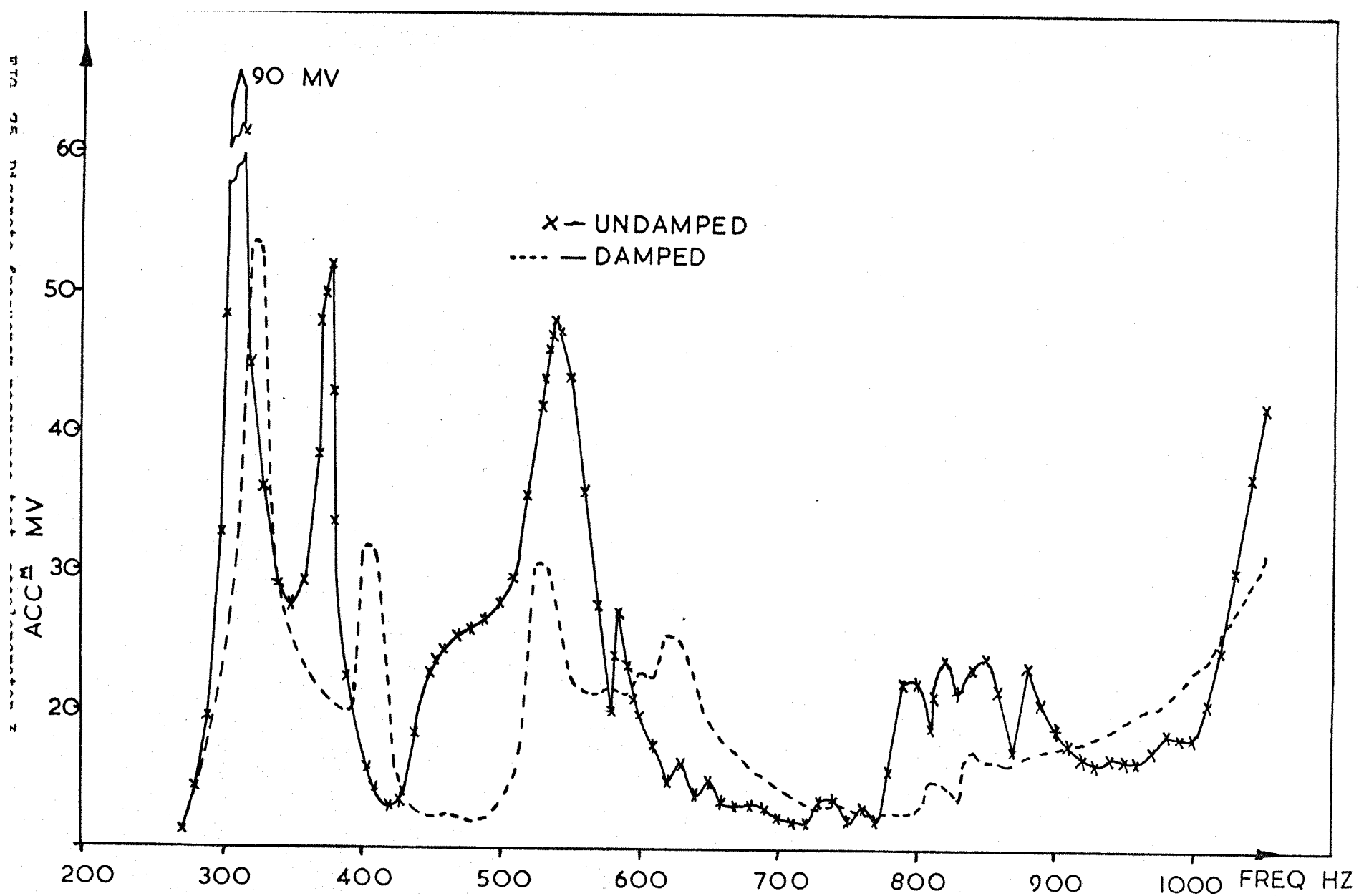
90 MV
X — UNDAMPED
---- — DAMPED
ACC MV
6G
5G
4G
3G
2G
200
300
400
500
600
700
800
900
1000
FREQ HZ

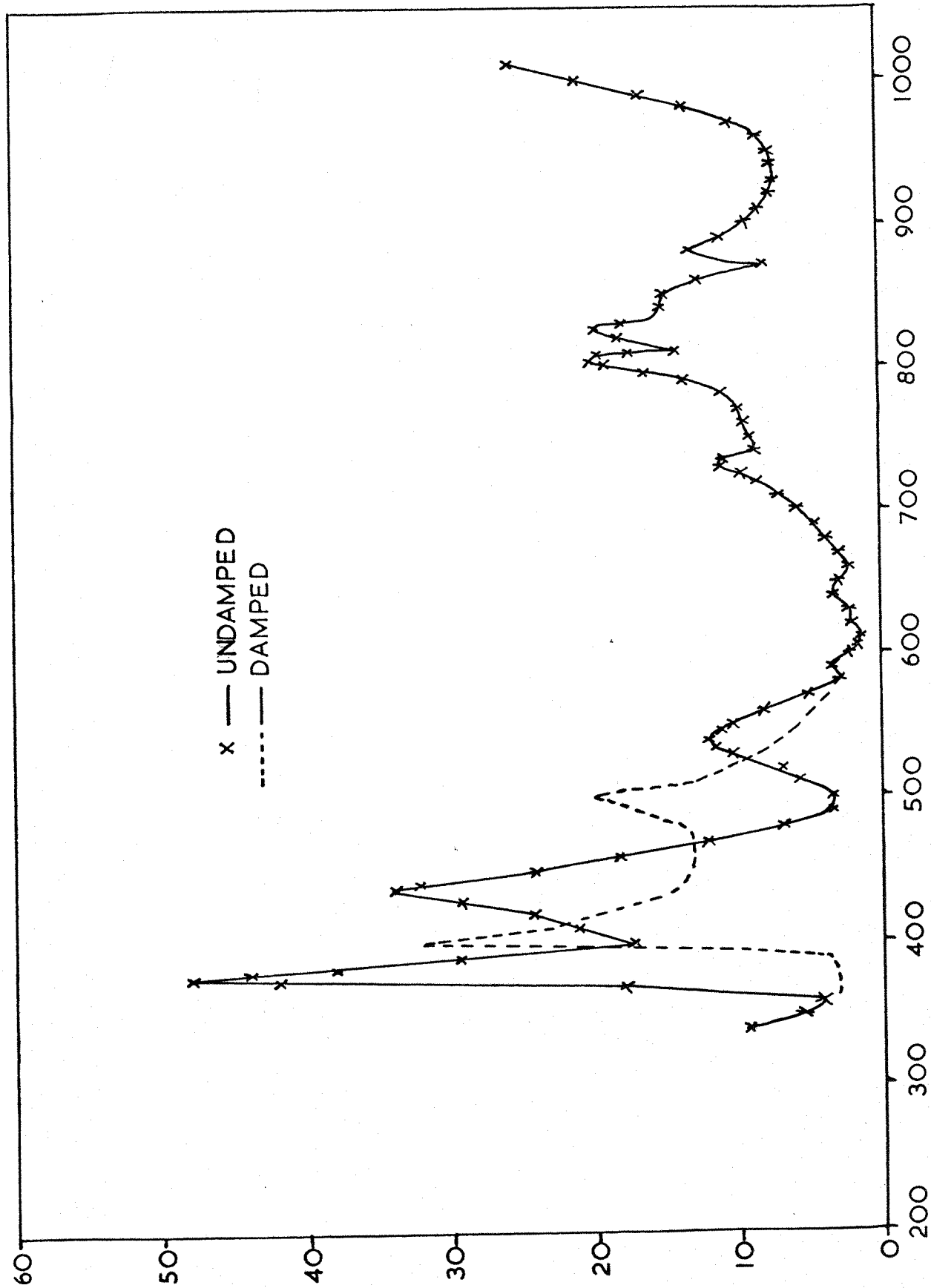


FIG. 76 Discrete frequency response test, accelerometer 5

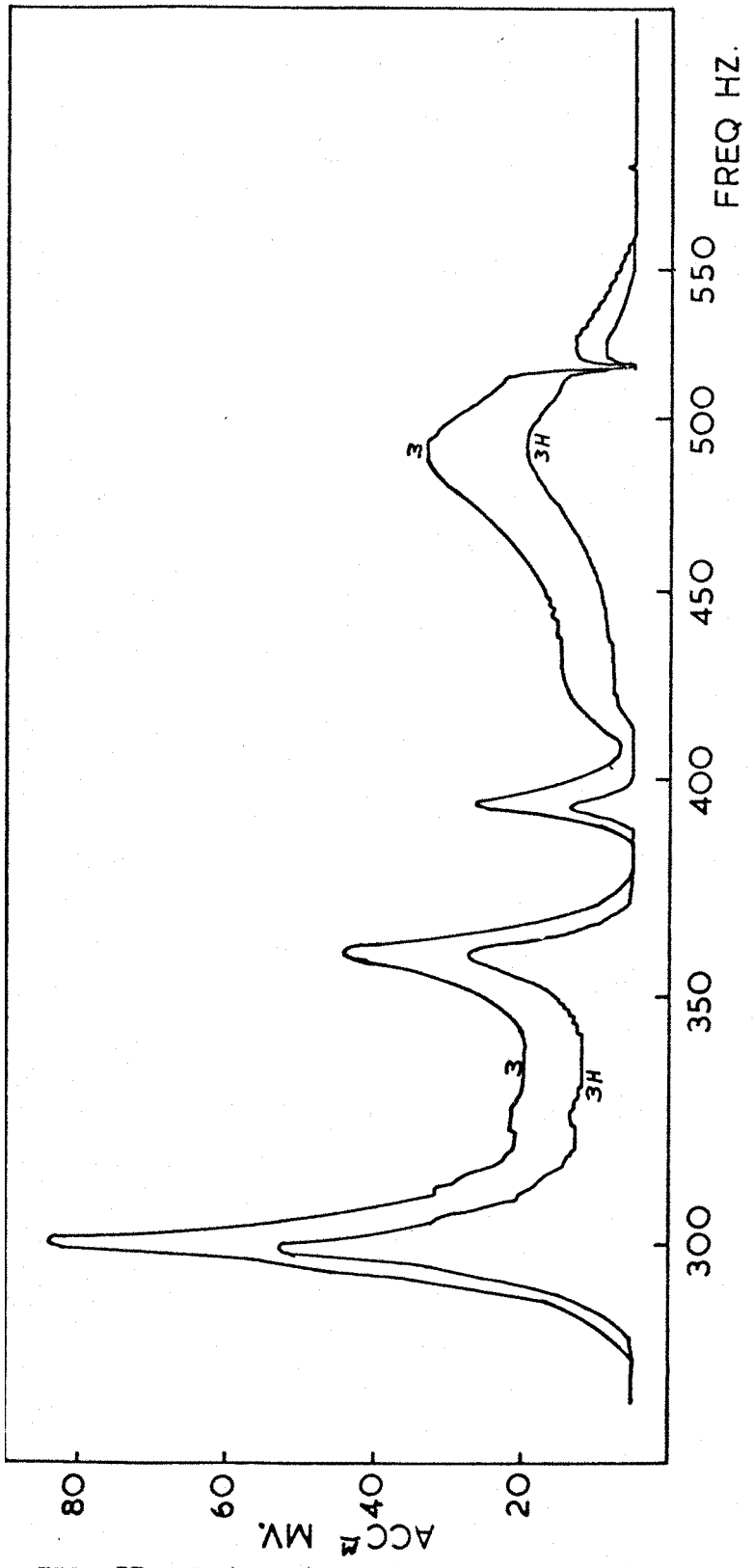


FIG. 77 Undamped panel response to slow frequency sweep, accelerometers 3

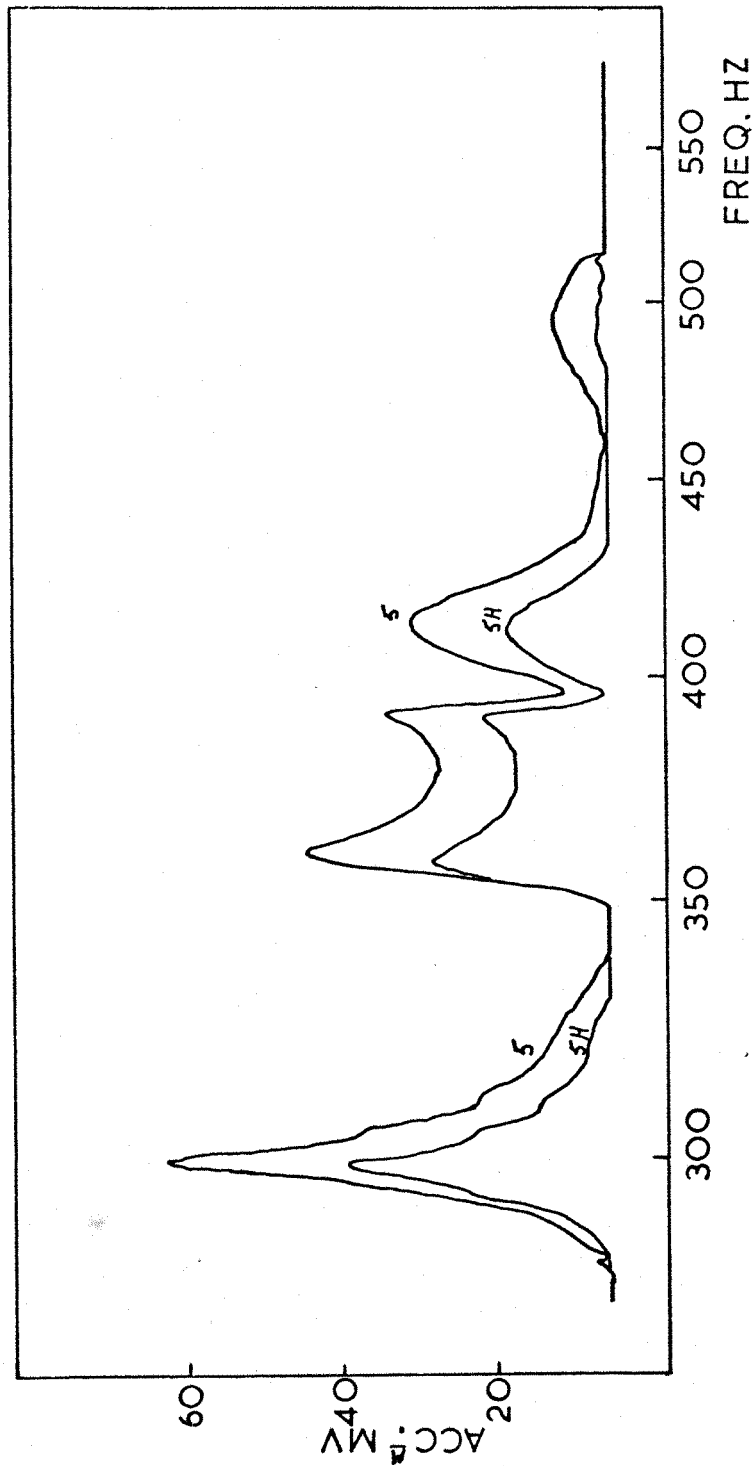


FIG. 78 Undamped panel response to slow frequency sweep, accelerometers 5

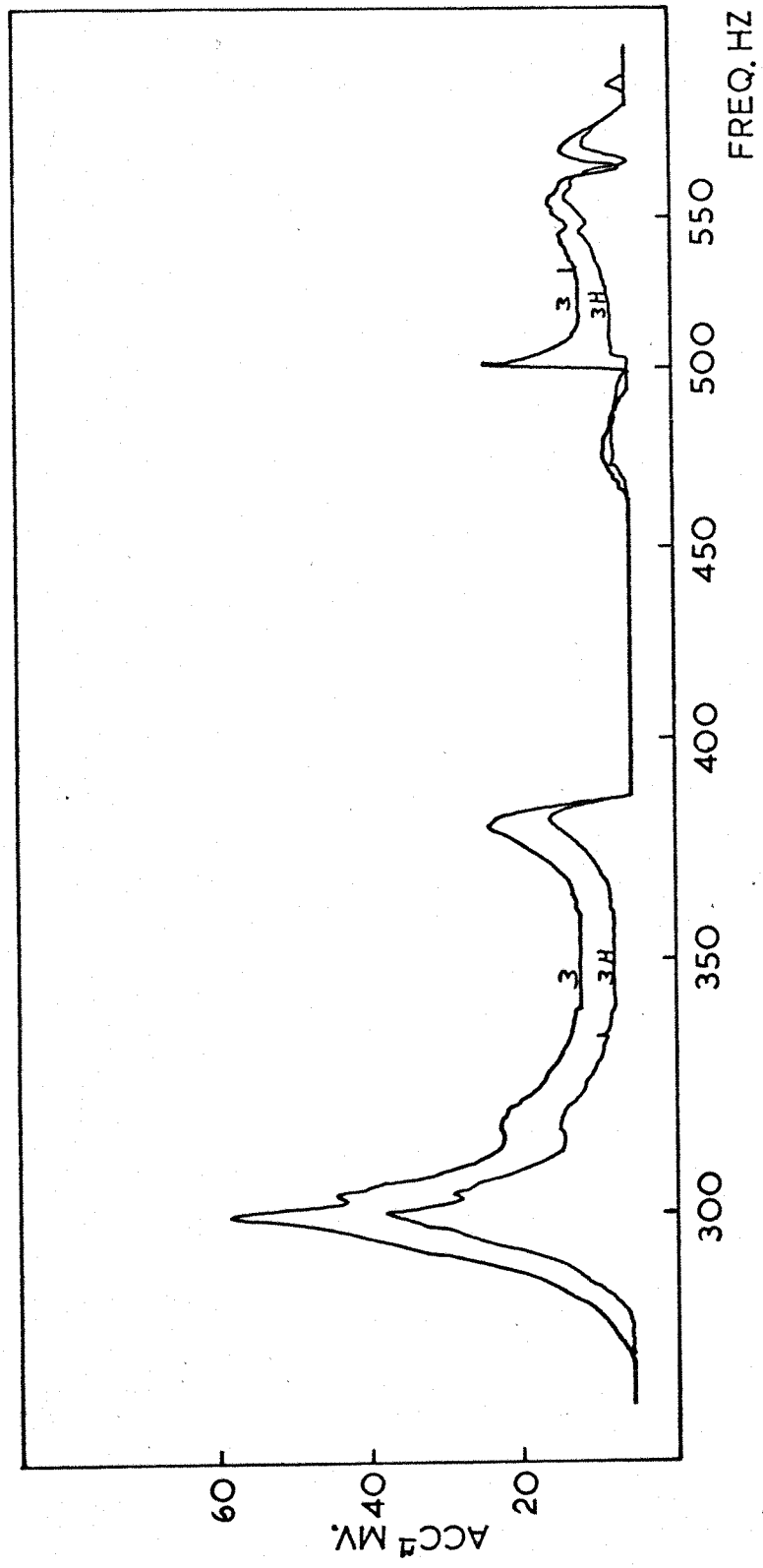


FIG. 79 Damped panel response to slow frequency sweep, accelerometers 3. Type I damping beam attached

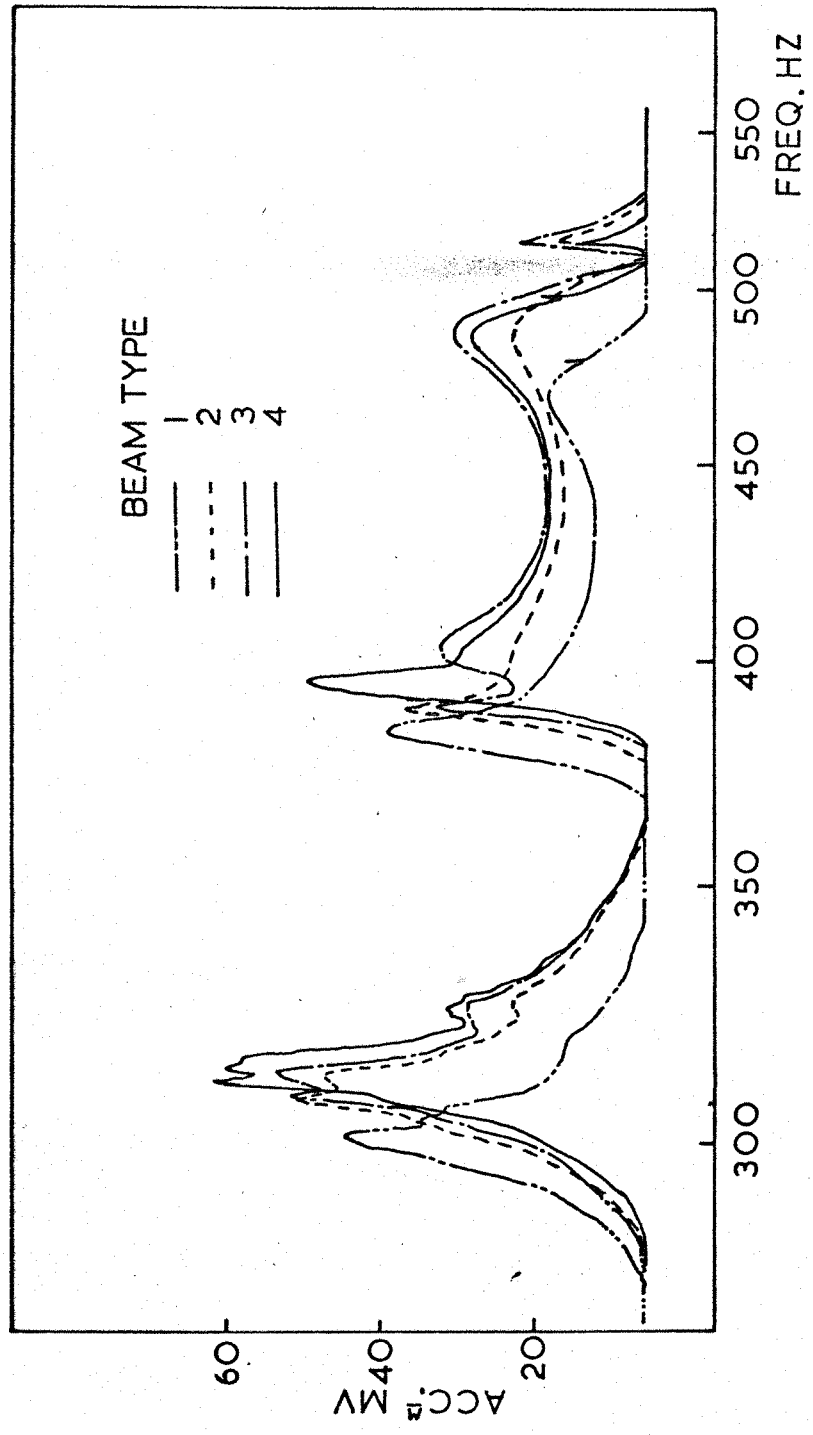


FIG. 80 Damped panel response to slow frequency sweep, accelerometers 5. Types 1, 2, 3, 4 damping beams attached.

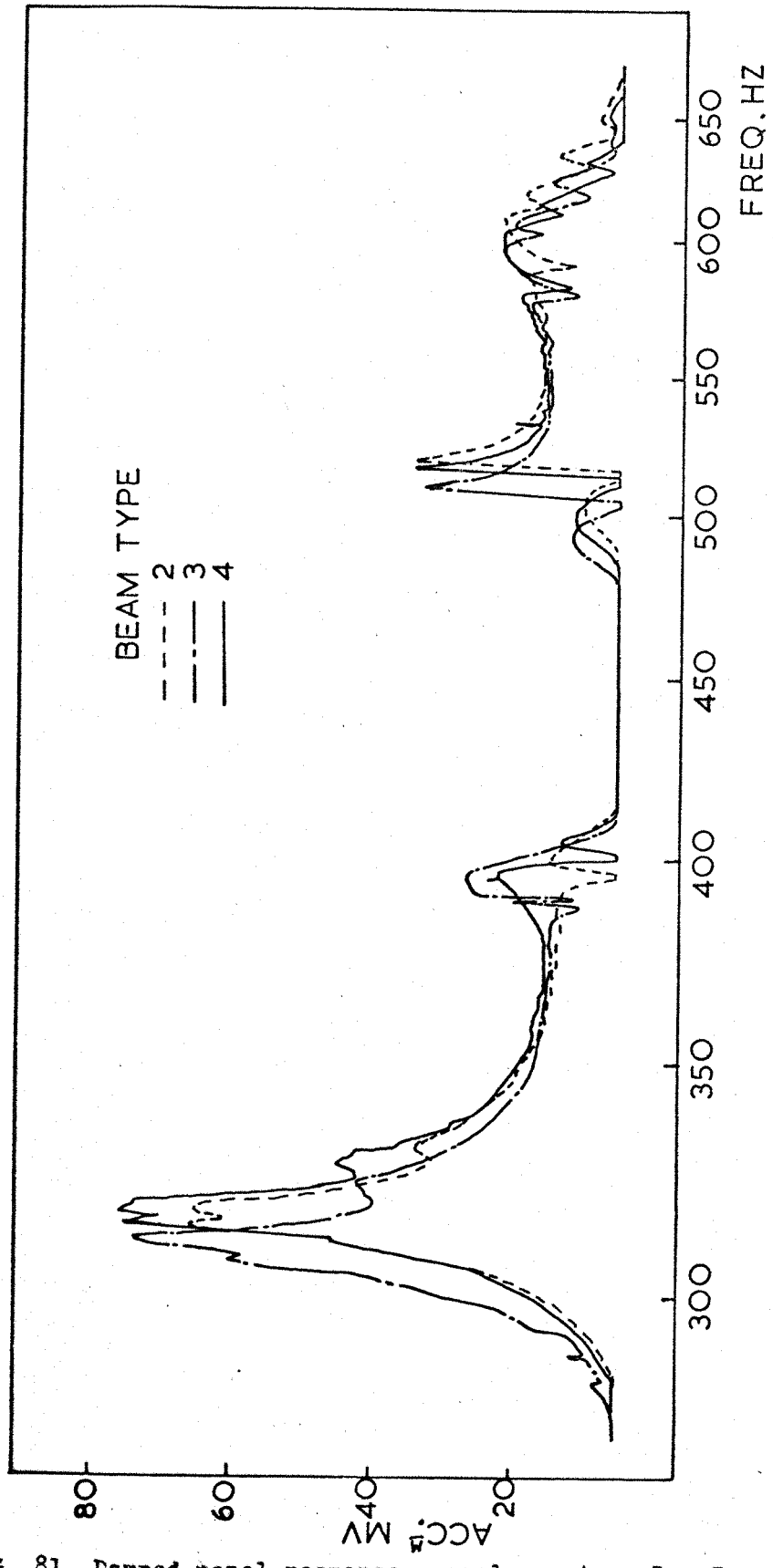


FIG. 81 Damped panel response, accelerometers 3. Type 2,3,4 damping beams.

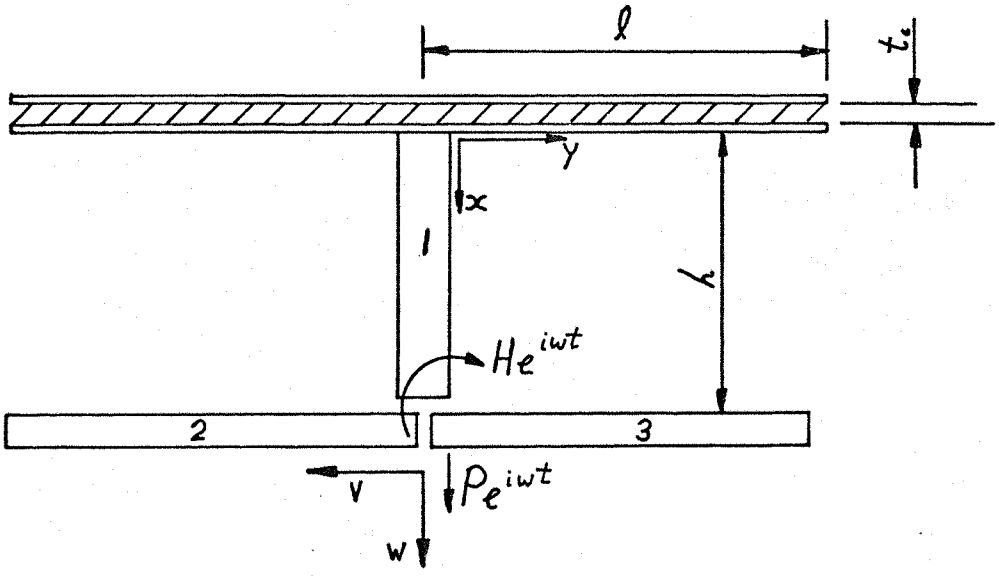


FIG. 82 Three beam element theoretical model

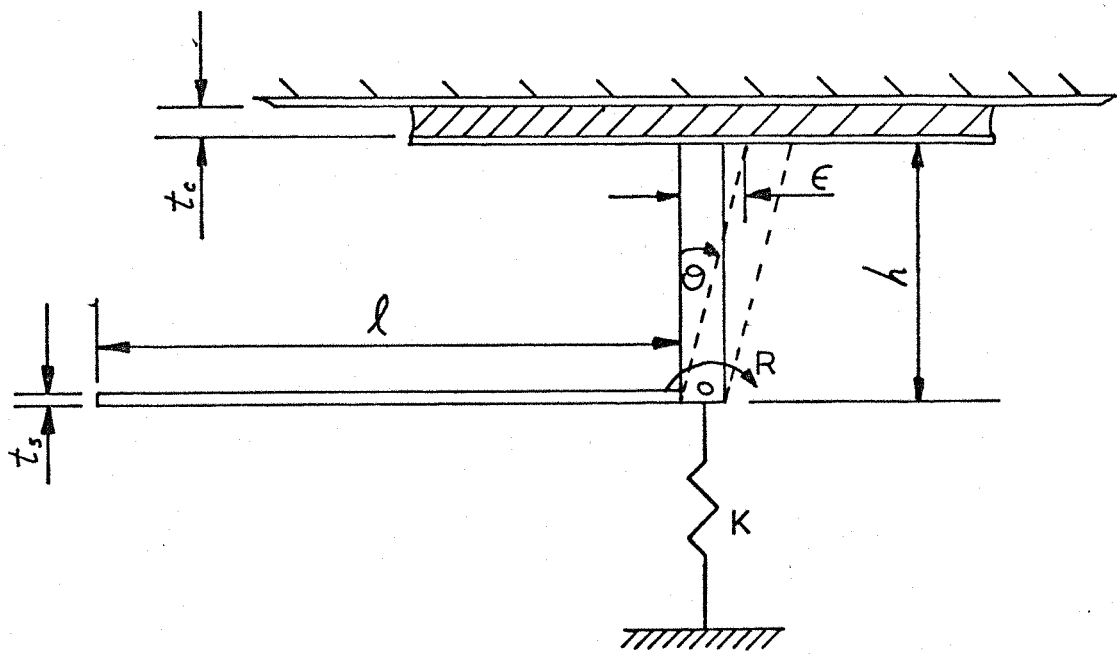


FIG. 83 Single element model for transfer matrix theory



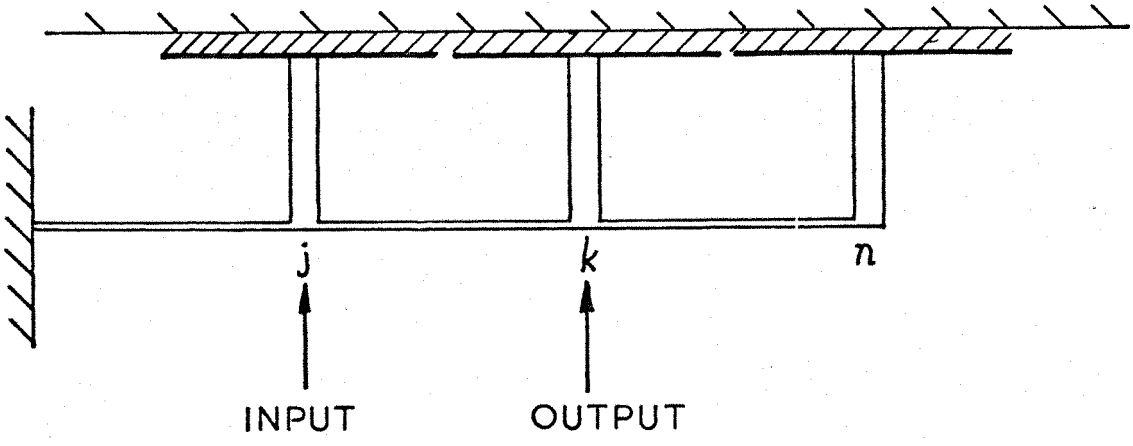


FIG. 84 Transfer matrix model of panel cross-section

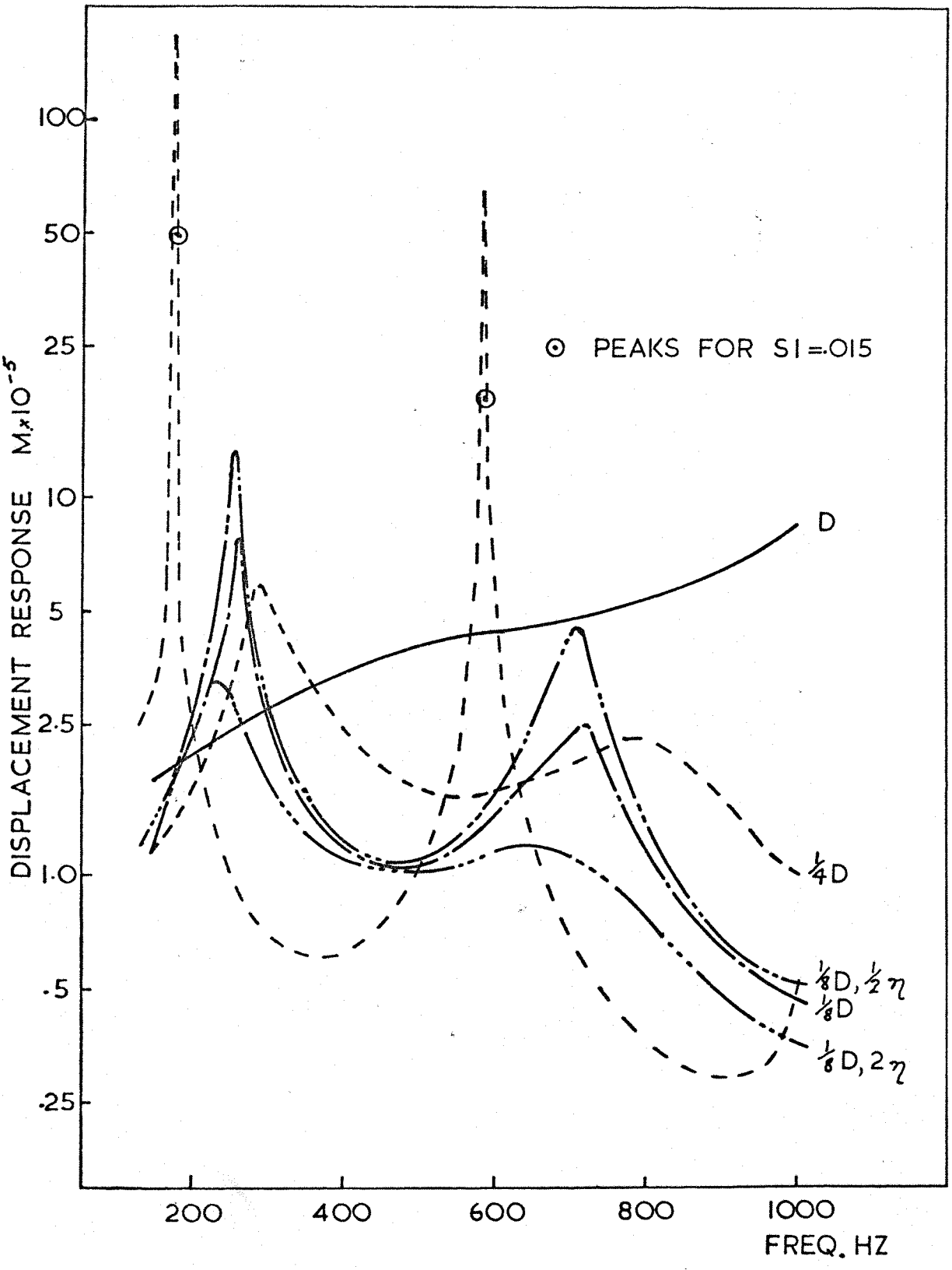


FIG. 85 Calculated panel response in anti-symmetric modes using transfer matrix theory

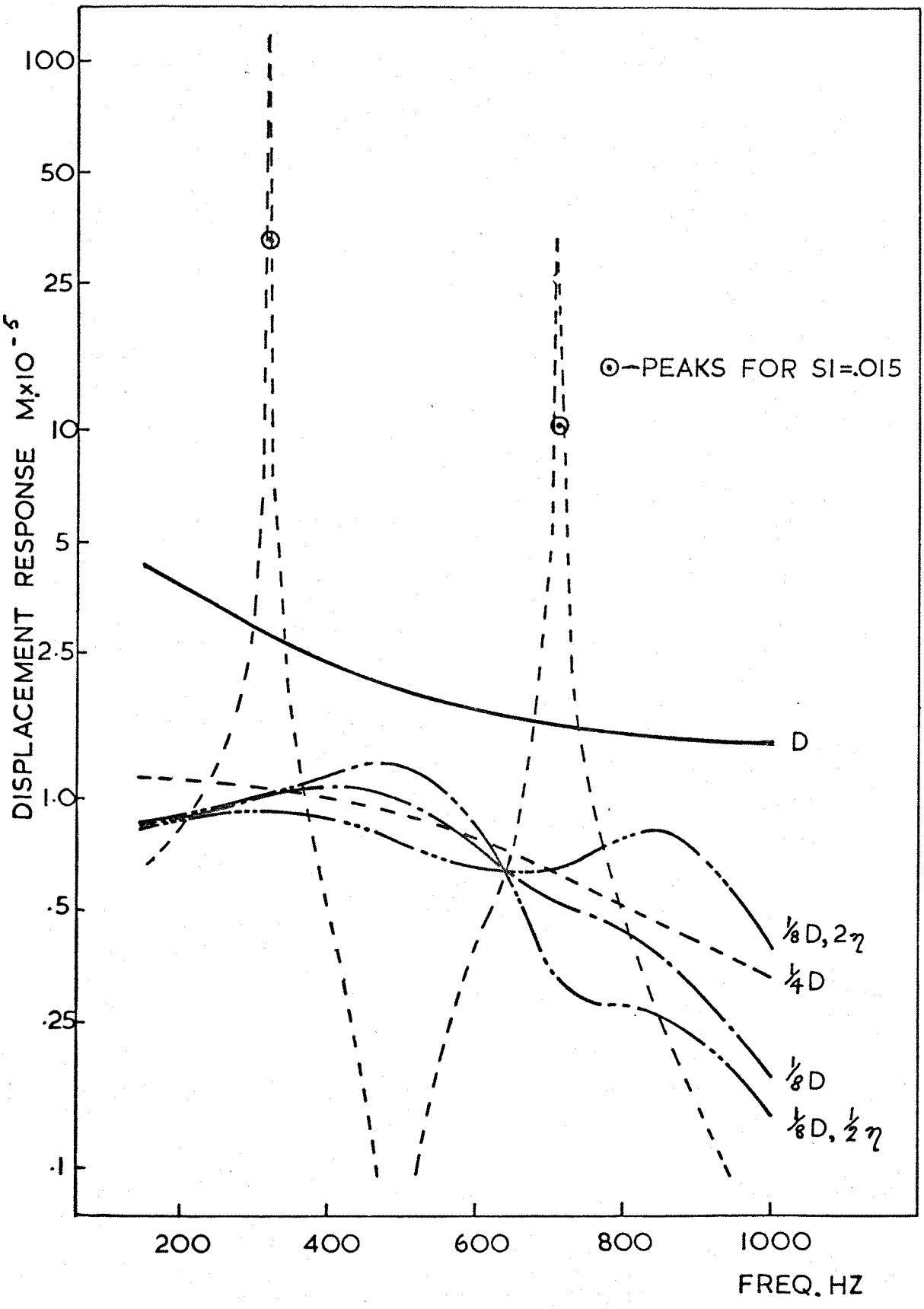


FIG. 86 Calculated panel response in symmetric modes using transfer matrix theory

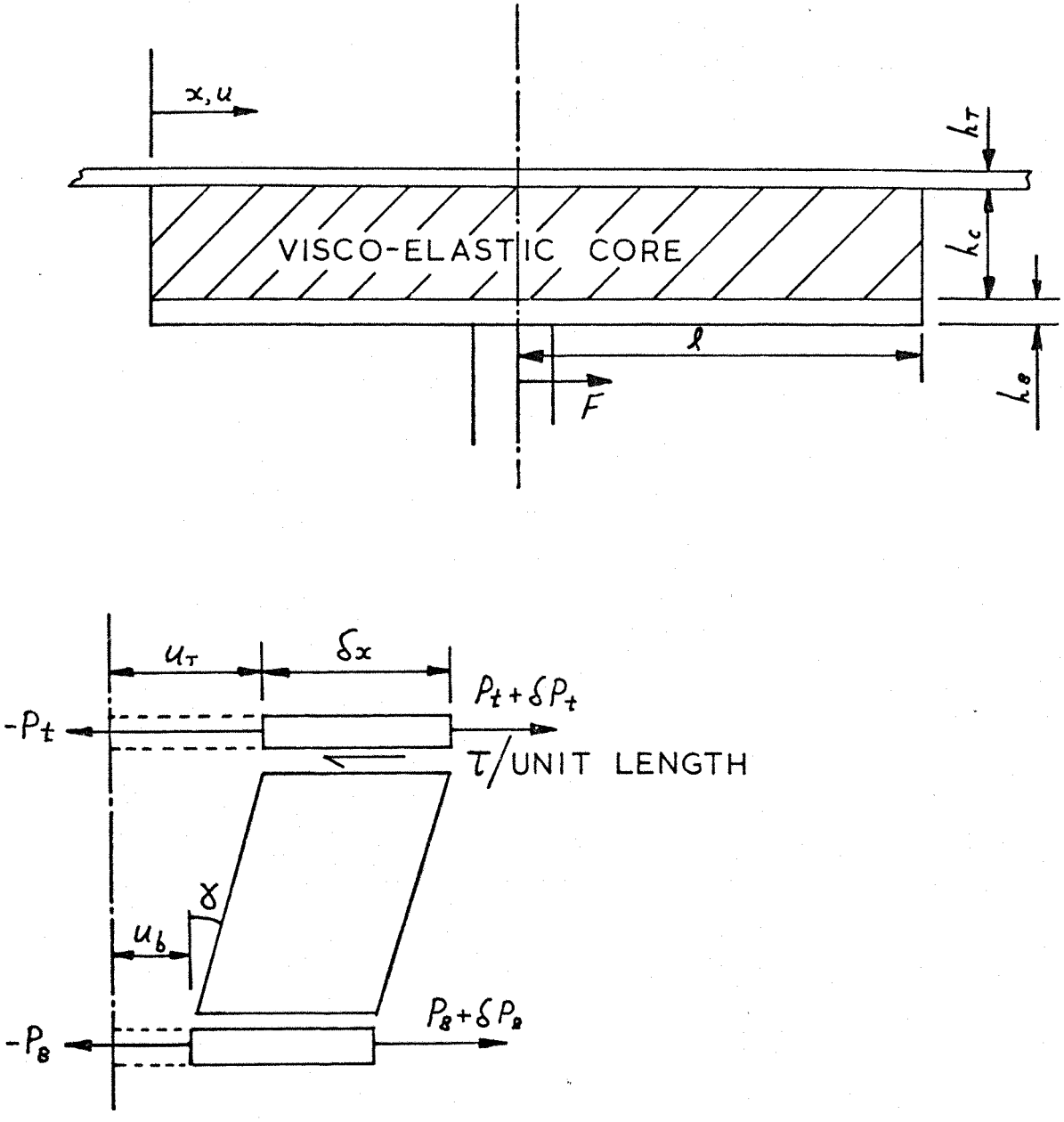


FIG. A.III Notation for calculation of shear stress distribution in damping beam core as Appendix III

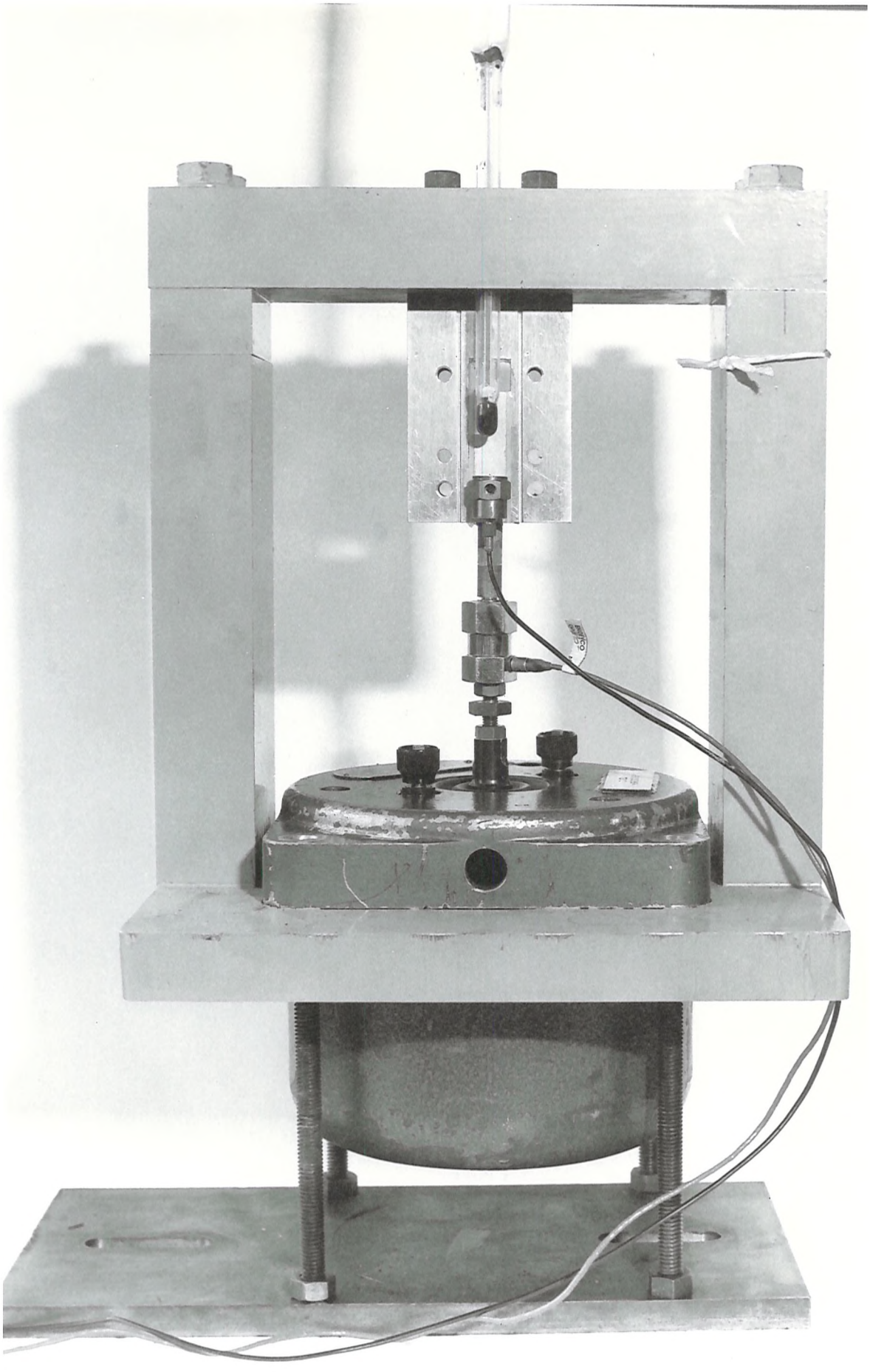

PLATE I  Basic Shear Test Apparatus

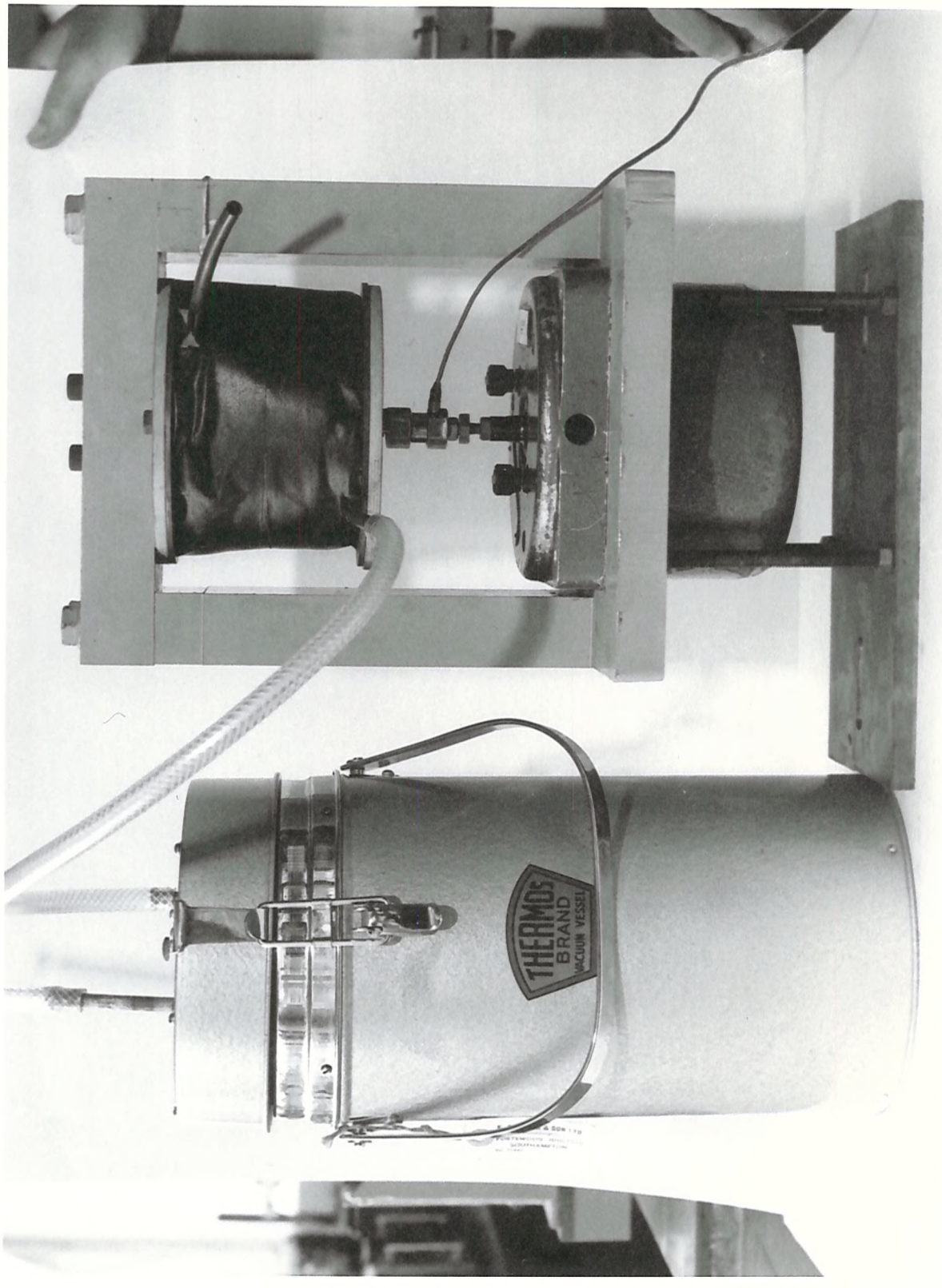


PLATE 2 Shear Test Apparatus with Coolant Resevoir and Chamber

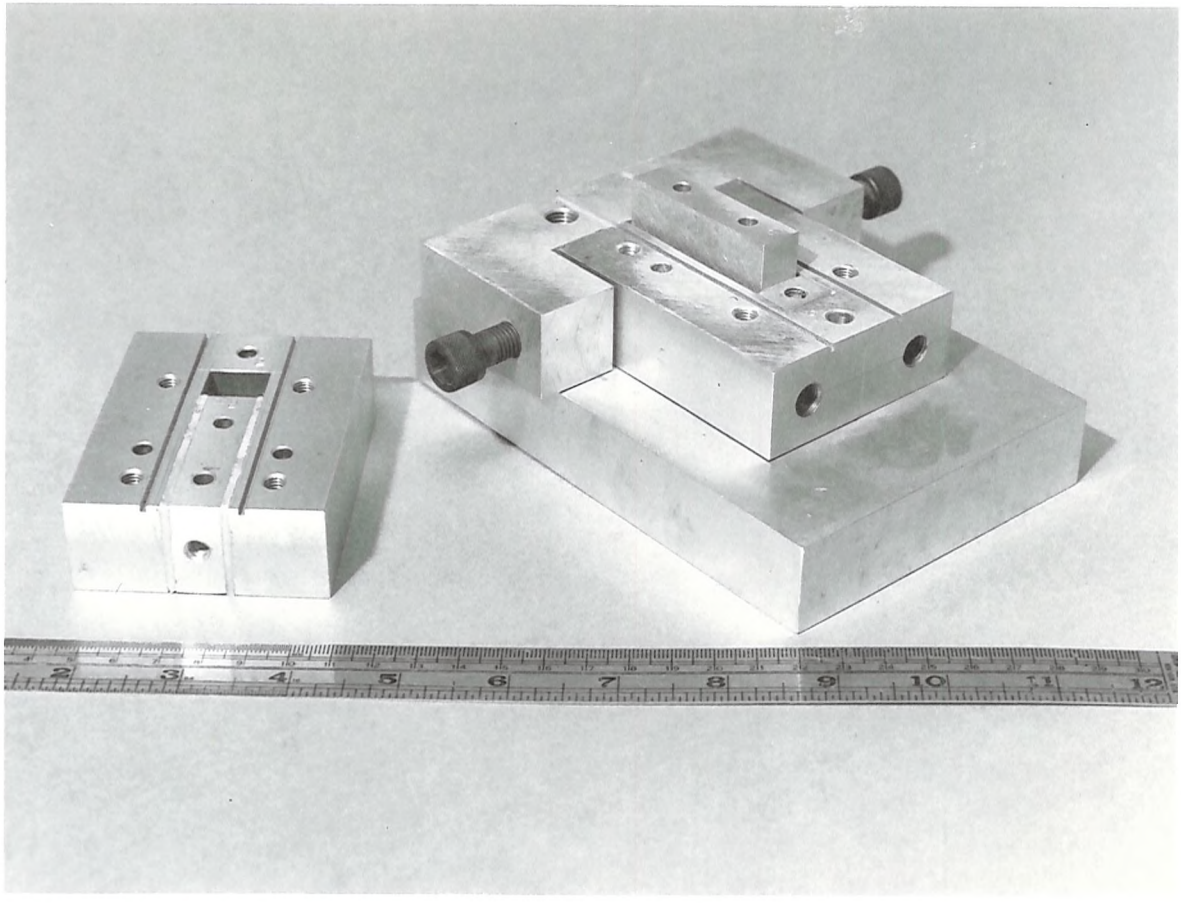

PLATE 3 Shear Test Specimen and Mould Assembly

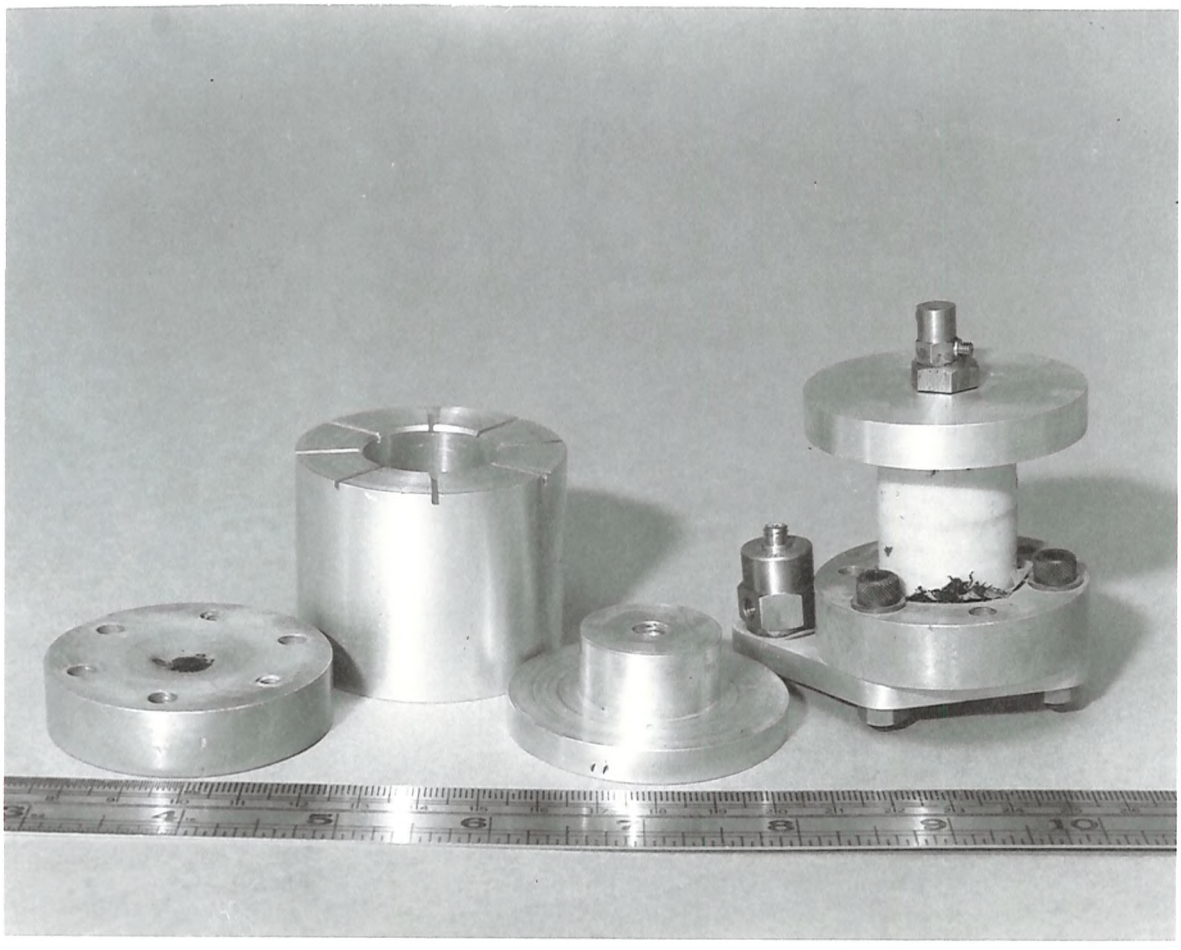

PLATE 4 Single Slug Test Specimen and Mould Assembly

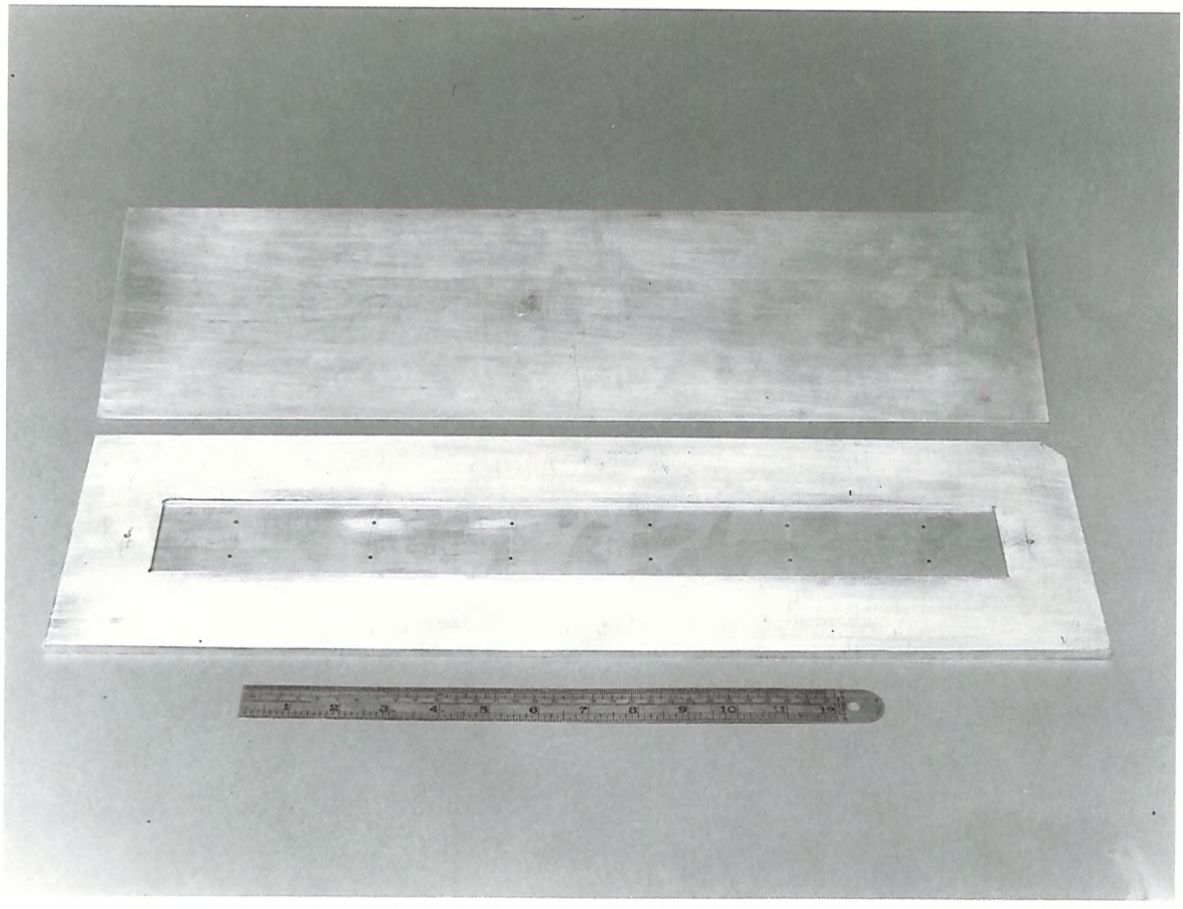

PLATE 5 Mould for Producing Damping Beams

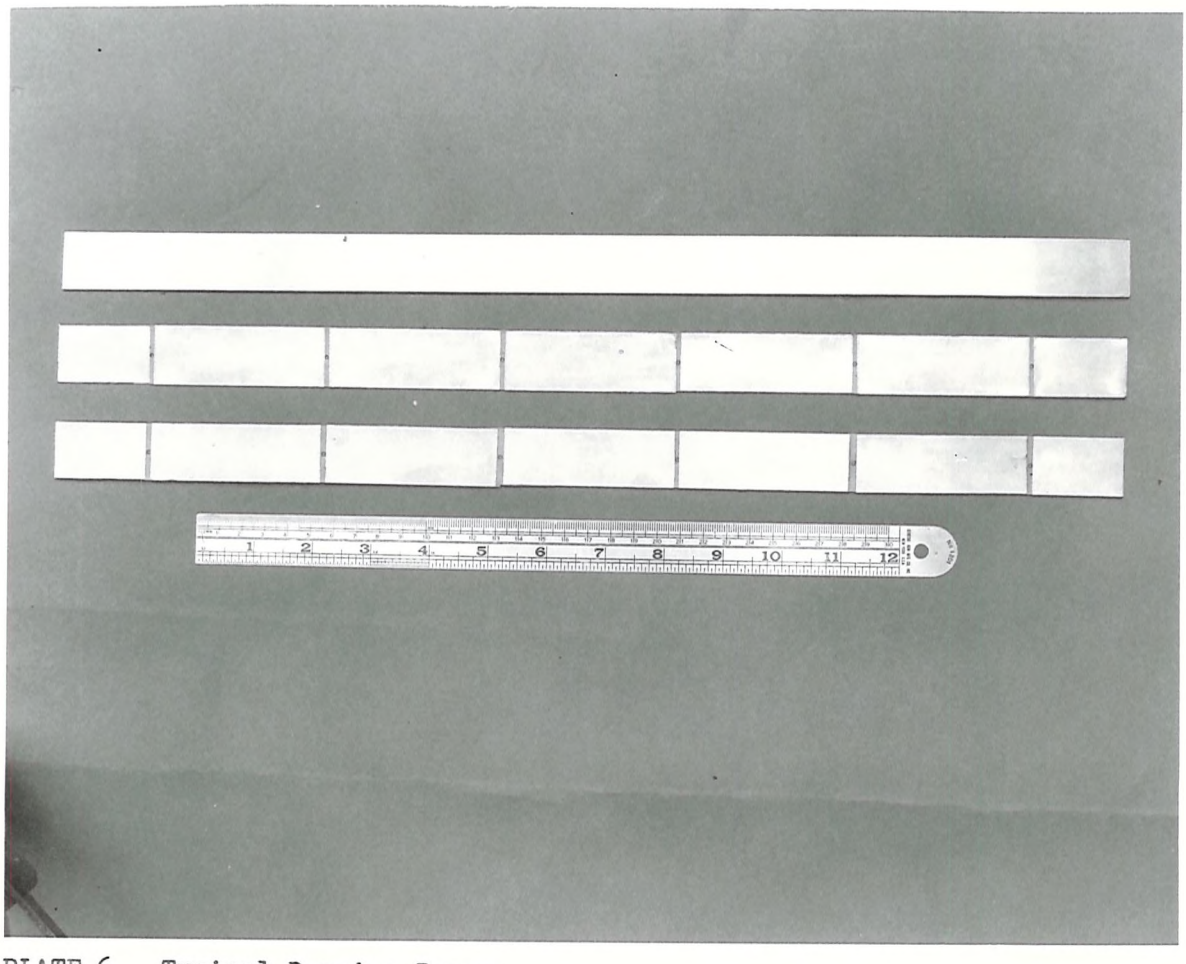

PLATE 6 Typical Damping Beams

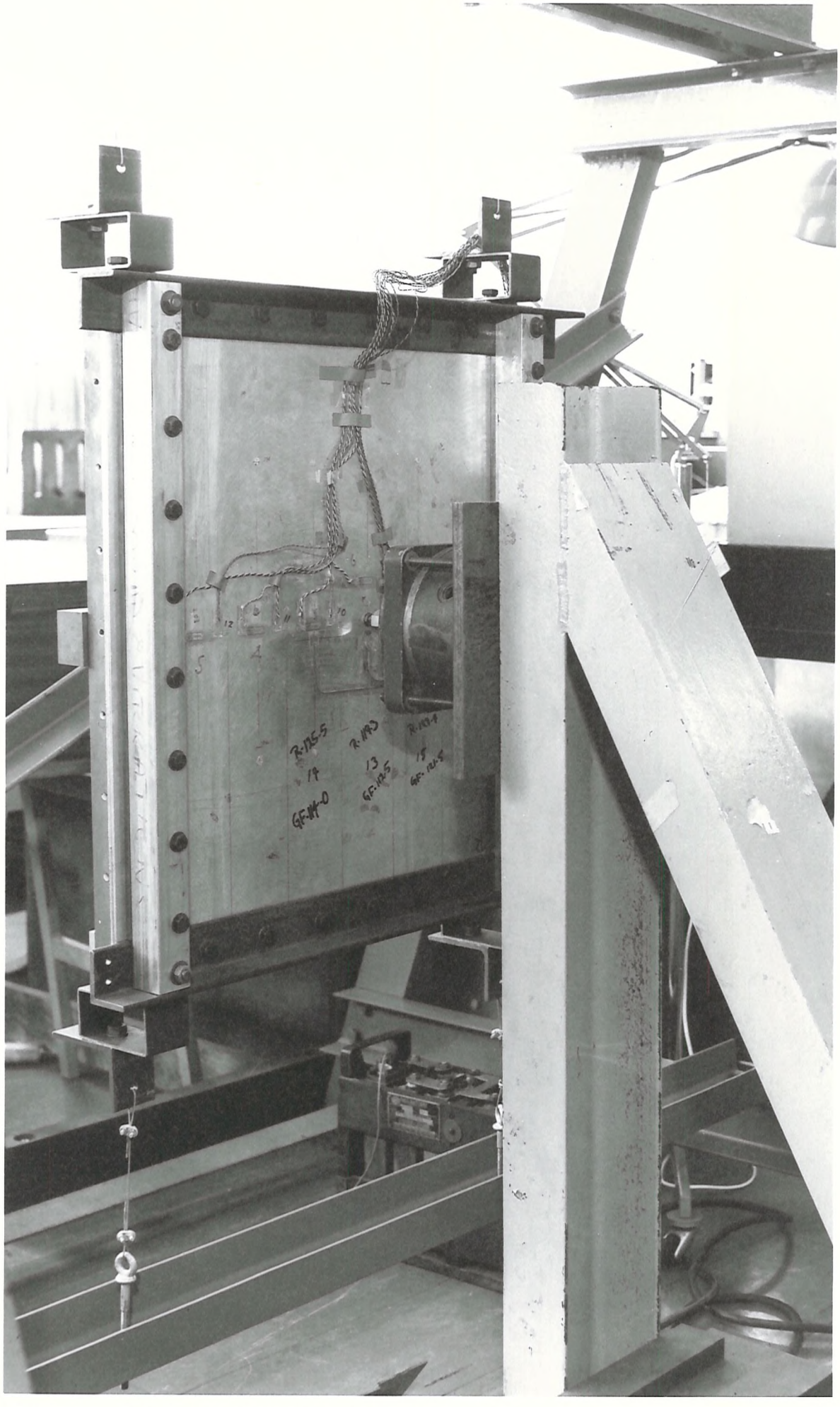

PLATE 7 Panel and Shaker Mounting for Single Point Excitation

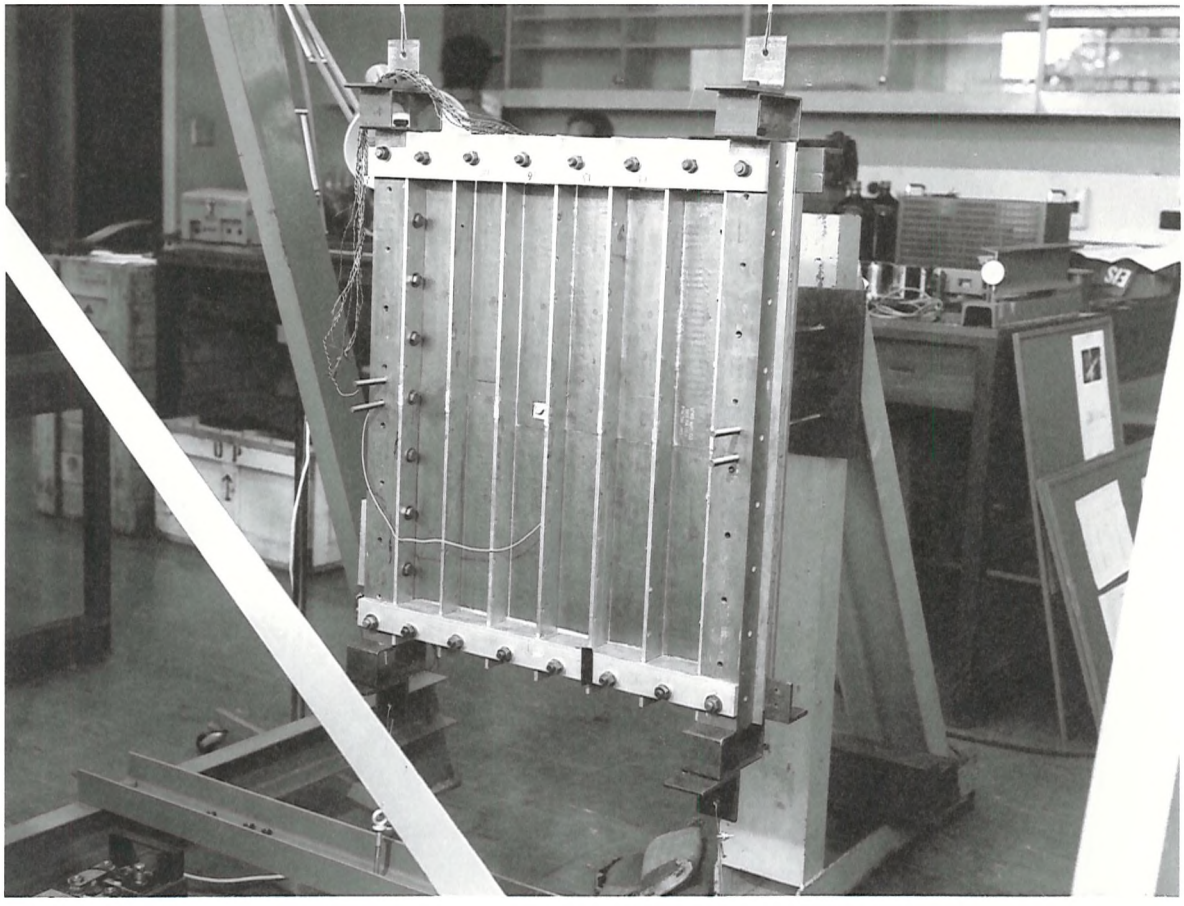

PLATE 8 Undamped Panel Mounting

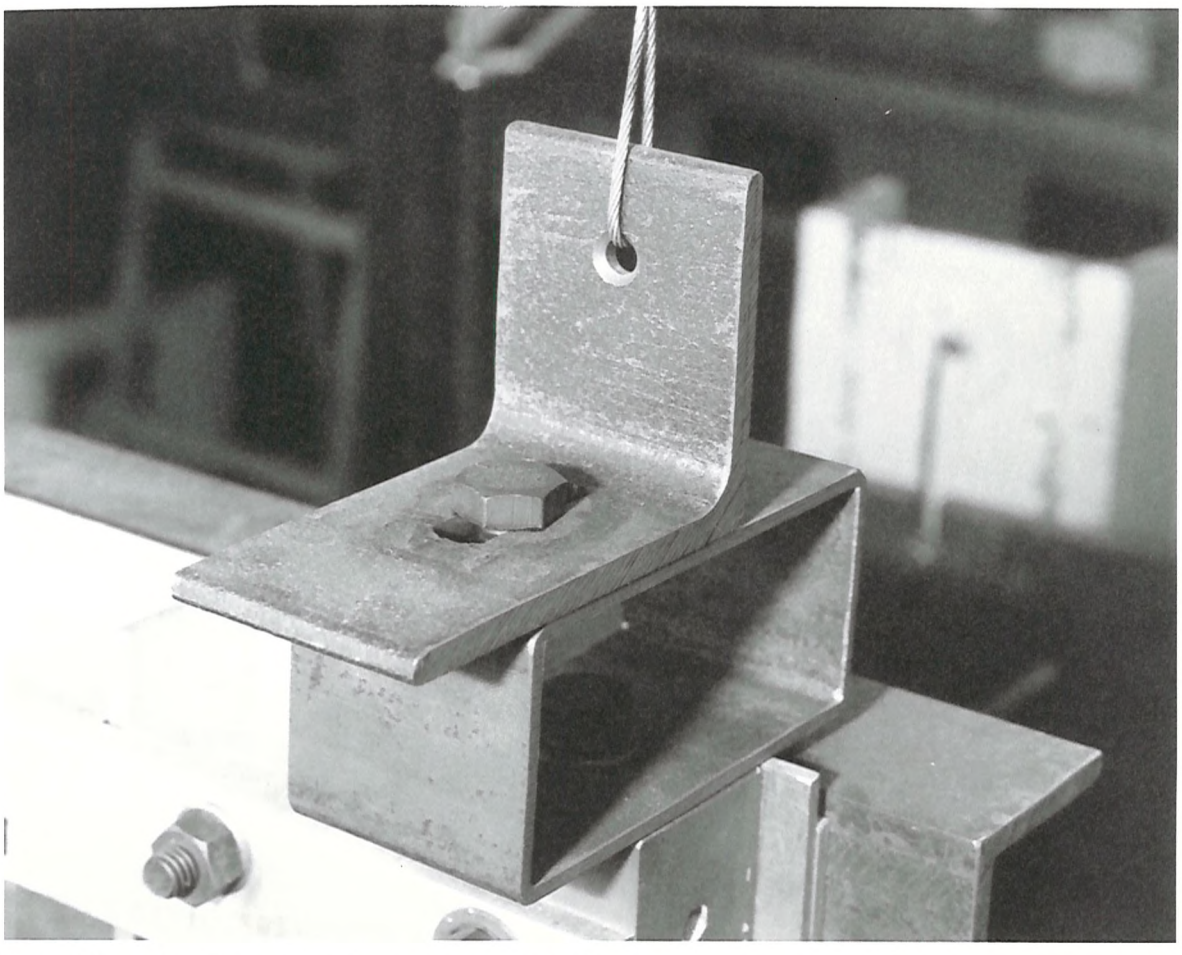

PLATE 9 Panel Frame Suspension Details

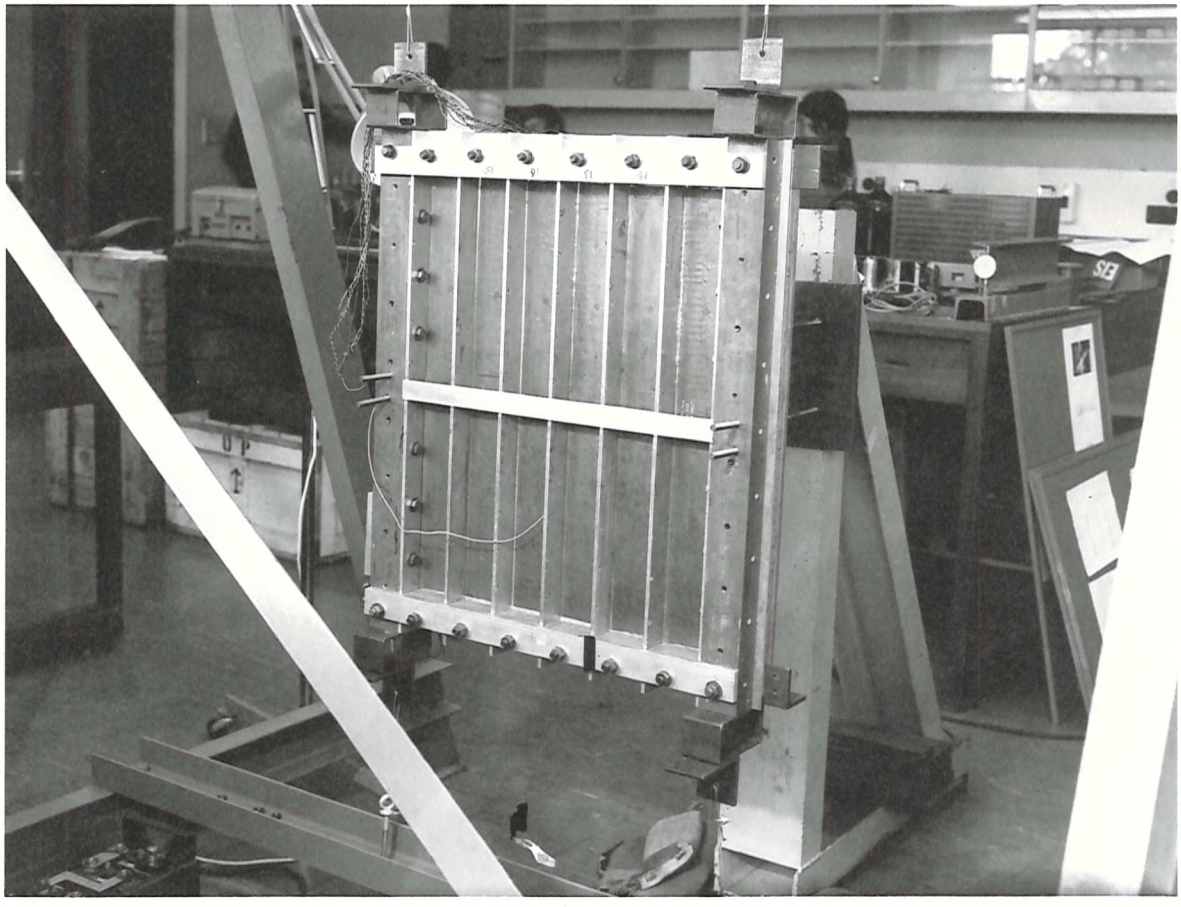

PLATE 10 Damped Panel with Single Damping Beam Attached

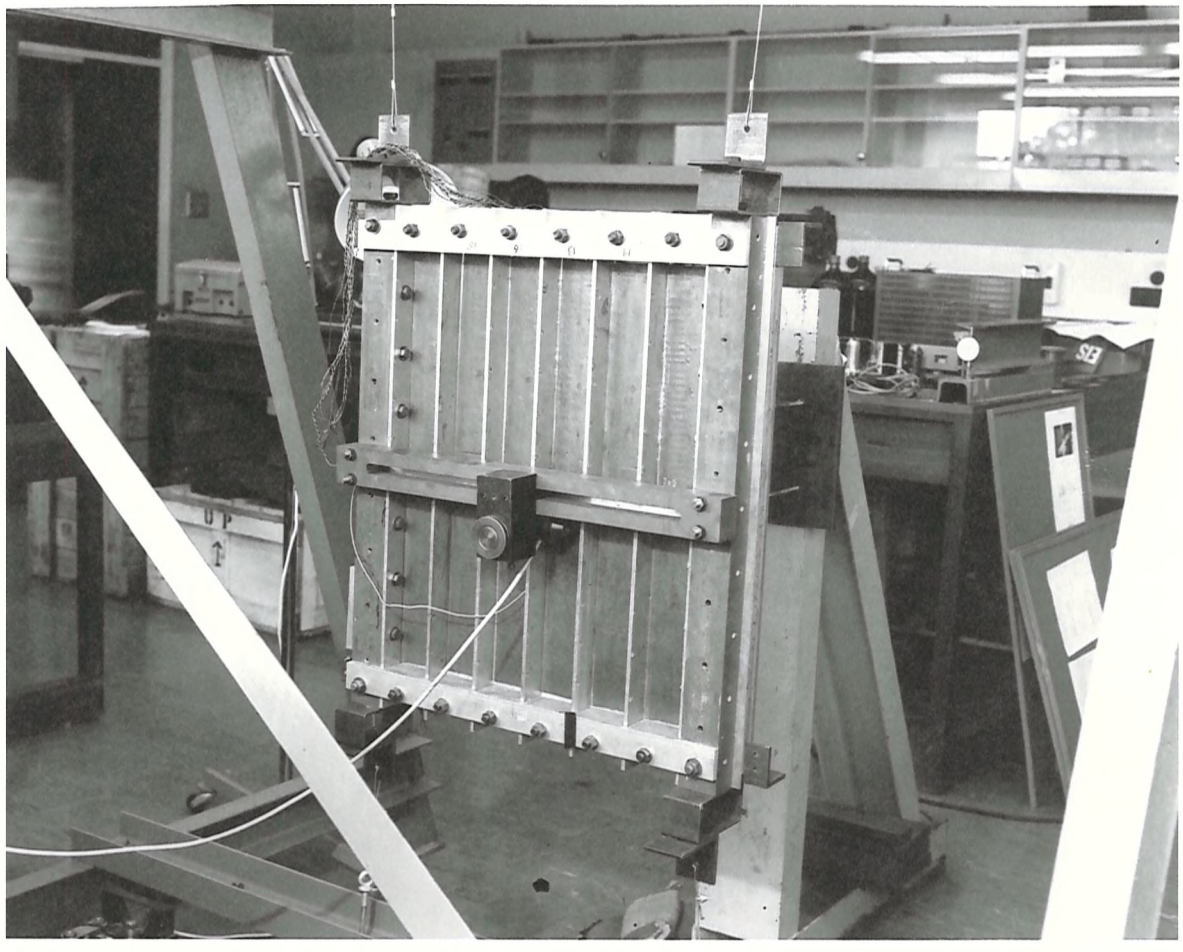

PLATE 11 Damped Panel with Displacement Probe for Stringer Deflexion Tests